APPLICATION OF SYSTEM IDENTIFICATION BASED METHODS ON POWER SYSTEM OSCILLATION CHARACTERIZATION AND MITIGATION

by

Sheikh Jakir Hossain

A dissertation submitted to the faculty of
The University of North Carolina at Charlotte
in partial fulfillment of the requirements
for the degree of Doctor of Philosophy in
Electrical Engineering

Charlotte

2019

Approved by:

_____
Dr. Sukumar Kamalasadan

_____
Dr. Robert Cox

_____
Dr. Valentina Cecchi

_____
Dr. Vincent Ogunro

ABSTRACT

SHEIKH JAKIR HOSSAIN. Application of system identification based methods on power system oscillation characterization and mitigation. (Under the direction of DR. SUKUMAR KAMALASADAN)

This dissertation presents measurement-based system identification methods that help to improve the reliability and operational stability of modern power systems. One of the important factors in maintaining stability is to know the damping and frequency of the oscillatory modes for all system operating conditions. Widespread use of synchrophasors has paved the way for several measurement-based approaches for estimating oscillation modes, damping, and frequency. These methods provide more accurate results than model-based approaches. This dissertation studies the effectiveness of state-of-the-art mode-estimation and proposes a framework based on subspace identification that provides a more accurate modal estimation in real-time. The proposed framework can also classify the oscillation types overserved in the measurements. Oscillatory modes are not observable at all measurement locations. Towards this, in this work, an optimal signal selection method is proposed based on subspace affinity. This helps to reduce the computational time of the modal estimation algorithms, which is critical for any real-time monitoring tool. This work also proposes approaches for mitigating oscillations. First, a method for locating the source of oscillations using the energy of oscillations is presented. Second, a framework for updating power system models based on measurements is proposed that helps system operations and planning. Finally, an integrated control framework for a wide-area damping controller (WADC) is proposed which mitigates different types of oscillations observed in the system. Effectiveness of the overall framework is tested with IEEE test systems and with real-life models with relevant data-sets.The studies show that the proposed approaches can improve the system's situational awareness.

ACKNOWLEDGEMENTS

I want to express my sincere gratitude to my advisor, Dr. Sukumar Kamalasadan, who provided me with an opportunity to be a part of his research team and helped me grow both as a researcher and an individual. I would also like to appreciate the time and support provided by the advising committee of Dr. Robert Cox, Dr. Valentina Cecchi, and Dr. Vincent Ogunro. I sincerely thank UNC Charlotte for offering me GASP, which aided in continuing the course smoothly. Also, I would like to thank EPIC for providing the right atmosphere and research assistantship for performing research. I want to thank students of UNC Charlotte and in particular, PEISL lab who supported directly or indirectly on this work. Last but not least, I would like to express my gratitude towards my wife, Mollika, who has been a constant source of inspiration for me in this long journey.

DEDICATION

This dissertation is dedicated to the two most influential people in my life, my wife Mollika and my mother Jesmin Naher.

TABLE OF CONTENTS

LIST OF TABLES

LIST OF FIGURES

LIST OF ABBREVIATIONS

ARMAX Auto Regressive Moving Average Exogenous Model.

ARX Auto Regressive Exogenous Model.

DEF Dissipating Energy Flow.

FO Forced Oscillations.

MIMO Multiple Input Multiple Output.

MRAS Model Reference Adaptive System.

MVC Minimum Variance Control.

NO Natural Oscillations.

OE Oscillation Energy.

PMU Phasor Measurement Unit.

PSS Power System Stabilizers.

RCDSSI Recursive Combined Deterministic Stochastic Subspace Identification.

RLS Recursive Least Square.

RSSI Recursive Stochastic Subspace Identification.

SI System Identification.

SSI Stochastic Subspace Identification.

WAMS Wide Area Measurement System.

CHAPTER 1: INTRODUCTION

Electromechanical oscillations are an inherent attribute of an interconnected power system (9). For reliable operation of the power system, it is essential that these oscillations are well damped. Undamped oscillations can lead the system towards instability and eventually can cause cascading outages (11). In order for the power system operators to take preventive measures, it is essential to have real-time information about the oscillation frequency and the associated damping. There are two methods for estimating oscillation modes 1) model-based method, and 2) measurement-based method. Model-based methods perform eigenvalue analysis of a linearized model of power grid at different operating conditions and compute the oscillatory modes (9). However, these approaches are suitable only for offline studies and rely heavily on an accurate model of the power system, which is very difficult to obtain. Lack of accurate models along with the widespread implementation of Phasor Measurement Units (PMUs), provides an opportunity to design measurement based methods that can estimate system oscillatory modes from measured data.Significant advances have been made and oscillation monitoring tools have been developed and integrated with system operation.

1.1 Literature Review and Research Challenges

Power system oscillations have been a very active research area over the last few decades. Because it's implication on reliable operation of power grid is huge. Also, wide spread development of synchrophasor applications have paved the way for a lot of new data driven methods for characterizing and mitigating power system oscillations. Significant development have been made in this field in recent years but there are still

a lot of issues that needs to be addressed. Researchers are actively working on these topics. Some of the research problems and associated challenges are discussed in the subsections below.

1.1.1 Power System Oscillations Overview

Over the past decade, significant research progress has been made on measurement based methods for estimating electromechanical modes (12). These methods are mainly divided into three categories based on the type of input power system signals. These categories are a) ringdown signals (the response of power system during event, e.g., line trip, generator trip) b) ambient signals (the response of power system during random load changes), and c) probing signals (non-intrusive signals that excite the power system through probing inputs). Several methods have been proposed for estimating oscillatory modes from ringdown signals such as prony method, eigensystem realization (12), and matrix pencil method to name the few. Methods for analyzing oscillations due to ambient signals are called mode-meter methods such as Yule-Walker algorithm, subspace identification methods, and frequency domain decomposition (12). Some of these methods are performed on an offline data-set which cannot be implemented in real-time due to computational complexity.

For implementation purposes, recursive algorithms are proposed that can make the computation faster for online/real-time applications and changing operating conditions of the system. Some of these methods use variants of a recursive least square algorithm for ARMAX, ARX model structures (13) and some others use subspace identification methods (14), (15). Subspace identification methods are robust and use model order determination as an intermediate step in the identification process which helps to track multiple modes simultaneously. Authors of (14) have proposed recursive adaptive subspace identification which works well for identifying electromechanical oscillations from ambient signals. This method uses covariance-based stochastic subspace identification (SSI-COV). Some method uses non-recursive (block process-

ing) data-driven stochastic subspace identification (SSI-Data) to identify oscillation properties from the ringdown signal (15) in order to mitigate error in data such as in error co-variance variance (SSI-COV)(16).

Besides, detecting the type of oscillation is exceptionally critical. Analysis of synchrophasor data has revealed that oscillations in a system can be due to internal factors such as cyclic loads, malfunction of equipment's (17). These oscillations are known as forced oscillations. When natural oscillations have low damping and forced oscillation frequencies are closer to natural oscillations frequencies it becomes increasingly difficult to identify and distinguish the oscillatory modes and types. Recently, (3) showed that the covariance based recursive SSI algorithm can estimate oscillation modes in the presence of both natural and forced oscillation. However, this method does not explicitly separates natural oscillations from forced oscillations. Ref. (18) have shown how the input information can be used to separate the system characteristics from input characteristics. Researcher are working actively on developing methods for detecting forced oscillations and estimating electromechanical oscillation in the presence of forced oscillations.

1.1.2 Optimal Signal Selection for Mode Estimation

Recent widespread deployment of phasor measurement units (PMUs) have paved the way for a lot of new synchrophasor applications. One important synchrophasor application is the wide area measurement system (WAMS). WAMS enables the development of situational awareness tools which provides operators information about real-time power system stability and archives data which is used for post event analysis. One key indicator of power system stability is the oscillation modes and the associated damping. For reliable operation of the power system it is pivotal for all the modes to be well damped. Recent report from North American Electric Reliability Corporation (NERC) lists several oscillatory events observed in Eastern,Western and ERCOT interconnections (19). Traditionally, such oscillatory behaviours related

to small signal stability is studied using modal analysis of linearized power system models . But, post event analysis of August 10, 1996 blackout reveals significant mismatch between the oscillation characteristics predicted from modal analysis and the actual oscillations observed in the system (20). Several events like this has shown the need of measurement based mode estimation methods and has drawn significant attention from researchers in past couple of decades.

Several methods have been proposed by the researchers for mode estimation using PMU measurements. These methods have been categorized into three categories depending on the type of measured power system responses a) ringdown b) mode meter and c) probing (21). Ringdown response means the response of a the system following a large disturbance (e.g faults, line/generation trip etc) and mode estimation methods for ringdowns signals are prony, matrix pencil, eigensystem realization. Mode meter methods are yule-walker parameter estimation, least mean square method, stochastic subspace identification etc. These methods are used to extract modal information from ambient data which represents the continuous random load variations occurring the system (22).Probing response means the response of the system when a low intrinsic signal is injected to excite and estimate system modes (23).

Moreover, careful investigation of the PMU data has revealed not all the oscillations are related to system electromechanical modes which in sense means not an inherent characteristics of the system, rather are because of periodic external disturbance. Such oscillations are termed as forced oscillations and has been observed in power system across Europe (24), North America (25) etc. Irrespective of the oscillation type it is important to detect the oscillation frequency and damping for both ringdown and ambient conditions. One key characteristic of oscillations is that oscillatory behaviour is not observable in all available PMU signals and hence does not provide enough information to estimate the modes. For most of the available mode estimation methods only a handful of PMU signals which are selected based on prior knowledge

of the system are used. Another limitation is most of the time such methods are tuned to monitor the damping of previously known inter-area modes. Furthermore, concurrent use of large number of PMU signals affect the computational time of existing algorithms. Another important requirement which has been mentioned in NERC reliability guideline (25), is to determine to what extent an oscillation is affecting in the system. This helps to coordinate between multiple regional coordinators which in turn helps in taking proper corrective steps. All these consideration leads to the concept of finding optimal group of signals which are suitable for mode estimation as well as gives information about the spread of the oscillations.

Authors in (26) has used a two level estimation architecture to use large number of PMU signals and uses weighting factors to determine signal quality. Authors have shown that if an ISO running a mode estimation tool is not monitoring the right PMU signal then it might miss the oscillatory behaviour. A modal power contribution (MPC) index is proposed in (27) to rank signal according their suitability for mode estimation. But these methods are based on heuristic approach and does not provide any mathematical proof. Authors in (4) proposes an analytic expression for estimating the variance of damping ratio which uses only identified system parameters. But, the proposed method ranks signals for one oscillatory mode at a time and can not account for multiple modes simultaneously. In this dissertation proposal, a spectral clustering based grouping method is used which first characterizes each PMU signals in terms of identified subspaces. Then it calculates the affinity between the subspaces identified at each location to form a fully connected similarity graph. Spectral clustering is applied on the similarity graph to select the optimal group of signals. The proposed grouping has selects optimal signals for ambient and ringdown condition which ensures less variance of the damping ratio. Additionally, such grouping reduces number of signals to be shared among different utilities or regional operators in the wake of system wide oscillations.

1.1.3 Oscillation Source Location Methods

Damped oscillations are a normal phenomenon for any disturbed system showing that the system is approaching back to its equilibrium. However, sustained oscillations could happen in reality where the possible causes include improper operating conditions, periodic disturbances or malfunctioning controllers. Such unexpected sustained oscillations may reduce the power transfer limit and even result in detrimental consequences on the system equipment. To solve this problem, researches on the analysis, detection, classification, location and control design have always been active during the past several decades while only a few of them have been integrated into system control centers to help system operators (28). Since sustained oscillations represent a risk for instability or insecurity of power systems, they should be mitigated as soon as possible. The location of the oscillation source is usually a prerequisite of the mitigation actions and the elimination of the source would always be the most straightforward and effective remedy.

In the current literature, two types of mechanisms for sustained oscillations, i.e. poorly damped natural oscillations and forced oscillations, have been extensively investigated and explained for observed oscillation events, while some other mechanisms have also been discovered in analyses which are based either on Hopf bifurcation caused by slowly varying parameters or on practically impermissible nonlinear behavior of the system, e.g. outof- step condition. The discoveries and investigations of these mechanisms not only provide a better understanding of the oscillation phenomenon in power systems, but also are of fundamental importance for laying foundations for different location methods. Usually, the oscillation source is implicitly defined as a physical device which causes oscillations following a certain mechanism. In practice, causes of sustained oscillations could be the excitation system (29), diesel engine, synchrotron as a cyclic load (30), control valve , turbopressure pulsation , governor control , asynchronous parallelizing of synchronous generators and

improper parameters for the steam turbine controller, et al.Different methods have been developed for oscilaltion source location. Traveling wave based methods utilize the principle of the electromechanical wave propagation (31) to locate the oscillation source. In the damping torque based methods, the generator with a negative damping torque coefficient is identified as the oscillation source (32).Mode shape represents the relative magnitude and phasing of the oscillation throughout the system. It is defined based on the right eigenvectors of the state matrix of the linearized system model. However, the accurate system model is often difficult to obtain and the model based mode shape analysis has only been applied to test systems for a better understanding. To utilize the mode shape information in real systems, many measurement based methods for estimating the mode shape have been proposed. An overview on existing estimation techniques using either ring-down signals or ambient signals can be found in [34] and its references (33).Transient energy function (TEF) is an application of Lyapunov function in power system stability analysis (34), which is usually defined as the sum of the kinetic and potential energies of all generators in the synchronous coordinate framework.

1.1.4 Model-Measurement Based Method for Model Validation

Oscillations are inherent characteristics of dynamic systems. They are broadly classified into electromagnetic and electromechanical oscillations. Electromagnetic oscillations have high frequency and are generally well damped because of internal damping of the power system. However, electromechanical oscillations have a lower frequency and requires additional controllers to damp. Based on the oscillation frequency electromechanical oscillations are divide into local oscillations (0.7 Hz to 2 Hz) and inter-area oscillations (01 Hz to 0.8 Hz) (9). Growing and sustained oscillations pose a serious threat to the reliable operation of the power system and limit the power transfer capacity of interconnected power systems (35). Traditionally, oscillations have been studied as a part of stability studies for different contingencies.

Modes determined through modal analysis give the oscillations frequencies and associated damping of each oscillations(9). Modal analysis gives the modes using a linearized model of power system but the actual system is nonlinear in nature. So, the actual response of a power system model can be significantly different from the linearized response. Authors in (36) present an analysis of the major power outage event occurred in western North America on August 10, 1996 and they conclude that there was a significant difference between the simulated model response and the actual system response. Although the simulated response showed significant damping for the oscillatory modes in actual system, there were negative damping which caused widespread outage. So, a model of the power system cannot always reliably estimate the actual oscillation frequency and damping present in the system.

Recently, real-time measurement devices such as phasor measurement unit (PMU) have been installed throughout the power system and coverage area is increasing very fast (37). PMU acquires data with a higher sample rate (120 or 240 samples per second), and this data is able to capture the fast changes happening in the power system. In the last decades, several researchers have worked on these measurement data and several methods have been proposed that can estimate the modes and mode shapes using these data (12). Increased availability of PMU data allowed to capture oscillations in the frequency range of 0.1 HZ to 2 Hz which are not part of system natural response rather they are created by periodic external sources (38). These oscillations are termed as forced oscillations. The sources of forced oscillations include but not limited to cyclic load, stable limit cycles, wind plant controllers, malfunction of generator governor controller etc (39). The characteristics of forced oscillations are different than natural electromechanical oscillations. To take proper control action the type of oscillation needs to be identified. The authors of (5) have shown analytically the characteristics of forced oscillations and natural oscillations but these characteristics are difficult to extract if the oscillation sinusoids cannot be extracted

from the noise. In (40) authors present a method that can simultaneously detect natural and forced oscillations, but the proposed method needs to be studied extensively for scenarios mentioned in the test case library (41). In (42) authors propose a method which analyses oscillation envelope shape to detect forced oscillation.

In spite of the advancements made in the measurement based methods on forced oscillation detection, these methods lack an analytic approach based on the mathematical model of the power system. Several researchers have proposed different methods which take the linearized model of the system and forms an analytic expression for characterizing the system response to forced oscillations (43). However, these analytic methods work well for linearized models but for the actual power system, the performance of these methods decreases because of the nonlinearity and unmodeled dynamics. Nonlinearity can have a significant effect on the estimated modes from measurement data (44). It is clear that system model update critical to capture dynamic changes in the system. With the help of measurements that happens after an event, these updates are possible and can be characterized as unmodeled dynamics. How to capture the difference between model and measurement response is a growing research area.

1.1.5 Oscillation Mitigation Overview

Generally, WADC are designed using linear feedback control techniques based on the small signal model obtained by linearizing the dynamic model of the system around an operating point. Control techniques reported in literature utilizing DER is based upon either mimicking the droop based control (45), PSS (46; 47), compensator based (48), or by injecting the power into the system out of phase with the inter-area oscillation(49). Other studies based on optimization algorithm and energy function approach has been demonstrated in (47; 50). However, one of the issues related with these previous studies is that their success is dependent on having an accurate knowledge of system and linearization of the non-linear dynamic system such as power

grid. Also, the controllers are static and designed for a particular operating condition, considering a particular mode of oscillation which may not work well for different operating condition especially with higher penetration of variable renewable resources. Artificial intelligence (AI) based techniques have been demonstrated to capture the nonlinearities and uncertainties in the power grid and can learn and map the system dynamics from set of system inputs and outputs (51). However, the issues related to such AI based techniques is that they require sets of offline data for training and performance validation and has larger computational burden.

Several measurement based methods have also been developed to estimate the modes of the system from wide area measurements (WAMs) data. These methods identify the model of the system from measurement data in two forms 1) subspace state space form (52) and 2) transfer function form (53). In (53), it has been demonstrated that both the subspace state space and MIMO transfer function model can capture the dominant modes of the system accurately from both ring-down data (data generated from event like line tripping, generation loss etc.) and ambient data (data obtained from random small load changes). These identified models can be used to design adaptive and coordinated damping controller (DC). Compared to subspace state space model MIMO transfer function model has improved computational efficiency and lower order aggregation capability. In (8), the parameters of conventional WADC form as well as time delay compensator are updated online based on low order single-input single-output (SISO) model determined based on the residue analysis of the MIMO model. In (8), it was assumed that the critical inter-area mode can be well represented by the mode with largest residue in the identified transfer function model of the system. This approach ignores the other nearby modes whose residue can be in close approximation with the electromechanical modes that may have significant impact on system low frequency oscillations. Such modes are generally associated with the poor design of controllers (54).

1.2 Dissertation Objectives, Motivation and Contribution

1.2.1 Objectives

The research work has the following objectives:

- Study the state of the art methods for power system mode estimation and oscillation characterization.
- To develop a method for estimating the oscillation modes accurately in the presence of forced oscillations.
- To develop a method for selecting optimal number of signals for oscillation mode estimation.
- To study the existing oscillation source location method and then develop a method for oscillation source location from measurements.
- To develop a measurement based model generation method that can capture the effect of unmodeled dynamics.
- To develop wide area damping controller that is adaptive in nature and can effectively damp oscillations. Also the controller should be able to control multiple resources to damp oscillations.

1.2.2 Contribution

Following are the research contributions which facilitates new methods for oscillation characterization and mitigation:

- A method for applying combined deterministic-stochastic subspace identification framework for accurately estimating the electromechanical modes of the system from measurements. The main advantages of the proposed architecture are a) it provides closed loop online identification of power system oscillation

modes which addresses the issues related to the online implementation of subspace identification b) provides accurate estimation of electromechanical modes in the presence of forced oscillation c) it can distinguish between natural and forced oscillations and d)it can dynamically tracks the multiple changing oscillatory modes as operating condition changes.

- A novel method for finding out the optimal number of signals for mode estimation is developed which uses spectral clustering to group the signals. The main advantages of the proposed method are a) it is a general method for ranking the synchrophasor signals for mode estimation methods using both ringdown and ambient data b)The developed method considers both the spatial and temporal characteristics of synchrophasor signals and takes that into account to classify the signals into strong and weak groups and c)The proposed methods can select optimal signals in the presence of multiple oscillation modes.

- A new method for locating the source of oscillation is proposed. This method can estimate the mode shape of generator which does not have any phasor measurement unit (PMU) located at it's terminal. This also uses the subspace affinity based grouping developed in previous chapter to preselect the potential location of source buses. Then it uses the phase angle relationship between the bus speed and branch power to find the direction of oscillation energy flows. Tracing the directions of oscillation energy flow the source of oscillation is located

- A method for using both model and measurement are proposed. In this method mathematical models are obtained to represent the undmoeled dynamics which is the mismatch between the model and measurement response. Then the identified mode is used to perform what if scenarios to improve system reliability. The proposed method uses subpace identification developed in previous chapter.

- A novel damping controller framework is proposed which augments the existing control architecture of distributed energy resources (DER) to perform oscillation damping. The main advantages of the propose methods are a)it is based on the online identification of the system dynamics which results in adjusting the controller output as the system operating condition changes b)It is independent of the network topology and only requires wide area measurement system (WAMs) for identification and control c) it can be augmented with the existing local control in the DER and d)it adapts to various operating conditions and can consider the complete order of identified system model as opposed to considering the mode with highest residue

1.2.3 Intellectual Merit and Broader Impact

The intellectual merit of the work is

- This dissertation provides a method for detecting forced oscillation from measurement data and proposes an integrated framework for estimating the electromechanical mode characteristics in the presence of forced oscillations. This will help to enhance the capability of state-of-art situational awareness tool used by power system operators.

- This work provides a method for selecting optimal number of signals for mode estimation based on subspace affinity. It uses spectral clustering to group the signals into weak and strong group for the mode estimation algorithms. Decreasing the number of signals for mode estimation method helps to decrease the computation burden on the mode estimation algorithm. It also enables transmission operators (TO) to coordinate across multiple balancing authorities (BA).Moreover, it helps to pre-screen number of potential oscillation source location.

- This work also presents a new method of locating the source of oscillations

which can detect the source of oscillations reliably even if there are no PMU measurement available at the source location. This method can help the system operators on locating the source of oscillation and can help them taking fast corrective actions.

- One of the limitation of power system planning is that it depend on the model of the system. Power system models does not always give an accurate representation of the system. In this work a model measurement based hybrid method is proposed that can construct mathematical model of the system based on measurements and can help identifying the accuracy of power system models. This can also help operator running different scenarios.

- In this work a wide area damping controller(WADC) is developed. It uses a multiple input multiple output (MIMO) system identification to identify the system. The proposed method is adaptive in nature and can mitigate oscillations with varying system conditions. This is helpful for ensuring system reliability speciality with the uncertainty and variability introduced by the increased renewable penetration.

Broader impact of the work is

- This dissertation proposes a recursive combined deterministic stochastic subspace identification framework which can be applied to other fields of study where system identification based technique is required

- The proposed method increases the capability of the existing situational awareness tools used in the system operating centers. This will improve the overall reliability of the power system.

- The proposed method helps to tackle the increased variability and uncertainty associated with increased renewable integration by enhancing the oscillation

monitoring and mitigation schemes.

- The proposed oscillation mitigation can allow controllable renewable resources like energy storage to participate in improving the bulk power system stability.

1.3 Dissertation Organization

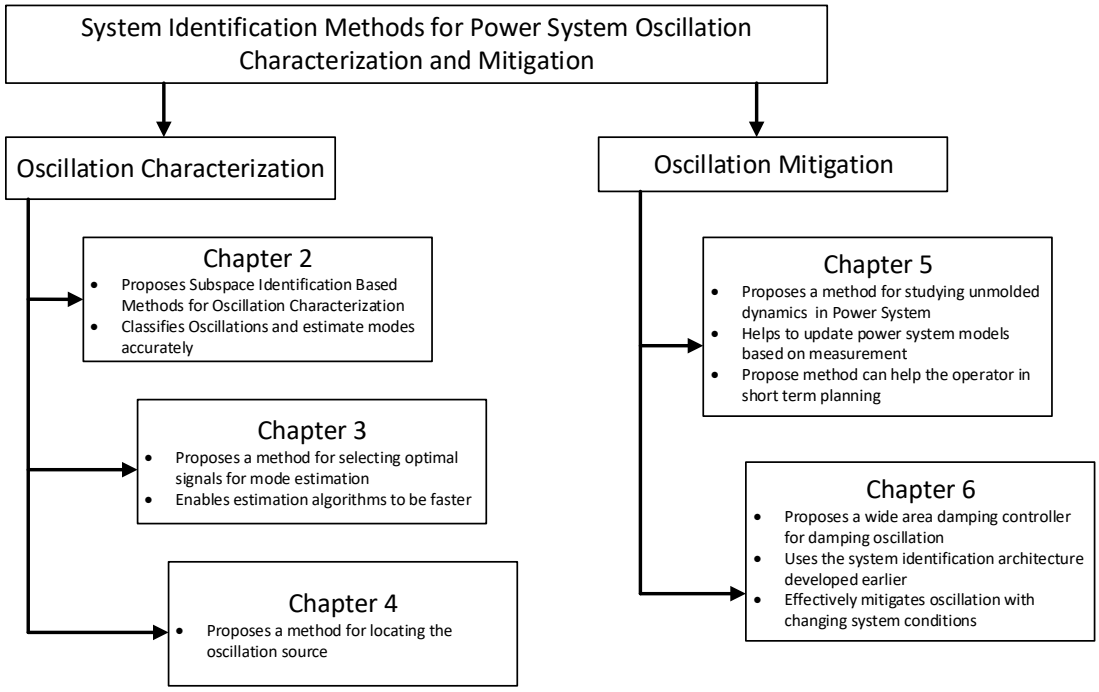

Figure 1.1: Overview of the thesis proposal.

Chapter 1 provides an introduction to the oscillation monitoring tool and current state of the art related to system operator situational awareness tool in the Energy Management System (EMS) operation. The objectives, motivation, and contribution of the dissertation is presented in Chapter 1. Chapter 2 introduces a novel approach for oscillation characterizations. Chapter 3 discusses a method for optimal signal selection for oscillation monitoring. Chapter 4 proposes a new method for locating the source of power system oscillations. Chapter 5 shows how the techniques developed in previous chapters can be used to update the power system models and how it helps to capture the effect of unmodeled dynamics. A combined framework is presented

that incorporates the methods proposed in the thesis and uses it to develop mitigation techniques. A subspace identification based oscillation mitigation framework is presented in chapter 6, which helps to damp the power system oscillations faster and improves system stability. Conclusions and future works are discussed in chapter 7.

CHAPTER 2: AN INTEGRATED FRAMEWORK FOR OSCILLATION CHARACTERIZATION

Measurement-based methods for power system oscillatory modes estimation provide situational awareness and power system operational strategies to ensure overall grid stability. This chapter presents a combined deterministic-stochastic framework for online identification of oscillatory modes using synchrophasors data. The proposed method recursively solves the deterministic-stochastic model structure and addresses the issues related to the online implementation of such an oscillation monitoring tool. Further, It proposes a method for forced oscillation detection and uses that as input information to obtain accurate mode estimation of all relevant electromechanical modes. Simulation results from two area test system and IEEE 68 bus test system show the potential advantage of the proposed method.

2.1 Introduction

Electromechanical oscillations are an inherent attribute of an interconnected power system (9). For reliable operation of the power system, it is essential that these oscillations are well damped. Undamped oscillations can lead the system towards instability and eventually can cause cascading outages (11). In order for the power system operators to take preventive measures, it is essential to have real-time information about the oscillation frequency and the associated damping. There are two methods for estimating oscillation modes 1) model-based method, and 2) measurement-based method. Model-based methods perform eigenvalue analysis of a linearized model of power grid at different operating conditions and compute the oscillatory modes (9). However, these approaches are suitable only for offline studies and rely heavily on

an accurate model of the power system, which is very difficult to obtain. Lack of accurate models along with the widespread implementation of Phasor Measurement Units (PMUs), provides an opportunity to design measurement based methods that can estimate system oscillatory modes from measured data.

Over the past decade, significant research progress has been made on measurement based methods for estimating electromechanical modes (12). These methods are mainly divided into three categories based on the type of input power system signals. These categories are methods that uses a) ringdown signals (the response of power system during event, e.g., line trip, generator trip) b) ambient signals (the response of power system during random load changes), and c) probing signals (non-intrusive signals that excite the power system through probing inputs). Several methods have been proposed for estimating oscillatory modes from ringdown signals such as prony method, eigensystem realization (12), and matrix pencil method. Methods for analyzing oscillations due to ambient signals are called mode-meter methods such as Yule-Walker algorithm, subspace identification methods, and frequency domain decomposition (12). Some of these methods are performed on an offline data-set which cannot be implemented in real-time due to computational complexity.

For implementation purposes, recursive algorithms are proposed that can make the computation faster for online/real-time applications and changing operating conditions of the system. Some of these methods use variants of a recursive least square algorithm for ARMAX, ARX model structures (13) and some others use subspace identification methods (14), (15). Subspace identification methods are robust and use model order determination as an intermediate step in the identification process which helps to track multiple modes simultaneously. Authors of (14) have proposed recursive adaptive subspace identification which works well for identifying electromechanical oscillations from ambient signals. This method uses covariance-based stochastic subspace identification (SSI-COV). Some method uses non-recursive (block process-

ing) data-driven stochastic subspace identification (SSI-Data) to identify oscillation properties from the ringdown signal (15) in order to mitigate error in data such as in error co-variance variance (SSI-COV)(16).

Besides, detecting the type of oscillation is exceptionally critical. Analysis of synchrophasor data has revealed that oscillations in a system can be due to external factors such as cyclic loads, malfunction of equipment's (17). These oscillations are known as forced oscillations. When natural oscillations have low damping and forced oscillation frequencies are closer to natural oscillations frequencies it becomes increasingly difficult to identify and distinguish the oscillatory modes and types. Recently, (3) showed that the covariance based recursive adaptive SSI (RASSI) algorithm can estimate oscillation modes in the presence of both natural and forced oscillation. However, this method does not explicitly separates natural oscillations from forced oscillations. Ref. (18) have shown how the input information can be used to separate the system characteristics from input characteristics. Such mode estimation and classifications are very important for reliable operation of power grid (55) as well as mitigation of oscillations (56),(57).Authors in (58) have proposed a transfer function based (ARMA+S) approach for estimating electromechanical modes in the presence of forced oscillations. However, the method requires detection and time localisation of forced oscillations.

In this Chapter, a data-driven Recursive Combined-Deterministic Stochastic Subspace Identification (RCDSSI) algorithm is designed and tested which takes the input characteristics into account and extracts only the systems natural modes. In this approach, the conventional recursive stochastic subspace identification (RSSI) is enhanced to include the input information and both RSSI and the RCDSSI algorithm are part of one combined framework. As RSSI algorithm gives both system and input/forced modal information and RCDSSI gives only system modal characteristics, oscillations are classified. The proposed method solves the combined state space

structure recursively and avoids numerically exhaustive steps like QR decomposition and Singular Value Decomposition (SVD).

The main contributions are the architecture can:

- Provide closed loop online identification of power system oscillation modes based on a combined deterministic stochastic structure which can isolate system natural characteristics in the presence of external disturbances.
- Provide accurate estimation of electromechanical modes for both ambient and ringdown signals.
- Provide accurate estimation of electromechanical modes in the presence of forced oscillations.
- Detect the presence of forced oscillations
- Characterization of the oscillations based on oscillation types
- Dynamically tracks the multiple changing oscillatory modes as condition changes.

The rest of the chapter is organized as follows. Section 5.2 provides a brief discussion on the methodology proposed for RCDSSI and oscillation classification. Section 2.3 gives an illustrating example of the proposed architecture. Simulation results for different scenarios are discussed in section 6.5 and conclusions are in section 5.7.

2.2 Proposed Methodology

In this section, first the power system model is described. Then the combined deterministic stochastic subspace identification is presented and the recursive method of implementing it is then introduced.

2.2.1 Power System Model

The power system response in the presence of external periodic disturbance and ambient noise is represented by a discrete linear model (59) as,

$$\dot{x_{k+1}} = Ax_k + Bu_k + \sum_{j=1}^{P} B_{Nj} W_{jk} \tag{2.1}$$

$$y_k = Cx_k + Du_k + \sum_{j=1}^{P} V_{jk}$$

where, $x \epsilon \mathbb{R}^n$ is the system state matrix, $y \epsilon \mathbb{R}^l$ is the vector of PMU measurements,$u \epsilon \mathbb{R}^m$ is the vector of input, $A \epsilon \mathbb{R}^{n \times n}$ is the state matrix,$B \epsilon \mathbb{R}^{n \times m}$ is the input matrix,$C \epsilon \mathbb{R}^{l \times n}$ is the input matrix t is the integer time sample, $W_j k$ is the process noise with zero mean Gaussian noise sources which typically represents the random load changes and $V_j k$ is the measurement noise representing disturbances or sensor error.

$$\mathbf{E}[\begin{pmatrix} W_p \\ V_p \end{pmatrix} (W_q^T \quad V_q^T)] = \begin{pmatrix} Q & S \\ S^T & R \end{pmatrix} \delta \tag{2.2}$$

where, $Q \epsilon \mathbb{R}^{n \times n}$, $R \epsilon \mathbb{R}^{l \times l}$ and $S \epsilon \mathbb{R}^{n \times l}$ are the co variance matrix of the noise vectors, $\mathbf{E}$ denotes the expected value operator and δ the kronecker delta.

The time domain solution of (2.1) gives the system response $y(t)$ as,

$$y(t) = \underbrace{\sum_{i=1}^{N} C\psi_i\phi_i X(0) e^{\lambda_i t}}_{Transient} + \underbrace{\sum_{j=1}^{M} [(\sum_{i=1}^{N} C\psi_i\phi_i B_{Nj} e^{\lambda_i t}) \circledast Q_{Nj}(t)]}_{Noise} \tag{2.3}$$

where ψ, ϕ, λ are the left eigenevector , right eigenvector and eigenvalues of the A matrix respectively. $\circledast$ is the convolution operator.

If there is a nth lightly damped natural oscillation mode and no forced oscillation present then (2.3) can be rearranged in frequency domain as,

$$y_N(\omega) = \underbrace{\frac{C\psi_n\phi_n X(0)}{j\omega - \lambda_n}}_{NO_1} + \underbrace{\sum_{j=1}^{M}[\sum_{i=1,i\neq n}^{N} \frac{C\psi_n\phi_n B_{Nj}}{j\omega - \lambda_i}]Q_j(\omega)}_{NO_2} + \underbrace{\sum_{j=1}^{M}(2C\psi_i\phi_i B_{Nj}Q_j(\omega))\delta(\omega - \omega_n)}_{NO_3} \tag{2.4}$$

where, the term NO_1 represents the transient response, NO_2 represents random noise colored by system dynamics and NO_3 represents the sinusoidal noise term which contains the lightly damped mode frequency ω_n.

2.2.2 Combined Deterministic Stochastic Subspace Identification

In this section, a Recursive Combined Deterministic Stochastic Subspace Identification (RCDSSI) framework is presented. The goal is to obtain the model of the system from measurement data. PMU measurements are typically located at selected buses in the power system network and measures the voltage magnitude, voltage angle, current magnitude, current angle and frequencies at the bus. When a disturbance occurs oscillation is seen at different PMU locations. The type and magnitude of oscillations depends on the severity and location of disturbance. Depending upon the location of PMU measurements, it can be classified in output and input (e.g load buses) (60)). This input and output is used to form the output block Hankel matrix H_y and input block Hankel matrix H_u.

$$\mathbf{H_y} = \left[\frac{Y_p}{Y_f}\right] = \frac{\begin{bmatrix} y_1 & \cdots & y_j \\ y_2 & \cdots & y_{j+1} \\ \vdots & \cdots & \vdots \\ y_i & \cdots & y_{j+i-1} \end{bmatrix}}{\begin{bmatrix} y_{i+1} & \cdots & y_{i+j} \\ y_{i+2} & \cdots & y_i + i + j + 1 \\ \vdots & \cdots & \vdots \\ y_{2i} & \cdots & y_{2i+j-1} \end{bmatrix}} \epsilon \mathbb{R}^{2i \times j} \tag{2.5}$$

$$\mathbf{H_u} = \left[\frac{U_p}{U_f}\right] = \frac{\begin{bmatrix} u_1 & \cdots & u_j \\ u_2 & \cdots & u_{j+1} \\ \vdots & \cdots & \vdots \\ u_i & \cdots & u_{j+i-1} \end{bmatrix}}{\begin{bmatrix} u_{i+1} & \cdots & u_{i+j} \\ u_{i+2} & \cdots & u_i + i + j + 1 \\ \vdots & \cdots & \vdots \\ u_{2i} & \cdots & u_{2i+j-1} \end{bmatrix}} \epsilon \mathbb{R}^{2i \times j} \tag{2.6}$$

where i is the number of block rows which is an user-defined index and must be larger than the order $2n$ of the system to capture all the system modes, and $j = l - 2i + 1$ and l is data window length. The input and output block Hankel matrices are divided into past and future input-output matrices Y_p, Y_f, U_p and U_f. The response of the system contains both stochastic and deterministic part. The state sequence x_k and output response y_k is divided into stochastic and deterministic part.

$$x_k = x_k^d + x_k^s \tag{2.7}$$

$$y_k = y_k^d + y_k^s \tag{2.8}$$

The system in (2.1) is represented in matrix form after performing recursive substitution as,

$$\begin{aligned} Y_p &= \Lambda_i X_p^d + H_i^d U_p + Y_p^s \\ Y_f &= \Lambda_i X_f^d + H_i^d U_f + Y_f^s \\ X_f^d &= A_i X_p^d + \Delta_i^d U_p \end{aligned} \tag{2.9}$$

where, x_f^d is the past deterministic states, x_p^d is the future deterministic states, Y_p^s is the past stochastic output and Y_f^s is the future stochastic output.

$$H_i^d = \begin{bmatrix} D & 0 & \cdots & 0 \\ CB & D & \cdots & 0 \\ \vdots & \vdots & \cdots & \vdots \\ CA^{i-2}B & CA^{i-3}B & \cdots & D \end{bmatrix} \epsilon \mathbb{R}^{li \times mi} \tag{2.10}$$

$$\Delta_i^d = \begin{bmatrix} A_d^{i-1}B & A_d^{i-1}B & \cdots & A_d B_d B_d \end{bmatrix} \epsilon \mathbb{R}^{2n \times mi} \tag{2.11}$$

where Δ_i^d is the reverse extended controllability matrix, H_i^d is the low block triangular Toeplitz matrix (61) and Y_p^s,Y_f^s represents the stochastic part of the measured signals. The key idea of subspace identification (SI) is the use of state as a finite di-

mensional space between past and future. it uses the projection theorem to eliminate the influence of noise and extracts the extended observability matrix from the block equations (2.9). Authors in (61) provides a general framework for treating most of the SI algorithms. However, does not provide any methods for recursive subspace identification algorithms which is essential for online oscillation monitoring application. The key idea is to compute the oblique projection of future output Y_f on past input output along the direction of future inputs. One of the algorithm that helps to compute the oblique projection is "Multivariable Output-Error State Space" algorithm (MOESP). It uses LQ decomposition of the Hankel matrix to compute the column space of the projection matrix O (61).

$$\underset{\mathbb{R}^{2(m+l)i\times j}}{H_{1:j}} = \begin{bmatrix} U_f \\ W_p \\ Y_f \end{bmatrix} = \begin{bmatrix} L_{11} & 0 & 0 \\ L_{21} & L_{22} & 0 \\ L_{31} & L_{32} & L_{33} \end{bmatrix} \begin{bmatrix} Q_{11}^T \\ Q_{21}^T \\ Q_{31}^T \end{bmatrix} \tag{2.12}$$

$$(Y_f/_(U_f)W_p) = \Lambda_i X_i/U_f^| = L_{32}Q_{21}^T \tag{2.13}$$

where W_p is the combined subspace of both past input and output block Hankel matrices U_p and Y_p. Eqn. (5.18) calculates the oblique projection of the future outputs on the past input/output along the future inputs. Column space of L_{32} is equal to the column space of extended observability matrix Λ_i. So only extracting L_{32} from the LQ decomposition of the whole subspace is enough to get the system characteristics. This algorithm takes both input and output measurements into account and we refer to this algorithm as RCDSSI algorithm. If only output measurements are used then this algorithm reduces to Recursive Stochastic Subspace identification (RSSI). Different variations of this algorithm have been proposed in the literature (14),(62). In that case orthogonal projection is used instead of oblique projection and the projection matrix O is computed through LQ decomposition as

$$\underset{\mathbb{R}^{2(m+l)i\times j}}{H_{1:j}} = \begin{bmatrix} Y_p \\ Y_f \end{bmatrix} = \begin{bmatrix} L_{11} & 0 \\ L_{21} & L_{22} \end{bmatrix} \tag{2.14}$$

$$Y_f/Y_p = L_{21}Q_{11}^T; L_{21}Q_{11}^T = \Lambda_i X_i \tag{2.15}$$

where L_{ij} represents the lower triangular matrix of LQ decomposition and Q_{ij} represents the orthogonal matrix. Eqn. (5.14) shows that the extended observability matrix (Λ_i) can be calculated from the column space of $\mathbf{L_{21}}$.For online mode estimation and detecting time varying system, it is crucial for the method to be fast and recursive in nature. Recursive Subspace identification based algorithms fall under the broad spectrum of block processing algorithm where at each iteration a fixed window (l discrete points) of data points are taken and only a small p number of data points are updated in each iteration. It uses mathematical tools like LQ decomposition and Singular value Decomposition (SVD) which makes it reliable and numerically stable. However, to reduce the computational burden a method is proposed to update the LQ decomposition as shown in eqns. (5.17) and (5.14) recursively with new p data points at every iteration.

For both RSSI and RCDSSI method the Hankel matrix is used as shown in eqns. (5.14) and (5.17) respectively.If $H_{1:j}$ is a rectangular matrix and $j > 2(m+l)i$, then the columns beyond $2(m+l)i$ of lower triangular matrix of LQ decomposition of $H_{1:j}$ will consist of entirely of zeros. So, $H_{1:j}$ is made a square matrix of size $2(m+l)i \times 2(m+l)i$ and the rest of the columns are truncated. Without losing generality, the Hankel matrix for a known size $j = 2(m+l)i$ can be given as shown in (2.16), where $\mathbf{L_1}\epsilon\mathbb{R}^{j\times j}$ is a square lower triangular matrix and $\mathbf{Q_1}\epsilon\mathbb{R}^{j\times j}$ is a square and orthogonal matrix. When new data points are added then old p data points are deleted and the new LQ decomposition is calculated as shown in (2.17). Then $\mathbf{L_2}$is

calculated recursively from $\mathbf{L_1}$ by applying two successive numerical methods known as Givens rotation. First Givens rotation decouples the past s data points from the Hankel matrix according to (2.18). Then a new set of s data points are appended to the $H \epsilon \mathbb{R}^{j \times j}$ and rearranged as shown in (2.19). Then a second Givens rotation is applied to transform $\bar{L_2}$ to a lower triangular matrix (see (2.20)).

$$\mathbf{H_{1:j}} = \mathbf{L_1 Q_1} \tag{2.16}$$

$$\mathbf{H_{1+s:j+s}} = \mathbf{L_2 Q_2} \tag{2.17}$$

$$\begin{aligned}
\mathbf{H_{1:j}} = \mathbf{L_1 Q_1} &= (\mathbf{L_1 G_1^T})(\mathbf{G_1 Q_1}) \\
&= [\mathbf{H_{1:s}} \quad \bar{\mathbf{L_1}}] \begin{bmatrix} I_s & 0 \\ 0 & \bar{Q}_1 \end{bmatrix} \\
&= [\mathbf{H_{1:s}} \bar{\mathbf{L_1}} \bar{\mathbf{Q_1}}] = [\mathbf{H_{1:s}} \quad \mathbf{H_{s+1:j}}] \qquad (2.18) \\
\mathbf{H_{1+s:j+s}} &= [\mathbf{H_{s+1:j}} \quad \mathbf{H_{j+1:j+s}}] \qquad (2.19) \\
&= [\bar{\mathbf{L_1}} \bar{\mathbf{Q_1}} \quad \mathbf{H_{j+1:j+s}}] \\
&= [\mathbf{H_{j+1:j+s}} \quad \bar{\mathbf{L_1}}] \begin{bmatrix} 0 & I_s \\ \bar{Q}_1 & 0 \end{bmatrix} = \bar{\mathbf{L_2}} \bar{\mathbf{Q_2}} \\
\mathbf{H_{1+s:j+s}} &= (\bar{\mathbf{L_2}} \mathbf{G_2})(\mathbf{G_2^T} \bar{\mathbf{Q}}_\mathbf{2}) = \mathbf{L_2 Q_2} \qquad (2.20)
\end{aligned}$$

where G_1 and G_2 are the givens rotation matrix.

The projected matrix O is expressed as,

$$\underset{\mathbb{R}^{i \times j}}{O} = \begin{cases} L_{21}, \text{if only output measurements are used} \\ L_{32}, \text{if both input and output measurements are used} \end{cases} \tag{2.21}$$

2.2.3 Extraction of Modal Information

After the projected matrix is obtained from the PMU measurements system modal characteristics needs to be extracted. One key characteristics of PMU measurements is the low rank property (63). This means that the rank of projected matrices are low compared to matrix size. Mathematically this can be achieved using SVD. This process reduce the model order and capture only the dominant n modes from the projected matrix O as follows.

$$W1OW2 = [U_1 \quad U_2] \begin{bmatrix} S_1 & 0 \\ 0 & S_2 \end{bmatrix} \begin{bmatrix} V_1^T \\ V_2^T \end{bmatrix} \tag{2.22}$$

When there is measurement noise present in the data, the selection of n dominant modes is not trivial by observing only the singular values of W. Also, for online implementation of such techniques, the process of selecting n dominant modes needs to be automated. Let α_r be the r^{th} singular values of O . Two criteria are used to select n largest singular values from a total of r singular values based on two parameters γ and β. A user can set the values based on the prior knowledge of the system. γ represents the relative difference between two consecutive singular values, and β represents the ratio of n largest singular values to total r number of singular values. Reduced projected matrix based on this is as follows.

$$O_r = U_1 S_1 V_1^T \tag{2.23}$$

$$|\frac{\alpha_i - \alpha_{i+1}}{\alpha_i}| \geq \gamma \tag{2.24}$$

$$\frac{\sum_{i=1}^{n} \alpha_i}{\sum_{j=1}^{r} \alpha_j} \geq \beta \;\; where, \beta = M \;\; \text{a large number} \tag{2.25}$$

The extended observability matrix is expressed as in eqn (2.39) and relates to system matrices A and C.

$$\Lambda_i = \begin{bmatrix} C \\ CA \\ \cdots \\ CA^{i-1} \end{bmatrix} = U_1\sqrt{S1} \tag{2.26}$$

Although eqns. (2.39) and (2.40) help to select the model order dynamically following SVD, it is computationally burdensome to compute SVD for every iteration of a recursive algorithm (64).And SVD is only need to be performed if there is a change in system operating condition or a new mode gets excited or an periodic external disturbance is introduced. In this chapter, recursive way of calculating the extended observability matrix Λ_i is presented which uses the similarities between recursive subspace identification and adaptive signal processing techniques like the propagator method (65). But, in the recursive calculation of Λ_i the size of Λ_i is determined by the model order. And, the model order is determined through SVD and eqns. (2.39), (2.40) only if there is a change in the system. The change in the system is captured by monitoring the change in the mode estimates. It has been observed heuristically that whenever there is a change in the system operating condition the deviation in the mode estimation is significantly higher than if there is no change but random load variations. The deviation is compared with predefined threshold $\Delta\lambda_{Threshold}$ to detect the change in system order and then SVD is performed to update the model order.

$$\boldsymbol{\Delta}\lambda = |\lambda_{\mathbf{k}} - \lambda_{\mathbf{k-1}}| \tag{2.27}$$

Once the model order is selected the recursive algorithm is used to compute the extended observability matrix Λ_i. The propagator can be determined recursively by solving a least square problem mentioned in (2.30). Detail equations are as follows.

$$col(\Lambda_i) = col \begin{pmatrix} I_n \\ P^T \end{pmatrix} \tag{2.28}$$

$$Z_f(t) = \begin{bmatrix} Z_{f1}(t) \\ Z_{f2}(t) \end{bmatrix} \tag{2.29}$$

$$V(P) = E||z_{f2}\zeta^T - P^T z_{f1}\zeta^T||_F^2 \tag{2.30}$$

$$g_t = (R_{z_{f2}}\zeta_t \quad z_{f2t}) \tag{2.31}$$

$$A_t = \begin{pmatrix} -\zeta_t^T\zeta_t & \lambda \\ \lambda & 0 \end{pmatrix} \tag{2.32}$$

$$w_t = R_{z_{f1}}\zeta_t \tag{2.33}$$

$$\psi_t = (w_t \quad z_{f_1,t}) \tag{2.34}$$

$$K_t = (A_t + \psi_t^T M_{t-1}\psi_t)^{-1}\psi_t^T M_{t-1} \tag{2.35}$$

$$P_t^T = P_{t-1}^T + (g_t - P_{t-1}^T\psi_t)k_t \tag{2.36}$$

$$M_t = \frac{1}{\lambda^2}(M_{t-1} - M_{t-1}\psi_t K_t) \tag{2.37}$$

$$\Lambda_t = P_t^T \tag{2.38}$$

where P is a linear operator called propagator which expresses the linearly dependant vectors of extended observability matrix Λ_i as a linear combination of n independent vectors, $Z_f(t)$ is the observation vector, K_t is the gain vector, $R_{z_{f1}}$ is the expected value of observation vector and λ is the forgetting factor.

The discrete time system matrix A can be calculated using the extended observability matrix as shown in (2.40). Then mode frequency and damping properties can

be obtained by performing eigenvalue analysis of the discrete A matrix as follows.

$$\Lambda_i = \begin{bmatrix} C \\ CA \\ \cdots \\ CA^{i-1} \end{bmatrix} = U_1\sqrt{S1} \tag{2.39}$$

$$A = \underline{\Lambda_i}^* \bar{\Lambda}_i \tag{2.40}$$

Further this can be converted into continuous domain equivalent.

$$Eig(A_s) = \sigma + j\omega = \frac{1}{T_s}\log Eig(A) \tag{2.41}$$

The proposed RCDSSI framework is able to estimate behaviour of the power system in the presence of input excitation and noise. This helps to estimate system electromechanical modes accurately even in the presence of forced oscillations at the same time can also classify oscillations between forced and natural electromechanical modes. Fig. 2.1 shows the overall flowchart of the proposed architecture.

2.2.4 Detection of Forced Oscillations

In case a forced oscillation is present in the system the input u_k is expressed as a periodic disturbance,

$$f_k = \sum_{p=-\infty}^{\infty} A_p e^{jp\omega k} \tag{2.42}$$

The time domain solution of (2.1) gives the system response $y(t)$ as,

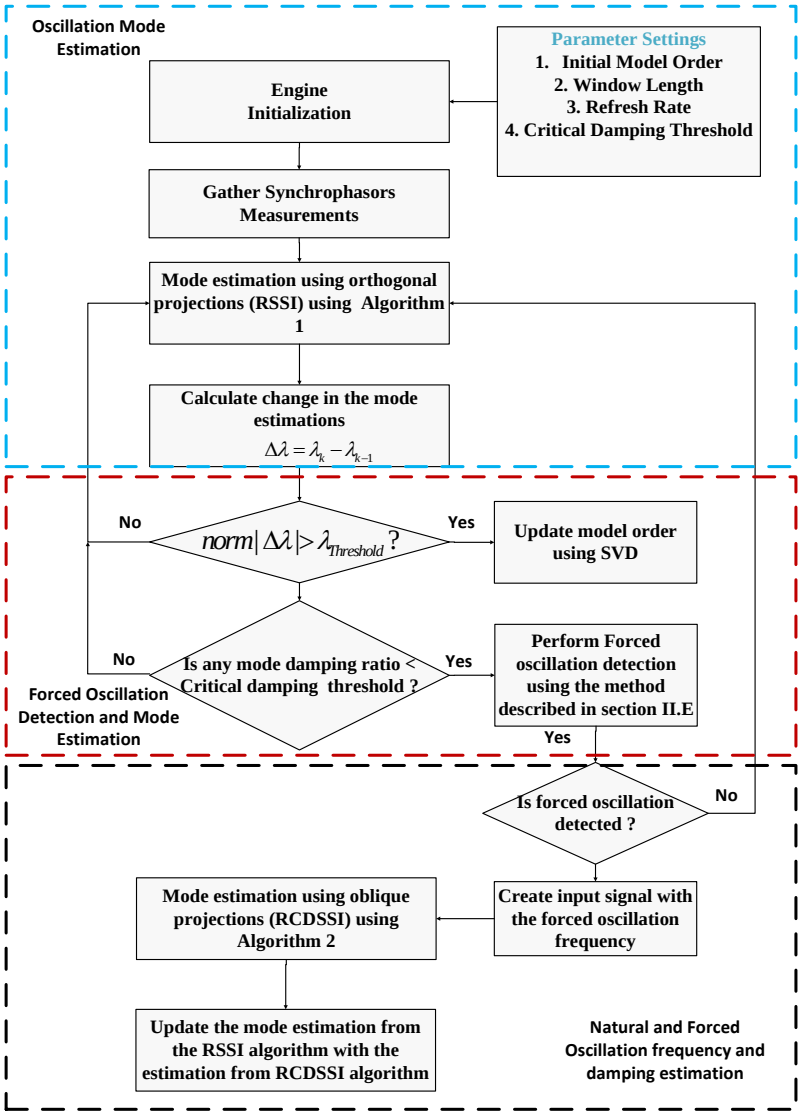

Figure 2.1: Flow Chart for the proposed integrated framework for online oscillation monitoring and classification.

$$y(t) = \underbrace{\sum_{i=1}^{N} C\psi_i\phi_i X(0)e^{\lambda_i t}}_{Transient} + \underbrace{\sum_{p=1}^{\infty}[(\sum_{i=1}^{N} C\psi_i\phi_i B e^{\lambda_i t}) \circledast A_p e^{jp\omega t}]}_{Forced} + \underbrace{\sum_{j=1}^{M}[(\sum_{i=1}^{N} C\psi_i\phi_i B_{Nj} e^{\lambda_i t}) \circledast Q_{Nj}(t)]}_{Noise} \tag{2.43}$$

If all the modes of the system are well damped and a forced oscillation is present then after rearranging (2.43) is represented in frequency domain as,

$$y_F(\omega) = \underbrace{\sum_{p=1}^{\infty}[\sum_{i=1}^{N}\frac{C\psi_n\phi_n X(0)}{j\omega-(\lambda_n-p\omega_0)}]}_{FO_1} + \underbrace{\sum_{j=1}^{M}[\sum_{i=1}^{N}\frac{C\psi_n\phi_n B_{Nj}}{j\omega-\lambda_i}]Q_j(\omega)}_{FO_2} \tag{2.44}$$

Close observation of forced $y_N(\omega)$ and natural $y_F(\omega)$ response of the system in equation (2.4) and (2.44) show that a sinusoidal noise term NO_3 is present if a lightly damped Natural oscillatory mode exists. This is used later in section 2.2.4 to develop a method for forced oscillation detection.

2.2.4.1 System matrices extraction using RSSSI Algorithm

In cases where only the output measurements are available the extended observability matrix Λ_i extracted in section 2.2.2. Then the C matrix of the system is is calculated after solving the following equation using a least square method,

$$\frac{\Lambda_{i-1}^{\dagger}.R_{i+1}}{H_y} = (\frac{A}{C}).\Lambda_I^{\dagger}.R_i \tag{2.45}$$

$$\Lambda_{i-1} = \underline{\Lambda_i} \tag{2.46}$$

where, $R_i = Y_f/(W_pU_f)$ is the orthogonal projection of future output on the subspace formed by past and future input and past output and $R_{i+1} = Y_f^-/(W_p^+U_f^-)$.

2.2.4.2 Time Varying Kalman Filtering for State Estimation

The system model A and C, identified in previous section is used in this section to estimate the state sequence $\hat{x_k}$ with the help of non steady state kalman filter.

$$\hat{x_k}^- = A\hat{x_{k-1}} + Bu_k \tag{2.47}$$

$$P_k^- = AP_{k-1}A^T + Q \tag{2.48}$$

$$K_k = \frac{P_k^- C^T}{CP_k^- C^T + R} \tag{2.49}$$

$$\hat{x_k} = \hat{x_k}^- + K_k(y_k - Cx_k^-) \tag{2.50}$$

$$P_k = (I - K_k C)P_k^- \tag{2.51}$$

2.2.4.3 Signal Segmentation

After calculating the Model of the underlying system A and C and the state sequence $\hat{x_k}$, these are used to estimate the response Y_k^{est} of the underlying dynamic system. The difference between the actual response Y_k and the estimated response Y_k^{est} is termed as Noise response Y_k^{Noise}.

$$Y_k^{ext} = C * (A * \hat{x_{k-1}}) \tag{2.52}$$

$$Y_k^{Noise} = Y_k - Y_k^{ext} \tag{2.53}$$

2.2.4.4 Proposed Oscillation Classification Method

As mentioned in section 2.2.1 one of the key characteristics of undamped natural oscillation is that the frequency of oscillation is present in the noise part of the response as well as the oscillating part of the signal too. The Power Spectral Density (PSD) is used to create an index that indicates the presence of natural or forced oscillations. The power spectral density of estimated signal(part NO_1 and part FO_1) and the noise signal (part NO_2+NO_3 and part FO_2) are given by,

$$P_{est} = \lim_{k->\infty} (\frac{1}{nk} \sum_{0}^{nk} |Y_{kext})|^2) \tag{2.54}$$

$$P_{Noise} = \lim_{k->\infty} (\frac{1}{nk} \sum_{0}^{nk} |Y_{kNoise})|^2) \tag{2.55}$$

$$P_{estN} = \frac{P_{est}}{max(P_{est})} \tag{2.56}$$

$$P_{NoiseN} = \frac{P_{Noise}}{max(P_{Noise})} \tag{2.57}$$

$$I_D(f) = P_{estN}(f) \star P_{NoiseN}(f) \tag{2.58}$$

$$I_D(f) = \begin{cases} 1, & \text{if the oscillation is natural} \\ < 1, & \text{if the oscillation is forced} \end{cases} \tag{2.59}$$

Algorithm 1 Recursive Stochastic Subspace Identification (RSSI)-Algorithm

1) Define identification parameters sampling frequency, window length, observed frequency limit and refresh rate.
while 1=1 **do**
a) Gather PMU measurements, and perform low pass filtering and down sampling
b) Form the block Hankel output matrix (5.12)
c) Perform orthogonal projection of future output Y_f on past output Y_p (5.14) and perform LQ factorization recursively using eqns. (2.16)-(2.20)
d) Calculate the projected matrix O (5.19)
e) Calculate the extended observability matrix Λ_i recursively using (2.28)-(2.38)
f) Calculate system state matrix A (2.40)
g) Calculate oscillation frequency and damping from (2.41)
end while

2.2.5 Implementation Methodology

Fig. 2.1 shows the overall flow chart of the proposed framework and Fig. 2.2 shows the implementation scheme of the proposed architecture in the power grid. For each power system area the PMU measurements are first aggregated through lo-

Algorithm 2 Recursive Combined Deterministic Stochastic Subspace Identification (RCDSSI)-Algorithm

1) Define identification parameters sampling frequency, window length, observed frequency limit and refresh rate.
while 1=1 **do**
a) Gather PMU measurements, and perform low pass filtering and down sampling

b) Form the block Hankel output matrix (5.12) and input matrix (5.14)
c) Perform oblique projection of future output Y_f on past output Y_p along the direction of past input U_p (5.18) and perform LQ factorization recursively using eqns. (2.16)-(2.20)
d) Calculate the projected matrix O (5.19)
e) Calculate the extended observability matrix Λ_i recursively using (2.28)-(2.38)

f) Calculate system state matrix A (2.40)
g) Calculate oscillation frequency and damping from (2.41)
end while

cal PDC. The lcal PDC data is then transferred to the control center PDC through communication channels. Depending on the communication medium and distance a propaghation delay of todayâs wide-area communication networks can be in the range of 6 ms to 1 s. Fiber optics latency for Bonneville Power Administration (BPA) system is considered to be less than 26 ms (66). Control center PDC gathers all the local PDC measurements and time aligns them. Then the PMU measurements are send to the Wide Area Monitoring System (WAMS) in the form of data packet over the ethernet network. The proposed algorithms are part of the WAMS. PMU data obtained from the power grid is first processed for missing data, outliers, detrending and down-sampling. The proposed framework is implemented and both the RCDSSI and RSSI algorithms are run according to the flow chart shown in Fig. 2.1. Parameters that control the performance of the algorithms such as window length, refresh rate, sampling frequency and forgetting factor are given as inputs. The algorithm work on blocks of data and window length represents the data length. Refresh rate is the part of window length that is updated when new data is available. Sampling frequency determines which frequencies are observable and can be extracted by the

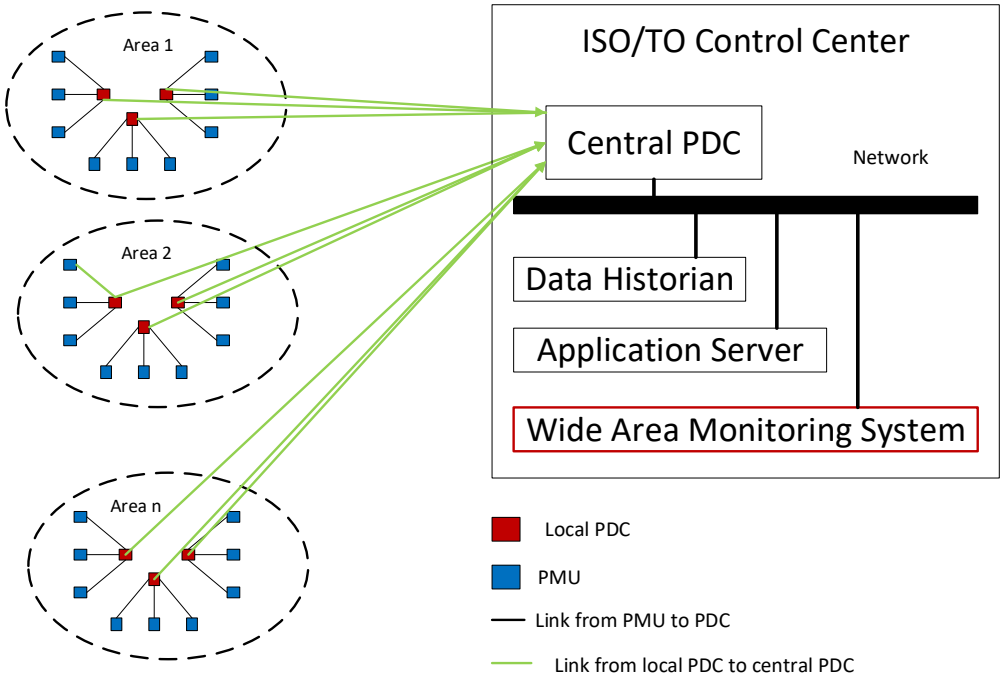

Figure 2.2: Wide area monitoring scheme.

algorithms and, forgetting factor controls the ability of the algorithms to track fast changes in system operating condition. Initial model orders are selected based on prior knowledge of the system and then model orders are calculated the dynamically as part of the algorithm mentioned in previous sections.This helps to track multiple modes if there is a change in operating condition.

2.3 An Illustrative Example

A single machine infinite bus system (SMIB) is shown in Fig. 3.1 to illustrate the functionalities of the integrated framework proposed in Fig. 2.1. For simplicity the machine is modelled as a classical second order model and the small signal analysis of the system shows oscillatory modes with 1.015 HZ frequency and 11.2%. A random Gaussian noise is added to the load to simulate an ambient condition. Fig. 2.4 shows the synthetic simulated frequency response as measured at Bus 2. 5 minute in the simulation a three phase fault is applied on Bus 2 for 10 cycles, on minute 10 a forced oscillation is introduced with 2 Hz frequency and on minute 15 a forced oscillation

is simulated with 1.03 Hz frequency to create a resonance scenario where the forced oscillation frequency is close to the system's natural oscillation frequency. The next subsections discuss the performance of proposed method for this different scenarios.

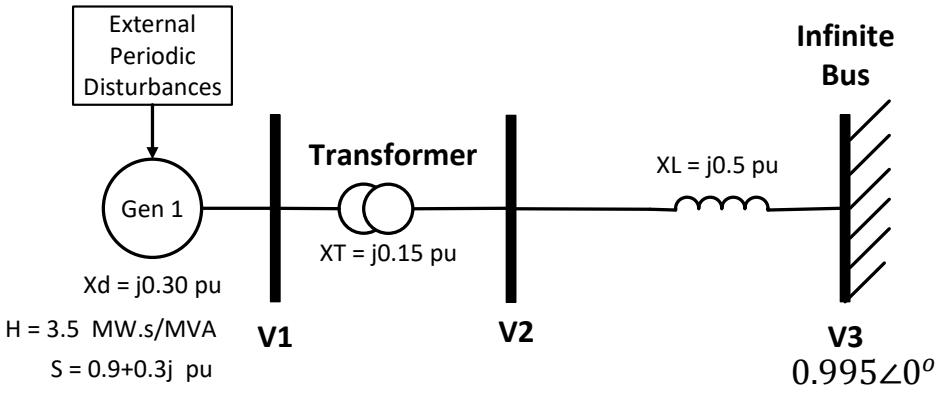

Figure 2.3: Single Machine Infinite Bus system.

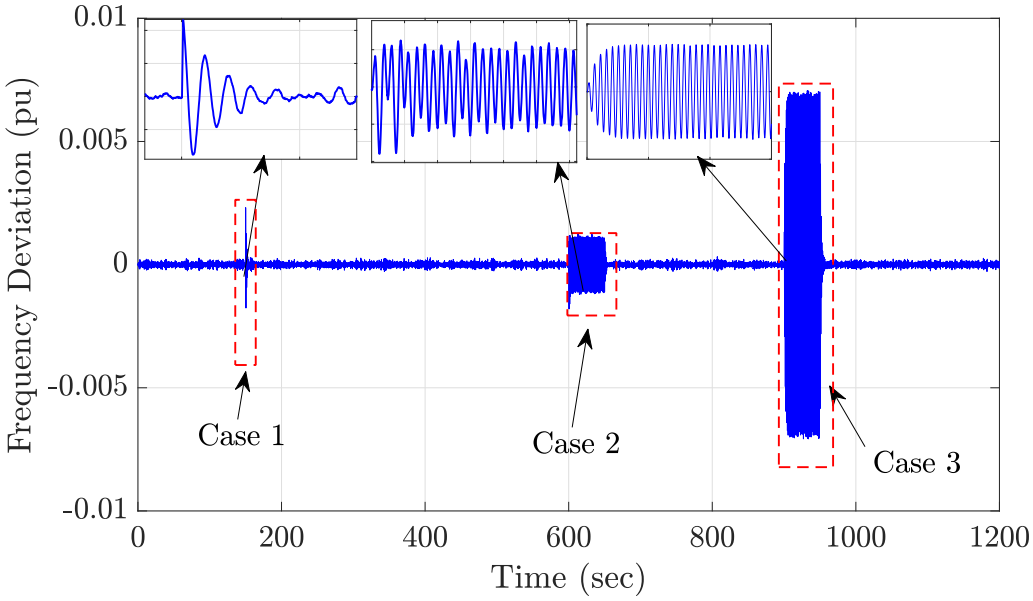

Figure 2.4: Frequency deviation signal used as a synthetic PMU measurement

2.3.1 Case 1: Estimation of Oscillatory Modes

This section shows the performance of proposed oscillation monitoring framework for both ringdown and ambient conditions. This case focuses on the time period

between $150s$ to $200s$ where a ringdown event occurs because of a three phase fault. The engine is initialised with a model order 2, window length 60 seconds and refresh rate 1 second. Fig. 2.5 shows the time varying model order and the selection criteria for the model order and the corresponding threshold. Close observation shows that for case 1 the deviation in Norm of estimated eigenvalues does not goes beyond the predefined threshold $\eta_{Threshold}$ and as a result the model order does not change. The synthetic PMU data is used and the method discussed in subsection 2.2.2 to obtain the projection matrix. Then the model order is selected and the modal information is extracted using the method described in subsection 2.2.3. After that method discussed in subsection 2.2.2 is used to implement the modal information extraction in a recursive manner to avoid computing QR decomposition and SVD at every time step. Figs. 2.6 and 2.7 shows the oscillation monitoring window for natural and forced oscillation respectively. From Fig. 2.6 it is clear that it is a natural oscillation with 1.01 Hz frequency and 11.2% damping which matches with the small signal stability analysis values. The standard deviation of the frequency and damping ratio estimates are 0.005% and 0.01% respectively.

2.3.2 Case 2: Mode Estimation and Detection in the Presence of Forced Oscillations

This case shows how the proposed method detects forced oscillation and can determine both natural and forced oscillation modes accurately. This case focuses on the period between 600 seconds to 650 seconds in fig. 2.4. As this is a block processing algorithm one block of data is shown in Fig. 2.8 to show how forced oscillation is detected by the proposed framework. The methods described in subsections 2.2.4.1, 2.2.4.2 and 2.2.4.3 are used to split the measurement signal into two parts oscillatory part Y^{est} and noisy part Y^{Noise}. Figs. 2.8a and 2.8c shows the estimated oscillatory part and the noisy part. Figs. 2.8b and 2.8d shows the amplitude spectrum of the extracted signals. The equations (2.54) are used to calculate the identification index

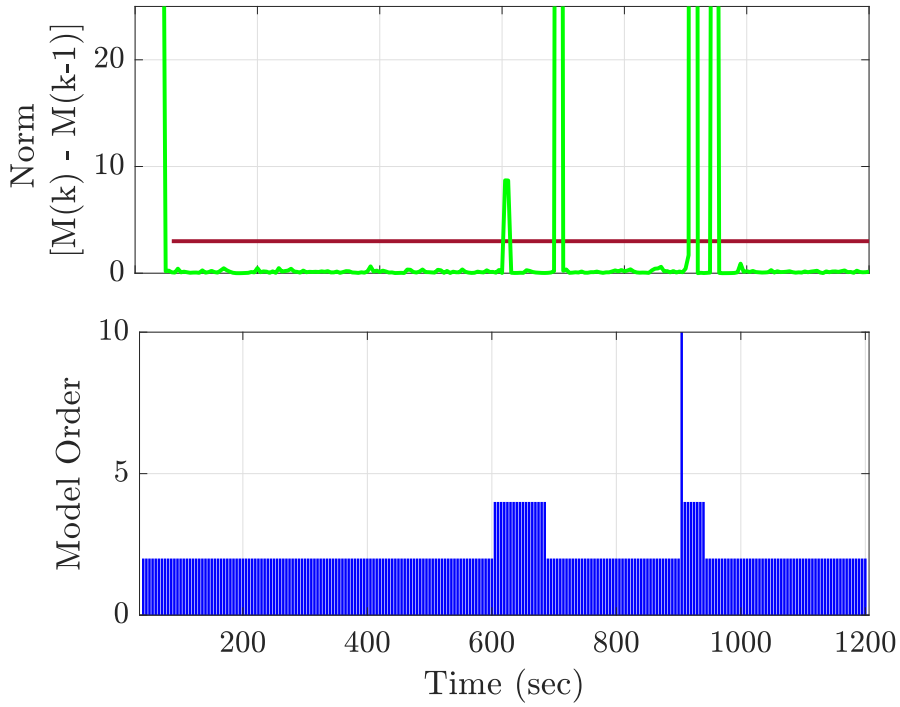

Figure 2.5: Time varying model order selection a) threshold for model order calculation and b) model order

$I_D(2)$ and it is 0.15. As the value of $I_D(2)$ is less than 1 it indicates that the oscillatory mode with 2 Hz frequency is a forced oscillation. Fig. 2.9 shows that as soon as forced oscillation is introduced it is detected in less than 2 seconds.

2.3.3 Case 3: Mode Estimation and Distinguishing Between Natural and Forced Oscillations During Resonance

This case shows the ability of the proposed method to estimate the natural modes frequency and damping accurately during resonance conditions. When forced oscillation frequency is close or superimposes on the natural oscillation frequency it creates a resonance condition (3). Although there have been a lot of methods proposed in the literature, most of these methods provide biased estimation of natural modes in the presence of forced oscillations (67). The proposed framework detects the presence of forced oscillation and uses the frequency of forced oscillation to create an input

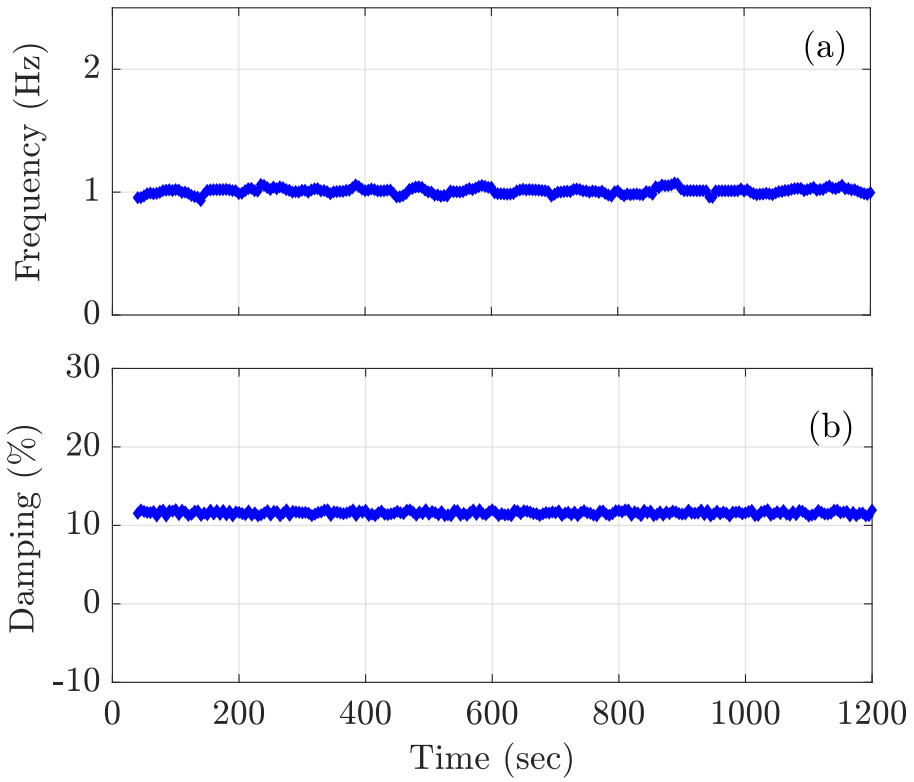

Figure 2.6: Natural oscillation monitor a) frequency and b) damping ratio

signal. Then the proposed RCDSSI framework is used to incorporate the input information and it helps to estimate the natural modes accurately. This case focuses on the signal between 900 seconds to 950 seconds in fig. 2.4. Fig. 2.7 shows that the proposed framework detects the forced oscillation around 900 seconds and also rightly estimates the associated damping. Fig. 2.6 shows that between 900 and 950 second the method gives a proper estimate of natural oscillation frequency and damping. This shows that the proposed method can simultaneously detect forced oscillations and can also estimate the natural oscillation accurately.

2.4 Simulation Results and Discussion

Fig. 2.11 shows the experimental setup used for the simulation cases. Power system models are run in Real Time Digital Simulators (RTDS). Then PMU measurements are broadcasted using software PMU in RTDS. One workstation is used as Phasor Data Concentrator (PDC) and the proposed algorithm is implemented along with the

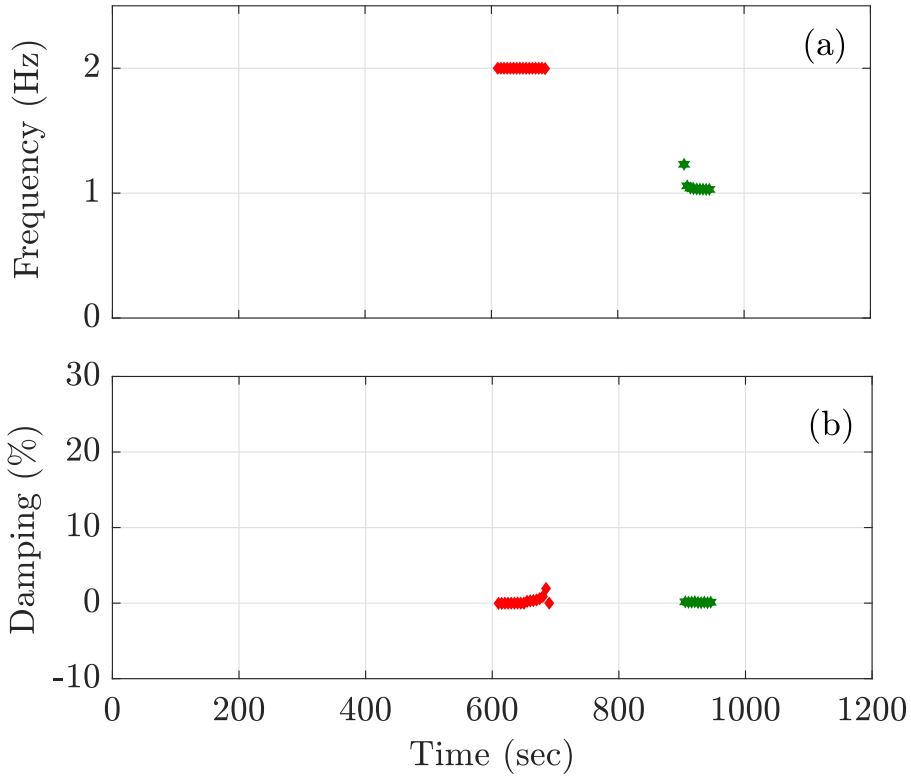

Figure 2.7: Forced oscillation monitor a) frequency and b) damping ratio

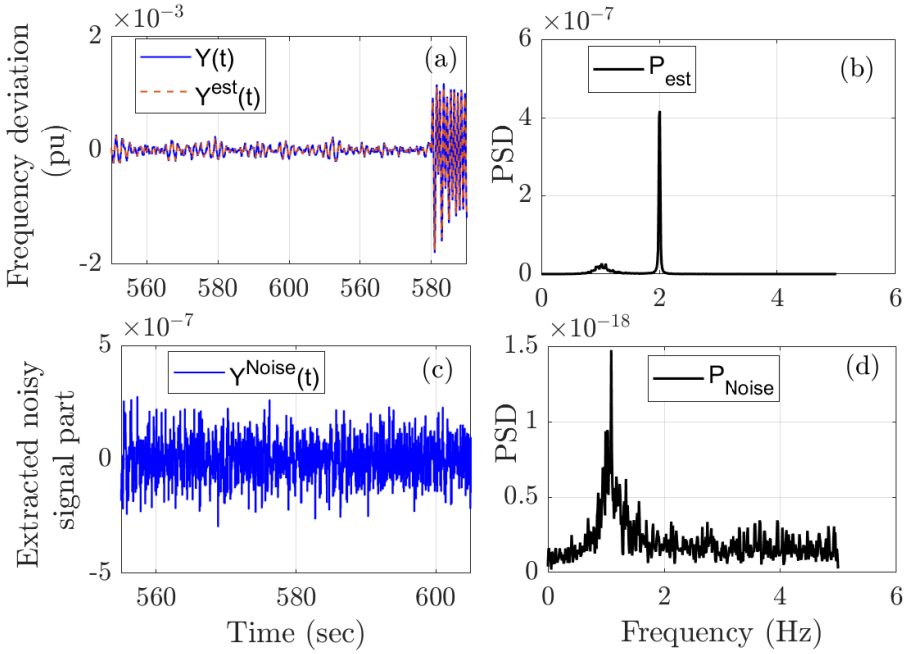

Figure 2.8: Time varying model order selection a) threshold for model order calculation and b) model order

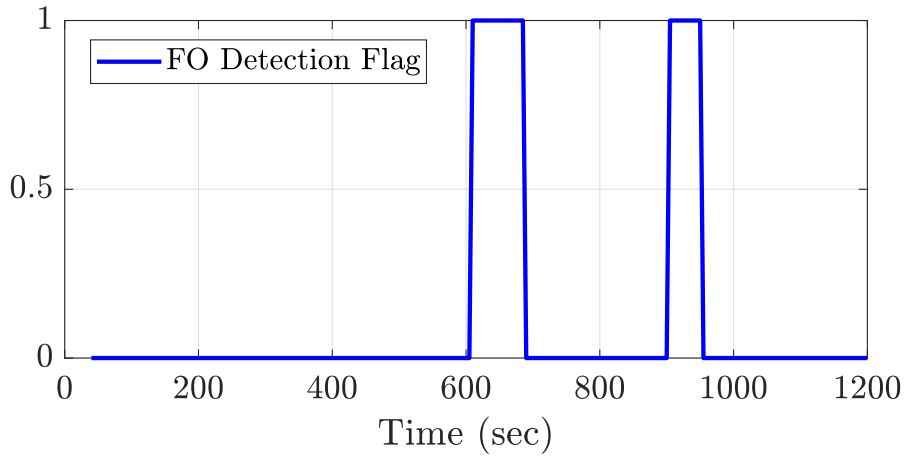

Figure 2.9: Forced oscillation detection flag

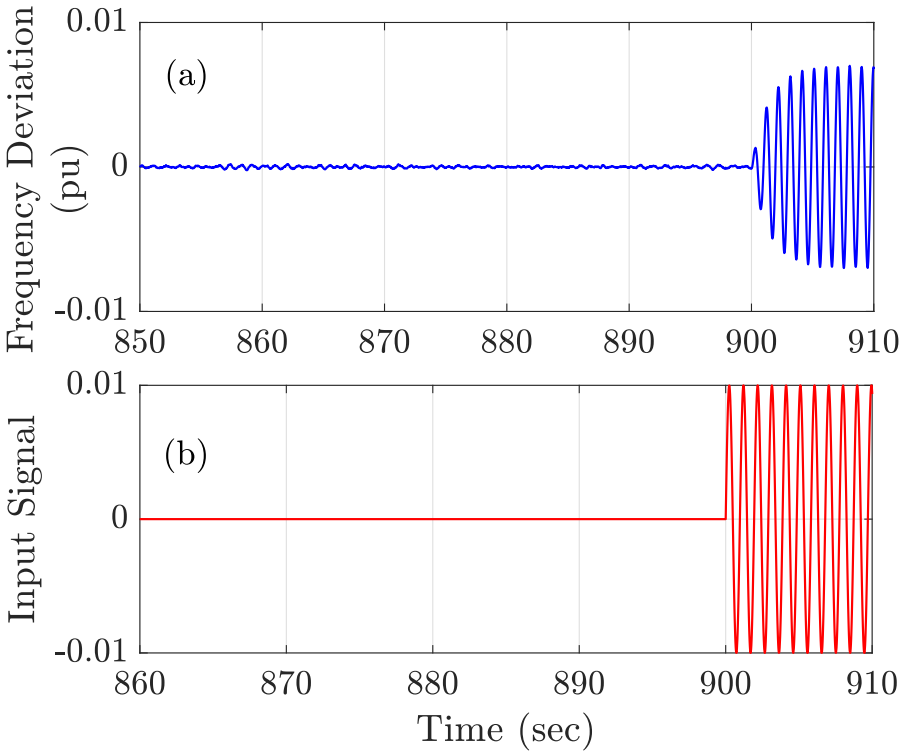

Figure 2.10: One window length input and output data used for the RCDSSI algorithm in Fig. 2.1

PDC. The output from the algorithm is send back to RTDS through GTNET using ethernet connection.

Two systems are used to study the performance of the proposed algorithm using RTDS. The first one is a two area power grid (9). This is a widely used system

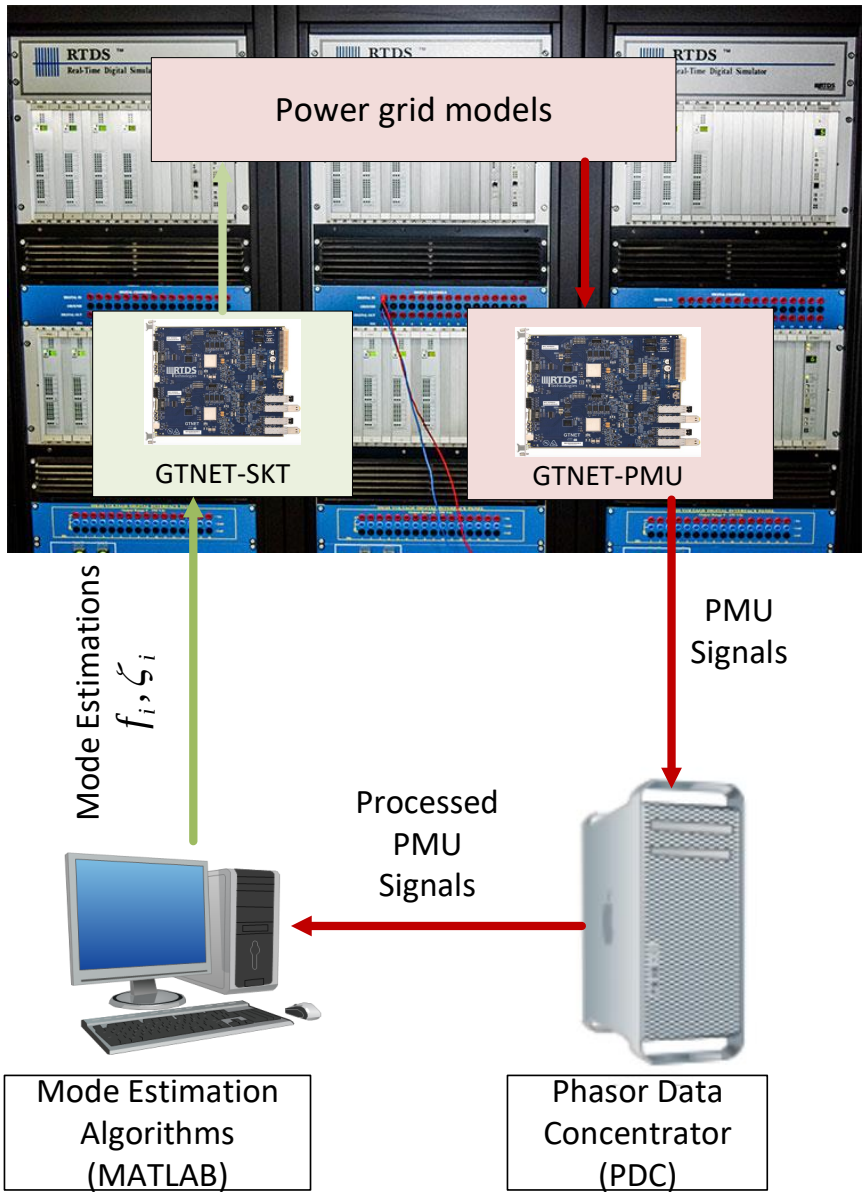

Figure 2.11: Experimental setup for the simulation results.

to study inter-area oscillation. The second system is IEEE 68 bus test system which represents the NETS-NYPS system model. This system is used to show the scalability of the proposed algorithm to perform well on large systems.

2.4.1 Two Area Test System

The two area power grid is shown in Fig. 6.3. The details are in (9).

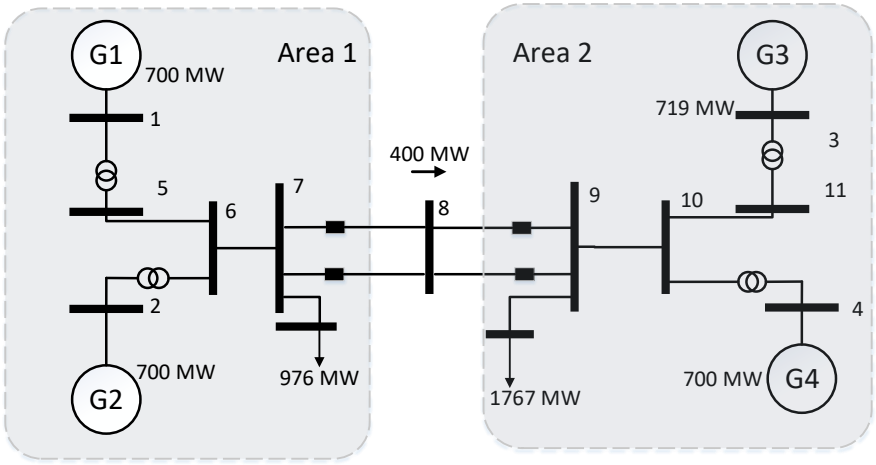

Figure 2.12: Two-area four-machine study system.

2.4.1.1 Case 1: Dynamic mode tracking

This case shows the dynamic capability of the proposed method to track low-frequency oscillations for varying operating conditions. Under the normal operating condition, a power system is always in motion because of random load variations occurring continuously in the system. These responses are typically termed as an ambient responses. The spectral analysis of ambient response shows that it can be approximated well by white noise (68). White noise with a magnitude of 1% of each rated load (active and reactive power) is added to the corresponding load to simulate ambient response, and there is no other disturbance in the system. In this case two operating conditions as shown in Table. 2.1 are studied to monitor only the inter-area oscillation frequencies. First operating condition represents a case where the inter-area mode is well damped. Small signal stability analysis (SSAT) shows that an inter-area oscillation has 0.6192 Hz frequency and 10.08% damping. Around 10 minutes into the simulation the power system stabilizers (PSS) malfunctions are simulated and the damping of the inter-area mode decreases. SSAT results show that inter-area mode of 0.6150 Hz has poor damping ratio of 0.74%. Table. 2.1 also shows that RSSI and RCDSSI gives similar estimate for both operating condition and the results are

similar to the RASSI method in literature (14).However, for first operating condition the mode is well damped, so the RCDSSI algorithm is not triggered for this operating condition. Fig. 2.13 shows that the proposed RCDSSI algorithm is initialized around 180 seconds and it estimates the inter-area mode for the first operating condition accurately. Around 600 seconds when the system operating condition changes, the algorithm could track the changing operating condition quickly. The spike between $900s$ and $1000s$ is because of the numerical calculation at the fault inception, but it converges very fast. The average computational time for RCDSSI algorithm on a Windows computer with 16 GB RAM and I-7 processor(4 GHz) is 0.2 second. Next case shows the advantage of taking the input characteristics into account in RCDSSI.

Table 2.1: Estimated modes for two area test system Case 1.

Operating Condition	Methods	Frequency (Hz)	Damping (%)
Operating Condition 1	SSAT	0.62	10.08
	RCDSSI	–	–
	RSSI	0.621	10.02
	RASSI (14)	0.621	10.03
Operating Condition 2	SSAT	0.6150	0.74
	RCDSSI	0.6149	0.75
	RSSI	0.6152	0.74
	RASSI (14)	0.6153	0.73

2.4.1.2 Case 2: : Mode estimation with forced oscillations

One of the major advantages of the proposed method is that it can estimate the electromechanical modes of the system accurately even in the presence of forced oscillation. This case shows the performance of the proposed algorithm for such a scenario and compares the results with existing methods (2). Two algorithms which are extensively used both in research and commercial applications for oscillation monitoring are modified for comparisons (Yule-Walker ARMA method and recursive stochastic subspace identification (RSSI)) (2). In this case, a forced oscillation of 0.62 Hz which

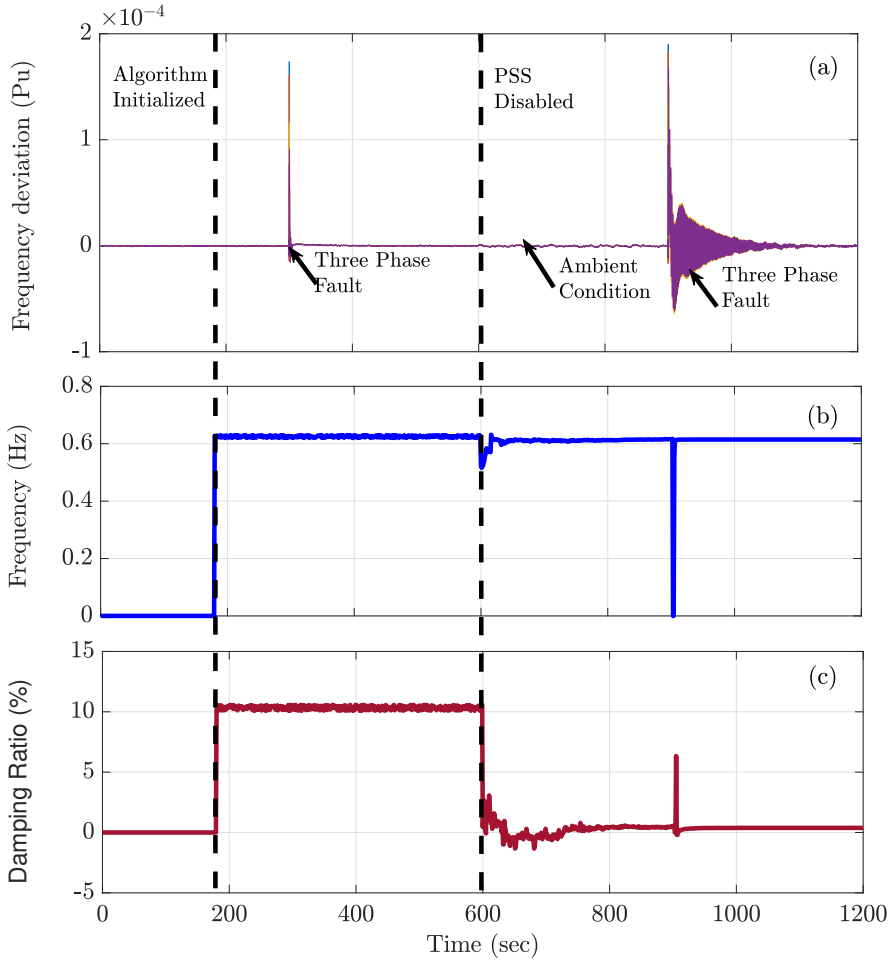

Figure 2.13: Case 1 a) Frequency deviation of the machine buses b) Frequency estimate and c) Damping ratio estimates..

coincides with the inter-area mode of the system is simulated by injecting a periodic disturbance at the load connected at Bus 7. Injecting periodic disturbances through load simulates the behavior of a cyclic load. For simplicity, only a single frequency sinusoidal signal is considered here as the main goal is to show the performance of mode estimation algorithms for such cases. Fig. 2.14a shows frequency deviation signal at bus 7, and it shows that at 10 minutes a forced oscillation is injected which stays for 5 minutes. Modified Yule-Walker method uses a predefined model order of ($n_a = 8$ and $n_m = 6$), and the estimated model order for both RSSI and RCDSSI are two, based on the criterion mentioned in (2.24) and (2.25). Fig. 2.14b shows that all three methods give an accurate estimate of the mode frequency. Fig. 2.14c

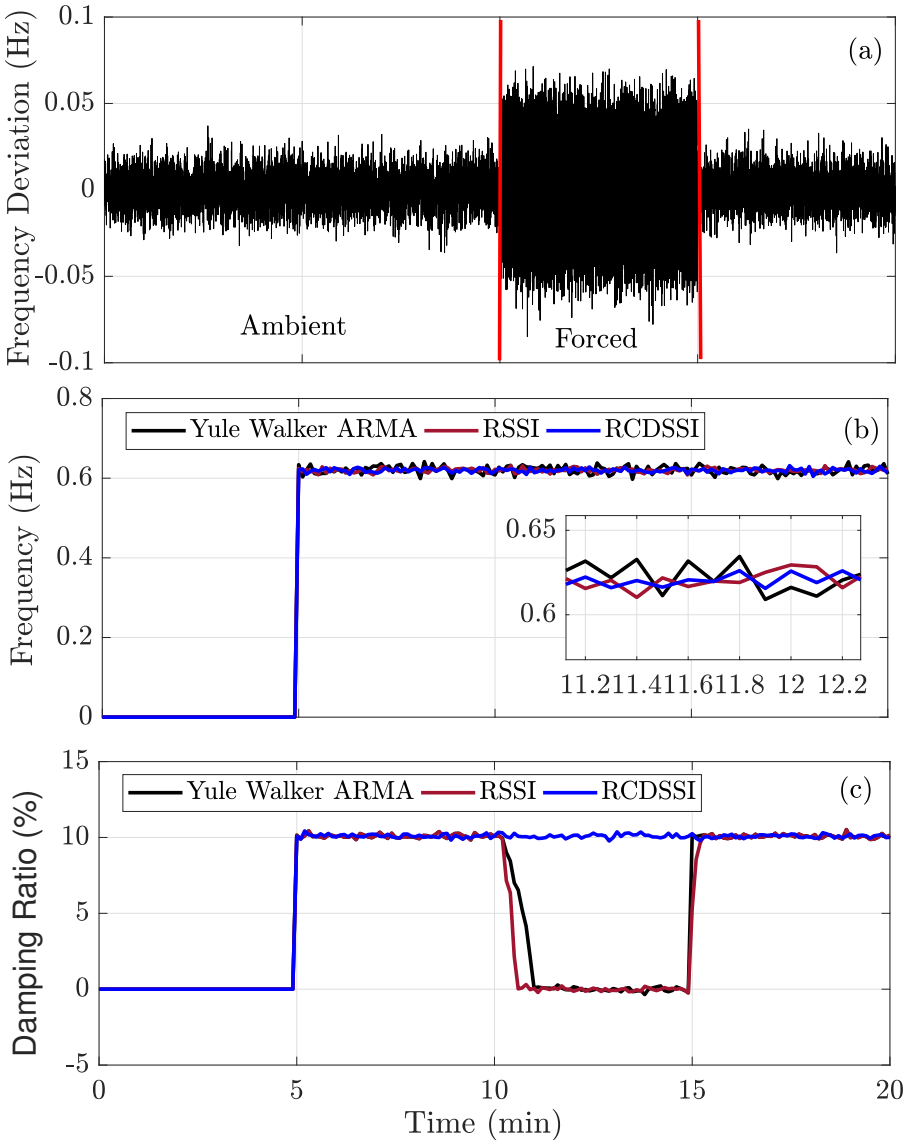

Figure 2.14: a) Time domain system frequency deviation signal b)comparison of mode frequency estimates and c) comparison of mode damping ratio estimates.

shows that the damping ratio estimate gets biased to the damping ratio of forced oscillation and shows approximately 0% damping when forced oscillation is present between 10 and 15 minutes. However, the proposed method (RCDSSI) can estimate the damping ratio of inter-area mode properly even in the presence of forced oscillations. This accurate estimation is important to help the power system operators take proper decision.

2.4.1.3 Case 3: Oscillation classification

This case shows how the proposed method can classify power system oscillations based on combined deterministic-stochastic subspace identification (RCDSSI) framework based on Fig. 2.1. In this case, the inter-area mode of the system has an oscillation frequency of $0.619Hz$ and a damping ratio of 0.74%. Moreover, a periodic signal of $0.625Hz$ frequency is added to the load connected at area 2 at Bus 9 to simulate the behavior of cyclic load as in case 2. Fig. 2.15 shows the power output of the load at bus 9 and the spectral characteristics of the load. It illustrates that the load is injecting a periodic disturbance of 0.62 Hz. It is noticed from Figs. 2.17a and 2.17b that the RCDSSI algorithm separates the effect of input and noise from the output and only extracts information related to inter-area mode of $0.62Hz$ and 0.74% damping. As mentioned before, the RSSI algorithm only separates the effect of noise from the output, so it picks up both input characteristics (in this case the periodic disturbance of the load) and inter-area mode characteristics. Figs. 2.17c and 2.17d shows that the RSSI algorithm identifies two modes one with $0.62HZ$ and 0.74% damping and another with $0.625HZ$ and 0% damping. Since both the oscillations are sustained oscillations, it is difficult for only the stochastic subspace identification algorithm to distinguish the type. However, comparing the estimate of RCDSSI and RSSI it can be concluded that since $0.62Hz$ mode is estimated in both method, so it is the inter-area mode of the system, and the $0.625Hz$ mode is a forced oscillation which is not an inherent characteristic of the system.

2.4.2 IEEE 68 Bus Test System

This case study presents how the proposed method works for a large scale power system where different modes are excited at different time. The tie lines in the 68 bus system are marked red in Fig. 3.13. The details of the power grid is in (10) so not discussed here.

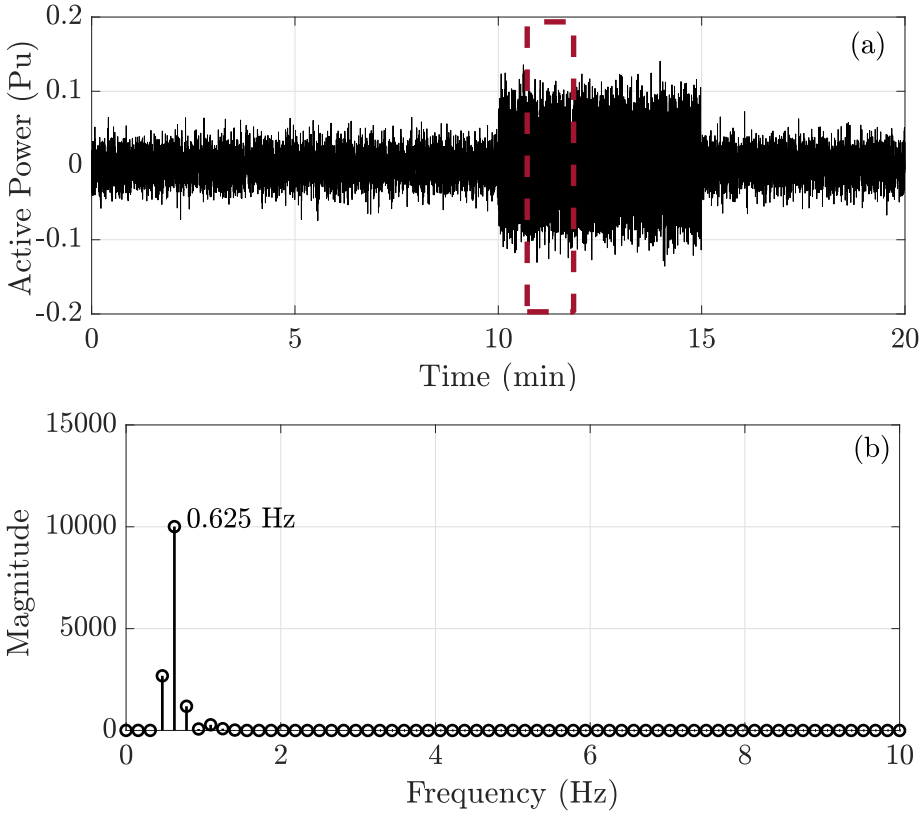

Figure 2.15: a)Load power output at bus 9 and b) frequency spectrum of the load power output for marked time length.

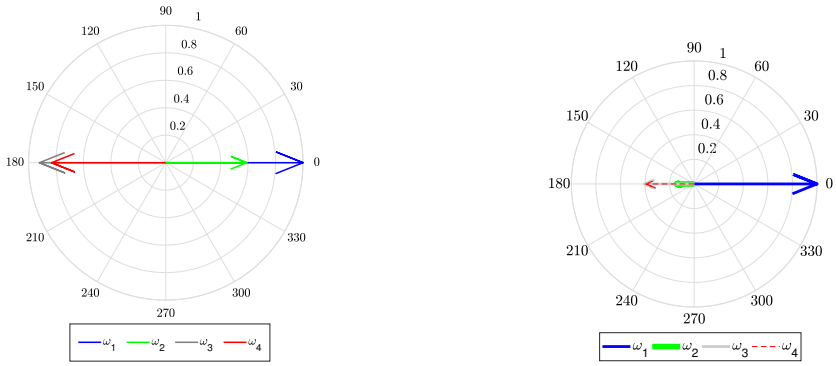

Figure 2.16: a) Oscillation shape for the 0.625Hz inter-area mode and b) Oscillation shape for the 0.62Hz inter-area mode

2.4.2.1 Case 1

This case study presents how the proposed method works for a large scale power system where different modes are excited at different time. The tie lines in the 68 bus system are marked red in Fig. 3.13. The details of the power grid is in (10) so

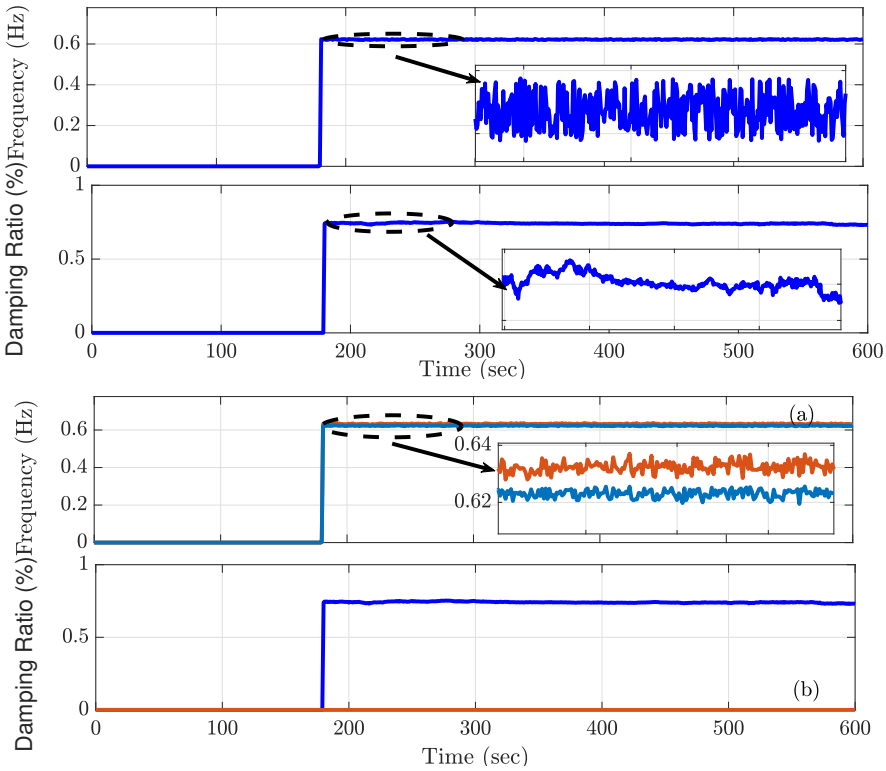

Figure 2.17: a) Time domain frequency signals b)frequency with RCDSSI c) damping ratio with RCDSSI d)frequency with RSSI and e) damping ratio RSSI.

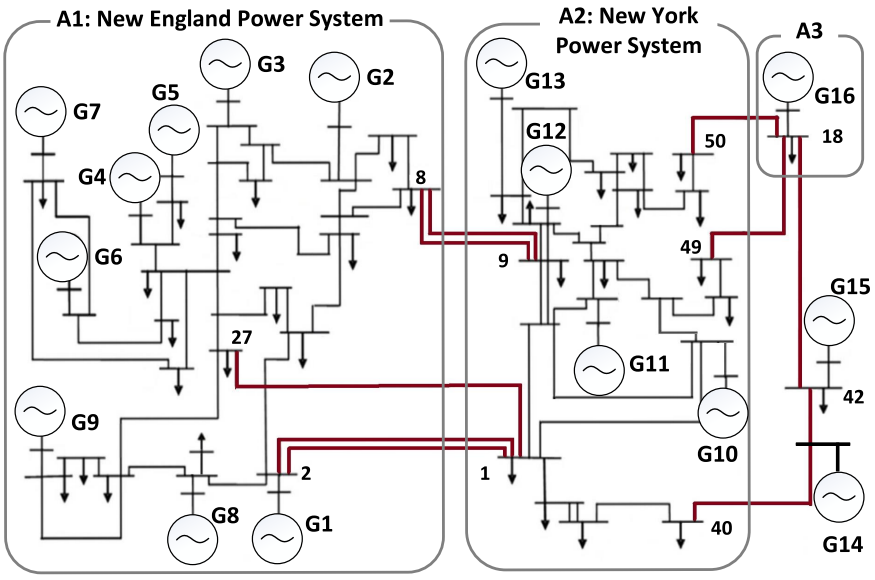

Figure 2.18: IEEE 68 Bus study system.

not discussed here. The simulation starts with operating condition one where a fault is applied near generator 14 to excite the $0.52Hz$ mode. A periodic disturbance is introduced at 10 min with a frequency of $0.526Hz$ which coincides with the system

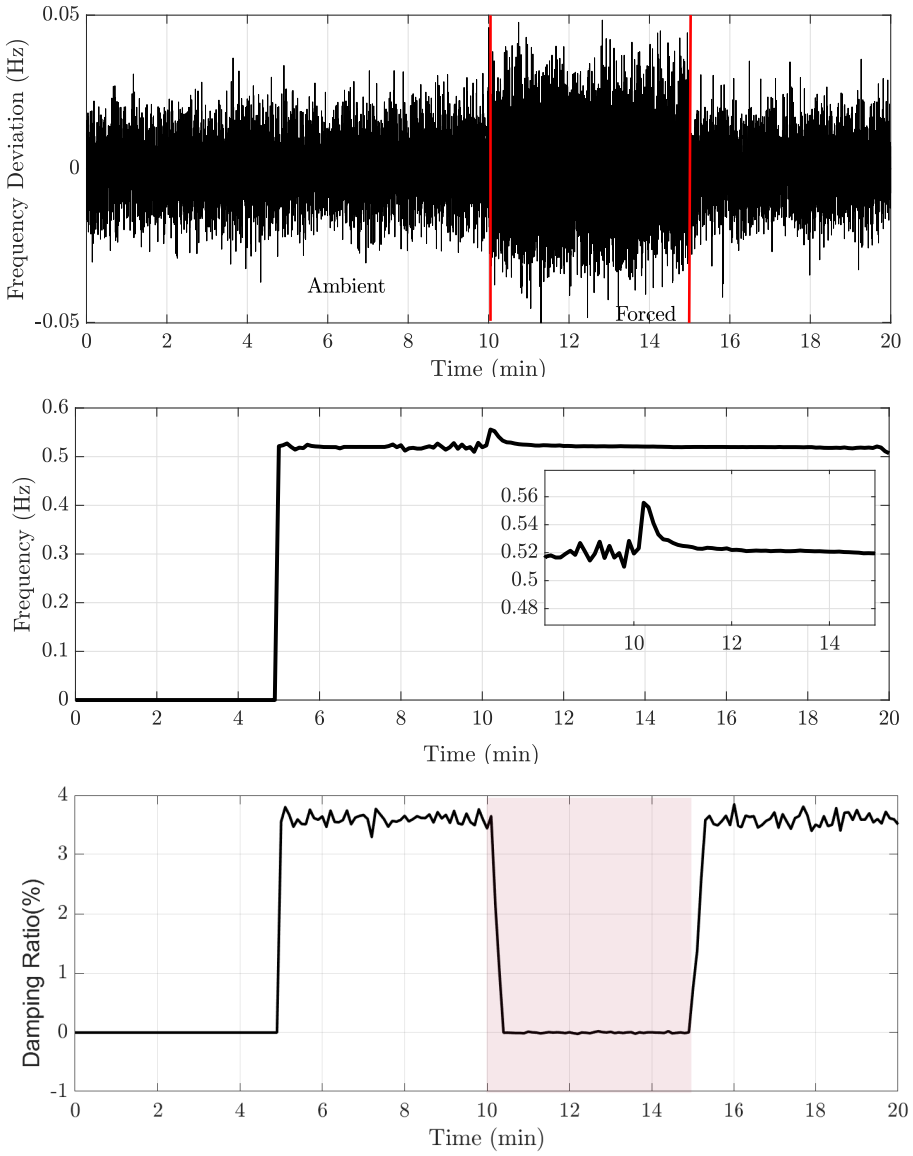

Figure 2.19: Yule Walker Method (2) a) Time domain ambient frequency deviation signal b) Frequency estimate and c) Damping ratio estimates.

inter-area frequency of $0.52Hz$ mode. Modified Yule-Walker method (2) with a pre-defined model order of ($n_a = 20$ and $n_m = 20$) is applied to estimate the inter-area -oscillatory mode frequency and damping. Fig. 2.19 shows that the Yule- Walker method fail to estimate the damping of target inter-area oscillatory mode accurately. Authors in (3) has claimed that the proposed Recursive Adaptive Subspace Identification (RASSI) method can estimate the electromechanical modes accurately in the presence of forced oscillations. Although this works well for an offline environ-

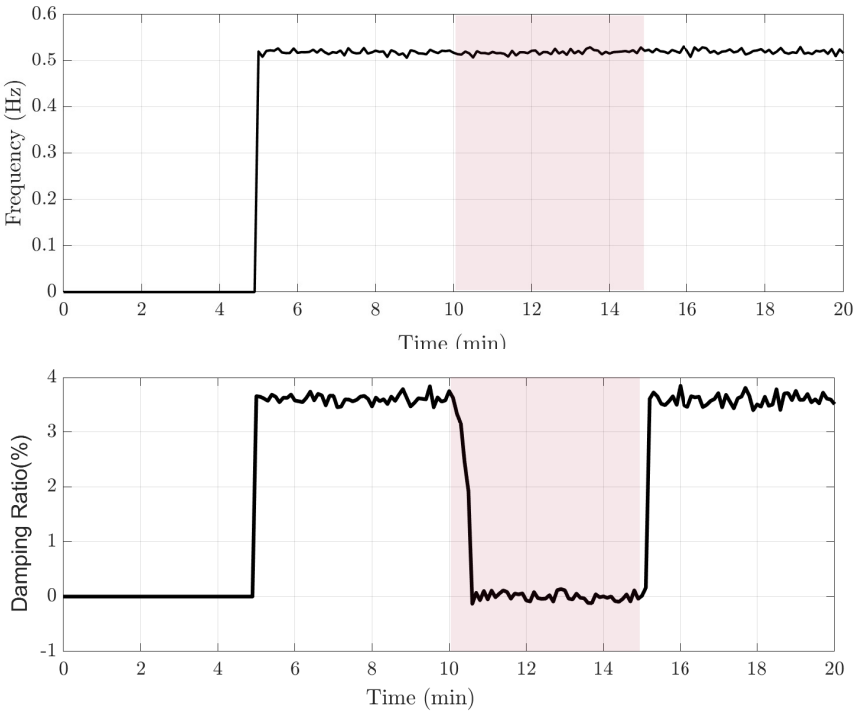

Figure 2.20: RASSI Method (3) a) Frequency estimate and b) Damping ratio estimates.

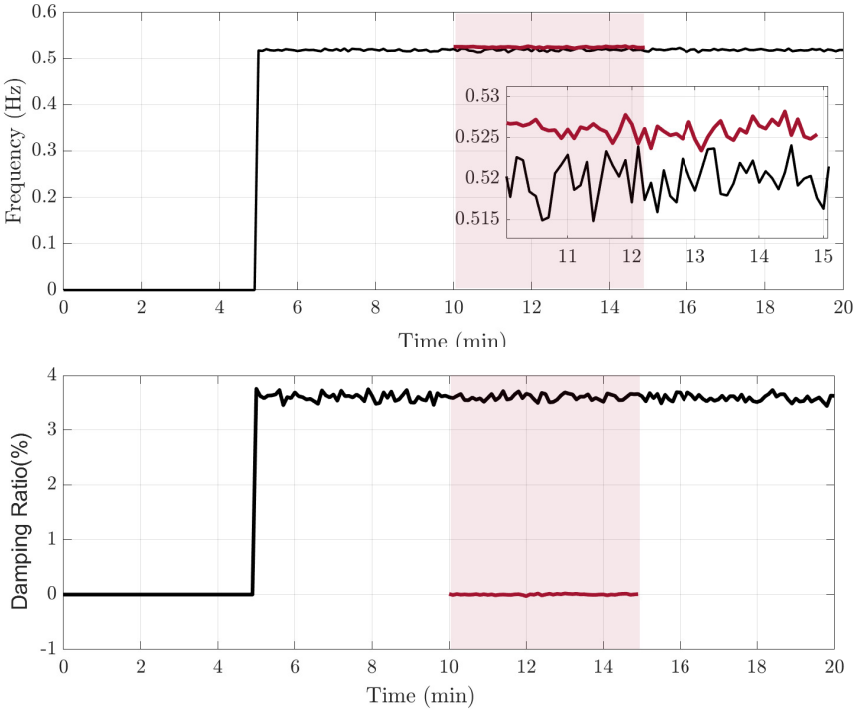

Figure 2.21: RASSI Method (3) when the order is known ahead of time a) Frequency estimate and b) Damping ratio estimates.

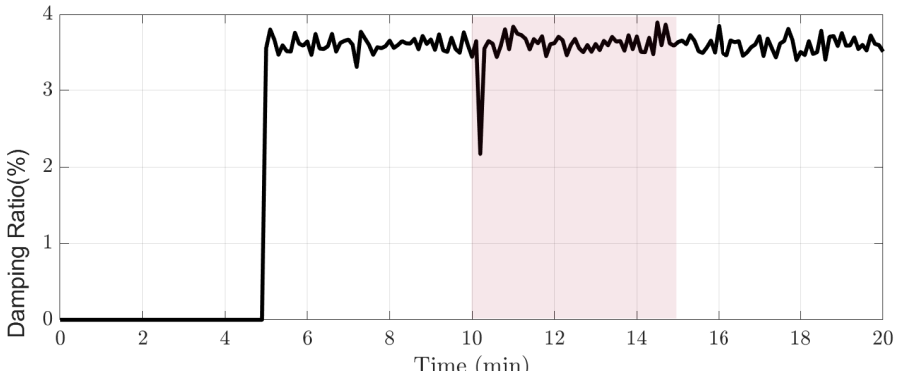

Figure 2.22: Proposed RCDSSI Method damping ratio estimate of target inter-area mode.

ment but in an online environment where the model order is selected automatically through SVD, this method can not always guarantee estimating the oscillatory modes accurately in the presence of forced oscillations, especially if the forced oscillation frequency is close to the inter-area oscillation frequency. Another popular method is transfer function based Yule-Walker method (2), which also gets biased in the presence of forced oscillation.This phenomenon is highlighted in Figs. 2.19 and 2.20. Fig. 2.20 shows that the subspace identification based method gets biased in the presence of forced oscillation and shows 0% damping. Similar issue exists for the Yule-Walker method as shown in Fig. 2.19. Fig. 2.21 shows that if the order of the system is known beforehand then only the RASSI method is able to estimate both natural and forced oscillatory modes accurately. But, in real-time operation that it is not feasible to know the number of modes seen in the measurement ahead of time. Fig. 2.22 shows that the proposed method gives an accurate estimate of inter-area mode damping for both low and high amplitude forced oscillations.

2.4.3 Experimental Results on Real PMU Measurements

In this section the proposed framework is tested for real time measurement data from ISO New-England system. Oscillations data for ISO New-England is available publicly (1). Several test cases from the library are tested. Fig. 2.23 shows the results for the case 1 from the library. In this case a system wide oscillation of 0.27

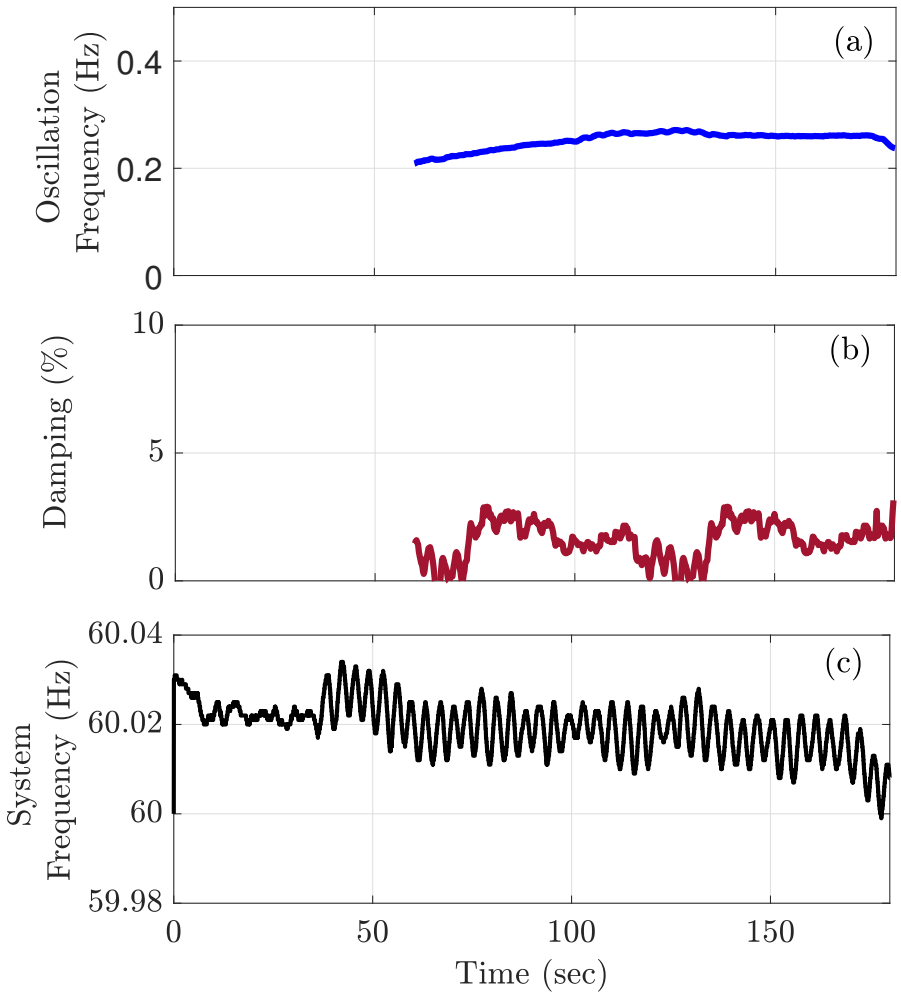

Figure 2.23: Results from ISO-NE real event data a) estimated oscillation frequency and b)estimated damping ratio and c) PMU measured system frequency signal

HZ frequency is seen in the system and the generator outside the NEW-England system is identified as the source of oscillation. Initialisation window length is 60s and refresh rate is 0.2s. Fig. 2.23c shows the frequency of the system at substation 5 and Fig. 2.23a shows the estimated frequency of around 0.27 Hz and Fig. 2.23b shows the estimated damping ratio indicating poor damping. Table 2.2 summarizes the results for other cases in the library and the proposed method provide an accurate estimate.

Table 2.2: Experimental Results on Actual PMU data (1)

Case	Modes	Methods	Frequency (Hz)	Damping (%)
Case 1	1	Actual	0.27	0.0
		RCDSSI	0.265	0.5
Case 2	1	Actual	0.25	0.0
		RCDSSI	0.252	0.3
Case 3	1	Actual	1.13	Growing
		RCDSSI	0.1.124	-0.13

2.4.4 Comparison with Existing State of the Art Methods

In this section the proposed method is compared with existing state of the art method from literature. As mentioned earlier authors in (14) has implemented recursive subspace identification based method for mode estimation. The proposed method is compared with the existing method for different scenarios run in the 68 bus test system and results are summarized in Table 2.3. Results show that the proposed RCDSSI framework gives similar mode estimations like the RASSI algorithm from literature. However, the RASSI algorithm can not change the model order dynamically and every time there is a change in model order the identification engine needs to be reinitialized. Because of this limitation RASSI fails to estimate the forced oscillation modes. On the contrary, the proposed framework is able to detect the type of oscillation as well as the oscillatory mode for all cases. Table 2.4 shows the average execution time of 300 seconds of window length used in the algorithm for both the methods. Both the method has similar execution time on a Intel core i7 processor with 3.7 GHz clock speed and 16 GB memory. Although the proposed method can dynamically track the changes in the model order and do not need to reinitialise the engine every-time the model order changes. Hence, the proposed method enhances the effectiveness of existing method by incorporating the ability of detecting oscillation type and estimating modes dynamically.

Table 2.3: Comparison of proposed method with existing methods.

Cases	Method	Mode	Oscillation Type	Frequency(Hz)		Damping Ratio(%)	
				Mean	Std Dev	Mean	Std Dev
Case 1	SSAT	Natural	-	0.52	0	3.621	0
	RCDSSI	Mode 1	NO	0.519	0.004	3.59	0.15
	RASSI(14)		-	0.517	0.006	3.63	0.27
Case 2	SSAT	Natural		0.52	0	3.621	0
	RCDSSI	Mode 1	NO	0.517	0.003	3.55	0.18
	RASSI(14)		-	0.518	0.005	3.58	0.26
	SSAT	Natural		0.591	0	9.625	-
	RCDSSI	Mode 2	NO	0.593	0.0035	9.88	0.82
	RASSI(14)		-	0.597	0.004	9.72	0.78
Case 3	SSAT	Natural	-	0.52	0	3.621	0
	RCDSSI	Mode 1	NO	0.515	0.005	3.60	0.17
	RASSI(14)		-	0.514	0.005	3.52	0.24
	SSAT	Natural	-	0.591	0	9.625	0
	RCDSSI	Mode 2	NO	0.592	0.002	9.71	0.76
	RASSI(14)		-	0.590	0.002	9.69	0.79
	SSAT	Forced	FO	0.8	0	0	0
	RCDSSI	Mode 1	FO	0.8	0.0025	0.001	0.0005
	RASSI(14)		-	-	-	-	-
Case 4	SSAT	Natural		0.52	0	3.621	0
	RCDSSI	Mode 1	NO	0.518	0.0025	3.59	0.16
	RASSI(14)		-	0.517	0.004	3.57	0.24
	SSAT	Forced	FO	0.526	0	0	0
	RCDSSI	Mode 2	FO	0.525	0.001	0.002	0.0.001
	RASSI(14)		-	-	-	-	-

Table 2.4: Computational Time for Different Cases.

Case	RCDSSI	RASSI(14)
Case 1	0.08 s	0.083 s
Case 2	0.085 s	0.086 s
Case 3	0.083 s	0.084 s
Case 4	0.079 s	0.080 s

2.5 Summary

The proposed combined deterministic and stochastic framework extends the the conventional SSI algorithm structure used widely in power system mode estimation, to take the effect of input on system response into account. It also applies subspace identification to detect the presence of forced oscillations. One portion of the results are published in the form of paper (69). Based on the results presented in the chapter it is noticed that the proposed framework can reliably estimate the modes of the system in an online environment. Moreover, The framework can also provide information about the type of oscillation, forced or natural. The proposed method enhances the capability of state-of-the-art and provide more accurate information about oscillation characteristics. One of thing that is noticed during the implementation that the computational time of the algorithm increases with the number of PMU measurements. A large number of signals significantly increases the computational time of the algorithm and hence can affect it's real-time implementation. To decrease the computational time a method is proposed in next chapter that reduces the number of signals used in the algorithm from the available PMU measurements.

CHAPTER 3: SUBSPACE IDENTIFICATION BASED OPTIMAL SIGNAL SELECTION FOR WIDE AREA MONITORING SYSTEM

In this chapter an approach for identifying and selecting optimum number of signals for monitoring power system oscillations is proposed. First, a formal method for ranking the signal based on their suitability for mode estimation is illustrated. The method considers both spatial and temporal characteristics of the synchrophasor signals and classifies the signals into strong and weak signals groups. Secondly, a method is shown for identifying optimum number of signals evolved from spectral clustering technique. This method takes into consideration of the affinity between two signals thus representing the characteristics of oscillation propagation. The main advantages of the proposed architecture is that a) such classifications can distinguish natural and forced oscillations typically observed in the Phasor Measurement Unit (PMU) measurements, b) such classification can identify the most suitable signals for oscillation mitigation, and c) the approach can find the closest signal to the oscillation source. The efficacy of the proposed method is validated using IEEE 68 bus and miniWECC 179 bus test systems and compared with the existing methods using IEEE 39 Bus test system.

3.1 Introduction

Recent widespread deployment of phasor measurement units (PMUs) have paved the way for a lot of new synchrophasor applications. One important synchrophasor application is the wide area measurement system (WAMS). WAMS enables the development of situational awareness tools which provides operators information about real-time power system stability and archives data which is used for post event analysis. One key indicator of power system stability is the oscillation modes and the associated damping. For reliable operation of the power system it is pivotal for all the modes to be well damped. Recent report from North American Electric Reliability Corporation (NERC) lists several oscillatory events observed

in Eastern,Western and ERCOT interconnections (19). Traditionally, such oscillatory behaviours related to small signal stability is studied using modal analysis of linearized power system models . But, post event analysis of August 10, 1996 blackout reveals significant mismatch between the oscillation characteristics predicted from modal analysis and the actual oscillations observed in the system (20). Several events like this has shown the need of measurement based mode estimation methods and has drawn significant attention from researchers in past couple of decades.

Several methods have been proposed by the researchers for mode estimation using PMU measurements. These methods have been categorized into three categories depending on the type of measured power system responses a) ringdown b) mode meter and c) probing (21). Ringdown response means the response of a the system following a large disturbance (e.g faults, line/generation trip etc) and mode estimation methods for ringdowns signals are prony, matrix pencil, eigensystem realization. Mode meter methods are yule-walker parameter estimation, least mean square method, stochastic subspace identification etc. These methods are used to extract modal information from ambient data which represents the continuous random load variations occurring the system (22).Probing response means the response of the system when a low intrinsic signal is injected to excite and estimate system modes (23).

Moreover, careful investigation of the PMU data has revealed not all the oscillations are related to system electromechanical modes which in sense means not an inherent characteristics of the system, rather are because of periodic external disturbance. Such oscillations are termed as forced oscillations and has been observed in power system across Europe (24), North America (25) etc. Irrespective of the oscillation type it is important to detect the oscillation frequency and damping for both ringdown and ambient conditions. One key characteristic of oscillations is that oscillatory behaviour is not observable in all available PMU signals and hence does not provide enough information to estimate the modes. For most of the available mode estimation methods only a handful of PMU signals which are selected based on prior knowledge of the system are used. Another limitation is most of the time such methods are tuned to monitor the damping of previously known inter-area modes.

Furthermore, concurrent use of large number of PMU signals affect the computational time of existing algorithms. Another important requirement which has been mentioned in NERC reliability guideline (25), is to determine to what extent an oscillation is affecting in the system. This helps to coordinate between multiple regional coordinators which in turn helps in taking proper corrective steps. All these consideration leads to the concept of finding optimal group of signals which are suitable for mode estimation as well as gives information about the spread of the oscillations.

Authors in (26) has used a two level estimation architecture to use large number of PMU signals and uses weighting factors to determine signal quality. Authors have shown that if an ISO running a mode estimation tool is not monitoring the right PMU signal then it might miss the oscillatory behaviour. A modal power contribution (MPC) index is proposed in (27) to rank signal according their suitability for mode estimation. But these methods are based on heuristic approach and does not provide any mathematical proof. Authors in (4) proposes an analytic expression for estimating the variance of damping ratio which uses only identified system parameters. But, the proposed method ranks signals for one oscillatory mode at a time and can not account for multiple modes simultaneously. In this paper a spectral clustering based grouping method is used which first characterizes each PMU signals in terms of identified subspaces. Then it calculates the affinity between the subspaces identified at each location to form a fully connected similarity graph. Spectral clustering is applied on the similarity graph to select the optimal group of signals. The proposed grouping selects optimal signals for ambient and ringdown condition which ensures less variance of the damping ratio. Additionally, such grouping reduces number of signals to be shared among different utilities or regional operators in the wake of system wide oscillations. The proposed method is applied on synthetic signals from IEEE 68 bus system for ambient conditions and then compared with other signal selection methods (4),(27) on IEEE 39 Bus test system. It is then applied on reduced WECC 179 bus system to show the advantage of proposed grouping in coordination between different utilities.

The main contributions of the proposed approach presented in this chapter are,

- A general method for ranking the synchrophasor signals for mode estimation methods

using both ringdown and ambient data.

- The developed method considers both the spatial and temporal characteristics of synchrophasor signals and takes that into account to classify the signals into strong and weak groups.

- The proposed methods can select optimal signals in the presence of multiple oscillation modes.

3.2 Problem Formulation and Proposed Methodology

In this section, mainly first power system propagation characteristics are described. Then subspace affinity is defined and a method for grouping signal based on spectral clustering is introduced. Also a method for reconstructing signal mode shape based on network sensitivities have been proposed.

3.2.1 Preliminaries

A power grid with network equation of a n machine system can be written as

$$\mathbf{I_G} = \mathbf{Y_R}\mathbf{E_G} \tag{3.1}$$

where $\mathbf{Y_R} \epsilon \mathbb{R}^{n \times n}$ is the reduced admittance matrix after eliminating all the nodes apart from generator nodes. $\mathbf{E_G}$ is the generator internal source voltage vector and $\mathbf{I_G}$ is the generator current injection vector. From (3.1), the ith row and jth column element of $\mathbf{Y_R}$ can be written as

$$y_{ij} = G_{ij} + jB_{ij} = \frac{1}{R_{ij} + jX_{ij}} \tag{3.2}$$

Let the electric power output(P_e) of ith machine is

$$P_{ei} = Real(\mathbf{E_i I_i}^*) = Real(\mathbf{E_i} \sum_{j=1}^{n} \mathbf{y_{ij} E_j^*}) \tag{3.3}$$

$$= \mathbf{E_i^2 G_{ii}} + \sum_{j=1, j\neq i}^{n} \mathbf{E_i E_j}[B_{ij} sin(\delta_i - \delta_j) + G_{ij} cos(\delta_i - \delta_j)] \tag{3.4}$$

$$= \mathbf{E_i^2 G_{ii}} + \sum_{j=1, j\neq i}^{n} [C_{ij} sin(\delta_i - \delta_j) + D_{ij} cos(\delta_i - \delta_j)] \tag{3.5}$$

$$\mathbf{C_{ij}} = \mathbf{E_i E_j B_{ij}}, \ \ \mathbf{D_{ij}} = \mathbf{E_i E_j G_{ij}} \tag{3.6}$$

Per-unitizing P_{ei} at an initial operating point ($\delta = \delta_i - \delta_j = \delta_0$),

$$T_{ei} = P_{ei} \tag{3.7}$$

where

$$\Delta T_{ei} = \frac{\partial T_{ei}}{\partial \delta} \Delta\delta = \sum_{j=1, j\neq i}^{n} [C_{ij} cos\delta_0 - D_{ij} sin\delta_0] \Delta\delta \tag{3.8}$$

Generalizing, for ith machine in a n machine system

$$\frac{d}{dt}(\Delta\omega_i) = \frac{(P_{mi} - P_{ei} - D_i \Delta\omega_i)}{2H_i} \tag{3.9}$$

$$\frac{d}{dt}(\delta_i) = \omega_0 \Delta\omega_i \tag{3.10}$$

For a n-machine classical (only considers the swing equation) model, the state-space repre-

sentation of the electromechanical model is

$$\begin{bmatrix} \Delta\dot{\omega} \\ \Delta\dot{\delta} \end{bmatrix} = \begin{bmatrix} \mathbf{MK_D} & \mathbf{MK_S} \\ \omega_\mathbf{0}.\mathbf{I_n} & \mathbf{0} \end{bmatrix} \begin{bmatrix} \Delta\omega \\ \Delta\delta \end{bmatrix} \tag{3.11}$$

$$\mathbf{\Delta}\dot{\omega} = \begin{bmatrix} \Delta\omega_1 & \cdots & \Delta\omega_n \end{bmatrix}$$

$$\mathbf{\Delta}\dot{\delta} = \begin{bmatrix} \Delta\delta_1 & \cdots & \Delta\delta_n \end{bmatrix}$$

$$\mathbf{M} = diag(\frac{1}{2H_i})$$

$$\mathbf{K_D} = diag(K_{Di})$$

$$\mathbf{K_S} = diag(K_{Sij})$$

$$K_{Sij} = \sum_{j=1, j\neq i}^{n} [C_{ij}cos\delta_{ij0} - D_{ij}sin\delta_{ij0}] \tag{3.12}$$

$$where\ i, j = 1, ..., n$$

The time response of the machine speed and rotor angle deviation of free state components can then be represented as

$$\mathbf{\Delta}\omega_\mathbf{i}(\mathbf{t}) = \sum_{i=1}^{n}\sum_{j=1}^{n} C_{ij}\psi_{ij}e^{\lambda_i t} \tag{3.13}$$

where

$$\mathbf{C_{ij}} = \sum_{i=1}^{n}\sum_{j=1}^{n} \psi_{ij}X_j(0) \tag{3.14}$$

3.2.2 Oscillation Propagation Characteristics

Once excited, oscillation propagation in the power grid (the magnitude and phase angle at different location) depends on several factors such as damping of the machine(s), network topology, operating conditions, stress level of the power system, disturbance severity etc. It can be stated that the an oscillation mode has different magnitude and phase at different

locations it varies with time.

A oscillation mode has different magnitude and phase at different location in power system and it varies with time. Let eigenvalue $\lambda_i = \sigma_i + j\omega_i$, where σ_i represents the damping and ω_i represent the oscillation frequency. Then the time domain response measured at different location given by (3.13) can be expanded as

$$\mathbf{\Delta}\omega_\mathbf{i}(\mathbf{t}) = \sum_{i=1}^{n}\sum_{j=1}^{n} |\phi_{ij}^M|\angle\phi_{ij}^A|C_{ij}^M|\angle C_{ij}^A e^{\sigma_i t} e^{j\omega_i t} \tag{3.15}$$

where

$$|\phi_{ij}^M|\angle\phi_{ij}^A = \frac{-K_{Sij}}{K_{Di} + \sqrt{(}K_{Di}^2 - 8H_i K_{Sij}\omega_0)}$$

and

$$|\psi_{ij}^M|\angle\phi_{ij}^A = \phi_{ij}^{-1} = f(K_{Sij}, K_{Di}) \tag{3.16}$$

With algebraic modifications

$$\mathbf{\Delta}\omega_\mathbf{i}(\mathbf{t}) = \sum_{i=1}^{n}\sum_{j=1}^{n} e^{\sigma_i t}[\underbrace{(acos(\omega t) - bsin(\omega t))}_{x} \tag{3.17}$$

$$+j\underbrace{(asin(\omega t) + Bcos(\omega t))}_{y}] \tag{3.18}$$

This can be summarized as

$$\mathbf{\Delta}\omega_\mathbf{i}(\mathbf{t}) = \sum_{i=1}^{n}\sum_{j=1}^{n} e^{\sigma_i t}|\sqrt{x^2+y^2}|\angle tan^{-1}\frac{y}{x} \tag{3.19}$$

From (3.18) it can be concluded that the magnitude and phase angle of the changes in the speed at different locations depends on y and x and specifically the value of a and b. Further, from (3.2.2) and (3.16, it is observed that the magnitude and angle increases if K_{sij} increases and decreases if K_{Di} increases. Also, it can be observed that for a fixed initial condition the value of k_{sij} increases if the susceptance (B_{ij}) of the network increases or

conductance (G_{ij}) of the network decreases. This two parameters are inversely proportional to the network impedance as shown in (5.35). Finally, this proofs that oscillation phase and magnitude varies at different locations in the power system.

For a simple two machine system the second order model of each machine can be represented as (3.20),

$$A = \begin{bmatrix} \Delta\dot{\omega} \\ \Delta\dot{\delta} \end{bmatrix} = \begin{bmatrix} \frac{K_{Di}}{2H_i} & \frac{MK_{Si}}{2H_i} \\ \omega_0 & 0 \end{bmatrix} \begin{bmatrix} \Delta\omega \\ \Delta\delta \end{bmatrix} \tag{3.20}$$

Singular value decomposition is performed on the matrix AA' to obtain the left orthonormal basis U_1 of the matrix as shown in (3.21)

$$W = AA' = \begin{bmatrix} \frac{K_{Di}^2+K_{Si}^2}{4H^2} & \frac{-K_{Di}\omega_0}{2H_i} \\ \frac{-K_{Di}w_0}{2H_i} & \omega_0^2 \end{bmatrix} \tag{3.21}$$

Eigenvalues of this matrix is calculated as,

$$\lambda_{1,2} = \frac{K_{\mathrm{Di}}^2 + 4\omega_0^2 H_i^2 + K_{\mathrm{si}}^2}{8H_i^2} \pm \frac{j\sqrt{\left(-K_{\mathrm{Di}}^2 - 4\omega_0^2 H_i^2 - K_{\mathrm{si}}^2\right)^2 - 16\omega_0^2 H_i^2 K_{\mathrm{si}}^2}}{8H_i^2} \tag{3.22}$$

The subspaces identified at different locations has different

3.2.3 Subspace Identification Method

Let us denote the PMU measurements obtained from a p bus power system at time t as $\mathbf{Y(t)}\epsilon\mathbb{R}^p$. The high dimensional PMU data recorded in power systems has a low rank property. This property has been used significantly to recover missing data (70), classifying events (63).The time series data of window length l at each PMU location can be expressed

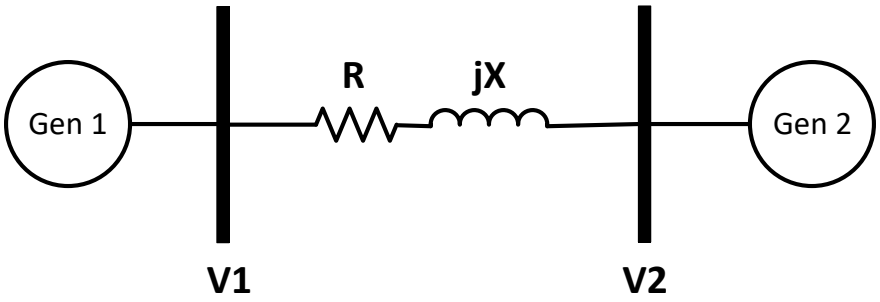

Figure 3.1: Two machine system.

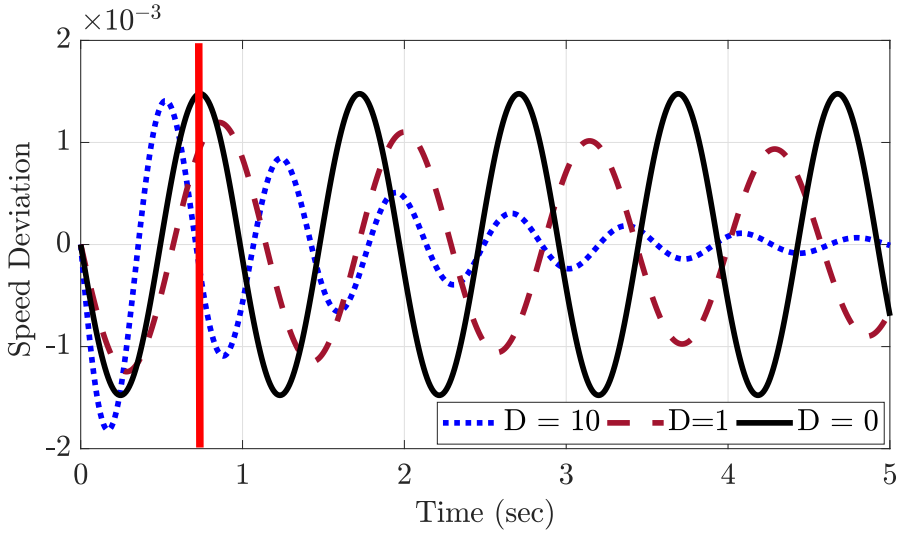

Figure 3.2: Effect of damping and network parameter on the machine speed deviation.

as,

$$\mathbf{Y_x(t)} = \underset{1\times 1}{\left[\begin{array}{cccc} y_x(t-l) & \dots & y_x(t-1) & y_x(t) \end{array}\right]^{\mathbf{T}}} \quad x = 1, 2, ..., p \tag{3.23}$$

These PMU time series data is used to identify the system dominant modes. From the measurement data first block Hankel matrices are formed as below,

$$\underset{2i\times j}{H_x} = \left[\frac{Y_{px}}{Y_{fx}}\right] = \frac{\begin{bmatrix} y_x(1) & \cdots & y_x(j) \\ y_x(2) & \cdots & y_x(j+1) \\ \vdots & \cdots & \vdots \\ y_x(i) & \cdots & y_x(j+i-1) \end{bmatrix}}{\begin{bmatrix} y_x(i+1) & \cdots & y_x(i+j) \\ y_x(i+2) & \cdots & y_x(i+j+1) \\ \vdots & \cdots & \vdots \\ y_x(2i) & \cdots & y_x(2i+j-1) \end{bmatrix}} \tag{3.24}$$

Based on Lemma 3.2.3, proper choice of number of rows(i) and the length of data(l) ensures that the identified subspace can capture the dominant modes present in the system.

if m is the maximum desired order of the identified system and l is the length of data vector, then number of block rows $i \geq m$ and number of column is $j = l - 2i + 1$ assuming that whole data length is used in the identification process.

Let m be the maximum number of order which needs to be identified(this can be known from prior knowledge of the system). Maximum possible rank of the identified system is $Rank(H_x) = min(i, j)$. Now the data length l is

$$l = \begin{cases} finite, & \text{if } Y_x\text{is from ringdown signal} \\ \text{inf}, & Y_x\text{is from ambient signal} \end{cases} \tag{3.25}$$

If the whole data length is used then $j >> i$. The order of identified system $n = Rank(H_x) = i$. So if the maximum identified system is m, then $m = n = i$. The number of block rows i needs to be at least m. If whole data length needs to be used then number of columns $j = l - 2i + 1$.

Subspaces are identified with the use of orthogonal projection. Projection is an important step to identify subspaces from ambient data where the signal to noise ratio is low. The

time series PMU data is divided into two data sequence matrix Y_{fx} and Y_{px}. The orthogonal projection of Y_{fx} on Y_{px} is given by,

$$\mathbf{Y_{fx}} = R_A Q^T, \ \mathbf{Y_{px}} = R_B Q^T \tag{3.26}$$

$$\begin{aligned} O_x = \mathbf{Y_{fx}}/\mathbf{Y_{px}} &= \phi_{[Y_{fx},Y_{px}]}.\phi_{[Y_{px},Y_{px}]}.\mathbf{Y_{px}} \\ &= [R_A Q^T Q R_B^T].[R_B Q^T Q R_B^T].R_B Q^T \\ &= R_A R_B^T.[R_B R_B^T]^{\dagger}.R_B Q^T \end{aligned} \tag{3.27}$$

The projected matrix (O_x) belongs to $\mathbb{R}^{i \times j}$. But the dominant number of modes in the PMU data is less than the matrix dimension. To find the number of dominant modes singular value decomposition (SVD) is performed on the matrices.

$$\begin{aligned} W_1 O_x W_2 = USV^T = [U_{P1} \quad U_{P2}] \begin{bmatrix} S_{P1} & 0 \\ 0 & S_{P2} \end{bmatrix} \begin{bmatrix} V_{P1}^T \\ V_{P2}^T \end{bmatrix} \\ = U_{P1} S_{P1} V_{P1}^T \end{aligned} \tag{3.28}$$

Where, W_1 and W_2 is a weighting matrix which determines the state space basis for the identified subspace and T is a similarity transformation.The extended observability matrix at each PMU location is given by,

$$\Gamma_x = W_1^{-1} U_{P1} S_{P1}^{\frac{1}{2}} T \tag{3.29}$$

To show that the physical interpretation of identified extended observability matrix, we use linear system analysis. Lets assume that the power system is linearized at an initial operating point .Overall power system response can be represented as a discrete time linear time invariant system

$$\mathbf{x_{k+1}} = \mathbf{Ax_k} + \mathbf{Bu_k} + \mathbf{w_k} \tag{3.30}$$

$$\mathbf{y_k} = \mathbf{Cx_k} + \mathbf{Du_k} + \mathbf{v_k}$$

where $u_k \epsilon R^m$ and where $y_k \epsilon R^l$ are the observations at the time k of respectively p inputs and q outputs, $w_k and v_k$ represents the process noise and measurement noise respectively. Let the order of matrix $\mathbf{A}$ be n. The expression for kth output is expressed as,

$$\begin{aligned} y(k) = CA^k x(k) + CA^{k-1}Bu(0) + ... + CBu(k-1) + Du(k) + \\ CA^{k-1}w(0) + ... + Cw(k-1) + v(k) \end{aligned} \tag{3.31}$$

With the assumption that the pair A, C is observable the extended observability matrix for a nth order system is given by,

$$\underset{np\times 1}{\begin{bmatrix} y(0) \\ y(1) \\ \cdots \\ y(n-1) \end{bmatrix}} = \underset{np\times n}{\begin{bmatrix} C \\ CA \\ \cdots \\ CA^{i-1} \end{bmatrix}} \times \mathbf{X(0)} \tag{3.32}$$

$$S_r = \underset{np\times n}{\begin{bmatrix} C & CA & \cdots & CA^{n-1} \end{bmatrix}^T} \tag{3.33}$$

From (3.37) it is clear that the extended observability matrix S_r is a function of system matrices A and C and it can be derived from data sequences.So, if the proper output signals are chosen then S_r contains information about the system modes.

Subspaces identified at different locations using the PMU data can capture the difference in phase and magnitude of oscillating signals as seen in the time domain response of PMU date.

$$\lambda_x = \frac{K_{\mathrm{Di}}^2 + 4\omega_0^2 H_i^2 + K_{\mathrm{si}}^2}{8H_i^2} \pm \frac{j\sqrt{\left(-K_{\mathrm{Di}}^2 - 4\omega_0^2 H_i^2 - K_{\mathrm{si}}^2\right)^2 - 16\omega_0^2 H_i^2 K_{\mathrm{si}}^2}}{8H_i^2} \tag{3.34}$$

$$\Gamma_x = U_1 S_1^{\frac{1}{2}} \ \textit{where, } U_1 \epsilon \mathbb{R}^{i \times n} \textit{ and } S_1 \epsilon \mathbb{R}^{n \times n} \tag{3.35}$$

Extended observability matrix is given by when $W_1 = I_{ij}$ and $T = I_{ij}$

3.2.4 Methods for Calculating the Affinity Between the Subspaces

There are several factors that needs consideration in dealing with PMU data. Subspace based methods deals with noise through the use of projections.

Then the system matrices A_z and C_z can be extracted from Γ_x using least square solutions (61).Then the modes of discrete A_z matrix is converted to continuous domain using (5.18). Thus the frequency and damping of dominant modes at each location can be calculated.

$$\lambda_i = \sigma_i + j\omega_i = \frac{1}{T_s} \log Eig(A_z) \tag{3.36}$$

The extracted subspaces is also used to calculate the oscillation shapes observed in the measured data. These oscillation shapes gives the relative magnitude and phase between different PMU signals which is also captured in the extended observability matrix Γ_x. The oscillation shapes are different from the typical mode shapes of linear systems. This oscillation shape depends on initial conditions, system mode shapes as well as the system inputs. Once the A matrix is identified the oscillation shape is calculated by calculating the right Eigenvector ϕ_i using eqn. (3.37), where λ_i represents the identified dominant modes .

$$A\phi_i = \lambda_i \phi_i \tag{3.37}$$

3.2.5 Method of Signal Clustering Based on Subspace Affinity

The intuition behind identifying the subspace is that the subspace captures the modal characteristics of system for a specific operating condition, disturbance magnitude and disturbance location. The affinity between the subspaces as seen at different location gives an indication of similarity between the signals at that locations. Let S_x be the subspace extracted from the extended observability matrix Γ_x, calculated at the previous section 3.2.3 for each PMU signal. The affinity between two subspaces S_i and S_j is calculated as,

$$A_{ij} = \sqrt{\frac{cos^2\theta_1 + cos^2\theta_2 + ... + cos^2\theta_n}{n}} \tag{3.38}$$

$$where, i, j = 1, 2, 3....n$$

$$\theta_n = acos(U_1(:,k)'.U_2(:,k)), \quad k = 1, 2, 3....n \tag{3.39}$$

Where, U_1 and U_2 represents the orthonormal bases of S_i and S_j respectively.v_n is the normalised length of the eigenvector. Ideally, $A_{ij} = 1$ if both the PMU signals i and j identifies same subspaces and $A_{ij} = 0$ if the PMU signals i and j identifies different independent subspaces.

A similarity matrix A is formed from the similarity graph shown in Figure. 4.4 and L is the laplacian matrix.

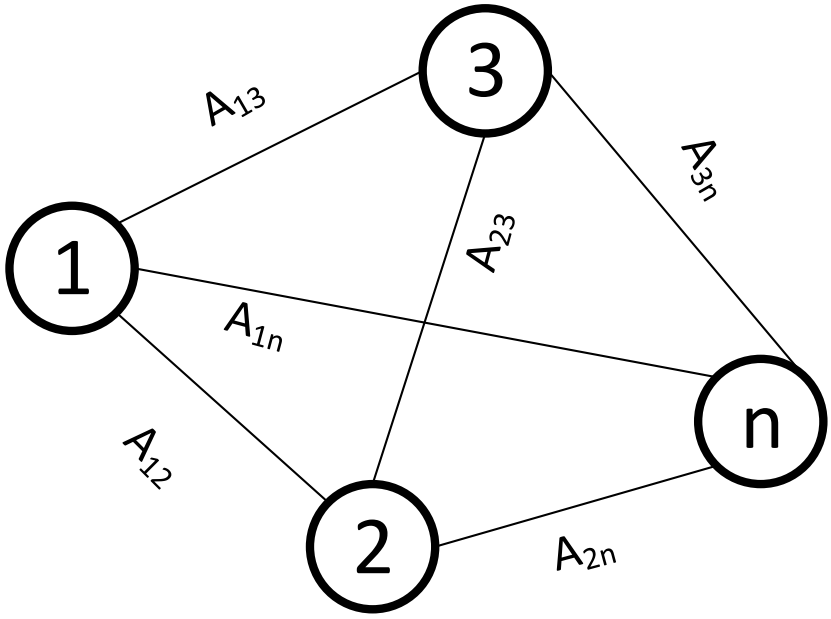

Figure 3.3: Similarity graph construction.

$$A = \begin{bmatrix} A_{11} & \cdots & A_{1n} \\ A_{21} & \cdots & A_{2n} \\ \vdots & \cdots & \vdots \\ A_{n1} & \cdots & A_{nn} \end{bmatrix} \tag{3.40}$$

$$D = \begin{bmatrix} \sum_{i=1}^{n} W(1,i) & \cdots & 0 \\ \vdots & \cdots & \vdots \\ 0 & \cdots & \sum_{i=1}^{n} W(n,i) \end{bmatrix} \tag{3.41}$$

$$L = D - A \tag{3.42}$$

As mentioned in the seminal work on graph partitioning by the authors of (71), one key criterion that ensures the optimal partitioning of graphs is the normalized cut between the graphs. Minimizing normalized cut (Ncut) ensures the similarity within a group is high and similarity between two different groups is low. If a graph $G = (V, E)$ is partitioned into two disjoint sets X and Y, then the Normalized cut is expressed as,

$$Ncut(X,Y) = \frac{cut(X,Y)}{assoc(X,V)} + \frac{cut(X,Y)}{assoc(Y,V)} \tag{3.43}$$

$$where, \tag{3.44}$$

$$cut(X,Y) = \sum_{a\epsilon X, b\epsilon Y} A(a,b) \tag{3.45}$$

$$assoc(X,V) = \sum_{a\epsilon X, c\epsilon V} A(a,c) \tag{3.46}$$

$$assoc(Y,V) = \sum_{b\epsilon Y, c\epsilon V} A(b,c) \tag{3.47}$$

$$Ncut(X,Y) = \frac{\sum_{(x_i=1,x_j=-1)} -A_{ij}x_ix_j}{\sum_{x_i=1}(\sum_{i=1}^{n}\sum_{j=1}^{n} A(i,j))} + \frac{\sum_{(x_i=-1,x_j=1)} -A_{ij}x_ix_j}{\sum_{x_i=-1}(\sum_{i=1}^{n}\sum_{j=1}^{n} A(i,j))} \tag{3.48}$$

where, $assoc(X,V)$ represents the total connections from nodes in group X to all the nodes in the graph and $assoc(Y,V)$.With the help of Rayleigh quotient (72) it is proven that finding the optimal solution of the problem of $min_x Ncut(x)$ is similar to finding the second smallest eigenvector of the laplacian matrix L (71) , where x is indicator vector and its value 1 means a node belongs to group X and -1 means a node belongs to group Y. However, there are some practical challenges in performing this clustering for practical data set. The indicator value is not always discrete in the second smallest eigenvector(V_{ss}) and can often take continuous values. It creates a problem of how to divide the values in the two groups to form to clusters. In this paper, an dynamic optimization is run to find the splitting point value C that minimizes $Ncut(x)$ value. The splitting values are chosen by taking m evenly spaced values between the minimum and maximum values of V_{ss}. The splitting value which gives minimum $Ncut(x)$ is chosen and groups are created.

3.2.5.1 Second Eigenvector Calculation

Let $S = S_1, S_2, ...S_p$ is a set of subspaces identified from p different PMU signal locations and $\lambda_\mathbf{i}$ where $i = 1, 2, ...n$ is the corresponding eigenvalues.The identified subspaces and eigenvalues at two different location i and j are expressed in terms of system parameters as,

$$u_{11}^{i} = -\frac{4\omega_0 K_{\mathrm{Di}} H_i}{\left(\sqrt{(-K_{\mathrm{Di}}^2 - 4\omega_0^2 H_i^2 - K_{\mathrm{si}}^2)^{\,2} - 16\omega_0^2 H_i^2 K_{\mathrm{si}}^2} - K_{\mathrm{Di}}^2 + 4\omega_0^2 H_i^2 - K_{\mathrm{si}}^2\right)} \tag{3.53}$$

$$\times \frac{1}{\sqrt{\frac{16\omega_0^2 K_{\mathrm{Di}}^2 H_i^2}{\left(\sqrt{\left(-K_{\mathrm{Di}}^2 - 4\omega_0^2 H_i^2 - K_{\mathrm{si}}^2\right)^2 - 16\omega_0^2 H_i^2 K_{\mathrm{si}}^2} - K_{\mathrm{Di}}^2 + 4\omega_0^2 H_i^2 - K_{\mathrm{si}}^2\right)^2} + 1}} \tag{3.54}$$

$$S_i = \begin{bmatrix} \frac{\mathbf{K_{Di}}}{\mathbf{2H_i}} & \frac{\mathbf{K_{Si}}}{\mathbf{2H_i}} \\ \omega_{\mathbf{0}}.\mathbf{I_n} & \mathbf{0} \end{bmatrix}; S_j = \begin{bmatrix} \frac{\mathbf{K_{Dj}}}{\mathbf{2H_j}} & \frac{\mathbf{K_{Sj}}}{\mathbf{2H_j}} \\ \omega_{\mathbf{0}}.\mathbf{I_n} & \mathbf{0} \end{bmatrix} \tag{3.49}$$

$$\lambda_i = \{\lambda_1^i, \lambda_2^i, ..., \lambda_n^i\}; \quad \lambda_j = \{\lambda_1^j, \lambda_2^j, ..., \lambda_n^j\} \tag{3.50}$$

if $(S_i, S_j)\epsilon S$ and S_i, S_j spans the same subspace, then affinity $A_{ij} - > 1$ which in turn means that the subspaces are closely related.The relation between the dominant modes of the identified subspaces is written as,

$$\lambda_{\mathbf{i}} = \lambda_{\mathbf{j}} + \gamma \tag{3.51}$$

$$\gamma = \begin{cases} \epsilon, \text{if affinity is close to 1} \\ M, \text{if affinity is close to 0} \end{cases}$$

The orthonormal basis for subspace S_i is given by ,

$$U_i = \begin{bmatrix} u_{11}^i & u_{12}^i \\ u_{21}^i & u_{22}^i \end{bmatrix} \tag{3.52}$$

$$u_{12}^{i} = -\frac{4\omega_0 K_{\mathrm{Di}} H_i}{\left(-\sqrt{(-K_{\mathrm{Di}}^2 - 4\omega_0^2 H_i^2 - K_{\mathrm{si}}^2)^{\,2} - 16\omega_0^2 H_i^2 K_{\mathrm{si}}^2} - K_{\mathrm{Di}}^2 + 4\omega_0^2 H_i^2 - K_{\mathrm{si}}^2\right)} \tag{3.55}$$

$$\frac{1}{\sqrt{\frac{16\omega_0^2 K_{\mathrm{Di}}^2 H_i^2}{\left(-\sqrt{\left(-K_{\mathrm{Di}}^2-4\omega_0^2 H_i^2-K_{\mathrm{si}}^2\right)^2-16\omega_0^2 H_i^2 K_{\mathrm{si}}^2}-K_{\mathrm{Di}}^2+4\omega_0^2 H_i^2-K_{\mathrm{si}}^2\right)^2}+1}} \tag{3.56}$$

$$u_{21}^{i} = \frac{1}{\sqrt{\frac{16H_i^2\omega_0^2 K_{Di}^2}{\left(+\sqrt{\left(-K_{Di}^2-4H_i^2\omega_0^2-K_{si}^2\right)^2-16H_i^2\omega_0^2 K_{si}^2}-K_{Di}^2+4H_i^2\omega_0^2-K_{Si}^2\right)^2}+1}} \tag{3.57}$$

$$u_{22}^{i} = \frac{1}{\sqrt{\frac{16H_i^2\omega_0^2 K_{Di}^2}{\left(-\sqrt{\left(-K_{Di}^2-4H_i^2\omega_0^2-K_{si}^2\right)^2-16H_i^2\omega_0^2 K_{si}^2}-K_{Di}^2+4H_i^2\omega_0^2-K_{Si}^2\right)^2}+1}} \tag{3.58}$$

Similarly, the orthonormal basis for subspace S_j is,

$$U_j = \begin{bmatrix} u_{11}^{j} & u_{12}^{j} \\ u_{21}^{j} & u_{22}^{j} \end{bmatrix} \tag{3.59}$$

The affinity A_{ij} between subspace S_i and S_j is calculated as,

$$A_{ij} = \frac{\sum_{i=1}^{n}\{cos^{-1}(U_{1i}^{T}U_{1j})\}}{n} \tag{3.60}$$

Without losing generality, the affinity matrix A from eqn. (3.40) is calculated for subspaces S_i and S_j as,

$$A_{ij} = \begin{bmatrix} A_{ii} & A_{ij} \\ A_{ji} & A_{jj} \end{bmatrix} \tag{3.61}$$

$$D_{ij} = \begin{bmatrix} A_{ii} + A_{ij} & 0 \\ 0 & A_{jj} + A_{ji} \end{bmatrix} \tag{3.62}$$

$$L_{ij} = \begin{bmatrix} (A_{ii} + A_{ij}) - A_{ii} & -A_{ij} \\ -A_{ji} & (A_{jj} + A_{ji}) - A_{jj} \end{bmatrix} \tag{3.63}$$

Eigenvalues and eigenvectors of the laplacian matrix L_{ij} is given by eqn. (3.64). L_{ij} is a symmetric positive semi-definite matrix which means all the eigenvalues are non-negative.

$$\lambda_1 = 0; \lambda_2 = \frac{1}{A_{ij} + A_{ji}} = \frac{1}{2A_{ij}}; A_{ij} = A_{ji} \tag{3.64}$$

The corresponding eigenvector is given by,

$$A_{ij} = \begin{bmatrix} 0.707 & \frac{2A_{\mathrm{ij}}^2 - 1}{\sqrt{-\frac{4}{A_{\mathrm{ij}}^2} + \frac{1}{A_{\mathrm{ij}}^4} + 8 A_{\mathrm{ij}}^2}} \\ 0.707 & \frac{2}{\sqrt{-\frac{4}{A_{\mathrm{ij}}^2} + \frac{1}{A_{\mathrm{ij}}^4} + 8}} \end{bmatrix} \tag{3.65}$$

3.2.6 Generation of Unobserved Network Variables

Power system has a limited number of PMU installed throughout the system. So, all the network variables associated with all the buses are not observable from the PMU measurements. So, there can be instances when the bus where a particular oscillation frequency is most prominent do not have a PMU located at it's location. This creates a need for a method that can help generating the network variables at different buses with PMU measurements from other buses. Authors in (73) has proposed a method for tracking the dominant oscillation path based on network sensitivities. In this work, the concept is used and only voltage sensitivities are used to find oscillation shape at unobserved PMU locations. Figure 4.1

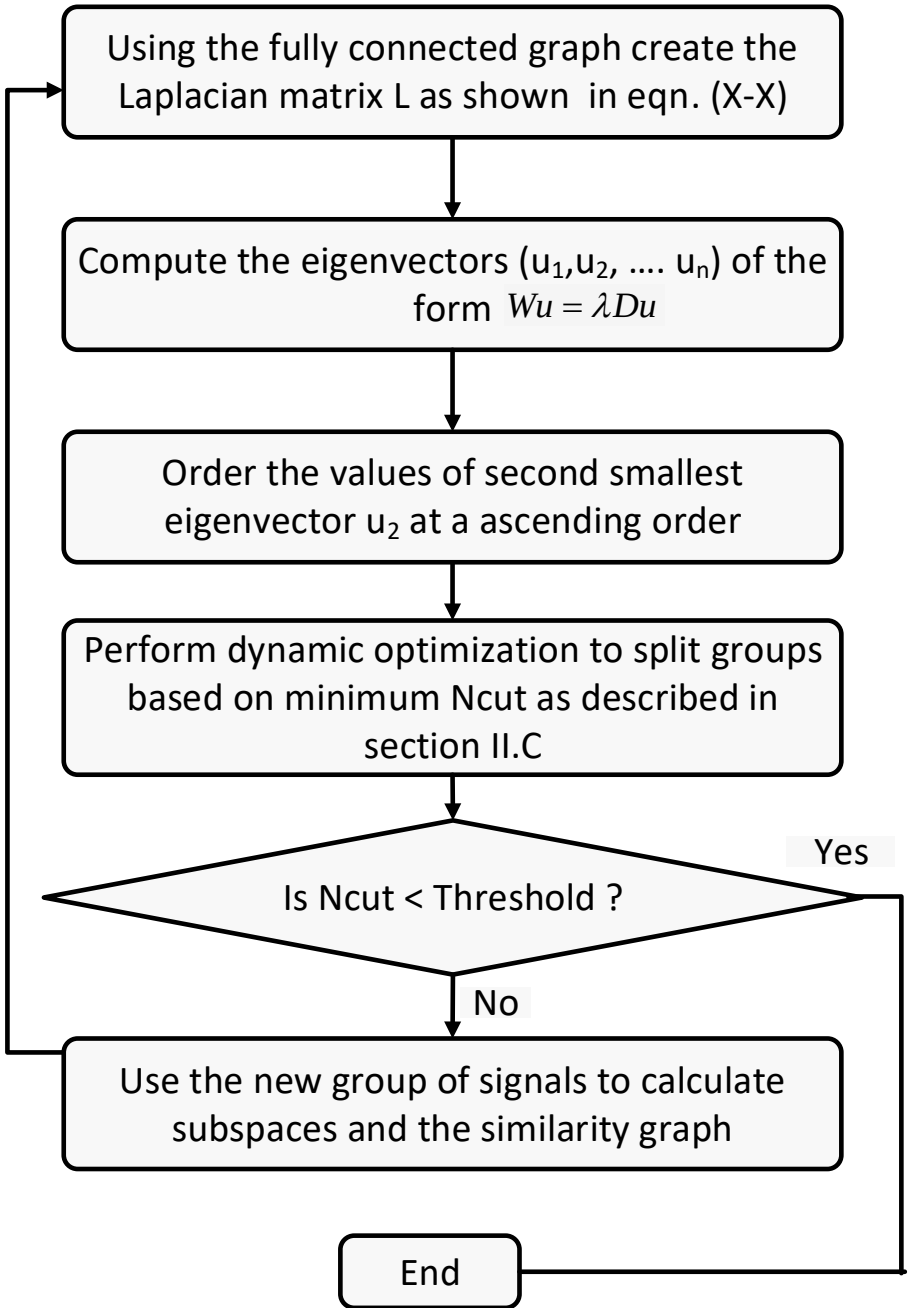

Figure 3.4: Flow chart for spectral clustering.

shows the n bus power system network with additional N bus for machine internal voltages. Loads are modeled as constant impedance and are added to the admittance matrix.So, current injections at all other nodes other than the generator nodes are zero. The node voltage equations for the network can be expanded as,

$$\begin{bmatrix} 0 \\ \mathbf{I_N} \end{bmatrix} = \begin{bmatrix} \mathbf{Y_{nn}} & \mathbf{Y_{nN}} \\ \mathbf{Y_{nN}^T} & \mathbf{Y_{NN}} \end{bmatrix} \begin{bmatrix} \mathbf{V_n} \\ \mathbf{E_n} \end{bmatrix} \tag{3.66}$$

$$\mathbf{V_n} = -\mathbf{Y_{nn}^{-1}} \mathbf{Y_{nN}} \mathbf{E_N} \tag{3.67}$$

Where, $\mathbf{I_N}$ denotes generator current injections, $\mathbf{E_N}$ refers to the generator internal voltages and $\mathbf{V_n}$ represents bus voltages. Equation (3.67) represents the bus voltages as a function of internal voltages and $-\mathbf{Y_{nn}^{-1}} \mathbf{Y_{nN}}$ depends on the network parameters.The generalised expression for bus voltage V_i can be written as,

$$\mathbf{V_i} = \sum_{j=1}^{N} \alpha_{ij} \mathbf{E_j}; \alpha = -\mathbf{Y_{nn}^{-1}} \mathbf{Y_{nN}} = \eta \angle \gamma \tag{3.68}$$

As shown in (3.68) the bus voltage depends on the magnitude and angle of machine internal voltage. A change in machine internal voltages causes the bus voltages to change. A generalised expression for network sensitivities have been derived in (73). Voltage magnitude sensitivities for $i-th$ bus with respect to the $j-th$ machine internal voltage and angles are given by,

$$\frac{\partial V_i}{\partial \delta_j} = \begin{cases} \frac{\beta}{|\mathbf{V_i}|}, j = p \\ \frac{-\beta}{|\mathbf{V_i}|}, j \neq p \end{cases} \tag{3.69}$$

$$\beta = -\sum_{x=1}^{N-1} \sum_{y=x+1}^{N} \alpha_{ix} \alpha_{iy} E_x E_y sin(\delta_x + \gamma_{ix} - \delta_y + \gamma_{iy}) \tag{3.70}$$

$$+ \sum_{x=1, x \neq j}^{N-1} \sum_{y=x+1, y \neq j}^{N} \alpha_{ix} \alpha_{iy} E_x E_y sin(\delta_x + \gamma_{ix} - \delta_y + \gamma_{iy})$$

$$|\mathbf{V_i}| = \sqrt{(\sum_{j=1}^{N} \eta_{ij} E_j)^2} \tag{3.71}$$

$$\frac{\partial \theta_i}{\partial \delta_j} = \frac{1}{|V_i|^2}[\eta_{ij}^2 E_j^2 + \sum_{y=1, y\neq j}^{N} \alpha_{ix}\alpha_{iy}E_x E_y cos(\delta_j + \gamma_{ij} - \delta_y + \gamma_{iy})] \tag{3.72}$$

Now the network sensitivities can be used to estimate the oscillation shape at different buses if the mode shapes are known at the machine terminals. The mode shapes at each machine terminal are obtained by calculating the right eigenvector of the identified A matrix from section 3.2.3 for each PMU location . The mode shapes as observed in the bus voltage magnitude and angle for the network buses are given by,

$$\mathbf{R_V} = \underbrace{\begin{bmatrix} \frac{\partial V_1}{\partial \delta_1} & \cdots & \frac{\partial V_1}{\partial \delta_j} \\ \vdots & \ddots & \vdots \\ \frac{\partial V_n}{\partial \delta_1} & \cdots & \frac{\partial V_n}{\partial \delta_j} \end{bmatrix}}_{S_V} \begin{bmatrix} W_1 \\ \vdots \\ W_N \end{bmatrix} \tag{3.73}$$

$$\mathbf{R}_\theta = \underbrace{\begin{bmatrix} \frac{\partial \theta_1}{\partial \delta_1} & \cdots & \frac{\partial \theta_1}{\partial \delta_j} \\ \vdots & \ddots & \vdots \\ \frac{\partial \theta_n}{\partial \delta_1} & \cdots & \frac{\partial \theta_n}{\partial \delta_j} \end{bmatrix}}_{S_\theta} \begin{bmatrix} W_1 \\ \vdots \\ W_N \end{bmatrix} \tag{3.74}$$

Where, $\mathbf{R_V} \epsilon \mathbb{R}^{n\times 1}$ and $\mathbf{R}_\theta \epsilon \mathbb{R}^{n\times 1}$ are the network bus voltage magnitude and angle oscillation shapes and $\mathbf{S_V} \epsilon \mathbb{R}^{n\times N}$ and $\mathbf{S}_\theta \epsilon \mathbb{R}^{n\times N}$ are voltage magnitude and angle sensitivity matrices. Oscillation mode shapes at different locations can be extracted from the PMU measurements using the identified subspaces. If PMU measurements are not available at every location then equations (3.73) and (3.74) can be used along with the mode shapes measured at available PMU locations to estimate the mode shapes at other unobserved network buses.This concept is demonstrated through a simple small system as shown in Fig. 3.6. The system matrix is calculated as below,

The eigenvalue analysis shows it has an oscillatory modes of 2.235 Hz and 3.83% damping.

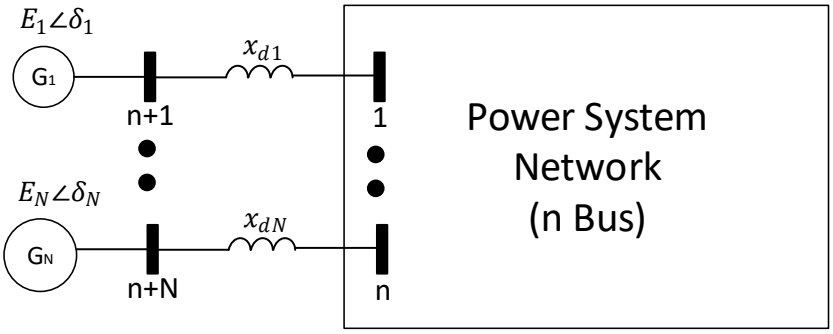

Figure 3.5: N machine n bus power system network.

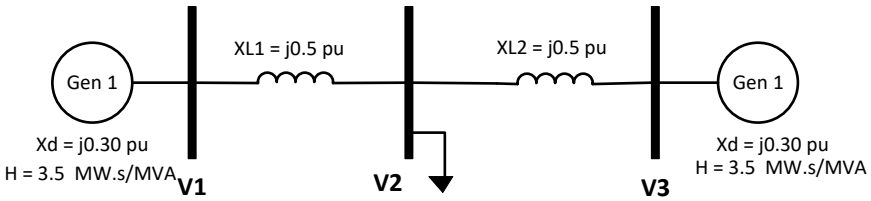

Figure 3.6: Two machine Three Bus system.

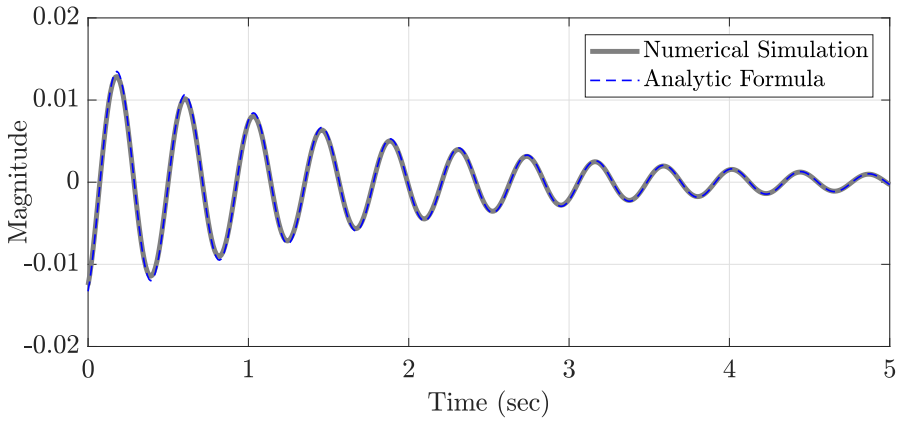

Figure 3.7: Validation of Analytic formula and Numerical simulation for Bus 3 mode shape.

The mode shape associated with machine angles are $[0.6940\angle -144.92 \quad 0.7190\angle 0]$. The network sensitivities and the mode shapes calculated using the method is compared with numerical simulation in Table 3.5.

3.3 Simulation Results

In order to illustrate the application of the proposed methodology for both ringdown and ambient system responses, reduced WECC 179 bus test system (1) and the IEEE 68 bus

Table 3.1: Network Buses Sensitivity Calculation and Mode shapes validation.

Bus	$\frac{\partial V_n}{\partial \delta_1}$	$\frac{\partial V_n}{\partial \delta_2}$	Mode Shapes	
			Analytic Formula	Numerical Simulation
1	0.0415	0.0179	$0.0197\angle -122.87$	$0.0187\angle -120.42$
2	0.0240	0.0405	$0.0180\angle -31.72$	$0.0189\angle -30.15$
3	0.0315	0.0340	$0.0142\angle -62.44$	$0.0149\angle -63.19$

benchmark test system (10) are used. Time domain simulated measurements from these systems can be considered as synthetic PMU measurements,making the method suitable using synchrophasors. Different scenarios are studied to show the performance of the proposed method.

3.3.1 Signal Selection for Ringdown Condition

WECC system is consist of a reduced WECC 179-bus, 29-machine system (1). The one-line diagram of the system is shown in Fig. 3.8. All generators are represented as a classical second-order differential model reflecting the motion of the rotor; damping parameter D for all generators are set to 4 in base case and all loads are modeled as constant MVA. Only generators where periodic disturbances are applied are represented as detailed model. Several test cases are provided covering different power system responses which includes normal oscillatory events because of local and inter-area modes, forced oscillations events, phenomenon of resonance, oscillations due to multiple oscillation sources etc. several cases in the library have been tested using the proposed method.

3.3.1.1 Case 1: Poorly Damped Natural Oscillation

Case 1 shows the step by step application of the proposed method for one of the cases in the test case library (1). In this case, the base model is modified to create a poorly damped local oscillation mode of 1.41 Hz with 0.01% damping. The damping of generator connected at bus 45 and bus 159 is modified from 4 to -2 and 4 to 1 respectively to create this scenario. It is assumed that there are PMU installed at the terminal of all 29 generator buses. Now the proposed method is applied to perform signal classification which helps the applications like mode estimation, oscillation classification, event classification etc. Fig. 3.9

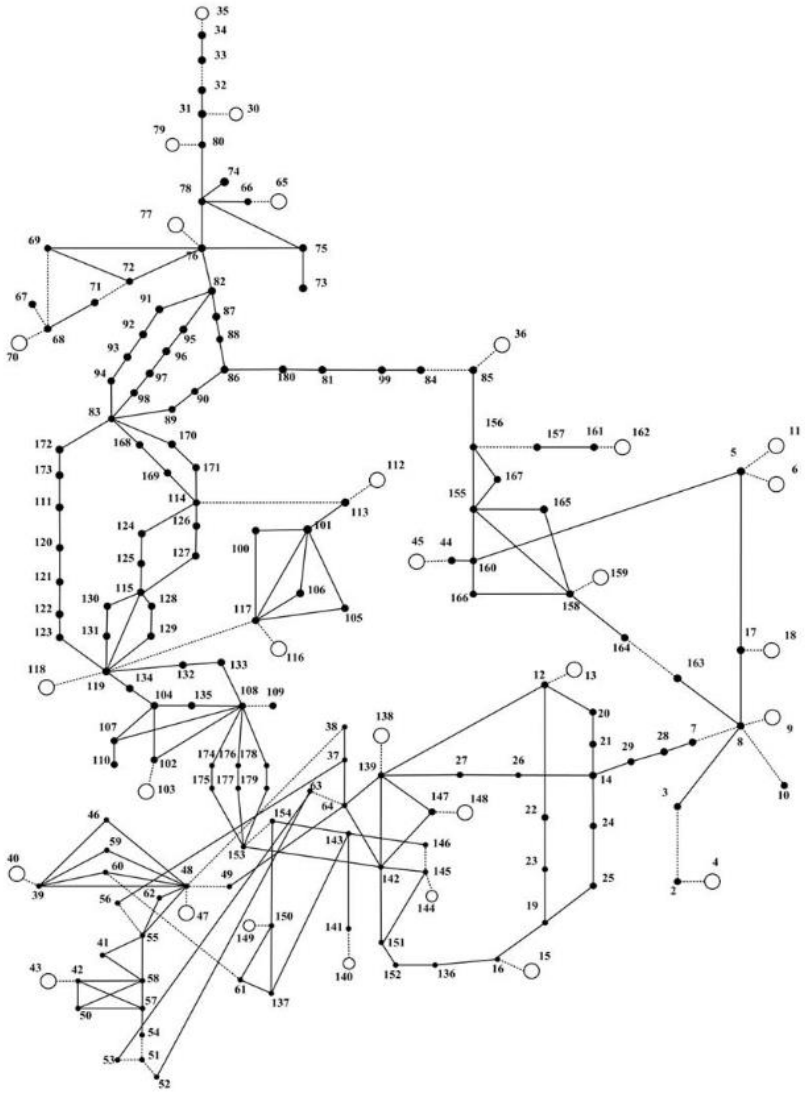

Figure 3.8: WECC 179 Bus Test System (1).

shows the time domain response of the system after a three phase fault at bus 159 for 0.05 second. Using these signals two sets of subspaces are calculated (subspaces with projection and without projection) as mentioned in sub section 3.2.3. Then the affinity between the subspaces are calculated and two weighted matrix W_{wp} and W_p are calculated as mentioned in sub section 3.2.4. Then the similarity matrix W is calculated using the two weighted matrices. Fig. 3.10 shows the matrix W for the first iteration of the proposed met

Al the diagonal elements are 1 indicating that the self affinity of the subspaces. Fig. 3.11 shows the second eigenvector values for each iteration and 3.12 shows the groups at each

iteration. It is noticeable that after each iteration the number of signals in the groups gets reduced. when the difference between values of second eigenvector is less than the threshold, the iterations stop. In this case, it takes 5 iterations to converge. After that, signal at bus 45 has the lowest value and it is identified as an input signal or is assumed to be close to the input.

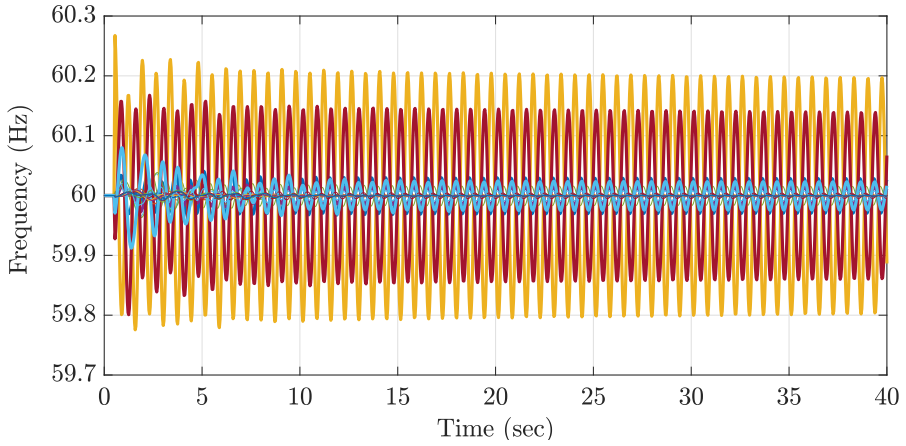

Figure 3.9: Time domain frequency signals of all the PMU locations.

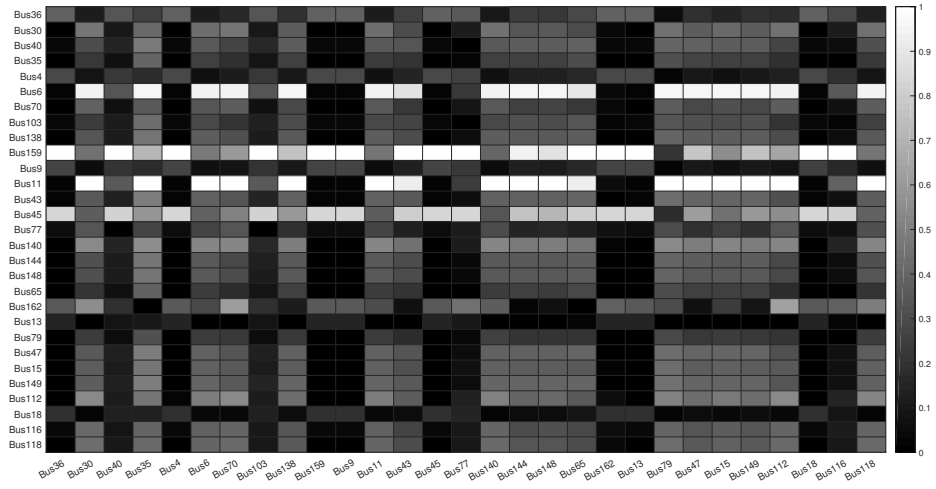

Figure 3.10: Case 1, Laplacian matrix for the first iteration.

3.3.1.2 Case 2: Resonance with Poorly Damped Natural Oscillation

In this case, the source bus signal 65 leads the other dominant signal 35 for the oscillation frequency of 0.37 Hz. In that case, methods based on phase shift is not able to track the input signals properly. The proposed method does not look into the phase shift between signals explicitly rather it looks into the subspace identified from the signals. Table. 3.2

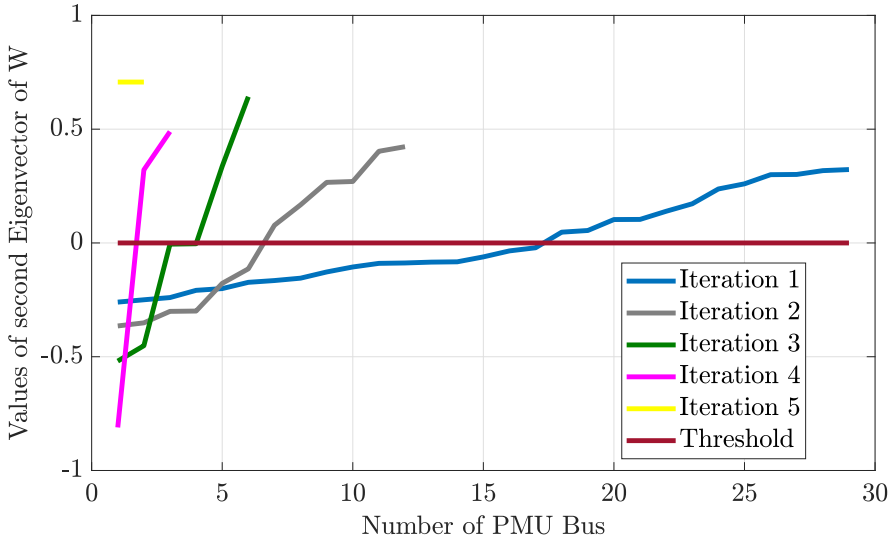

Figure 3.11: Case 1, values of second eigenvector of W for each iteration.

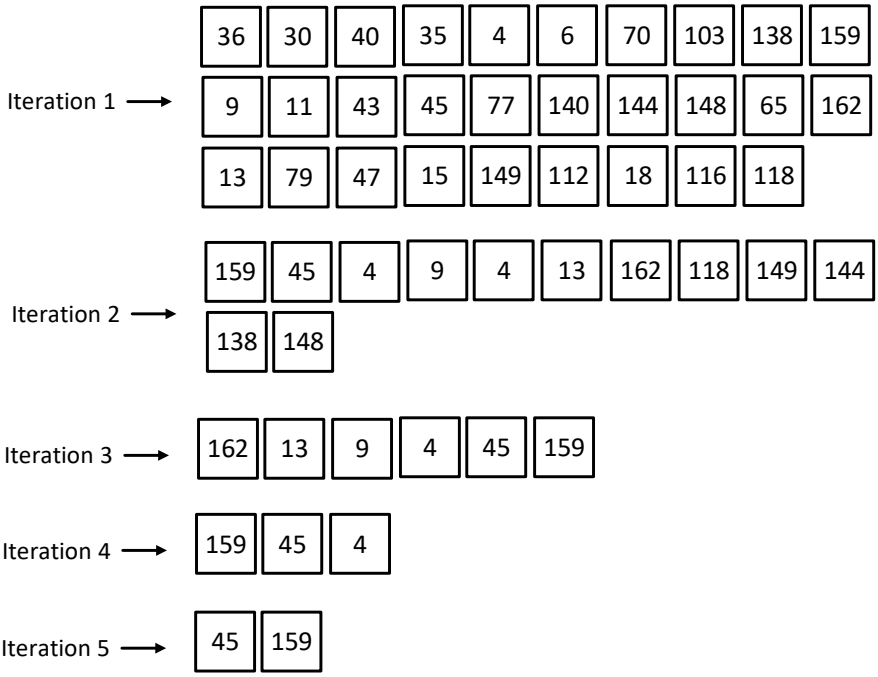

Figure 3.12: Case 1, Groups of signals for each iteration.

shows that for case PD_2 the proposed method ranked the signals as 65 and 35. The signal ranked 1 is considered to be close to the actual source. So, the proposed method can reliably classify the signals.

Table 3.2: Signal classification for the cases in test case library(1).

Case	D	Freq (Hz)	Damping Ratio	Source Bus	Fault Bus	Description	Signal Rank
PD_1	D45 =-2	1.41	0.01%	45	159	1 Source	45
	D159 =1					1 local mode	159
PD_2	D35 =0.5	0.37	0.02%	65	79	1 Source	65
	D65 =-1.5					1 inter-area mode	35
PD_3	D6 =2	0.46	2.22%	11	30	1 Source	11
	D11 =-6	0.70	1.15%			1 unstable local	30
		1.63	-0.54%			2 and 1 inter and area mode	35
PD_8	D45 =-2.5	1.27	-1.06%	45	159	2 Source	45
	D159 =-1.5	1.41	-0.22%	36		2 unstable	36
	D36 =-1					modes	159

Table 3.3: Signal classification for the forced oscillation cases in test case library(1).

Case Case	Injected Signal	Freq of Freq of (Hz)	Source Location	Description	Signal Rank
F_1	Sinusoidal	0.86	4	Resonance with local 0.86Hz mode	4,162,9
F_2	Sinusoidal	0.86	79	Resonance with local 0.86Hz mode	79,65,35
F_2	Sinusoidal	0.37	77	Resonance with inter-area 0.37Hz mode	65,35,79,77

3.3.2 Signal Selection for Ambient Conditions

Under normal operating condition,power system is always in motion because of random load variations occurring continuously in the system. These responses are typically termed as ambient response. The spectral analysis of ambient response shows that it can be approximated well by white noise (68). The IEEE 68 bus system from (10) is modified to add governors to the machines. The modified system is simulated in real time digital simulator (RTDS). To simulate ambient response,a white noise with a magnitude of 1% of each rated load (active and reactive power) is added to the corresponding load and there are no other disturbance in the system.

Fig. 3.14 shows the frequency as observed at different PMU locations. Then the proposed signal grouping algorithm is applied to these groups of signals to find the optimal number of signals for monitoring an inter-area oscillation mode of 0.52 Hz. Fig. 3.15 shows the results of grouping after each iteration. After the first iteration, it identifies 14 PMU locations where the effect of the mode under study is most prominent. Moreover, it also points out that the generators in the New England power system is oscillating against New York power system. Iteration 2, further simplifies the groups by selecting 7 PMU locations. And finally, after the third iteration, the optimal number of PMU locations are selected as bus 13, bus 18 and bus 14. The grouping process ends as the Ncut value exceeds the predefined threshold value. To validate that these are the optimal signals the criterion for predicting the variance of damping ratio from the identified model as proposed in (4), is applied for each iteration. Fig. 3.16 shows the average variance of the estimated damping ratio for each iteration. It shows that the estimated variance is decreasing with each iteration indicating that the grouping process is filtering out signals which gives a more accurate estimation.

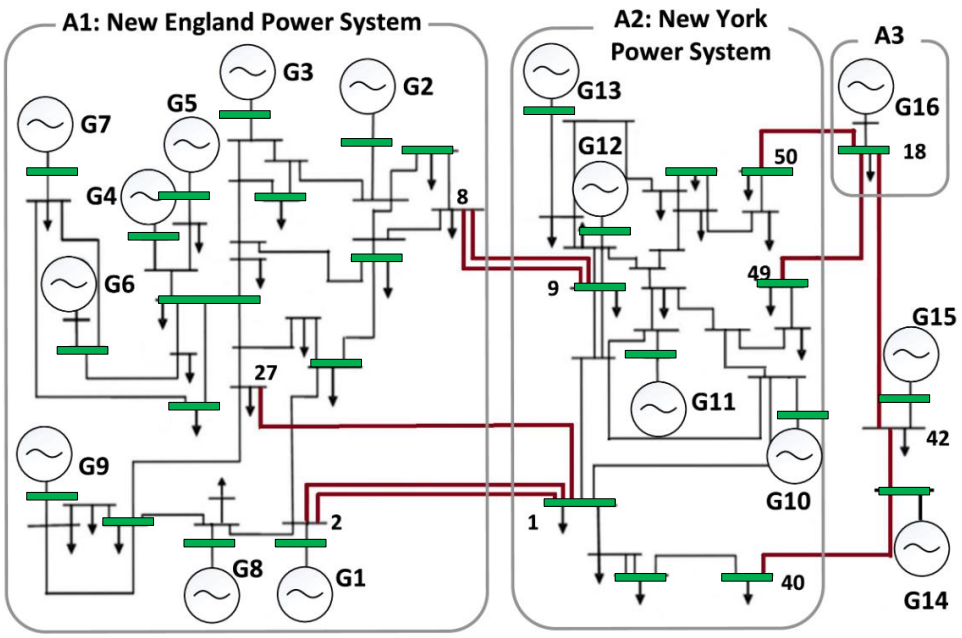

Figure 3.13: IEEE 68 Bus study system with PMU location .

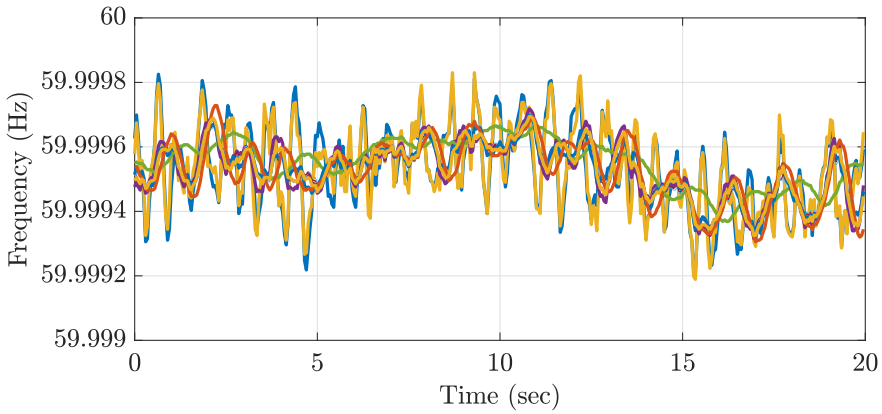

Figure 3.14: Time domain frequency signals of all the PMU locations.

3.3.3 Comparison with State-of-the-Art

In this section the optimal signal selection method is compared with other methods from the literature. Authors in (4) has compared the results of their proposed method with other methods in literature. The same IEEE 39 bus test system is used to compare the results of proposed method in this paper with other methods. IEEE 39 bus test system has an inter-area oscillation frequency of 0.6618 Hz and a damping ratio of 6.94% where the dominant state is related to the machine one speed. The frequency signals at each PMU locations are taken as input for the proposed methods as well as the existing methods. Tables 3.5 and 3.4 summarizes the result. Table 3.5 shows the signal ranking after using the method mentioned in (4).Table 3.4 shows the grouping obtained from the proposed method. It shows that the optimal signals selected from the proposed method overlap with the signal ranking obtained from the existing method. As a result of this, confirming the proposed method can give the best signals for accurate estimation â the advantage over existing methods that the proposed method does not require any signal pre-screening step and fast. It is also applicable in an online environment unlike the proposed other methods.

3.4 Computational Time of the Proposed Method

In this section the computational time of the proposed method is accessed and the results are compared with the most recent method of optimal signal selection in (4). Both the algorithms are implemented in an off-the-shelf personal computer (Intel i5, 2.4 GHz CPU,16

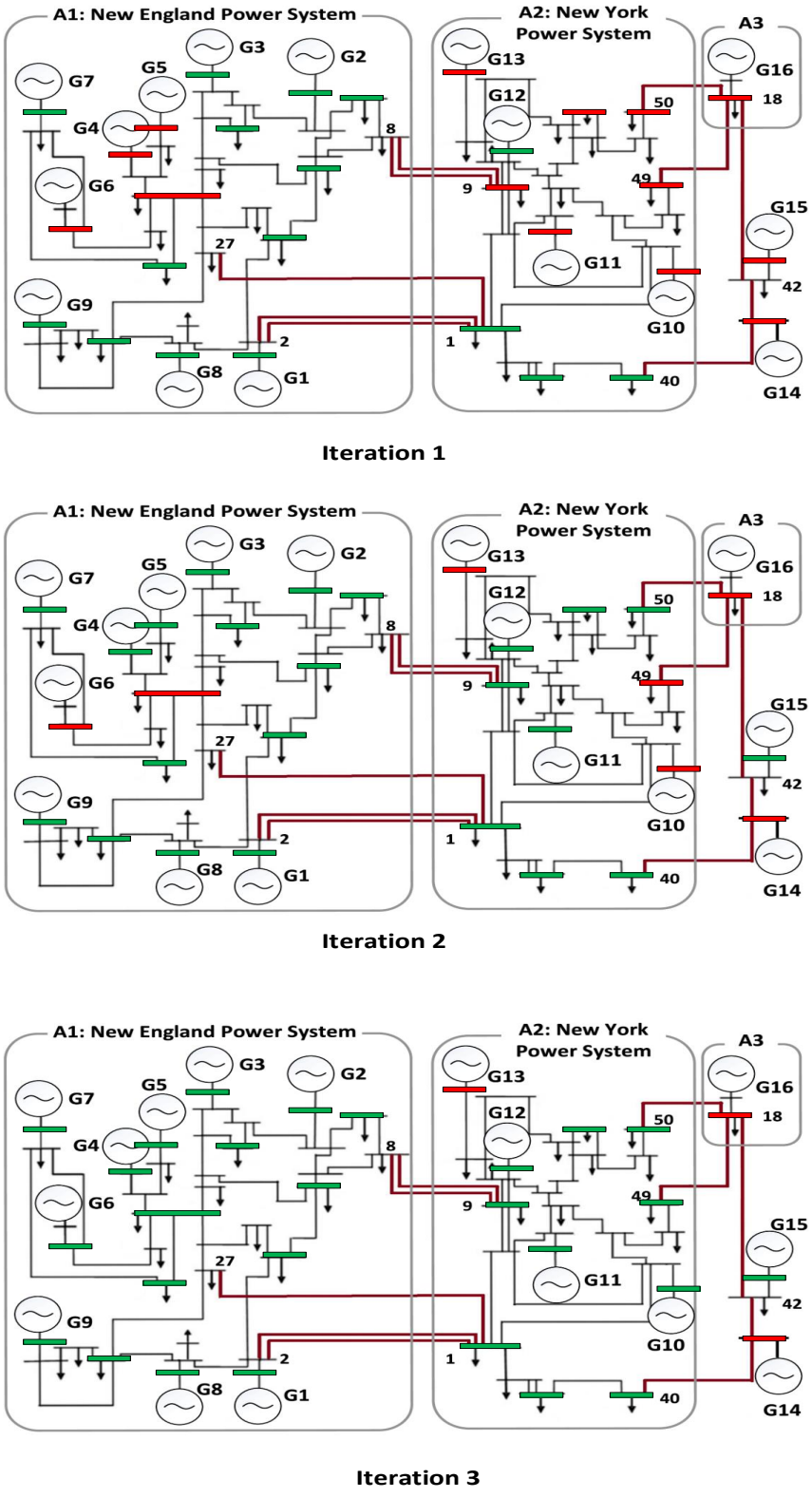

Figure 3.15: IEEE 68 Bus study system grouping for different iterations .

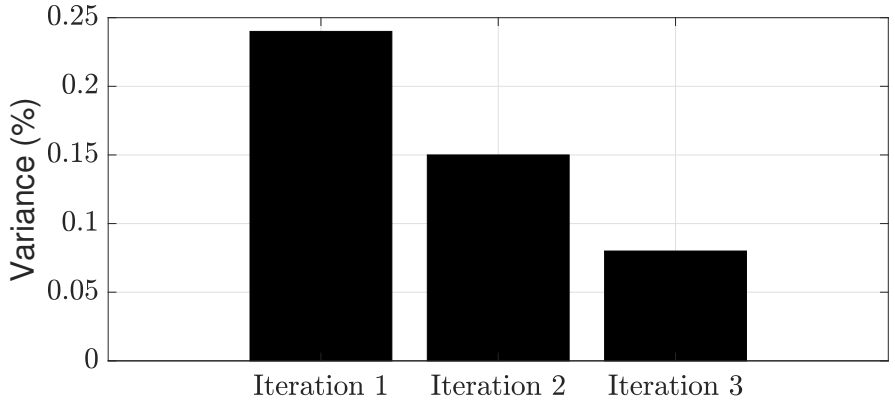

Figure 3.16: Average estimated damping ratio variance for each iterations .

Table 3.4: Signal groups based on proposed method.

Iteration	Signals	Variance
Iteration 1	31,33,34,32,39,37,30	0.136
Iteration 2	31,33,34,32,39	0.128
Iteration 3	31,33,34	0.121
Iteration 4	31,34	0.118

Table 3.5: Comparison of Different Signal Selection Algorithm for IEEE 39 Bus Test System.

PEC (4)		MPC(74)		CF1(75)	
31	0.115	33	0.123	32	0.136
34	0.121	34	0.131	34	0.148
33	0.129	31	0.145	31	0.157
32	0.137	37	0.152	33	0.169
39	0.142	30	0.165	30	0.181
30	0.149	32	0.169	39	0.189
37	0.162	39	0.175	35	0.197
36	0.184	35	0.189	37	0.205
35	0.199	36	0.196	36	0.215
29	0.230	29	0.220	29	0.235

GB of RAM). Figure 3.18 shows the computational time of the proposed algorithm for different model orders and different number of signals. The convergence time of the proposed signal selection time increases with both model order and number of signals. Fig. 3.19

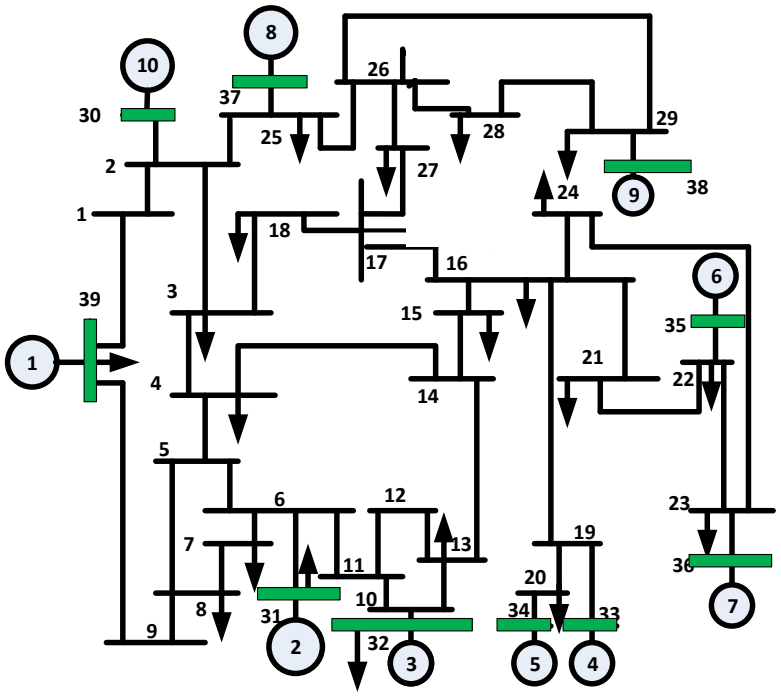

Figure 3.17: IEEE 39 Bus study system with PMU location.

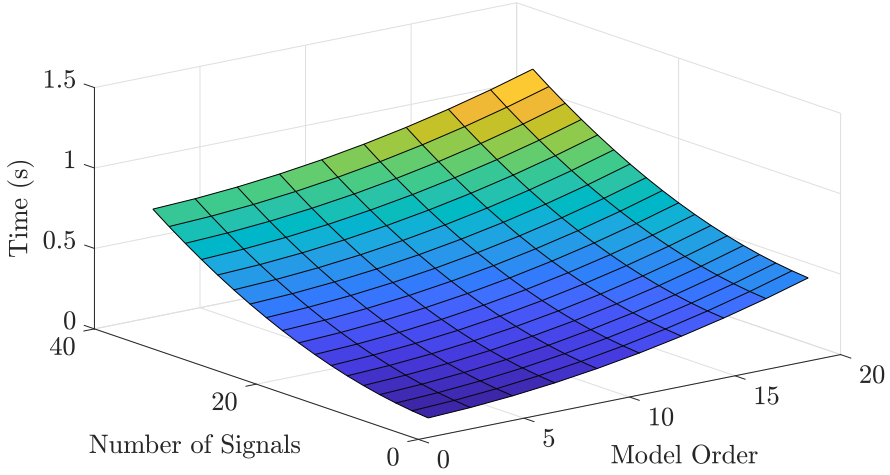

Figure 3.18: Computational time of the proposed method.

compares the results of proposed method with existing method. And the results show that the proposed method is able to group signals converges faster compare to the existing method. This is mainly due to the recursive subspace algorithm used for identification and the proposed method does not require any signal pre-slection based on Fast Fourier Transform (FFT) unlike the existing method.

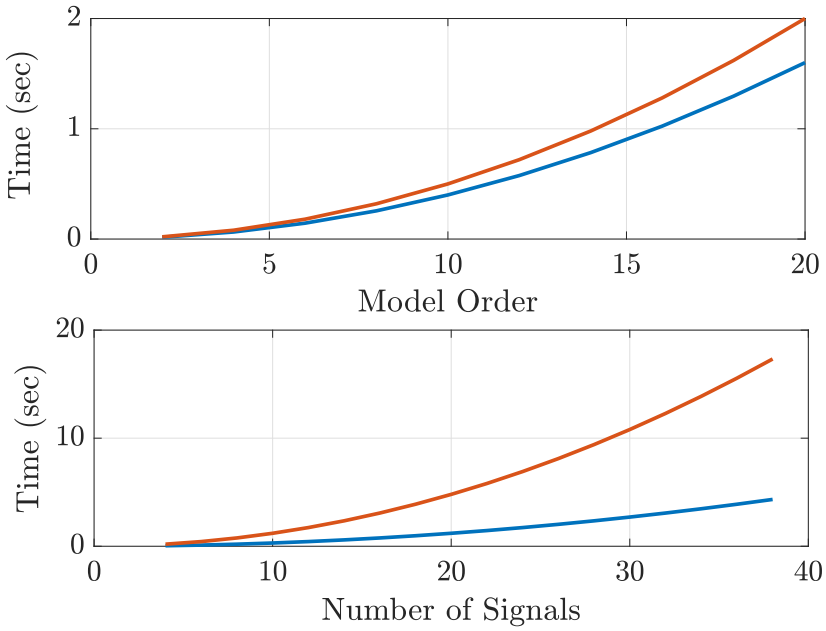

Figure 3.19: Computational time comparison with existing method (4) a)Time vs Model Order and b)Time vs Number of Signals.

3.5 Summary

In this chapter, a method for selecting optimal signals is presented. The proposed method can find an optimal group of signals for both ringdown and ambient conditions. The results based on IEEE 68 bus test system and WECC 179 bus system show that not only the proposed method can select the optimal signals, the optimal group also contains the source of forced oscillations. This can help in narrowing down the search area for the oscillation source location. The proposed method is implementable online and is faster than other states of the art methods available. The proposed method is used in the next chapter to develop an approach for locating the oscillation source.

CHAPTER 4: MEASUREMENT BASED OSCILLATION SOURCE LOCATION METHOD FOR MODERN POWER SYSTEM

In this chapter, a new method is presented, which identifies the location of the oscillation source using subspace-based identification method developed in earlier chapters. The proposed method derives a relationship between the phase angle of power and frequency signal of a machine from the energy function of the device. Then the relative phase difference between the machine power and frequency phase is utilized to locate the source of sustained oscillations. The proposed method can use the existing measurements to estimate the mode shapes of unobserved buses and can help to identify the location of forced oscillation more precisely. The efficacy of the proposed method is evaluated on the two-area system.

4.1 Introduction

Power system oscillations poses a serious threat to the reliable operation of the modern power grid.all the oscillatory modes need to be well damped for reliable operation of the power grid (35). Monitoring and analysis of the data captured by phasor measurement units (PMU) has revealed several instances of sustained oscillations in different power grids throughout the world (76),(77). The frequency range of these oscillations ranged from 0.05 Hz to 2 Hz. Depending on the source of oscillations these oscillations are broadly classified into two categories 1) natural oscillations and 2) forced oscillations. Natural oscillations are inherent characteristics of the system and typically caused by large power transfer over a weak and stressed tie-line, bad tuning of power system controllers etc. On the other hand, forced oscillations are caused by periodic external disturbances. The cause of these disturbances include but not limited to equipment failures, cyclic loads, control system malfunctions etc (78). Any type of sustained oscillations can lead to unstable grid conditions and can potentially cause cascading outages. It also can cause mechanical stress on the generator turbines which in turn can reduce the lifespan of the equipment and increased

maintenance cost. Depending on the type of sustained oscillations the mitigation method can be different. Regardless of the type, most efficient and safe way to mitigate oscillation is to locate the source of oscillation and disconnect the source from the power system.

However, locating the source of oscillations is not a trivial task. Over the past decade, several research work has been conducted to develop methods that can reliably locate the source of sustained oscillations. Authors in (79) have provided a comprehensive review of all the oscillation source location method available in the literature. Authors have also pointed out the pros and cons of each method. All these methods tries to analyse different attributes of oscillations to locate the source of oscillation. Such attributes include oscillation magnitude, phase angles, statistical signature, propagation speed and oscillation energy. Unfortunately, most of the methods are not practical for implementing in a power system as an oscillation monitoring tool. Authors in (77) has proposed a method based on calculating the dissipating energy of oscillations. The method tracks the dissipating energy flow in the network and generator with the positive dissipating energy is termed as the source of oscillations . This method is practically implemented in ISO-NE and only uses PMU measurements to calculate the dissipating energy. Although this method provide satisfactory results in practical scenarios the assumptions made in deriving the method needs further investigation. Authors in (80) has reported that lossy network and constant impedance load model can inject dissipating energy to the network and can lead to erroneous oscillation source location(81). The method also depends on the estimation of sustained oscillation frequency and on retrieving the phase and magnitude of all signals accurately through very sensitive signal filtering.

One of the limitation of dissipating energy flow method (DEF) (77) is that it can only locate the source upto buses where PMU measurements are available. So, it can only point to a area close to the oscillation source if PMU measurement is not available at the generator or plant bus. Authors in (82) proposes a method for locating the source of oscillation using frequency response function (FRF). Authors proposes the formulation of FRF for detailed machine model and then use that to locate the source of forced oscillations. Energy based method (83) is further enhanced to develop a two stage approach to detect the

source of oscillation up to control devices (governor and exciters) of the generators.However, the proposed method uses empirical mode decomposition (EMD) and total least square estimation to extract the phasor information of variable and is difficult to implement in an online environment because of computational complexity.

In this chapter, a new method is proposed for locating the source of oscillations. It uses the methods developed in previous chapter to construct the mode shapes for generator buses which does not have PMU installed. Then it leverage the method based on subspace affinity presented in previous chapter, for pre-selecting a group of potential oscillation source location signals. After that it uses the shape of power and frequency signals and the phase relationship between them to locate the source of oscillation source.

The main contributions of the proposed approach are :

- It can detect the source of sustained oscillation even if there are no PMU measurements available at the source generator bus
- It can be implemented as a practical tool for oscillation source location.
- It requires less amount of signals to determine the oscillation energy flow direction.

The rest of the chapter is organised as follow, section 4.2 describes the proposed methodology and section 4.3 presents the simulation results. Finally, section 4.4 concludes the chapter

4.2 Proposed Methodology

The proposed methodology has mainly three major steps a) extraction of unobserved generator buses mode shape , 2) signal pre-selection using subspace affinity and 3) locating the source of oscillations using phase relationship between generator power and frequency.

4.2.1 Extraction of Unobserved Machine Mode Shapes

Power system has a limited number of PMU installed throughout the system. So, all the network variables associated with all the buses are not observable from the PMU measurements. So, there can be instances when the bus where a particular oscillation frequency is most prominent do not have a PMU located at it's location. This creates a need for a method

that can help generating the network variables at different buses with PMU measurements from other buses. Authors in (73) has proposed a method for tracking the dominant oscillation path based on network sensitivities. In this work, the concept is used and only voltage sensitivities are used to find oscillation shape at unobserved PMU locations. Figure 4.1 shows the n bus power system network with additional N bus for machine internal voltages. Loads are modeled as constant impedance and are added to the admittance matrix.So, current injections at all other nodes other than the generator nodes are zero. The node voltage equations for the network can be expanded as,

$$\begin{bmatrix} 0 \\ \mathbf{I_N} \end{bmatrix} = \begin{bmatrix} \mathbf{Y_{nn}} & \mathbf{Y_{nN}} \\ \mathbf{Y_{nN}^T} & \mathbf{Y_{NN}} \end{bmatrix} \begin{bmatrix} \mathbf{V_n} \\ \mathbf{E_n} \end{bmatrix} \tag{4.1}$$

$$\mathbf{V_n} = -\mathbf{Y_{nn}^{-1}} \mathbf{Y_{nN}} \mathbf{E_N} \tag{4.2}$$

Where, $\mathbf{I_N}$ denotes generator current injections, $\mathbf{E_N}$ refers to the generator internal voltages and $\mathbf{V_n}$ represents bus voltages. Equation (3.67) represents the bus voltages as a function of internal voltages and $-\mathbf{Y_{nn}^{-1}} \mathbf{Y_{nN}}$ depends on the network parameters.The generalised expression for bus voltage V_i can be written as,

$$\mathbf{V_i} = \sum_{j=1}^{N} \alpha_{ij} \mathbf{E_j}; \alpha = -\mathbf{Y_{nn}^{-1}} \mathbf{Y_{nN}} = \eta \angle \gamma \tag{4.3}$$

As shown in (4.3) the bus voltage depends on the magnitude and angle of machine internal voltage. A change in machine internal voltages causes the bus voltages to change. A generalised expression for network sensitivities have been derived in (73). Voltage magnitude sensitivities for $i-th$ bus with respect to the $j-th$ machine internal voltage and angles are given by,

$$\frac{\partial V_i}{\partial \delta_j} = \begin{cases} \frac{\beta}{|\mathbf{V_i}|}, j = p \\ \frac{-\beta}{|\mathbf{V_i}|}, j \neq p \end{cases} \tag{4.4}$$

$$\beta = -\sum_{x=1}^{N-1} \sum_{y=x+1}^{N} \alpha_{ix}\alpha_{iy}E_xE_y sin(\delta_x + \gamma_{ix} - \delta_y + \gamma_{iy}) \tag{4.5}$$

$$+ \sum_{x=1, x\neq j}^{N-1} \sum_{y=x+1, y\neq j}^{N} \alpha_{ix}\alpha_{iy}E_xE_y sin(\delta_x + \gamma_{ix} - \delta_y + \gamma_{iy})$$

$$|\mathbf{V_i}| = \sqrt{(\sum_{j=1}^{N} \eta_{ij}E_j)^2} \tag{4.6}$$

$$\frac{\partial \theta_i}{\partial \delta_j} = \frac{1}{|V_i|^2}[\eta_{ij}^2 E_j^2 + \tag{4.7}$$

$$\sum_{y=1, y\neq j}^{N} \alpha_{ix}\alpha_{iy}E_xE_y cos(\delta_j + \gamma_{ij} - \delta_y + \gamma_{iy})]$$

Now the network sensitivities can be used to estimate the oscillation shape at different buses if the mode shapes are known at the machine terminals. The mode shapes at each machine terminal are obtained by calculating the right eigenvector of the identified A matrix from the subspace identification methods developed in previous chapters for each PMU location . The mode shapes as observed in the bus voltage magnitude and angle for the network buses are given by,

$$\mathbf{R_V} = \underbrace{\begin{bmatrix} \frac{\partial V_1}{\partial \delta_1} & \cdots & \frac{\partial V_1}{\partial \delta_j} \\ \vdots & \ddots & \vdots \\ \frac{\partial V_n}{\partial \delta_1} & \cdots & \frac{\partial V_n}{\partial \delta_j} \end{bmatrix}}_{S_V} \begin{bmatrix} W_1 \\ \vdots \\ W_N \end{bmatrix} \tag{4.8}$$

$$\mathbf{R}_\theta = \underbrace{\begin{bmatrix} \frac{\partial \theta_1}{\partial \delta_1} & \cdots & \frac{\partial \theta_1}{\partial \delta_j} \\ \vdots & \ddots & \vdots \\ \frac{\partial \theta_n}{\partial \delta_1} & \cdots & \frac{\partial \theta_n}{\partial \delta_j} \end{bmatrix}}_{S_\theta} \begin{bmatrix} W_1 \\ \vdots \\ W_N \end{bmatrix} \tag{4.9}$$

(4.10)

Where, $\mathbf{R_V} \epsilon \mathbb{R}^{n \times 1}$ and $\mathbf{R}_\theta \epsilon \mathbb{R}^{n \times 1}$ are the network bus voltage magnitude and angle oscillation shapes and $\mathbf{S_V} \epsilon \mathbb{R}^{n \times N}$ and $\mathbf{S}_\theta \epsilon \mathbb{R}^{n \times N}$ are voltage magnitude and angle sensitivity matrices. Oscillation mode shapes at different locations can be extracted from the PMU measurements using the identified subspaces. If PMU measurements are not available at every location then equations (4.8) and (4.9) can be used along with the mode shapes measured at available PMU locations to estimate the mode shapes at other unobserved network buses.This concept is demonstrated through a simple small system as shown in Fig. 4.2.

Typically PMU measures the voltage and current at the bus where it is located. similar to voltage sensitivities current sensitivities can also be developed and later used to create the current injection at unobserved PMU bus, The line current sensitivity in the line from bus m to n with respect to the jth machine angle are given by,

$$\frac{\partial I_{mn}}{\partial \delta_j} = \begin{cases} \frac{\alpha}{|\mathbf{I_{mn}}|}, j = p \\ \frac{-\alpha}{|\mathbf{V_i}|}, j \neq p \end{cases} \tag{4.11}$$

$$\alpha = -\sum_{x=1}^{N-1} \sum_{y=x+1}^{N} \Omega_{mnp}\Omega_{mnq}E_pE_q sin(\delta_p + \psi_{mnp} - \delta_q - \psi_{mnq})$$
$$+ \sum_{x=1, x\neq j}^{N-1} \sum_{y=x+1, q\neq j}^{N} \Omega_{mnp}\Omega_{mnq}E_pE_q sin(\delta_p + \psi_{mnp} - \delta_q - \psi_{mnq})$$

$$|I_{mn}| = \sqrt{(\sum_{j=1}^{N} \Omega_{mnj}E_j)^2} \tag{4.12}$$

The line current angle sensitivity with respect to jth machine can be calculated as,

$$\frac{\partial \chi_{mn}}{\partial \delta_j} = \frac{1}{|I_{mn}|^2}[\Omega_{mnj}^2 E_j^2 + \tag{4.13}$$
$$\sum_{y=1, y\neq j}^{N} \Omega_{mnj}\Omega_{mny}E_jE_y cos(\delta_j + \psi_{mnj} - \delta_y + \psi_{mny})]$$

where, $\mathbf{\Omega}$ is calculated from the pi model of a line segment between bus m and n. The current flow in the line can be written as ,

$$\mathbf{I_{mn}} = (\mathbf{y_{mn}} + \mathbf{y_{m0}})\mathbf{V_m} - \mathbf{y_{mn}}\mathbf{v_n} \tag{4.14}$$

$$\tag{4.15}$$

Now the line current flow can be expanded to express in terms of machine internal voltages by substituting $V_m = \eta_{mj}E_j$ where $j = 1, 2, 3, ...n$,

$$\mathbf{I_{mn}} = \sum_{\mathbf{j=1}}^{\mathbf{N}} (\mathbf{y_{mn0}} + \mathbf{y_{mn}})\eta_{\mathbf{nj}}\mathbf{E_j} - \mathbf{y_{mn}}\eta_{\mathbf{nj}}\mathbf{E_j} \tag{4.16}$$

$$= \sum_{j=1}^{N} \Omega_{mnj} E_j \tag{4.17}$$

where, $\mathbf{\Omega_{mnj}} = \Omega_{mnj}\angle\psi_{mnj}$ and $\Omega_{mnj} = |(y_{mn0} + y_{mn})\eta_{nj} - y_{mn}\eta_{nj}|$ and $\psi_{mnj} = \angle[(y_{mn0} + y_{mn})\eta_{nj} - y_{mn}\eta_{nj}]$. Details of the derivation can be found in Appendix A.

Once the voltage and current sensitivities are calculated the deviation in bus votlage magnitude and angles can be calculated as below,

$$\mathbf{\Delta V} = \underbrace{\begin{bmatrix} \frac{\partial V_1}{\partial \delta_1} & \cdots & \frac{\partial V_1}{\partial \delta_j} \\ \vdots & \ddots & \vdots \\ \frac{\partial V_n}{\partial \delta_1} & \cdots & \frac{\partial V_n}{\partial \delta_j} \end{bmatrix}}_{C_{V\delta}} \begin{bmatrix} \Delta_{\delta_1} \\ \vdots \\ \Delta_{\delta_N} \end{bmatrix} \tag{4.18}$$

$$\mathbf{\Delta}\theta = \underbrace{\begin{bmatrix} \frac{\partial \theta_1}{\partial \delta_1} & \cdots & \frac{\partial \theta_1}{\partial \delta_j} \\ \vdots & \ddots & \vdots \\ \frac{\partial \theta_n}{\partial \delta_1} & \cdots & \frac{\partial \theta_n}{\partial \delta_j} \end{bmatrix}}_{C_{\theta\delta}} \begin{bmatrix} \Delta_{\delta_1} \\ \vdots \\ \Delta_{\delta_N} \end{bmatrix} \tag{4.19}$$

$$\tag{4.20}$$

where, ΔV is the bus voltage magnitude and $\Delta\theta$ is bus angle.

The current magnitude deviation ΔI and angle deviation $\Delta\chi$ is calculated in a similar manner. The details of the derivation can be found in (73),

$$\mathbf{\Delta I_{mn}} = C_{Imn\delta}\Delta\delta \tag{4.21}$$

$$\mathbf{\Delta}\chi = C_\delta \Delta\delta \tag{4.22}$$

$$\tag{4.23}$$

The power deviation can be calculated from the voltage and current deviation values as,

$$\Delta P_{mn} = \Re[\Delta V_m \angle \Delta(\theta \Delta I_{mn} \angle \Delta\chi)^*] \tag{4.24}$$

If the generator terminal voltage is known then the internal voltage of the machine terminal can be calculated,

$$\Delta E_{ju} = V_m + Imjx_j \tag{4.25}$$

where E_{ju} refer to the unknown machine bus voltage and δ_{ju} is it's angle. Then the speed of the unknown machine bus ω_{ju} can be extracted by differentiating the angle with respect to time as $\omega_{ju} = \frac{d(\delta_{ju})}{dt}$

The eigenvalue analysis shows it has an oscillatory modes of 2.235 Hz and 3.83% damping. The mode shape associated with machine angles are $[0.6940\angle -144.92 \quad 0.7190\angle 0]$. The network sensitivities and the mode shapes calculated using the method is compared with numerical simulation in Table 3.5.

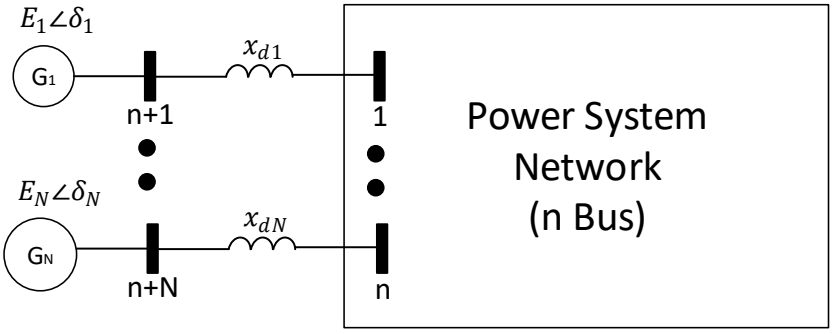

Figure 4.1: N machine n bus power system network.

4.2.2 Signal Pre Selection Using Subspace Affinity

The intuition behind identifying the subspace is that the subspace captures the modal characteristics of system for a specific operating condition, disturbance magnitude and dis-

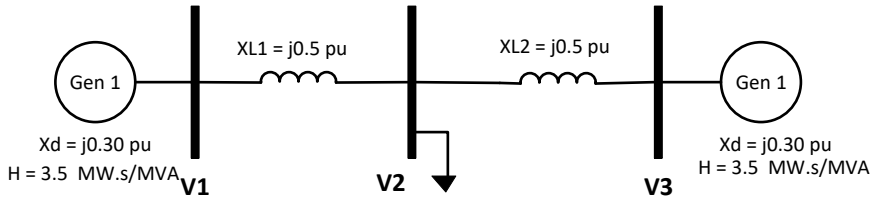

Figure 4.2: Two machine Three Bus system.

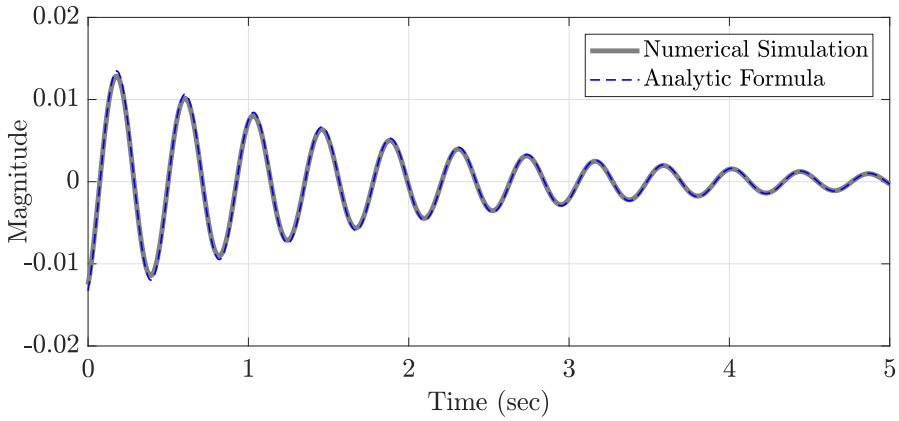

Figure 4.3: Validation of Analytic formula and Numerical simulation for Bus 3 mode shape.

turbance location. The affinity between the subspaces as seen at different location gives an indication of similarity between the signals at that locations. Let S_x be the subspace extracted from the extended observability matrix Γ_x, calculated at the previous chapters for each PMU signal. The affinity between two subspaces S_i and S_j is calculated as,

$$A_{ij} = \sqrt{\frac{v_1 cos^2\theta_1 + v_2 cos^2\theta_2 + ... + v_n cos^2\theta_n}{n}} \tag{4.26}$$

$$where, i, j = 1, 2, 3....n$$

$$\theta_n = acos(U_1(:,k)'.U_2(:,k)), \quad k = 1, 2, 3....n \tag{4.27}$$

Where, U_1 and U_2 represents the orthonormal bases of S_i and S_j respectively.v_n is the normalised length of the eigenvector. Ideally, $A_{ij} = 1$ if both the PMU signals i and j identifies same subspaces and $A_{ij} = 0$ if the PMU signals i and j identifies different independent subspaces.

A similarity matrix A is formed from the similarity graph shown in Figure. 4.4 and L is

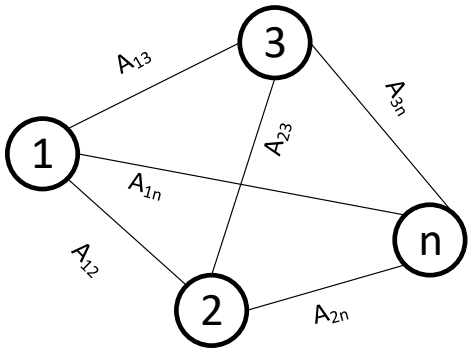

Figure 4.4: Similarity graph for a)without projection and b) with projection .

the laplacian matrix.

$$A = \begin{bmatrix} A_{11} & \cdots & A_{1n} \\ A_{21} & \cdots & A_{2n} \\ \vdots & \cdots & \vdots \\ A_{n1} & \cdots & A_{nn} \end{bmatrix} \tag{4.28}$$

$$D = \begin{bmatrix} \sum_{i=1}^{n} W(1,i) & \cdots & 0 \\ \vdots & \cdots & \vdots \\ 0 & \cdots & \sum_{i=1}^{n} W(n,i) \end{bmatrix} \tag{4.29}$$

$$L = D - A \tag{4.30}$$

As mentioned in the seminal work on graph partitioning by the authors of (71), one key criterion that ensures the optimal partitioning of graphs is the normalized cut between the graphs. Minimizing normalized cut (Ncut) ensures the similarity within a group is high and similarity between two different groups is low. If a graph $G = (V, E)$ is partitioned into two disjoint sets X and Y, then the Normalized cut is expressed as,

$$Ncut(X,Y) = \frac{cut(X,Y)}{assoc(X,V)} + \frac{cut(X,Y)}{assoc(Y,V)} \tag{4.31}$$

$$where, \tag{4.32}$$

$$cut(X,Y) = \sum_{a\epsilon X, b\epsilon Y} A(a,b) \tag{4.33}$$

$$assoc(X,V) = \sum_{a\epsilon X, c\epsilon V} A(a,c) \tag{4.34}$$

$$assoc(Y,V) = \sum_{b\epsilon Y, c\epsilon V} A(b,c) \tag{4.35}$$

$$Ncut(X,Y) = \frac{\sum_{(x_i=1,x_j=-1)} -A_{ij}x_ix_j}{\sum_{x_i=1}(\sum_{i=1}^{n}\sum_{j=1}^{n} A(i,j))} + \frac{\sum_{(x_i=-1,x_j=1)} -A_{ij}x_ix_j}{\sum_{x_i=-1}(\sum_{i=1}^{n}\sum_{j=1}^{n} A(i,j))} \tag{4.36}$$

where, $assoc(X,V)$ represents the total connections from nodes in group X to all the nodes in the graph and $assoc(Y,V)$.With the help of Rayleigh quotient (72) it is proven that finding the optimal solution of the problem of $min_x Ncut(x)$ is similar to finding the second smallest eigenvector of the laplacian matrix L (71) , where x is indicator vector and its value 1 means a node belongs to group X and -1 means a node belongs to group Y. However, there are some practical challenges in performing this clustering for practical data set. The indicator value is not always discrete in the second smallest eigenvector(V_{ss}) and can often take continuous values. It creates a problem of how to divide the values in the two groups to form to clusters. In this paper, an dynamic optimization is run to find the splitting point value C that minimizes $Ncut(x)$ value. The splitting values are chosen by taking m evenly spaced values between the minimum and maximum values of V_{ss}. The splitting value which gives minimum $Ncut(x)$ is chosen and groups are created.

4.2.3 Oscillation Source Location Using Phase Relationship

In this section the phase relationship between the power and frequency of generator signals are derived from energy functions. The phase relationship between the power and energy gives indication about the direction of oscillation energy flow.The detailed energy

function for generator models are not derive here. There is no generalised expression of energy function for multi-machine system. Only the energy function expression exists for single machine infinite bus models. Detailed derivation of the energy function can be found from (83). The second order equation of the generator are given by,

The classical second order model of the generator is given by,

$$\frac{1}{2H}\frac{d\Delta\omega}{dt} = \Delta P_m - \Delta P_e - D\Delta\omega \tag{4.37}$$

$$\frac{d\Delta\delta}{dt} = \Delta\omega \tag{4.38}$$

where, Δ is the steady state deviation, P_m is the mechanical torque, P_e is the electrical torque, H is the inertia constant and D is the damping torque coefficient. The energy function of classical generator model is given by,

$$\int \Im(-I^*_{Gi}dU_i) = (\frac{1}{2}T_{ji}\Delta{\omega_i}^2 - P_{mi}\delta_i) + \int D_i\Delta{\omega_i}^2 dt \tag{4.39}$$

where, I_{Gi} is the ith generator current injection , T_j is the per unit moment of inertia.

The transient energy function can be expressed in Hamiltonian realisation form as below

,

$$Hm_i = \frac{1}{2}T_{ji}\Delta{\omega_i}^2 + \int \Delta P_e d\Delta\delta_i \tag{4.40}$$

Let $x = [\Delta\delta\Delta\omega]$, $\nabla H = [\Delta P_e M\Delta\omega]$. The Hamiltonian realisation of (4.39) is ,

$$\dot{x} = T(x)\nabla H + G(x)u \tag{4.41}$$

$$\dot{H} = \nabla H^T\dot{x} \tag{4.42}$$

$$\dot{x} = \begin{bmatrix} 0 & \frac{1}{M} \\ \frac{-1}{M} & \frac{-D}{M^2} \end{bmatrix} [\Delta P_e M \Delta\omega] \begin{bmatrix} 0 & 0 \\ 0 & \frac{-1}{M} \end{bmatrix} \begin{bmatrix} 0 \\ \Delta P_m \end{bmatrix} \tag{4.43}$$

$$\dot{H} = E_{DM} + E_{IM}; E_{DM} = -D\Delta\omega^2; E_{iM} = \Delta P_m \Delta\omega \tag{4.44}$$

Here E_{DM} is the machine dissipation energy damping and E_I is the injection energy of prime mover . After solving the equation (4.45) we get the oscillation energy output(84) expression as $E_O = \Delta P_m \Delta\omega$

The oscillation energy can be calculated as below ,

$$\Delta P_e = A_p cos(\omega_f t + \phi_p) \tag{4.45}$$

$$\Delta\omega = A_\omega cos(\omega_f t + \phi_\omega) \tag{4.46}$$

$$\int E_O dt = \int \Delta P_e \Delta\omega dt \tag{4.47}$$

$$= \int \frac{1}{2} A_p A_\omega [cos(\phi_p - \phi_{omega}) - cos(2\omega_f t + \phi_p + \phi_{omega})] dt \tag{4.48}$$

$$= \int \frac{1}{2} A_p A_\omega cos(\phi_p - \phi_\omega) dt \tag{4.49}$$

where, A_p and A_ω are the amplitudes and ϕ_p and ϕ_{omega} are the phases of Δ_P and Δ_ω respectively. From the constant part of equation 4.45 it is seen that the oscillating energy will be positive inf $|\phi_p - \phi_\omega| \leq 90$ and it is negative if $|\phi_p - \phi_\omega| \geq 90$. The positive value indicates that the energy flows from bus i to bus j and the negative value indicates energy flows from bus j to bus i. By tracking the flow of the oscillation energy the source of oscillation can be detected.

4.3 Simulation Results

The two area system is studied to show the application of proposed method (9). The model is simulated in real time digital simulator (RTDS) and software PMUs are used in the simulation. In this test system, PMUs are not available at all generator buses. Different

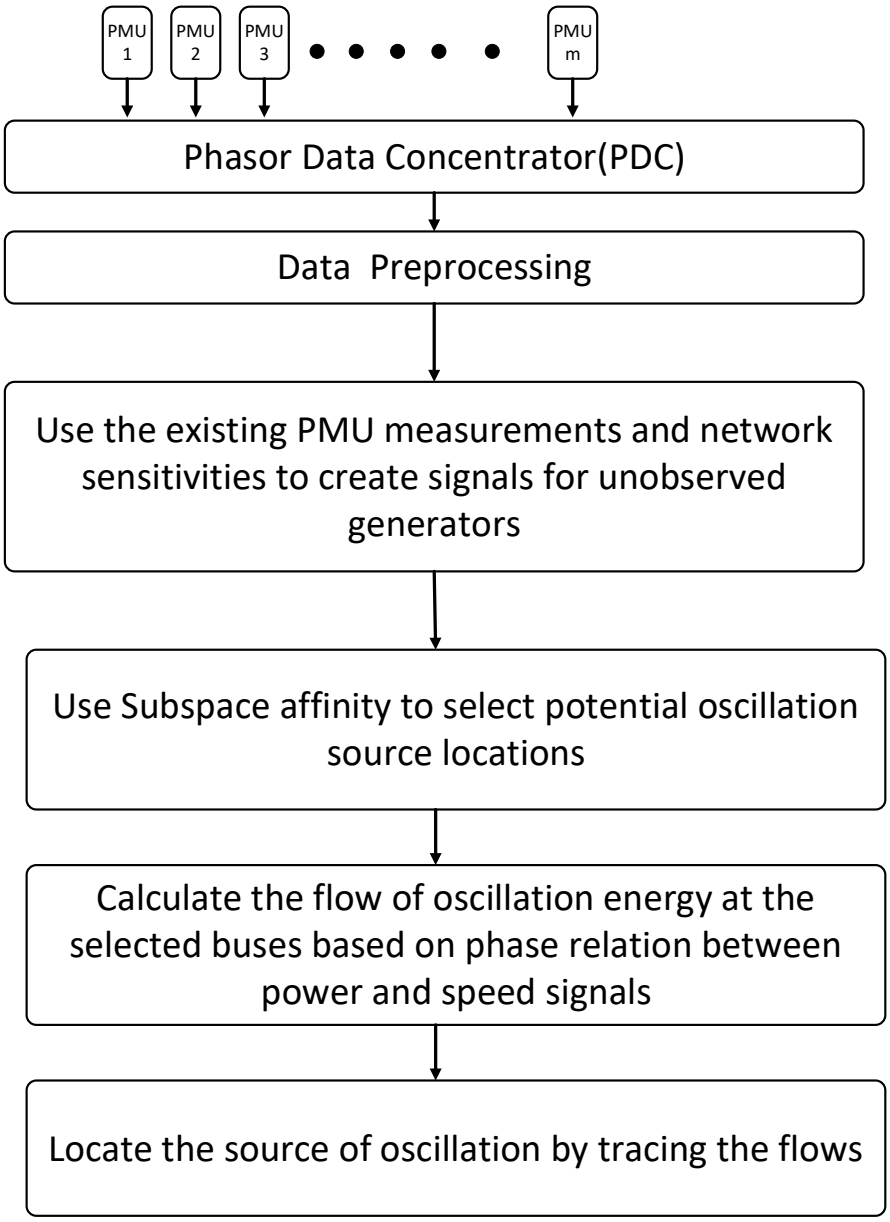

Figure 4.5: Flowchart of the proposed oscillation source location method.

cases are studied on this test system to test the peroformance of the proposed method.

4.3.1 Case 1:Single Frequency Oscillation Source

In this case a sinusoidal signal of 0.62 Hz is added as an external disturbance to the governor set point of generator 1. This is added to simulate the behaviour of a forced oscillations. In this case there are no PMU available at the terminal of the generators. So, the first step is to reconstruct power and speed signal of unobserved generator 1.Then affinity

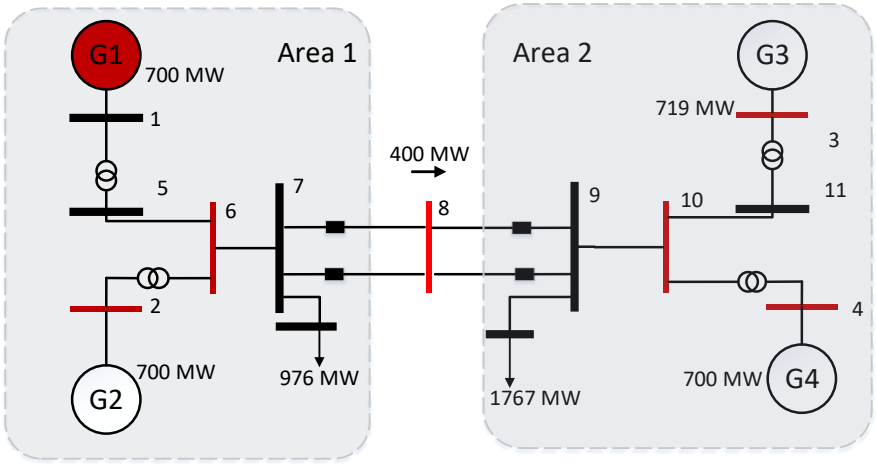

Figure 4.6: Modified two area four machine system with PMU.

based grouping is done to pre-select only a handful buses as a potential source. And then finally the phase difference between the power and speed signals are compared to find the direction of oscillation energy flow. Then by tracking the flow of oscillation energy source is located

4.3.1.1 Power and Speed Signal Reconstruction

In this section first the speed and power signal are reconstructed using the method described previously in the chapter. Fig. 4.7 shows the comparison of the reconstructed signals with the original signals.And the results show that the reconstructed signal follows the original signal very closely. So, if PMU is not available at the generator terminal or close by this method can be used to extract the modal information at the generator terminal.

4.3.1.2 Affinity based signal pre-selection

The affinity based grouping discussed in previous chapter have been used to find the group of signals where the oscillatory mode of interest is more prominent. The similarity graph is formed after calculating the affinity between each buses. After several iterations, the clustering algorithm provides four buses as a potential location of oscillation source. These buses are

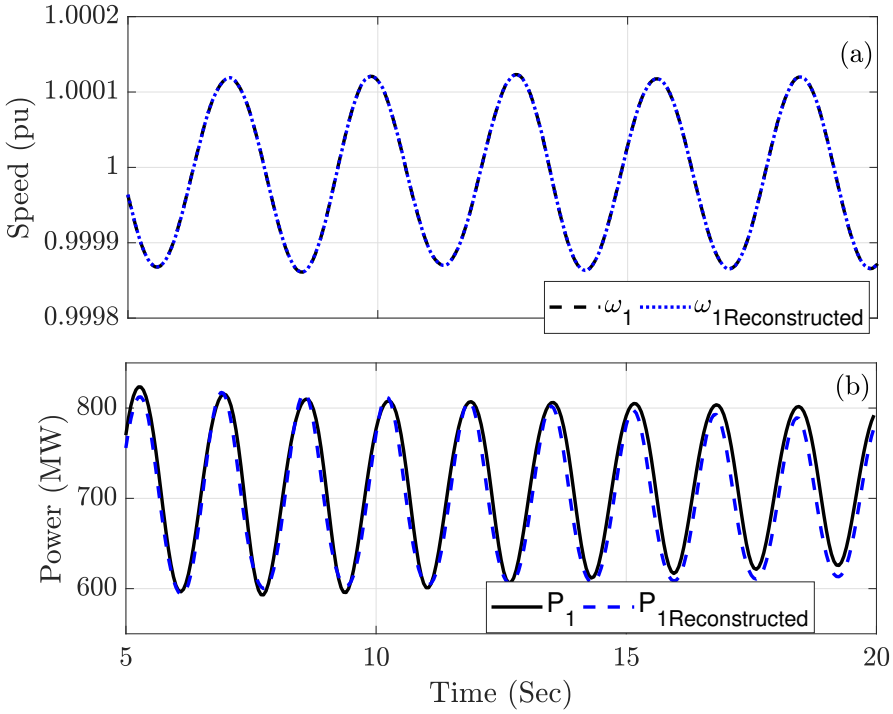

Figure 4.7: Power and speed signal reconstruction at generator 1.

4.3.1.3 Oscillation source location using the phasor relations

In this section the phase information of the power and speed signals are extracted using eigenvectors obtained from subspace identification. Table 4.1 shows the angles for each bus speed and branch power. Figure 4.8 shows the direction of energy flow in the network. By investigating the direction it is concluded correctly that the generator 1 is the source of oscillation.

Table 4.1: Case1: Oscillation Source Location .

Potential Location	ϕ_ω	Branch	ϕ_p	$\lvert\phi_p - \phi_\omega\rvert$	Energy Direction
1	5.3	1-5	39.45	29.15	1->5
5	-30.2	5-6	-84.30	54.1	5->6
2	-154.8	2-6	-45.20	109.6	6->2
6	-111.3	6-7	-35.14	76.16	6->7

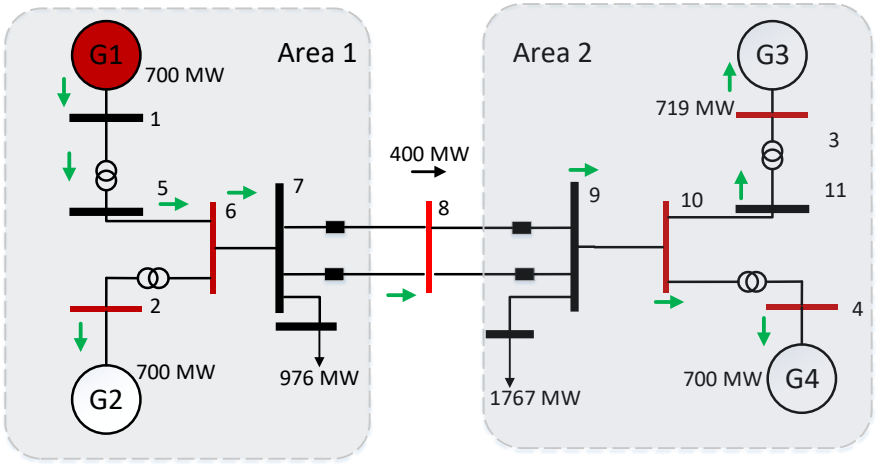

Figure 4.8: Oscillation energy direction.

4.3.2 Case 2:Multiple Oscillation Source

In this case a sinusoidal signal of 0.6 Hz is added as an external disturbance to the governor set point of generator 1 and another sinusoidal signal of 0.4 Hz is added to the governor set point of generator 4. This is added to simulate the behaviour of a forced oscillations. In this case there are no PMU available at the terminal of the generators. This is a case where multiple sources are present with two different frequencies. The subspace affinity grouping selects bus 1 ,5,2,6 as potential source locations for 0.6 Hz and bus 4,3,10,11 as potential source locations for 0.4 Hz. Table 4.2 shows the angles for each bus speed and branch power for 0.6 Hz and Table 4.3 shows for 0.4 Hz oscillation. Figure 4.9 shows the direction of energy flow in the network. similar to case 1 by investigating the direction it is concluded correctly that the generator 1 is the source of oscillation for 0.6 Hz oscillation frequency and generator 4 is the oscillation source for 0.4 Hz oscillation frequency .

Table 4.2: Case2: Oscillation Source Location for 0.6 Hz .

Potential Location	ϕ_ω	Branch	ϕ_p	$\lvert\phi_p - \phi_\omega\rvert$	Energy Direction
1	15.14	1-5	41.12	25.98	1->5
5	-38.48	5-6	-90.05	51.57	5->6
2	-168.2	2-6	-61.45	106.75	6->2
6	-101.4	6-7	-40.12	61.28	6->7

Table 4.3: Case2: Oscillation Source Location for 0.4 Hz .

Potential Location	ϕ_ω	Branch	ϕ_p	$\lvert\phi_p - \phi_\omega\rvert$	Energy Direction
4	15.41	4-10	39.45	29.15	4->10
3	-75.10	3-11	19.70	94.8	11->3
10	-85.75	10-9	-38.41	47.34	10->9
11	-125.41	11-10	-35.14	90.27	10->11

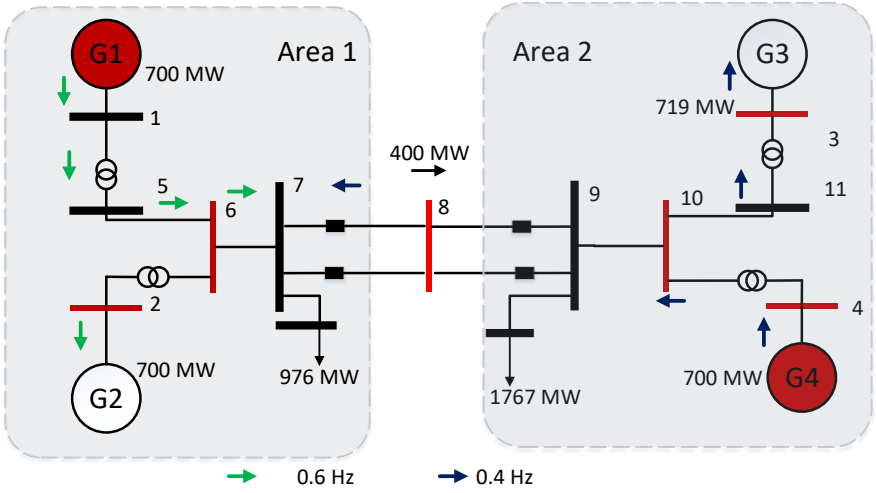

Figure 4.9: Oscillation energy direction.

4.4 Summary

In this chapter a method for locating the source of oscillation is proposed . The proposed method can detect the source of oscillations even if there is no PMU measurements available at the source generator buses. It gives accurate results for both single and multiple oscillation sources. Instead of calculating the large expression of dissipating energy it calculates only the phase difference between power and speed of each bus at the oscillation frequency. The method is easier to implement in an online environment and is not sensitive to data preprocessing. Location of oscillation source leads away the path to oscillation mitigation. In the next chapter, a model measurement based method will be presented that helps to capture the mismatch between model and measurement data.

CHAPTER 5: MEASUREMENT-MODEL BASED HYBRID APPROACH FOR MODEL VALIDATION

In this chapter, a new perspective is presented which analyses and characterize power system response based on developing the unmodeled dynamics of the system from event based measurement data. The approach uses a Multiple Input Multiple Output (MIMO) measurement based system identification that can be used to model the system dynamics utilizing the real system measurements. The unmodeled response of the power system is extracted using the model generated using measurements and the data from a linearized model of the power system at the same operating condition. With this information, system dynamics can be updated which can be further used for study and analysis of the grid under varying operating conditions. The simulation results show that analyzing unmodeled response helps to reliably detect the property of natural and forced oscillations. The results of this chapter has been published in the form of papers (85),(86).

5.1 Introduction

Oscillations are inherent characteristics of dynamic systems. They are broadly classified into electromagnetic and electromechanical oscillations. Electromagnetic oscillations have high frequency and are generally well damped because of internal damping of the power system. However, electromechanical oscillations have a lower frequency and requires additional controllers to damp. Based on the oscillation frequency electromechanical oscillations are divide into local oscillations (0.7 Hz to 2 Hz) and inter-area oscillations (01 Hz to 0.8 Hz) (9). Growing and sustained oscillations pose a serious threat to the reliable operation of the power system and limit the power transfer capacity of interconnected power systems (35). Traditionally, oscillations have been studied as a part of stability studies for different contingencies. Modes determined through modal analysis give the oscillations frequencies and associated damping of each oscillations(9). Modal analysis gives the modes using a lin-

earized model of power system but the actual system is nonlinear in nature. So, the actual response of a power system model can be significantly different from the linearized response. Authors in (9) present an analysis of the major power outage event occurred in western North America on August 10, 1996 and they conclude that there was a significant difference between the simulated model response and the actual system response. Although the simulated response showed significant damping for the oscillatory modes in actual system, there were negative damping which caused widespread outage. So, a model of the power system cannot always reliably estimate the actual oscillation frequency and damping present in the system.

Recently, real-time measurement devices such as phasor measurement unit (PMU) have been installed throughout the power system and coverage area is increasing very fast (37). PMU acquires data with a higher sample rate (120 or 240 samples per second offlate), and this data is able to capture the fast changes happening in the power system. In the last decades, several researchers have worked on these measurement data and several methods have been proposed that can estimate the modes and mode shapes using these data (12). Increased availability of PMU data allowed to capture oscillations in the frequency range of 0.1 HZ to 2 Hz which are not part of system natural response rather they are created by periodic external sources (38). These oscillations are termed as forced oscillations. The sources of forced oscillations include but not limited to cyclic load, stable limit cycles, wind plant controllers, malfunction of generator governor controller etc (39). The characteristics of forced oscillations are different than natural electromechanical oscillations. To take proper control action the type of oscillation needs to be identified. The authors of (5) have shown analytically the characteristics of forced oscillations and natural oscillations but these characteristics are difficult to extract if the oscillation sinusoids cannot be extracted from the noise. In (40) authors present a method that can simultaneously detect natural and forced oscillations, but the proposed method needs to be studied extensively for scenarios mentioned in the test case library (41). In (42) authors propose a method which analyses oscillation envelope shape to detect forced oscillation.

In spite of the advancements made in the measurement based methods on forced oscillation

detection, these methods lack an analytic approach based on the mathematical model of the power system. Several researchers have proposed different methods which take the linearized model of the system and forms an analytic expression for characterizing the system response to forced oscillations (43). However, these analytic methods work well for linearized models but for the actual power system, the performance of these methods decreases because of the nonlinearity and unmodeled dynamics. Nonlinearity can have a significant effect on the estimated modes from measurement data (44). It is clear that system model update critical to capture dynamic changes in the system. With the help of measurements that happens after an event, these updates are possible and can be characterized as unmodel dynamics.

In this chapter, a new perspective is adopted to develop the unmodeled dynamics of the system. In this approach first, a power system nonlinear model and a linearized model at that same operating condition are developed simultaneously and same disturbances are introduced in both the model. The response of both the models for different output signals is compared every 1 minute. the difference between the actual nonlinear power system response and the linearized model response accounts for the nonlinearity and unmodeled dynamics. Stochastic combined deterministic stochastic subspace identification (RCDSSI)is applied to these signals to estimate the modes and its damping.In recent years, a lot of research work has been conducted to develop methods which can detect and distinguish between forced and natural oscillations (87).(88). Some limitations of these methods include determining the start time of oscillation, and online estimation of detection threshold. In this chapter, a subspace identification based method is proposed which recursively identifies power system model and uses an offline dictionary to transform the identified model in a predefined state-space basis. Transforming the state space basis helps to compare the identified model with power system small-signal model. This comparison helps to detect the effect of nonlinearity and unmodeled dynamics (refer to power system components that are not modeled properly in power system model). Simulation results from two test systems and IEEE 39 bus test system show the efficacy of the proposed method. The main advantage of the proposed architecture is that with the technique updated power system model can be developed. Also, the estimated modes from the RCDSSI algorithm gives clear indication of the presence of

oscillations in the system. The main contributions are that the architecture:

- Proposes a generalized recursive algorithm for subspace identification, which reduces the computational burden by recursively performing Singular Value Decomposition (SVD) and LQ factorization.
- Identifies the model where the states represent the physical states of the power system. Identified model helps to understand the effect of nonlinearity and unmodeled dynamics.
- Identifies model in a state-space that helps to predict the dynamic response of the system, which is useful to predict the stability characteristics of the system.

The rest of the chapter is organized as follows. Section 5.2 provides a brief discussion on the methodology proposed to analyze unmodeled dynamics of system response and how this unmodeled response can be used to characterize system oscillations. Section 5.4 shows an illustrative example. The simulation results for different scenarios are discussed in section 6.5, and one application is illustrated in Section IV. The paper is concluded and the ongoing future work on this topic is discussed in section 5.7.

5.2 Proposed methodology

The proposed methodology is divided into three subsections. The first subsection discusses on how to extract unmodeled response and the characteristics of unmodeled response. The second section gives a brief description of the RCDSSI algorithm used for estimating system modes from measurement data. And the third section discusses the flow chart of the overall method.

5.2.1 Theory of Unmodeled Response

Fig. 5.1 shows the overall architecture of power system. Power system consists of many dynamic components and is in a constant state of motion due to changes in system dynamics. These dynamic changes can be due to load changes, control actions and known/unknown network topology changes. Also, internal or external disturbances in the system can cause changes in system dynamics. Mathematical models of power system have been used to

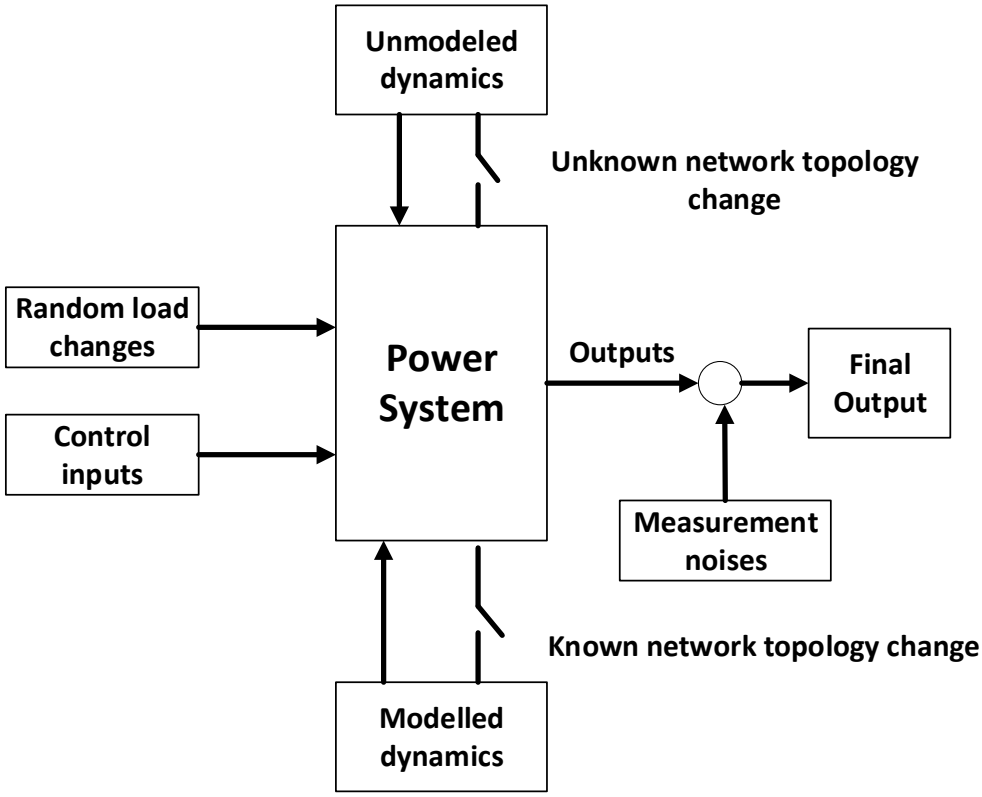

Figure 5.1: Overall architecture of power system response (5).

study the behaviors of the power system and these models give an accurate representation of the actual system if there are no unmodeled dynamics that exist in the system. However, most often in the actual system, there are some unmodeled dynamics because of nonlinear behaviors of loads, controllers etc. Unmodeled dynamics can be triggered due to events that occur internal or external to the system and can cause the actual system response to deviate a lot from the linearized response. Generally power system dynamic behaviors are mathematically modeled as (9)

$$\dot{\mathbf{x}} = \mathbf{f}(\mathbf{x}, \mathbf{u}) \tag{5.1}$$

$$\dot{\mathbf{y}} = \mathbf{g}(\mathbf{x}, \mathbf{u})$$

where $\mathbf{x}$ is the state vector and it's components x_i is state variable, $\mathbf{f}$ is the nonlinear function vector relating to the states and inputs to the rate of change of states, $\mathbf{y}$ is output vector and

$\mathbf{g}$ is the nonlinear function relating state variables and inputs to the outputs. The solution of (5.1) gives the state variables and output variables of the system.

To better understand and characterize the behaviour of power system, power system models are linearized around a known operating point. The fully deterministic linearized forms of equations can be represented as

$$\dot{\mathbf{x}} = \mathbf{A}\mathbf{x} + \mathbf{B}\mathbf{u} \tag{5.2}$$

$$\dot{\mathbf{y}} = \mathbf{C}\mathbf{x} + \mathbf{D}\mathbf{u}$$

where $\mathbf{A}$ is the state matrix of size $n \times n$, $\mathbf{B}$ is the input matrix of size $n \times r$, $\mathbf{C}$ is the input matrix of size $m \times n$ and $\mathbf{D}$ is the feedforward matrix of size $n \times r$. Performing Laplace transform of (5.2), the frequency domain representation is obtained as shown in (5.3). Rearranging (5.3) and after solving for output variables the expression for output is represented as (5.4) and the details can be found in (9).

$$s\mathbf{x}(\mathbf{s}) = \mathbf{A}\mathbf{x}(\mathbf{s}) + \mathbf{B}\mathbf{u}(\mathbf{s}) \tag{5.3}$$

$$\dot{\mathbf{y}(\mathbf{s})} = \mathbf{C}\mathbf{x}(\mathbf{s}) + \mathbf{D}\mathbf{u}(\mathbf{s})$$

$$\mathbf{y}(\mathbf{s}) = \mathbf{C}[\mathbf{s}\mathbf{I} - \mathbf{A}]^{-\mathbf{1}}[\mathbf{x}(\mathbf{0}) + \mathbf{B}\mathbf{u}(\mathbf{s})] + \mathbf{D}\mathbf{u}(\mathbf{s}) \tag{5.4}$$

After assuming that output $\mathbf{y}$ is not directly dependant on input $\mathbf{u}$ and transforming state variables, (5.4) can be rewritten as (5.5)

$$\mathbf{y}(\mathbf{s}) = [\mathbf{C}\mathbf{\Phi}[\mathbf{s}\mathbf{I} - \wedge]^{-\mathbf{1}}\mathbf{\Psi}\mathbf{B}]\mathbf{u}(\mathbf{s}) = \mathbf{G}(\mathbf{s})\mathbf{u}(\mathbf{s}) \tag{5.5}$$

where $\mathbf{\Phi} = [\mathbf{\Phi_1}\mathbf{\Phi_2}...\mathbf{\Phi_n}]$ is the right eigenvector and $\mathbf{\Psi} = [\mathbf{\Psi_1^T}\mathbf{\Psi_2^T}...\mathbf{\Psi_n^T}]$ is the left eigenvector. Eq. (5.5) is the general form of solution of output variables for linearized systems. Now depending upon the input $\mathbf{u}(\mathbf{s})$, the output response $\mathbf{y}(\mathbf{s})$ can be varied.

Inputs can be step changes or it can also be some periodic signals. Step changes in the input triggers the natural response of the system and periodic disturbances creates forced response. If the input is a step change then the the output variables of the system in time domain can be represented as in (5.6) and is termed as linear response.

$$\mathbf{y_{Linear}(t)} = \sum_{i=1}^{n} \mathbf{C\Phi_i\Psi_i B e^{\lambda_i t}} \tag{5.6}$$

The input can also be a periodic signal and can be of the form $\mathbf{u(t)} = ke^{jwt}$ to represent an external disturbance. Then the output response is termed as actual response and is given by (5.7)

$$\mathbf{y_{Actual}(t)} = \sum_{i=1}^{n} \mathbf{C\Phi_i\Psi_i B} \frac{\mathbf{k}}{\mathbf{j}\omega - \lambda_\mathbf{i}} (\mathbf{e^{j\omega t}} - \mathbf{e^{\lambda_i t}}) \tag{5.7}$$

The difference between actual and linear response is termed as unmodeled response and for a linear system an analytic expression can be written in the form

$$\mathbf{y_{Unmodeled}(t)} = \mathbf{y_{Actual}(t)} - \mathbf{y_{Linear}(t)} \tag{5.8}$$

$$\mathbf{y_{Unmodeled}(t)} = \sum_{i=1}^{n} \mathbf{C\Phi_i\Psi_i B} \frac{\mathbf{k}}{\lambda_\mathbf{i} - \mathbf{j}\omega} (\mathbf{e^{\lambda_i t}} - \mathbf{e^{j\omega t}}) - \sum_{i=1}^{n} \mathbf{C\Phi_i\Psi_i B e^{\lambda_i t}}$$

Eq. (5.8) can be rearranged as

$$\mathbf{y_{Unmodeled}(t)} = \sum_{i=1}^{n} (\mathbf{C\Phi_i\Psi_i B} \frac{\mathbf{k}}{\lambda_\mathbf{i} - \mathbf{j}\omega} - \mathbf{C\Phi_i\Psi_i B}) \mathbf{e^{\lambda_i t}} - \sum_{i=1}^{n} (\mathbf{C\Phi_i\Psi_i B} \frac{\mathbf{k}}{\lambda_\mathbf{i} - \mathbf{j}\omega}) \mathbf{e^{j\omega t}} \tag{5.9}$$

Eq. (5.9) shows that the contribution of natural response is less in unmodeled response compared to forced response in (5.7). In (5.9) a term is subtracted from the phase and

magnitude contribution of natural frequencies which means these frequencies have less contribution in the unmodeled response. Due to these characteristics, unmodeled response can be used to study the characteristics of external periodic forced oscillations as forced oscillations are more prominent in the unmodeled response.

There is no analytic expression for extracting unmodeled response from actual power system measurement data. System linear response is subtracted from measurement data to obtain the unmodeled response as given in (5.10)

$$\mathbf{y_{Unmodeled}}(\mathbf{t}) = \mathbf{y_{measurement}}(\mathbf{t}) - \mathbf{y_{Linear}}(\mathbf{t}) \tag{5.10}$$

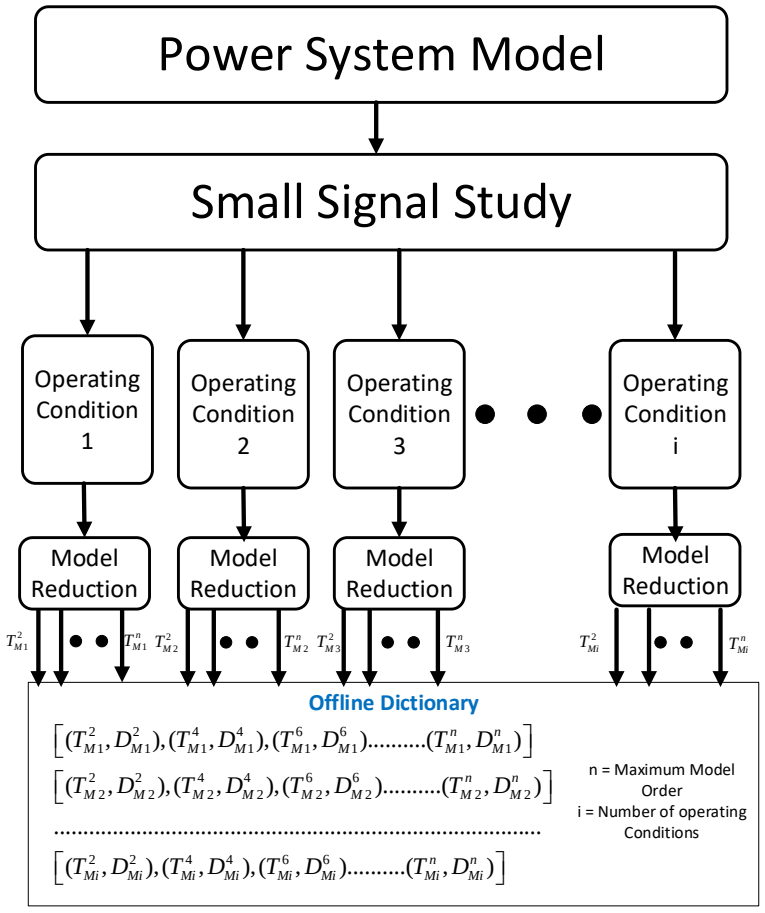

Figure 5.2: Flow Chart for the construction of model dictionary.

5.3 Methodology

Consider a power system response represented as a discrete time linear time invariant system

$$\mathbf{x_{k+1}} = \mathbf{Ax_k} + \mathbf{Bu_k} + \mathbf{w_k} \tag{5.11}$$
$$\mathbf{y_k} = \mathbf{Cx_k} + \mathbf{Du_k} + \mathbf{v_k}$$

where $u_k \epsilon R^m$ and $y_k \epsilon R^l$ are the observations at the time constant k of respectively m inputs and l outputs, w_k and v_k represents the process noise and measurement noise respectively, $\mathbf{A}$ is state transition matrix, $\mathbf{B}$ is input matrix and $\mathbf{C}$ is output matrix. The output response y_k as observed in PMU measurements contains the effect of system dynamics as defined by $\mathbf{A}$, input signals u_k, and also both process and measurement noises. The main goal of the subspace based methods to extract information only pertaining to $\mathbf{A}$ matrix which represents the system characteristics. The process is as follows.

5.3.1 Measurement Based Subspace Identification Models For Power Systems

From the PMU measurement data first input and output block Hankel matrices can be formed as below

$$\mathbf{H_y} = \begin{bmatrix} Y_p \\ \hline Y_f \end{bmatrix} = \frac{\begin{bmatrix} y_1 & \cdots & y_j \\ y_2 & \cdots & y_{j+1} \\ \vdots & \cdots & \vdots \\ y_i & \cdots & y_{j+i-1} \end{bmatrix}}{\begin{bmatrix} y_{i+1} & \cdots & y_{i+j} \\ y_{i+2} & \cdots & y_i + i + j + 1 \\ \vdots & \cdots & \vdots \\ y_{2i} & \cdots & y_{2i+j-1} \end{bmatrix}} \epsilon \mathbb{R}^{2i \times j} \tag{5.12}$$

$$\mathbf{H_u} = \left[\frac{U_p}{U_f}\right] = \frac{\begin{bmatrix} u_1 & \cdots & u_j \\ u_2 & \cdots & u_{j+1} \\ \vdots & \cdots & \vdots \\ u_i & \cdots & u_{j+i-1} \end{bmatrix}}{\begin{bmatrix} u_{i+1} & \cdots & u_{i+j} \\ u_{i+2} & \cdots & u_i + i + j + 1 \\ \vdots & \cdots & \vdots \\ u_{2i} & \cdots & u_{2i+j-1} \end{bmatrix}} \epsilon \mathbb{R}^{2i \times j} \tag{5.13}$$

where i is the number of block rows which is an user-defined index and must be larger than the order $2n$ of the system to capture all the system modes, and $j = l - 2i + 1$ and l is data window length. The input and output block Hankel matrices are divided into past and future input-output matrices Y_p, Y_f, U_p and U_f. When only output measurements are available with noise, then the system defined by (5.11) turns into a stochastic system as input u_k=0. The main goal of stochastic subspace identification (SSI) is to extract the extended observability matrix Λ_i from the orthogonal projection of Y_f on Y_p. The orthogonal projection can be computed using LQ decomposition,

$$\underset{\mathbb{R}^{i \times j}}{H_{1:j}} = \begin{bmatrix} Y_p \\ Y_f \end{bmatrix} = \begin{bmatrix} L_{11} & 0 \\ L_{21} & L_{22} \end{bmatrix} \tag{5.14}$$

$$Y_f / Y_p = L_{21} Q_{11}^T ; L_{21} Q_{11}^T = \Lambda_i X_i \tag{5.15}$$

where L_{ij} represents the lower triangular matrix of LQ decomposition and Q_{ij} represents the orthogonal matrix. Eqn. (5.14) shows that the extended observability matrix (Λ_i) can be calculated from the column space of $\mathbf{L_{21}}$.

The above can be represented as a combined deterministic-stochastic system identification (CDSSI) using both input and output information to isolate only the system characteristics

related to A matrix in (5.11). This can be written (89) as

$$\begin{aligned} Y_p &= \Lambda_i X_p + H_i^d U_p + Y_p^s \\ Y_f &= \Lambda_i X_f + H_i^d U_f + Y_f^s \\ X_f &= A_i X_p + \Delta_i U_p \end{aligned} \tag{5.16}$$

where Δ_i is the reverse extended controllability matrix, H_i^d is the low block triangular Toeplitz matrix (61) and Y_p^s,Y_f^s represents the stochastic part of the measured signals.

It is worth noting that only extracting Λ_i from the above set of equations is enough to extract the modal properties of the system. Λ_i can be extracted by applying LQ decomposition on the subspace expanded by the row space of input/output block Hankel matrices.

$$\underset{\mathbb{R}^{i\times j}}{H_{1:j}} = \begin{bmatrix} U_f \\ W_p \\ Y_f \end{bmatrix} = \begin{bmatrix} L_{11} & 0 & 0 \\ L_{21} & L_{22} & 0 \\ L_{31} & L_{32} & L_{33} \end{bmatrix} \begin{bmatrix} Q_{11}^T \\ Q_{21}^T \\ Q_{31}^T \end{bmatrix} \tag{5.17}$$

$$(Y_f /_{(} U_f) W_p) = \Lambda_i X_i / U_f^{|} = L_{32} Q_{21}^T \tag{5.18}$$

where W_p is the combined subspace of both past input and output block Hankel matrices U_p and Y_p. Eqn. (5.18) calculates the oblique projection of the future outputs on the past input/output along with the future inputs. Column space of L_{32} is equal to the column space of extended observability matrix Λ_i. So only extracting L_{32} from the LQ decomposition of the whole subspace is enough to get the system characteristics.

The projected matrix O is expressed as,

$$\underset{\mathbb{R}^{i\times j}}{O} = \begin{cases} L_{21}, \text{if only output measurements are used} \\ L_{32}, \text{if both input and output are used} \end{cases} \tag{5.19}$$

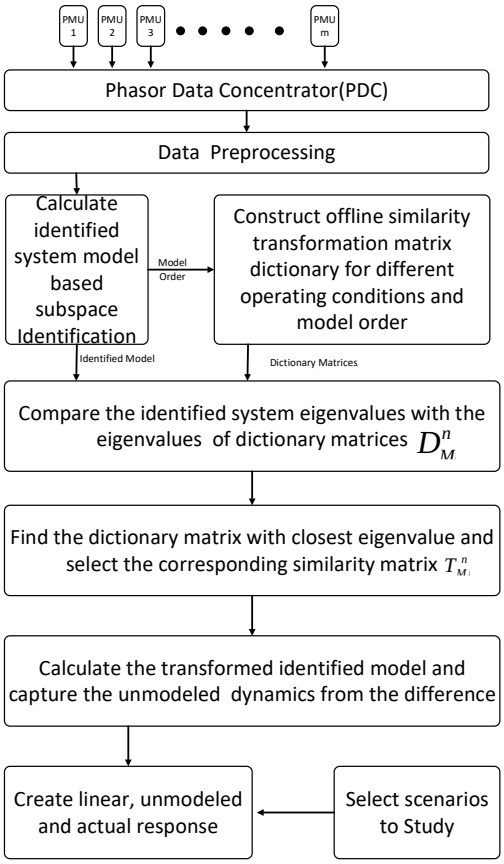

Figure 5.3: Flow Chart for the proposed model validation framework.

5.3.2 Determining Weighting Factors for Identified Models

In subspace identification, the state-space matrices are only recovered up to within a similarity transformation. This means although the response of the identified system matches with the response of the actual system, the states of the identified system does not necessarily match with the dynamical system, which is being identified. The state-space basis can be predefined by introducing weighting factors W_1 and W_2, and that by a proper choice of these weights, the basis can be altered in a user-controlled manner (61). Determining the values of the weighting factors are similar to finding the frequency weight balances used in balanced truncation for model reductions (90). The frequency weight balancing is used for model reduction to ensure the frequency of interest is captured in the reduced model. The key idea is to find the frequency weighted controllability Grammian $W_u(z)$ and observability Grammian $W_y(z)$. Then find the similarity transformation which makes the both

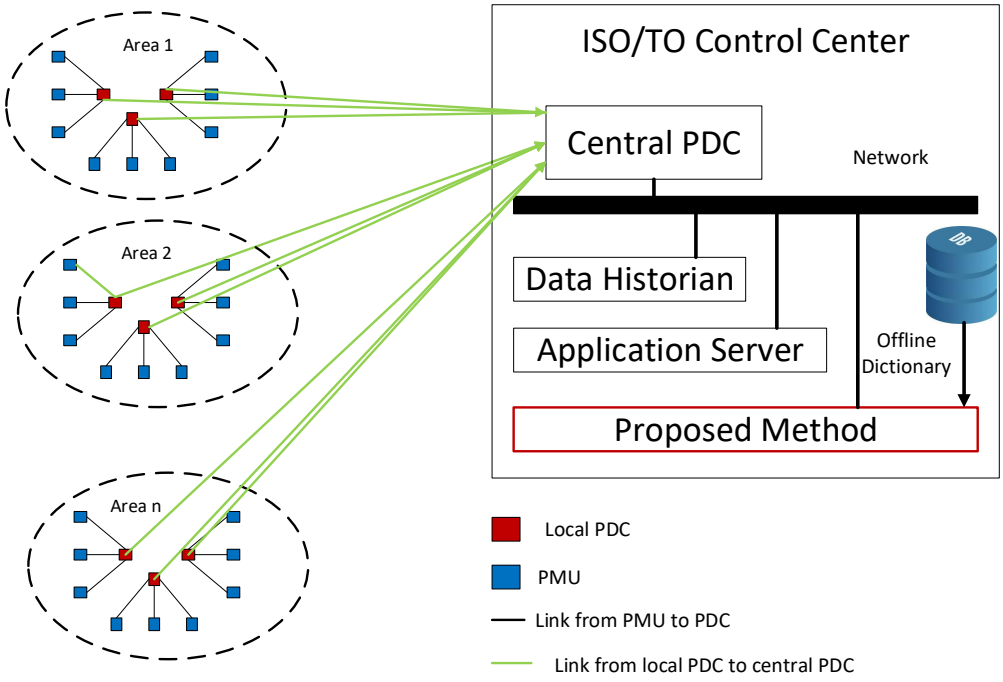

Figure 5.4: Practical Implementation framework of the proposed method.

Grammians diagonal and equal to each other (5.20).

$$W_u(z) = \Delta_i^d [W_u W_u^T] (\Delta_i^d)^T + \Delta_i^s (\Delta_i^s)^T \tag{5.20}$$

$$W_y(z) = \Lambda_i^T [W_y^T W_y] \Lambda_i \tag{5.21}$$

$$W_u(z) = W_y(z) = \sum_{i=1}^{N} \sigma_i \tag{5.22}$$

where Δ_i^d is the deterministic part of extended controllability matrix and Δ_i^s is the stochastic part of extended controllability matrix, σ_i is the frequency weighted Hankel Singular Values.

For an asymptotically stable system and when the data length of the system is infinite, the weighting factors W_1 and W_2 can be expressed as in eqns. (5.23). Details of the derivation can be found in (61).

$$W_1 = W_y \tag{5.23}$$

$$W_2 = U_p^T (R_P^{uu})^{-1} W_u (L_p^{uu})^{-1} U_p + \pi_{U_p^*} \tag{5.24}$$

$$W_u = \begin{bmatrix} D_u & \cdots & 0 \\ \vdots & \vdots & 0 \\ C_u A_u^{i-2} B_u & \cdots & D_u \end{bmatrix} \tag{5.25}$$

$$W_y = \begin{bmatrix} D_y & \cdots & 0 \\ \vdots & \vdots & 0 \\ C_y A_y^{i-2} B_y & \cdots & D_y \end{bmatrix} \tag{5.26}$$

$$W_u(z) = W_y(z) = S_1 \tag{5.27}$$

where L_p^{uu} is the Markov parameters of the spectral characteristics of input, U_p is past Block Hankel matrix formed from measurement data, S_1 is the singular values of extended observability matrix. The above equations implies that the frequency weighted observability and controllability matrices used in model reduction is equal to singular values of identified extended observability matrix (61).

5.3.3 Calculation of System Matrices

The system matrices A, B, C, D can be extracted with the help of weighted projection matrix O. Singular value decomposition (SVD) is performed on the weighted projected matrix to obtain U_1 and S_1. Both W_1 and W_2 are considered to be identity matrices.

$$W_1 O W_2 = U S V^T \tag{5.28}$$

$$U_1 = U(1:n); S_1 = S(1:n), n \;\; modelorder \tag{5.29}$$

$$\Gamma_i = U_1 \sqrt{S_1}, \Gamma_{i-1} = \bar{\Gamma}_i \tag{5.30}$$

Solve the set of linear equations for calculating A and C,

$$\frac{\Gamma_{i-1}^{\dagger}.Z_{i+1}}{Y_i} = (\frac{A}{C}).\Gamma_i^{\dagger}Z_i + KU_f + P \tag{5.31}$$

$$K = (\begin{bmatrix} B|\Gamma_{i-1}^{\dagger}.H_{i-1}^d - A.\Gamma_i^{\dagger}.H_i^d \\ D|0 - C.\Gamma_i^{\dagger.H_i^d} \end{bmatrix}) \tag{5.32}$$

where $Z_i = Y_f/[W_pU_f]$,$Z_{i+1} = [Y_f^- W_p^+ U_f^-]$ and P is the residual.And then B and D is calculated by solving the least square problem described in (6.10). The details of how to solve the least square problem can be found in (61).

$$\frac{\Gamma_{i-1}^{\dagger}.Z_{i+1}}{Y_i} = (\frac{A}{C}).\Gamma_i^{\dagger}Z_i + KU_f + P \tag{5.33}$$

$$K = (\begin{bmatrix} B|\Gamma_{i-1}^{\dagger}.H_{i-1}^d - A.\Gamma_i^{\dagger}.H_i^d \\ D|0 - C.\Gamma_i^{\dagger.H_i^d} \end{bmatrix}) \tag{5.34}$$

The matrices extracted are used to formulate the identified model of the system.

5.3.4 Balanced Truncation Based Reduced Order Model of Power System

Similarity transformation is first represented by Lyapunov equations as

$$\mathbf{AP} + \mathbf{PA^T} + \mathbf{BB^T} = \mathbf{0} \tag{5.35}$$

$$\mathbf{A^TQ} + \mathbf{QA} + \mathbf{C^TC} = \mathbf{0}$$

From this balancing equations can be constructed as

$$\tilde{\mathbf{x}} = \mathbf{T}\mathbf{x} \tag{5.36}$$

$$e^{\mathbf{A}t}\mathbf{B} = \mathbf{T}e^{\mathbf{A}t}\mathbf{T^{-1}}\mathbf{T}\mathbf{B} = \mathbf{T}e^{\mathbf{A}t}\mathbf{B} \tag{5.37}$$

$$\tilde{\mathbf{P}} = \mathbf{T}\mathbf{P}\mathbf{T}' \tag{5.38}$$

$$\mathbf{C}e^{\mathbf{A}t} = \mathbf{C}\mathbf{T^{-1}}\mathbf{T}e^{\mathbf{A}t}\mathbf{T^{-1}} = \mathbf{C}e^{\mathbf{A}t}\mathbf{T^{-1}} \tag{5.39}$$

$$\tilde{\mathbf{Q}} = \mathbf{T^{-1}}'\mathbf{Q}\mathbf{T^{-1}} \tag{5.40}$$

where $\tilde{\mathbf{P}}$ is the transformed controllability matrix and $\tilde{\mathbf{Q}}$ is the transformed observability matrix. Computing the balancing transformation T_B and ensuring that the states of the system are preserved, this problem will be equivalent to minimizing the following linear optimization problem.

$$\min_{\mathbf{T}\epsilon GL(N)} f(\mathbf{T}) = \min_{\mathbf{T}\epsilon GL(N)} trace(TPT' + T^{-1}{}'QT^{-1}) \tag{5.41}$$

$$\text{subject to}, f(\mathbf{T_B}) = 2\sum_{i=1}^{N}\sigma_i$$

$$\mathbf{A}\mathbf{P} + \mathbf{P}\mathbf{A^T} + \mathbf{B}\mathbf{B^T} = \mathbf{0}$$

$$\mathbf{A^T}\mathbf{Q} + \mathbf{Q}\mathbf{A} + \mathbf{C^T}\mathbf{C} = \mathbf{0}$$

$$\tilde{\mathbf{A}} = \mathbf{T_B}\mathbf{A}\mathbf{T_B^{-1}},\ \ \tilde{\mathbf{B}} = \mathbf{T_B}\mathbf{B},\ \ \tilde{\mathbf{C}} = \mathbf{C}\mathbf{T_B^{-1}}$$

$$\tilde{\mathbf{A}} = \begin{bmatrix} \tilde{A}_{11} & \tilde{A}_{12} \\ \tilde{A}_{21} & \tilde{A}_{22} \end{bmatrix},\ \ \tilde{\mathbf{B}} = \begin{bmatrix} \tilde{B}_1 \\ \tilde{B}_2 \end{bmatrix},\ \ \tilde{\mathbf{B}} = \begin{bmatrix} \tilde{C}_1 & \tilde{C}_2 \end{bmatrix}$$

$$\mathbf{A_r} = \tilde{A}_{11}\epsilon\mathbb{R}^{r\times r},\ \ \mathbf{B_r} = \tilde{B}_1\epsilon\mathbb{R}^{r\times p}$$

$$\mathbf{C_r} = \tilde{C}_1 = I_{q\times r}\epsilon\mathbb{R}^{q\times r},\ \ \mathbf{D_r} = 0\epsilon\mathbb{R}^{q\times p}$$

5.3.5 Offline construction of Model Dictionary

At a given time, the power system model is expressed as a combination of differential and algebraic equations.

$$\dot{x} = f(x, u) \tag{5.42}$$
$$\dot{y} = g(x, u)$$

where x is the state vector, u is the input vector and y is the output vector to the system. The differential equations represent different power system components and the algebraic equations represent the network topology. For stability analysis these nonlinear equations are linearized at an operating condition and the small signal model of the system is formed as

$$\Delta\dot{x} = A\Delta x + B\Delta u \tag{5.43}$$
$$\Delta y = C\Delta x + D\Delta u$$

where Δx is the state vector, Δy is the output vector, Δu is the input vector. A is the state matrix, B is the input matrix, C is the output matrix, and D is the feed-forward matrix. The frequency and damping ratio of the oscillatory model are calculated from the eigenvalues (9). The A matrix can then be converted to Canonical Jordan form using

$$D = T_M^{-1} A T_M \tag{5.44}$$

where T_M is the right eigenvector of A. The size of T_M varies depending on the size of A. This transformation matrix T_M is stored in the dictionary. Overall flowchart to construct the model dictionary is represented in Fig. 5.2. Small signal stability analysis is performed on the power system model of the power grid for different operating conditions. Also, reduced

order models are derived for each operating conditions. The similarity transformation matrix is calculated for each scenarios and are stored in an offline dictionary.

5.3.6 Approach for Studying the Unmodeled Response

In this section, how different responses are calculated and how these responses can be used to update the power system model continuously to perform what if scenarios to predict the response of actual nonlinear system is discussed. Moreover, how analysis of these responses can help to identify different oscillations are also discussed. Fig. 5.3 illustrates the steps of calculating different responses. First, the operating condition of the system is determined. Then the actual response of the power system is captured from measurement data and the linear response of the system is obtained from the linearized model. The difference between these two response is calculated to capture the unmodeled response. Then all three responses are passed to three RCDSSI algorithm block which applies the algorithm mentioned in section 5.3.3 on three separate response, identifies the mathematical models and estimates the modes for three responses. The combination of linear model and unmodeled response model gives the actual behavior of the power system obtained from measurement data. Then the combination of these two mathematical model can be used to study the actual behavior of the system for different what if scenarios. Ideally, only linear model of the system can not predict the response of power system. So, having an additional model for the unmodeled dynamics which captures nonlinearities, external disturbances, components which are not modelled in detail etc, helps to accurately predict the power system response. Moreover, these models helps to characterize power system oscillations as well. Combination of unmodeled response and knowledge about system modes at that operating condition helps to identify forced oscillation even if it has the same frequency as natural oscillation frequency. Forced oscillation frequencies are prominent in unmodeled response and the characteristics are easily identified from unmodeled response. After the forced oscillation frequencies are determined it is compared with the natural oscillation frequencies and decision are taken on the type of oscillation.

5.4 An Illustrative Example

In this section, a three machine 9 bus system (Fig. 5.5) is used to show a numerical example of the proposed method. For simplicity only classical models are considered here. The equation of motion of synchronous machine i is

$$\frac{2H_i}{\omega}\frac{d^2\delta_i}{dt^2} = P_{mi} - P_{ei} \tag{5.45}$$

where H_i is the inertia constant of ith machine, δ_i is the machine angle of ith machine, P_{mi} is the constant mechanical power and P_{ei} is the electrical power of the ith machine.

5.4.0.1 Dictionary Construction

The linearized model equations of the three machine system are given by

$$\frac{2H_i}{\omega}\frac{d^2\delta_{\Delta i}}{dt^2} + \sum_{i,j=1,j\neq i}^{n} P_{s(i,j)}\delta_{\Delta(i,j)} = 0 \tag{5.46}$$

After rearranging the equations (5.46) and then subtracting $3rd$ machine equation from the first two equations we get

$$\frac{d^2\delta_{\Delta 13}}{dt^2} + \underbrace{\left(\frac{\omega}{2H_1}P_{s12} + \frac{\omega}{2H_1}P_{s13} + \frac{\omega}{2H_3}P_{s31}\right)}_{a_{11}}\delta_{\Delta 13} \tag{5.47}$$

$$+ \underbrace{\left(\frac{\omega}{2H_3}P_{s32} - \frac{\omega}{2H_1}P_{s12}\right)}_{a_{12}}\delta_{\Delta 23} = 0$$

$$\frac{d^2\delta_{\Delta 23}}{dt^2} + \underbrace{\left(\frac{\omega}{2H_3}P_{s31} - \frac{\omega}{2H_2}P_{s21}\right)}_{a_{21}}\delta_{\Delta 13} \tag{5.48}$$

$$+ \underbrace{\left(\frac{\omega}{2H_2}P_{s21} + \frac{\omega}{2H_2}P_{s23} + \frac{\omega}{2H_3}P_{s32}\right)}_{a_{22}}\delta_{\Delta 23} = 0$$

The state space representation of the system is expressed as

$$\begin{bmatrix} \dot{\delta}_{13} \\ \dot{\delta}_{23} \\ \dot{\omega}_{13} \\ \dot{\omega}_{23} \end{bmatrix} = \underbrace{\begin{bmatrix} 0 & 0 & 1 & 0 \\ 0 & 0 & 0 & 1 \\ -a_{11} & -a_{12} & 0 & 0 \\ -a_{21} & -a_{22} & 1 & 0 \end{bmatrix}}_{A} \begin{bmatrix} \delta_{13} \\ \delta_{23} \\ \omega_{13} \\ \omega_{23} \end{bmatrix} \tag{5.49}$$

After plugging in the values of all the machine and network parameters (6) the calculated A matrix is

$$A = \begin{bmatrix} 0 & 0 & 1 & 0 \\ 0 & 0 & 0 & 1 \\ -104.096 & -59.524 & 0 & 0 \\ -33.841 & -153.460 & 0 & 0 \end{bmatrix} \tag{5.50}$$

The right eigenvector of the A matrix gives similarity transformation T_M4 which converts A to a Canonical Jordan form D. The similarity matrix T_M4 is stored in the dictionary.

$$D = \begin{bmatrix} -13.4164j & 0 & 1 & 0 \\ 0 & 13.4164j & 0 & 1 \\ 0 & 0 & -8.8067j & 0 \\ 0 & 0 & 0 & 8.8067j \end{bmatrix} \tag{5.51}$$

$$T_M4 = \begin{bmatrix} -0.0459j & 0 & 1 & 0 \\ -0.0585j & 13.4164j & 0 & 1 \\ 0.6154 & 0 & -0.9075 & -0.9075b \\ 0.7847 & 0.7847 & 0.4046 & 0.4046 \end{bmatrix} \tag{5.52}$$

5.4.0.2 Model identification

The response of the system is captured through nonlinear simulation (Fig. 5.14) following a load change at bus 8 of the 3 machine 9 bus system. The identified $4th$ order system matrix is given by,

$$A_{Identified} = \begin{bmatrix} 0.0035 & -4.8922 & 7.2137 & -1.5919 \\ 4.8879 & 0.0017 & -1.5599 & -11.4508 \\ -7.2159 & 1.5639 & 0.0010 & -6.7216 \\ 1.5804 & 11.4517 & 6.7350 & -0.0046 \end{bmatrix} \tag{5.53}$$

The identified model is expressed in Jordan canonical form as,

$$T_{Identified} = \begin{bmatrix} 13.4145j & 0 & 1 & 0 \\ 0 & -13.4115j & 0 & 1 \\ 0 & 0 & 8.7963j & 0 \\ 0 & 0 & 0 & 8.7963j \end{bmatrix} \tag{5.54}$$

5.4.0.3 Identified Model Transformation

The $T_{Identified}$ model is then converted to system small signal model with the help of similarity transformation matrix T_M4 stored in the dictionary. The transformed matrix $A_{Transformed}$ is comparable with the system small signal model state matrix A as the norm of $|A_{Transformed} - A|$ is 0.0103.

$$A_{Transformed} = T_M 4 * T_{Identified} * T_M 4^{-1} \tag{5.55}$$

$$= \begin{bmatrix} 0.0000 & 0.0000 & 0.9991 & 0.0000 \\ 0.0000 & 0.0000 & 0.0003 & 0.9996 \\ -104.0219 & -59.5621 & 0.0000 & 0.0001 \\ -33.8627 & -153.4175 & 0.0000 & 0.0001 \end{bmatrix}$$

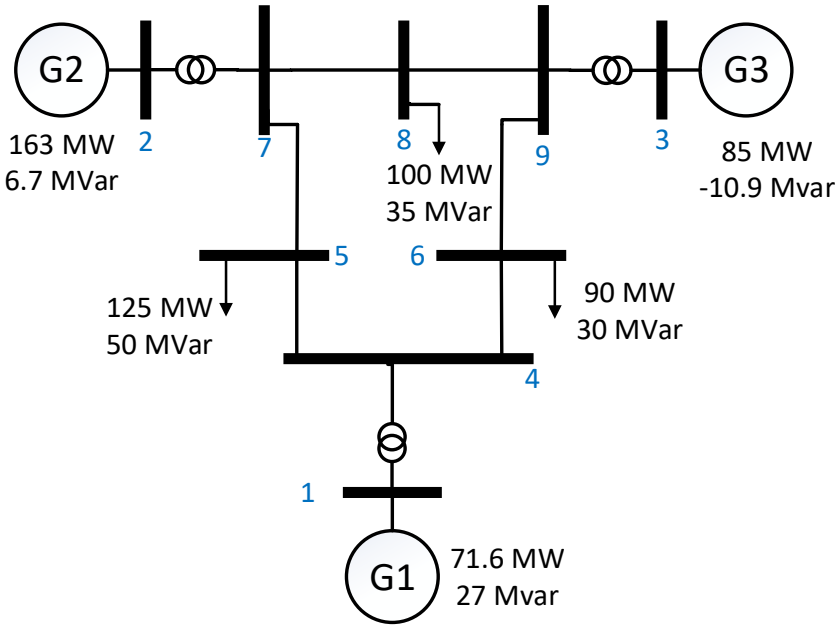

Figure 5.5: Three machine nine bus study system (6).

5.5 Simulation Results and Discussion

Fig. 6.3 shows the test system used for studying the proposed approach of analyzing unmodeled dynamics and how it can be used to characterize power system oscillations. The test system used is a classical two area four machine system which has been used widely in literature for studying oscillations. For the studies performed in this paper, all the generators are modeled in detail along with exciters, governors and power system stabilizers (PSS). The Power System Toolbox package (91) is used to perform linear simulations and Real-Time Digital Simulator (RTDS) is used for nonlinear simulations.

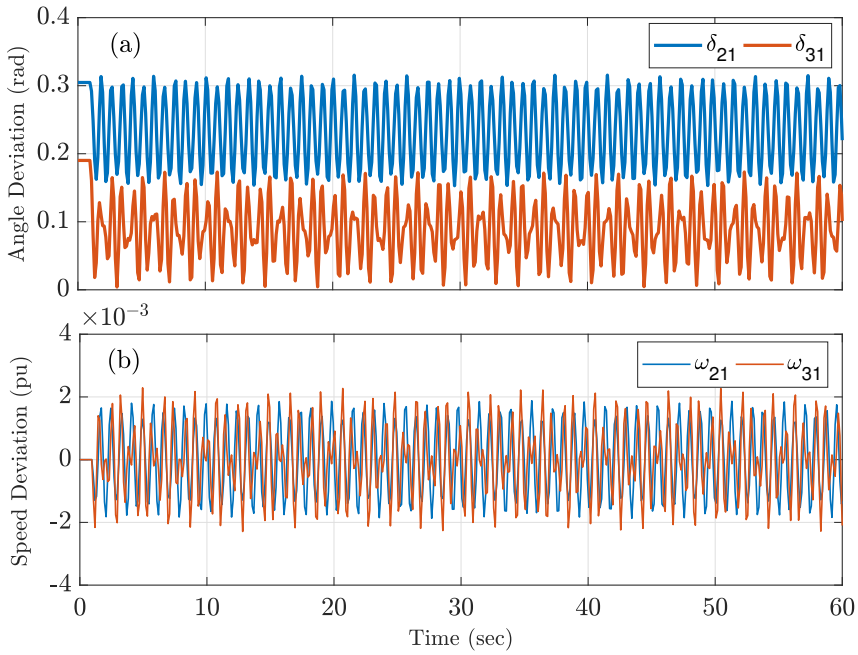

Figure 5.6: Machine a) angle deviation and b) speed deviation from nonlinear simulation after applying 20% load change in bus 8.

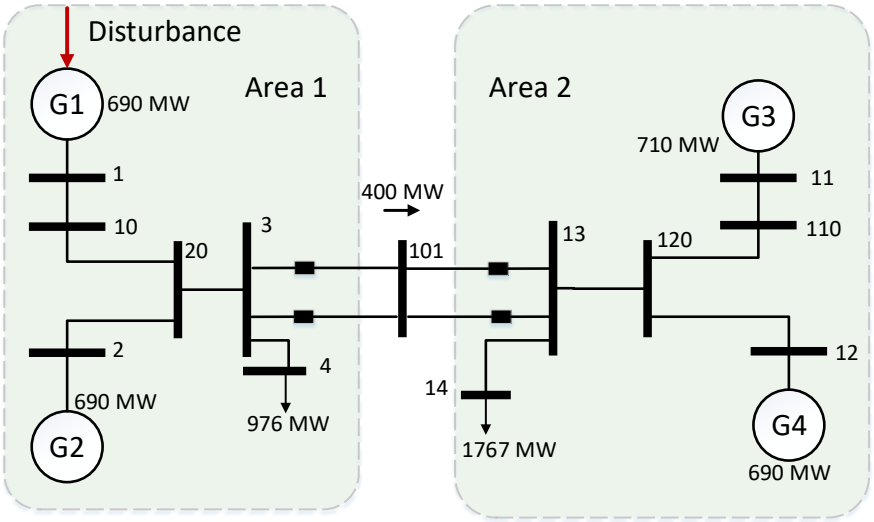

Figure 5.7: Two-area four-machine study system.

5.5.1 Case 1:Analysis of unmodeled response on a linear system

The goal of this study is to simulate a forced oscillation at a different frequency than natural oscillations and study how extracting the unmodeled dynamics helps to characterize forced oscillations. For, this case a linearized model of two areas system is used. System

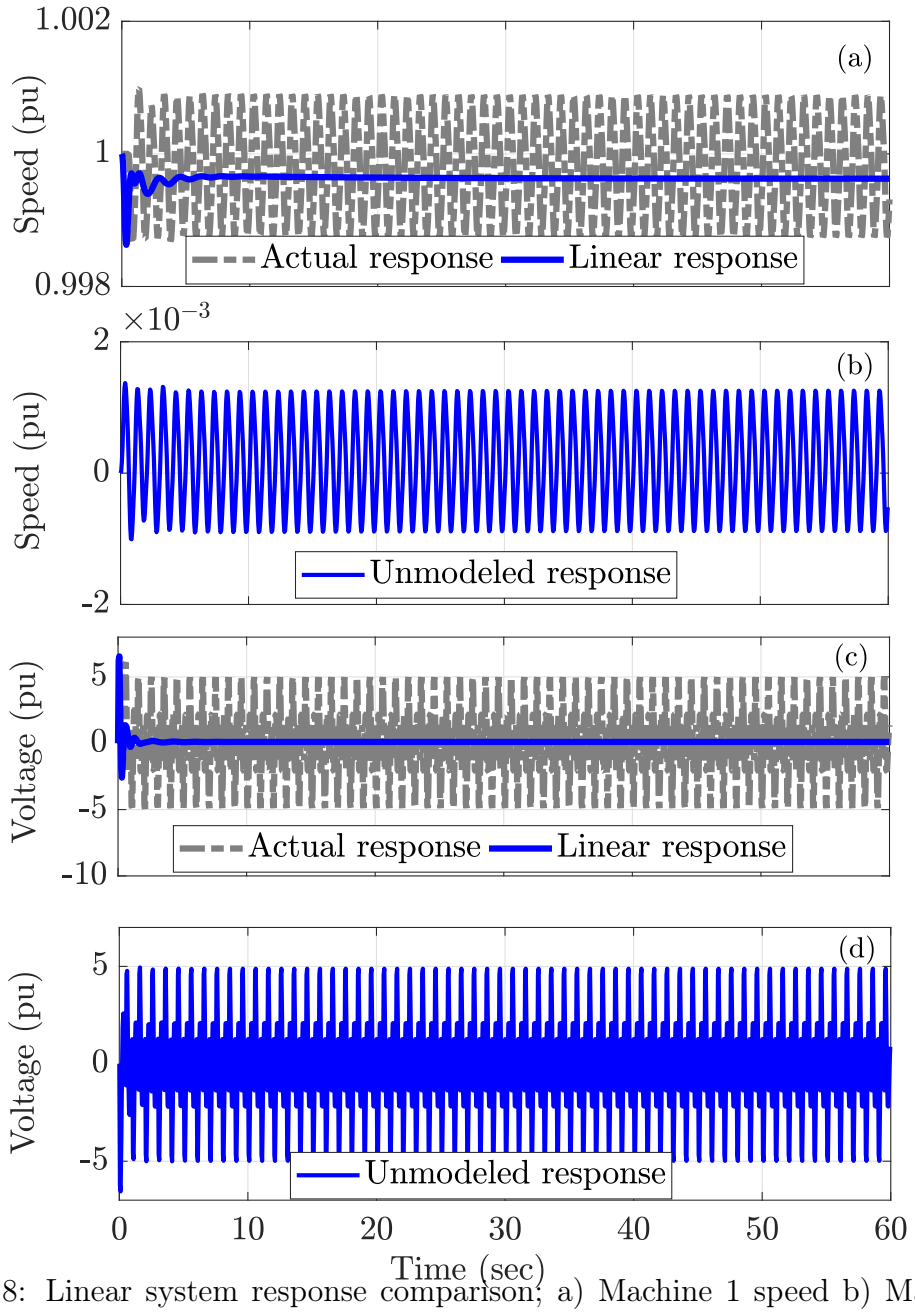

Figure 5.8: Linear system response comparison; a) Machine 1 speed b) Machine 1 speed unmodeled response c) Machine 1 field excitation voltage and d)Machine 1 field excitation voltage unmodeled response.

response to a step change is termed as linear response and to a periodic external disturbance is termed as actual response as it simulates system response with forced oscillation. Forced oscillation is simulated as a square wave of $1Hz$ frequency and $0.05pu$ magnitude, and is applied to exciter voltage reference of generator 1 to represent a limit cycle on the

exciter voltage limit. Modal analysis of the linear system gives the electromechanical modes that are mainly excited by applying disturbance to machine 1 exciter. These modes have frequencies of 1.36 Hz, 0.6125 Hz, 2.48 Hz, 1.31 Hz and damping ratio of 35.33%, 13.5%, 30.7% and 36.5% respectively. Machine speeds are recorded as output and machine field excitation voltages are taken as input to the RCDSSI algorithm for estimating the oscillation frequency and corresponding damping ratios. Fig. 5.8 shows the comparison of linear response of the systems with the actual response and it also shows the difference between these two response which is termed as unmodeled response. Fig. 5.8a illustrates that linear response dampens very quickly as all the excited modes have good damping ratios but actual response shows sustained oscillation throughout the simulation as it is excited by an external source. Fig. 5.8b, 5.8c and 5.8d gives the unmodeled response of speed, linear and actual response of voltage excitation and unmodeled response of voltage excitation respectively. Forced oscillation response is also visible in the extracted unmodeled response. Similarly, unmodeled dynamics are extracted for all machine speeds and excitation voltages. Then excited oscillation frequencies and damping ratios are estimated using RCDSSI for three types of response signals linear, actual and unmodeled. Normalized value of residue for the excited modes is also calculated to find out the relative contribution of each mode in the output signals. Table 5.1 summarizes the results for different, responses. As expected linear response properly estimates the excited modes. Actual response captures the natural modes as well as the forced oscillation frequencies. As the simulated forced oscillation is a square wave of 1 Hz frequency it consists of odd harmonics sinusoids. Presence of odd harmonics in the system response is an indication of the presence of forced oscillation (5). The forced oscillation frequency of 1 Hz and it's odd harmonics at 3 Hz and 5 Hz are identified. The unmodeled response also captures the forced oscillation and natural oscillation frequencies. It is noticeable from Table 5.1 that in unmodeled response the normalized residue of natural oscillation frequencies are very low compared to the forced oscillation frequencies which mean unmodeled response is dominated by the forced oscillations. Hence, analyzing the unmodeled response along with the natural response can help to get more insight into the oscillation type. Also, the identification of forced oscillation from unmodeled response helps

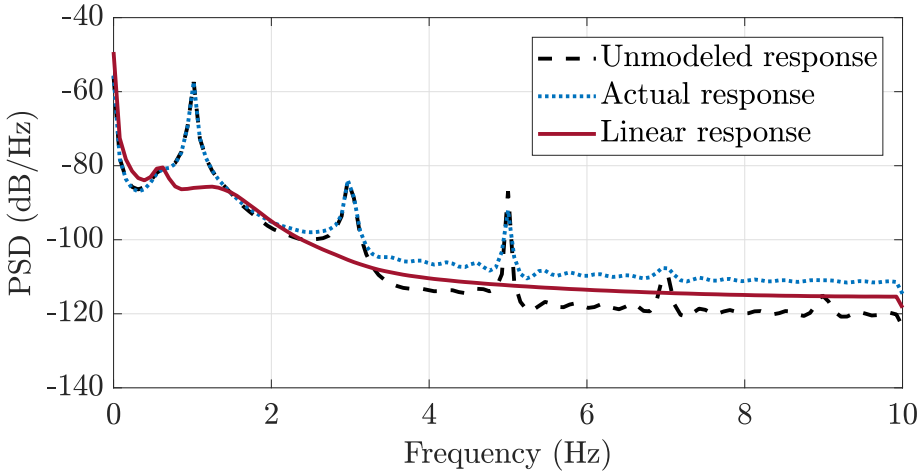

Figure 5.9: Power spectral density (PSD) comparison for different responses of linear system machine 1 speed.

to update the linear model of the system and give an external periodic signal of 1 Hz square wave to the linear model. In that case the linear model response matches exactly with the actual response. Thus, the model of the system can be constantly updated to match with the actual system response. The results of the RCDSSI algorithm is verified using a nonparametric method called Welch's Periodogram with a sampling frequency of 20 Hz, windows size of 1024 samples and an overlap of 128 samples. Fig. 5.9 illustrates power spectral density (PSD) for different responses. For actual and unmodeled response there are multiple peaks at the odd harmonics of 1 Hz and it matches with the results of RCDSSI algorithm.

5.5.2 Case 2: Analysis of unmodeled response on a non linear system with resonance

This case studies the effect of unmodeled response on an nonlinear system. In this case, the test system is solved by numerical integration to mimic the behaviour of a nonlinear power system. A forced oscillation is applied with a frequency of 0.62 Hz which is close to the inter-area oscillation frequency to simulate a resonance scenario. As the system is nonlinear, the effect of nonlinearity is also observed in this case. Fig. 5.10 shows that applying a forced oscillation at the reference voltage of voltage regulator of machine 1 with a magnitude of $0.05pu$, causes the exciter voltage to hit its limit of $5pu$. Because of this nonlinearity effect the estimated modes from the nonlinear system varies to some extent from the linear system modes. Fig. 5.11 shows the different captured response for the machine speeds. Fig. 5.11a

Table 5.1: Estimation of modes for different responses of linear system.

Responses	Frequency (Hz)	Damping ratio (%)	Normalized residue
Linear	0.6125	13.4300	0.6900
	1.3100	29.7000	1.0000
	1.3600	34.2700	0.3361
	2.4800	35.4500	0.6630
Actual	0.6125	13.5100	0.2900
	1.3100	36.4600	0.0080
	1.3600	35.2800	0.1900
	2.4800	36.2500	0.0080
	1.0000	0.0000	1.0000
	3.0000	0.0000	0.6900
	5.0000	0.0000	1.0000
Unmodeled	0.6125	13.5100	0.0190
	1.3100	36.4600	0.0080
	1.3600	35.2800	0.0800
	2.4800	36.2500	0.0080
	1.0000	0.0000	1.0000
	3.0000	0.0000	0.5700
	5.0000	0.0000	1.0000

illustrates the unmodeled dynamics as seen in the machine speeds, Fig. 5.11b presents the total actual response of the machine speeds which contains the effect of nonlinearities and forced oscillations. Finally, Fig. 5.11c shows the linear response of the system at the given operating point. RCDSSI algorithm is applied on the captured input-output signal as mentioned in Fig. 5.3. The results of the RCDSSI algorithm is summarized in Table 5.2. For the natural response, the estimated modes deviates a little from the modes estimate by the linear model for that operating condition and this happens because of nonlinearity effect. Actual response of the system shows zero damping for the inter-area oscillation frequency of 0.6134 Hz and for its odd harmonics. Other natural modes are also present in this response. Unmodeled response shows the similar results as the forced response case. However, it is noticed that in the unmodeled response the contribution of forced oscillation modes are significantly higher than natural oscillation modes. This conclusion is deduced by

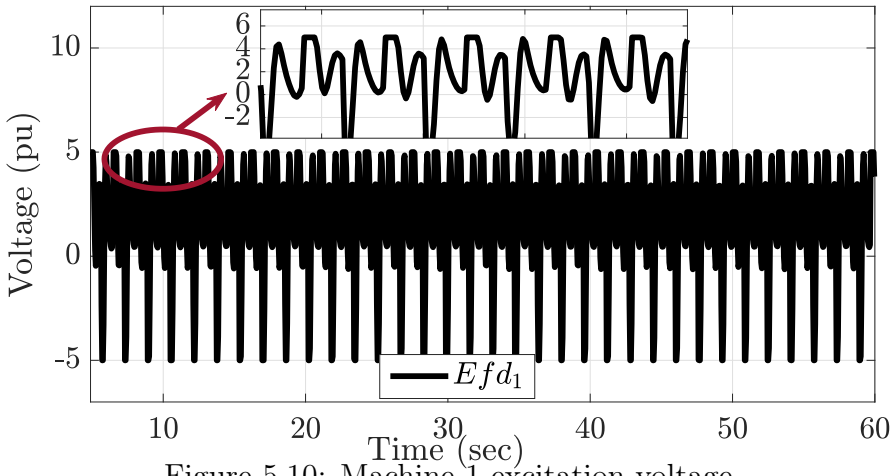

Figure 5.10: Machine 1 excitation voltage.

comparing the normalized residue values between the forced and natural response in Table 5.2. So, analyzing the unmodeled response for characterizing forced oscillations provides more reliable information. The linear response shows a well damped oscillation frequency of 0.6134 Hz. Unmodeled response shows sustained oscillation at 0.6199 Hz and represent the characteristics of forced oscillations (peaks at odd harmonics Fig. 5.12). Combining these information from linear and unmodeled response, decisions can be taken on classifying system oscillations into natural or forced. Additionally, the identified transfer function models of linear and unmodeled response can be used to dynamically track the changes in the actual system, which is shown in next case study.

5.5.2.1 Case 3: Validation of Identified Model

In this section, a simulation case is performed to show that the identified model based on measured data can accurately capture the dynamic response of the actual system. For this purpose, first, the nonlinear power system model is simulated, and a series of disturbances is applied in the form of load changes which is visible in fig. 5.14. The power system model has detailed generator models, exciters, power system stabilizers, and turbine governors. The machine bus frequencies are input, and the angle of tie-line bus 101 is output to the identification algorithm.

For larger power systems, the original model order can be significantly higher, and the identified model order depends on the number of modes which are excited following a disturbance. For a more extensive system, a reduced-order model is created from the system

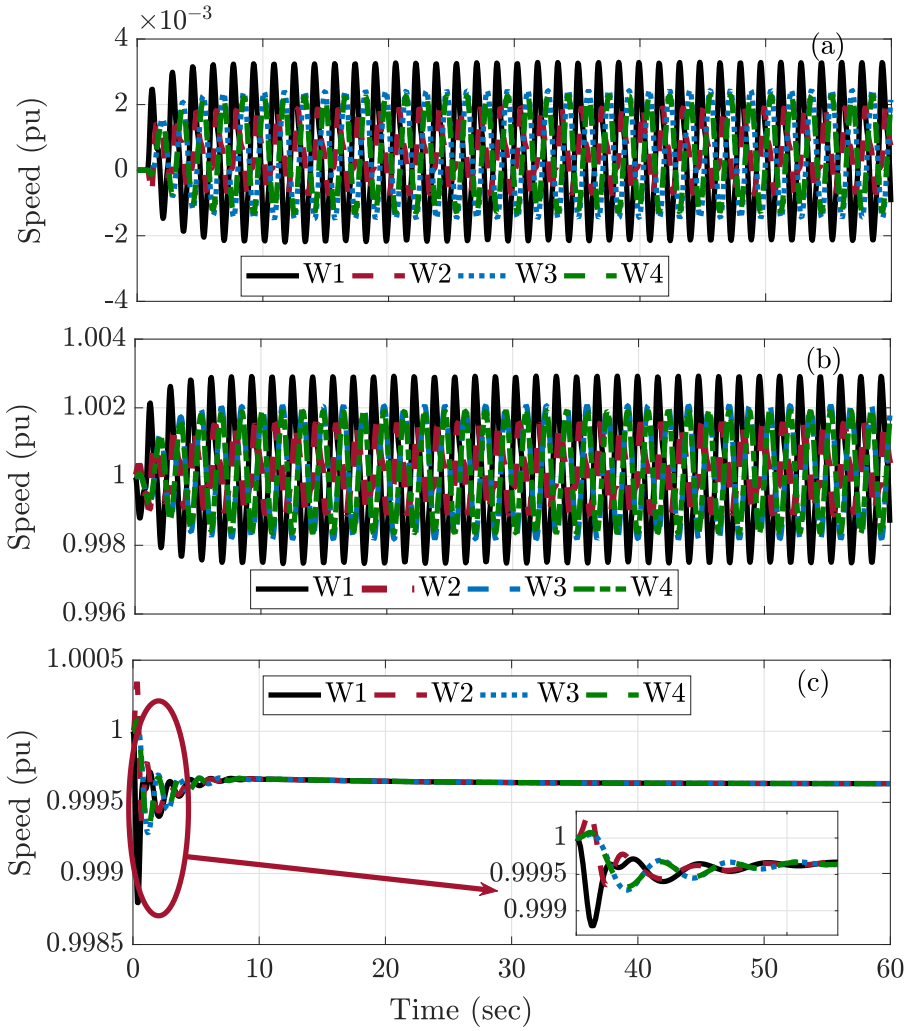

Figure 5.11: Different response of nonlinear system, a) unmodeled, b) actual and c) linear

model using the method described in section 5.3.4. A comparison is made between the identified model and the reduced-order model to compare the accuracy of the identified model. Due to page limitation, the detailed matrices are not presented here, but the norm of $|A_{ReducedModel} - A_{IdTransformedModel}| = 0.015$ shows the difference between the identified model and the reduced model. The norm is very negligible and which proves that the identified model does captures the system behavior if the modes are appropriately excited.

5.6 Applications of Proposed Architecture

One of the main advantage of developing a model of the system including unmodeled dynamics is that we can use this updated model for studying 'what if' scenarios in the

Table 5.2: Estimation of modes for different responses of nonlinear system.

Responses	Frequency (Hz)	Damping ratio (%)	Normalized residue
Linear	0.6197	13.1900	0.5300
	1.2500	25.4600	1.0000
	1.3914	36.7000	0.3600
	2.4700	23.4600	0.6957
Actual	0.6134	0.0000	0.0944
	1.3338	30.6400	0.0200
	1.3720	21.9200	0.0040
	2.4803	36.2500	0.0154
	1.8600	0.0000	1.0000
	3.1000	0.0000	0.1589
	4.3400	0.0000	1.0000
Unmodeled	0.6199	0.0000	1.0000
	1.3100	24.0200	0.0010
	1.3500	24.2900	0.0030
	2.4803	17.2600	0.0015
	1.8600	0.0000	1.0000
	3.1000	0.0000	0.1571
	4.3400	0.0000	0.1571

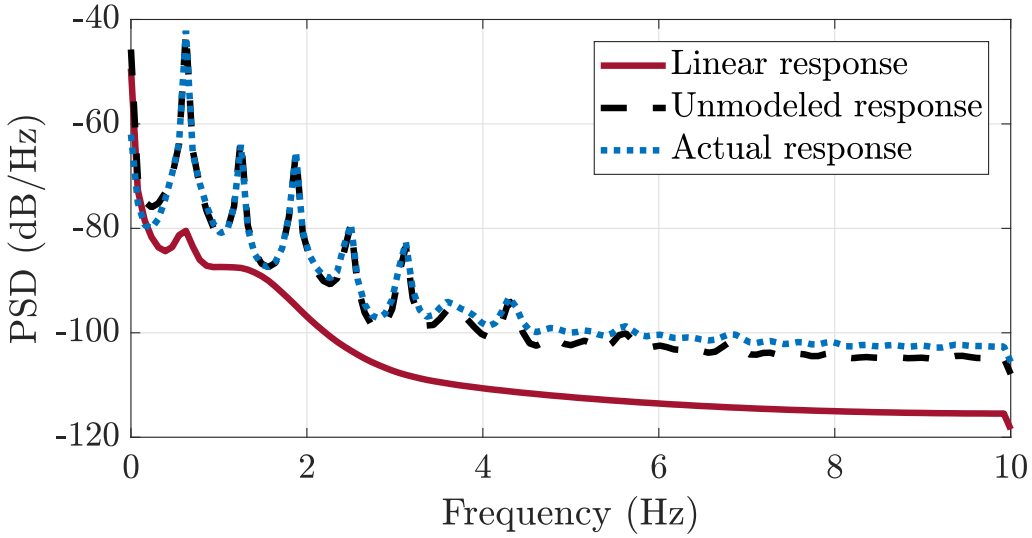

Figure 5.12: Power spectral density (PSD) comparison for different responses of nonlinear system machine 1 speed.

power grid. We are going to illustrate one possible application of developing a system architecture with unmodeled dynamics.

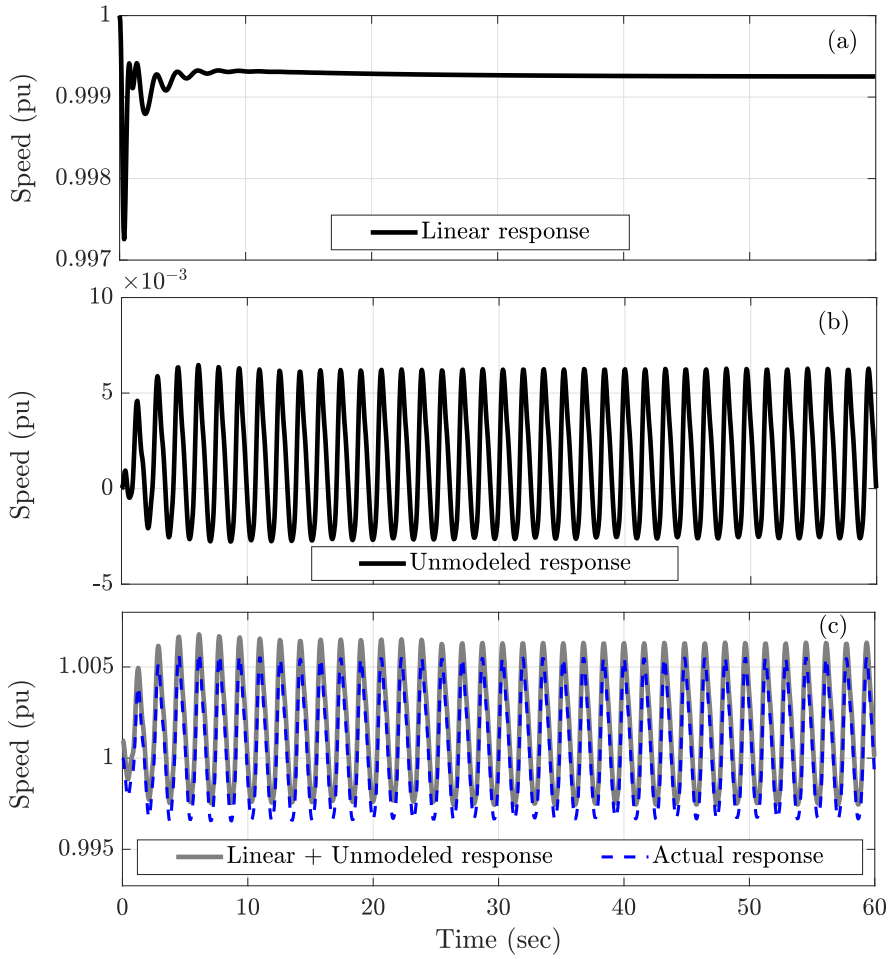

Figure 5.13: Power spectral density (PSD) comparison for different responses of nonlinear system.

5.6.1 Case 1: Study of Identified Unmodeled Response for Studying Different Scenarios

Previous sections shows that the combination of identified system models based on unmodeled response and linearized system model response can capture the actual behaviour of a nonlinear system. Now, these two identified models are used to study the behaviours of actual nonlinear system for different scenarios of interest. Ideally, it is very difficult to predict the true behaviour of a complex nonlinear power system and models can only match the actual system response to limited capacity. The proposed method enables to account for the mismatch between the model response and power system measurement data (which represent the actual system response) and can help to study how system unmodeled dynamics effect the overall behaviour of the system. This case uses the identified models for natural

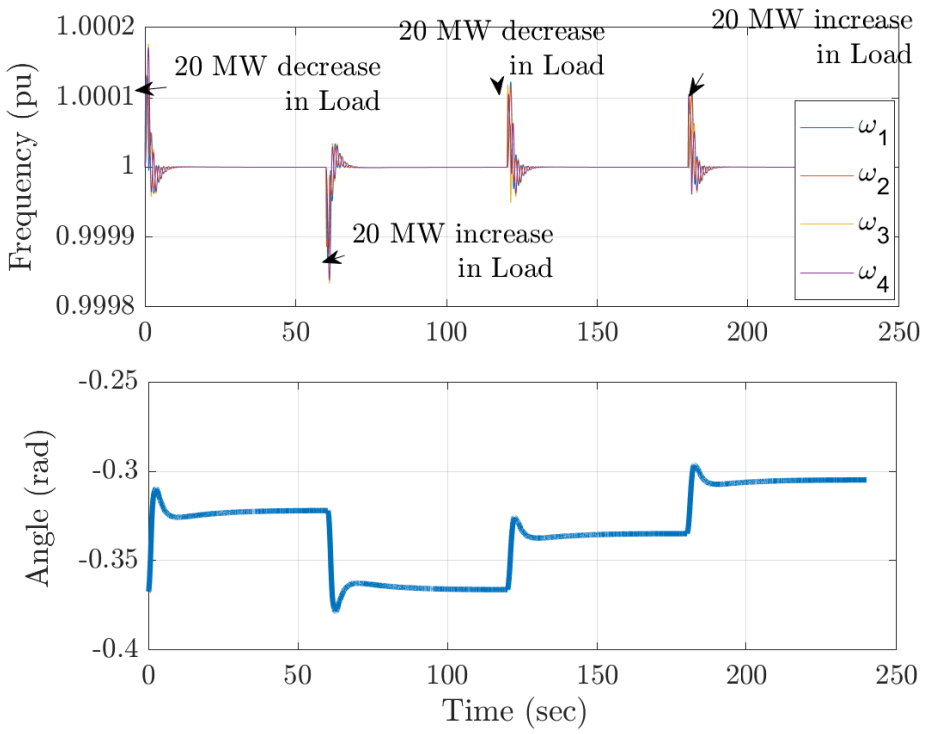

Figure 5.14: a) Input signals and b) output signals used for identification.

and unmodeled responses from section 5.3 . The identified models are perturbed with a periodic disturbance in the the voltage regulator reference of machine 1 with a frequency of $0.6125Hz$ and magnitude of $0.1pu$. The goal of the study is to predict the actual response of the power system using the identified linear and unmodeled response. First the identified models are given the disturbance and the linear and unmodeled response are shown in Fig. 5.13a and 5.13b respectively. Then the same disturbance is given to the nonlinear model of the power system which mimics the behaviour of an actual power system. The comparison of the actual power system response and the combined response of linear plus unmodeled response is shown in Fig. 5.13c. The predicted response from the identified models are almost same with the actual system response with an mean absolute percentage error (MAPE) of 0.1%. So, the proposed method can help to capture the unmodeled dynamics of the model and the can create identified mathematical models which helps to predict the nonlinear system behaviour.

5.6.2 Case 2: Use of Proposed Method for Predicting System Stability

The ability of the proposed architecture to capture the effect of unmodeled dynamics is presented in this case. This characteristics of the proposed architecture can also help updating the power system model. Malfunctions in generator control system can lead to lightly damped oscillations (92). To simulate such a scenario in time domain, the PSS gain is reduced from 100 to 50. This reduces the damping ratio of inter-area oscillation mode from 13.5% to 4.67%. The data from the simulation is used as synthetic PMU data. It can be noted that the system model used in the control center cannot incorporate such changes and predict the damping of the the oscillatory mode. Fig. 5.15a shows the change in governor reference set point which acts like disturbances and excites the inter-are oscillation mode. Fig. 5.15b shows the frequency of generator at bus1 and Fig. 5.15c shows the tie line power between bus 7 and 8 for three cases. Initially validation data is used to identify the model. Close observation shows that the identified model forecasts the system behaviors more closely than the system model. Thus, it can be concluded that such measurement based identified model can help in identifying the shortcomings of power system models which are usually validated not very frequently. The proposed architecture can capture the presence of unmodeled and nonlinear dynamics in system response.

5.6.3 Case 3: Application of Proposed Method for a Larger System

IEEE 39-Bus system is a reduced equivalent of the New England test system (NETS). Fig. A.4 shows the one line diagram of the test system (7).This system has 10 generators and 39 buses. Generator 1 located at bus is an aggregated generator and hence has high inertia and output power. Exciter model used for voltage regulation is of 'IEEE type 1' and governor model is of type 'TGOV'.The generator data and governor data is modified slightly for EMT simulation studies compared to (7). Forced oscillations are introduced using periodic disturbances at the governor mechanical torque output of the generators. Fig. A.4 shows the disturbance locations for different cases.

Similar to the response shown for the two area system, this section simulates a case for showing the combined response of a medium scale system. Random load changes are

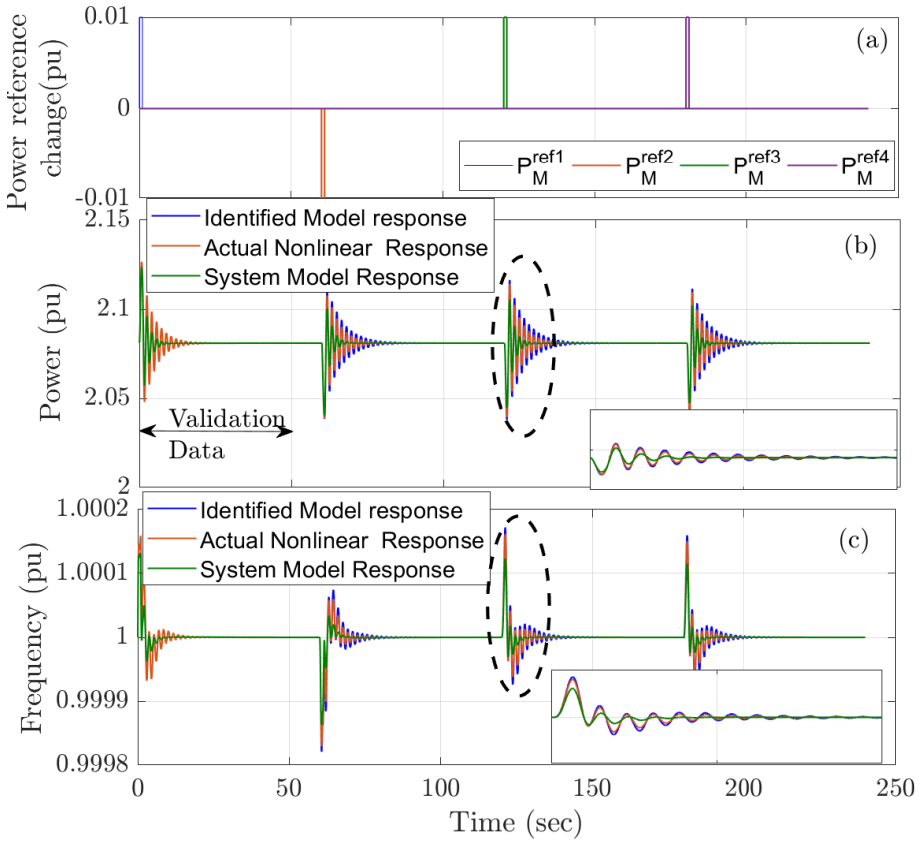

Figure 5.15: a) Input disturbance at the governor reference point , b) frequency at generator bus 1 c) tie-line power between line 7 and 8.

simulated by adding Gaussian white noise with a magnitude of 5% of the connected loads. A load increas is applied at bus 39 to simulate transient response. And an external disturbance of 0.4 Hz is applied to the generator 8 governor response to simulate forced response. Fig. 5.17a illustrates the combined response of the system for a 4 minute window.Fig. The result shows that the identified model can be used to predict the response of the system and it gives an accurate estimation of actual system response.Fig. 5.17b shows the time frequency analysis of the response The ambient response shows that a electromechanical frequency of 1.28 HZ is excited and this conforms with the small signal stability analysis of the system. Small signal stability analysis shows that generator 10 speed is the dominant state for the oscillation mode with 1.28 Hz frequency. The frequency of 1.28 Hz is more visible in the time between 70 second to 100 second when the transient response of the system is excited. Response of the system between time 140 second to 200 second shows the forced oscillation frequency of 0.4 Hz.

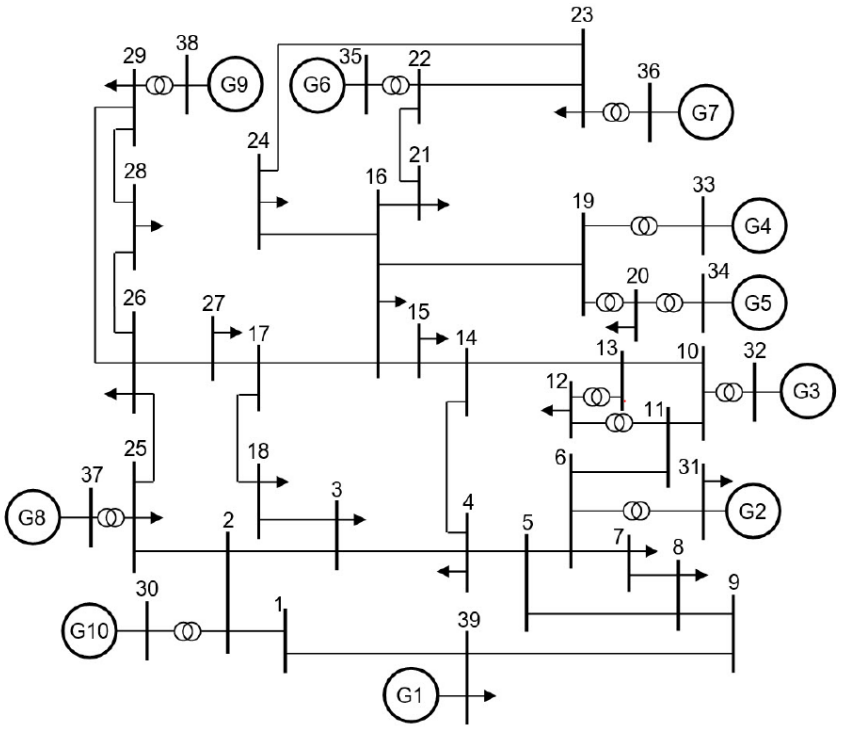

Figure 5.16: IEEE 39 bus test system (7).

5.7 Summary

This chapter illustrates an approach for identifying the unmodeled response of power system for characterizing system oscillations. The proposed method use a nonlinear power system model and the linearized model of the same power system to extract the unmodeled response of the system. This characteristics is then used to estimate the modes of oscillation from the unmodeled response. The method can not only find the reduced order model of the power grid based on system oscillation mode, but can also identify the order of the system and the physical states that is being excited. This helps one to understand and evaluate system nonlinearity and unmodeled dynamics. The methodology is evaluated with a numerical example and a test power grid model.It is observed that the approach can be used to differentiate between natural and forced oscillation if they have the same frequency. Also, the approach can be used to study scenarios of interest in the power grid. Future studies will be to test the architecture on real life data sets.The methodology proposed in

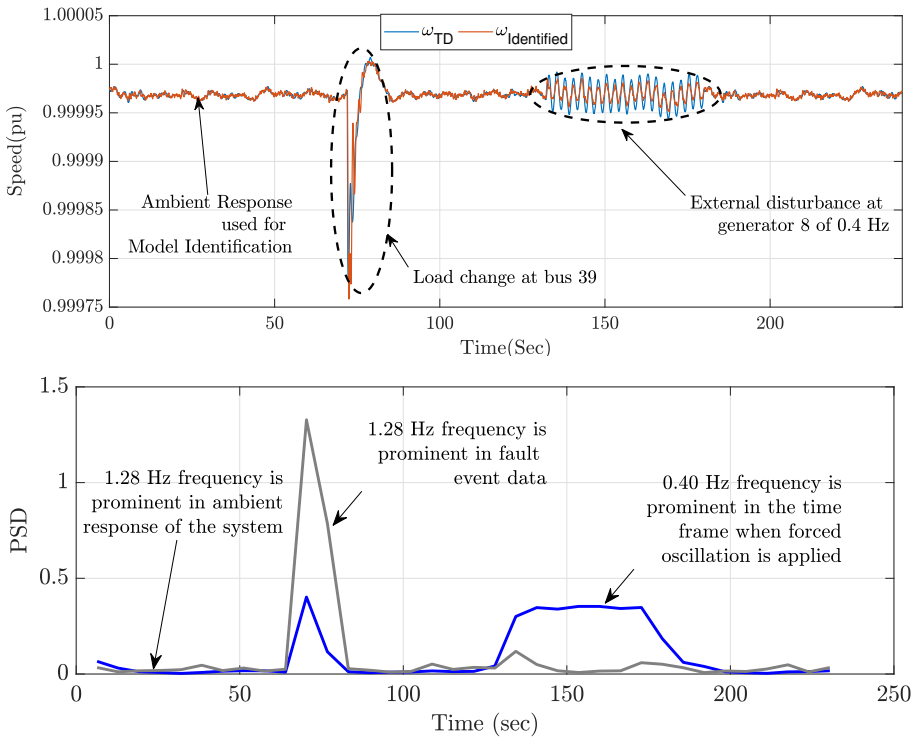

Figure 5.17: a) Time Domain(TD) and predicted machine speed for a load increase in bus 39 and b)Time frequency analysis of the response.

this chapter helps operator to take better corrective actions. But, with changing system conditions it is difficult for system operators to take corrective actions fast enough. For this an adaptive wide area damping controller is proposed in next chapter that can mitigate oscillations by controlling multiple damping resources.

CHAPTER 6: IDENTIFICATION BASED OSCILLATION MITIGATION APPROACH

In this chapter, a multi-channel system identification (SI) based adaptive wide-area damping controller (WADC) is proposed for a distributed energy resources (DER) integrated power grid. The proposed design identifies the multiple-input multiple-output (MIMO) reduced order transfer function model of the system using recursive least square (RLS) algorithm and utilizes adaptive control framework to adjust the power output of DER based upon the identified model to improve the transient stability of the system. The concept is to utilize the proposed controller to augment converter based local control of DER to damp the system oscillations faster. The benefit of the proposed control methodology has been validated by conducting simulation studies on a modified two area system to damp the inter-area oscillations. The results demonstrate that through coordinated control of different DERs, oscillations can be damped faster compared to using only local power system stabilizers (PSS) and conventional wide area damping controllers (WADC). The results of this chapter is summarized in the form of papers (93) and (94).

6.1 Introduction

Distributed energy resources are increasing their footprint in the power grid as there is a move towards clean energy demand. However, with the increase in DER and gradual replacement of conventional generation sources from the grid, the stability behavior of the grid is a concern. As most of the DER are asynchronous machines decoupled from the system with power electronic converters, the direct interaction between the synchronizing forces and the total system inertia is absent in these generation sources. With the increased penetration of DER the operating condition and the inertia of the system are increasingly time varying. This causes the frequency and damping ratio of electromechanical modes to change more frequently (95; 96). If these modes are not damped properly in time, it can create growing oscillations and can pose threat to reliable operation of the power system.

Conventionally, PSS (both local and wide-area) provide supplementary damping control. Generally, the DER do not take an active part in damping the power system oscillations. However, studies have shown that increased penetration of DER in power grid with reduced number of synchronous generators can have a damping effect that limit the power system oscillations. The studies also report that this behavior is dependent on the location of the DER and the way they impact the tie-line power flows (97; 98). So DER has the potential to suppress the oscillations by controlling the power output, if the power outputs from each units can be coordinated for this purpose. The coordination among all the DER can be performed through a WADC architecture.

Generally, WADC are designed using linear feedback control techniques based on the small signal model obtained by linearizing the dynamic model of the system around an operating point. Control techniques reported in literature utilizing DER is based upon either mimicking the droop based control (45), PSS (46; 47), compensator based (48), or by injecting the power into the system out of phase with the inter-area oscillation(49),(99). Other studies based on optimization algorithm and energy function approach has been demonstrated in (47; 50). However, one of the issues related with these previous studies is that their success is dependent on having an accurate knowledge of system and linearization of the non-linear dynamic system such as power grid. Also, the controllers are static and designed for a particular operating condition, considering a particular mode of oscillation which may not work well for different operating condition especially with higher penetration of variable renewable resources. Artificial intelligence (AI) based techniques have been demonstrated to capture the nonlinearities and uncertainties in the power grid and can learn and map the system dynamics from set of system inputs and outputs (51). However, the issues related to such AI based techniques is that they require sets of offline data for training and performance validation and has larger computational burden.

Several measurement based methods have also been developed to estimate the modes of the system from wide area measurements (WAMs) data. These methods identify the model of the system from measurement data in two forms 1) subspace state space form (52) and 2) transfer function form (53). In (53), it has been demonstrated that both the

subspace state space and MIMO transfer function model can capture the dominant modes of the system accurately from both ring-down data (data generated from event like line tripping, generation loss etc.) and ambient data (data obtained from random small load changes). These identified models can be used to design adaptive and coordinated damping controller (DC). Compared to subspace state space model MIMO transfer function model has improved computational efficiency and lower order aggregation capability. In (8), the parameters of conventional WADC form as well as time delay compensator are updated online based on low order single-input single-output (SISO) model determined based on the residue analysis of the MIMO model. In (8), it was assumed that the critical inter-area mode can be well represented by the mode with largest residue in the identified transfer function model of the system. This approach ignores the other nearby modes whose residue can be in close approximation with the electromechanical modes that may have significant impact on system low frequency oscillations. Such modes are generally associated with the poor design of controllers (54).

In this chapter, a multi-channel RLS identification based adaptive WADC has been proposed for DER integrated bulk power grid. RLS identification is used for SI, as opposed to the block processing algorithm (53). As RLS does not require fixed memory allocation, this approach is suitable for online applications. In this method, the MIMO transfer function model of the system is identified using autoregressive exogenous (ARX) model structure based on ring-down data obtained using measurements. Then a oscillation DC based on minimum variance control (MVC) architecture is designed using the transfer function model and is used to augment with the local controller (LC) of the DER. The advantage of the MVC control is that it looks certain steps ahead in the future and regulates the system output as close as possible considering the identification error and noise for control. The effectiveness of proposed method is demonstrated by case studies on a two area four machine system.

The major advantages of the proposed approach are:

- It is based on the online identification of the system dynamics which results in adjusting the controller output as the system operating condition changes.

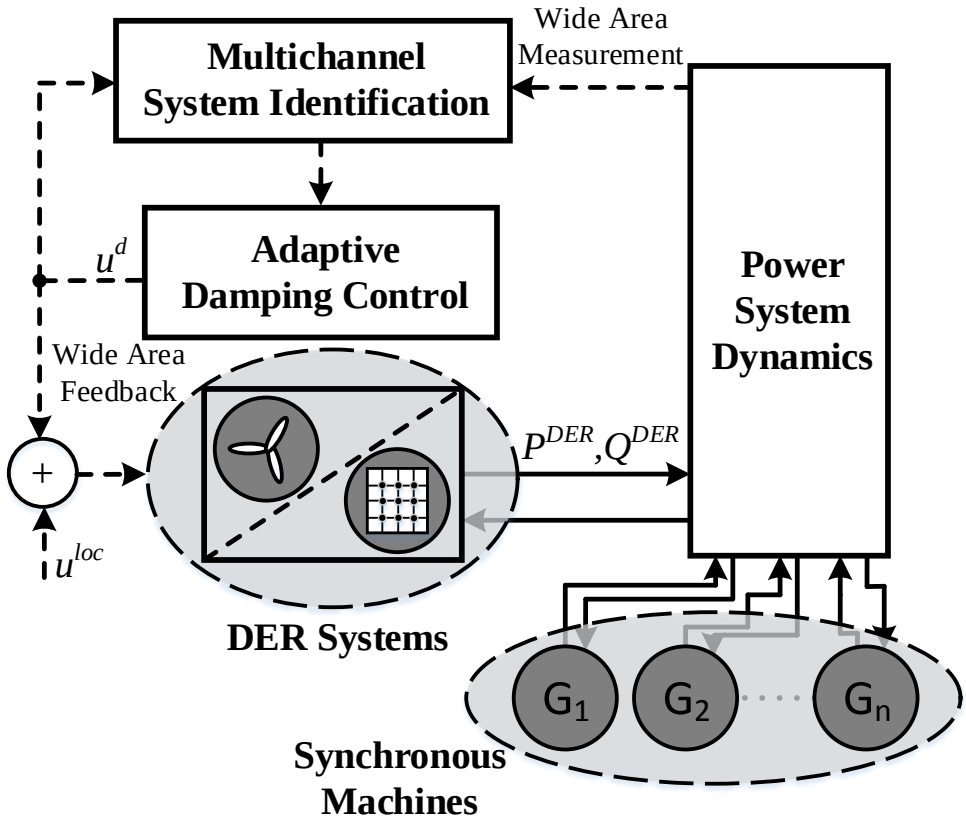

Figure 6.1: Proposed structure of DC based on SI.

- It is independent of the network topology and only requires WAMs for identification and control.
- It can be augmented with the existing LC in the DER.
- It adapts to various operating conditions and can consider the complete order of identified system model as opposed to considering the mode with highest residue.

6.2 System Modeling

The classical second order model of a synchronous machine is often used to study the transient stability of a power system during the period of time in which the system dynamics depend largely on the stored kinetic energy in the rotating masses (100). The equations of

motion for a classical representation of power system are given by,

$$\begin{aligned} \dot{\omega_i} &= \frac{1}{M_i}\left(P_{m_i} - D_i\omega_i - E_i\sum_{j=1}^{n} E_j(B_{ij}sin\delta_{ij} + G_{ij}cos\delta_{ij})\right) \\ \dot{\delta} &= \omega_i - \omega_s \qquad i = 1, \cdots, n \end{aligned} \tag{6.1}$$

where n is the number of synchronous machines, ω_s is the synchronous angular frequency, $\delta_{ij} = \delta_i - \delta_j$, $M_i = \dfrac{2H_i}{\omega_s}$, and H_i is the inertia constant in seconds and D_i is the damping coefficient of the machine i. B_{ij} and G_{ij} are the elements of the reduced admittance matrix Y at the internal nodes of the machine. The loads are modeled as constant impedances which are then absorbed into the admittance matrix.

The DER connected on the various buses modeled as a constant negative PQ load or a PV bus depending on the mode of control employed in the DER system. Considering DER as constant negative PQ load, (6.1) can be rewritten as,

$$\begin{aligned} \dot{\omega_i} &= \frac{1}{M_i}\left(P_{m_i} - D_i\omega_i - \sum_{i=1}^{n} P_{ld_i} - \sum_{i=1}^{m} P_{ls_i} + \sum_{i=1}^{o} P_i^{DER}\right) \\ \dot{\delta} &= \omega_i - \omega_s \qquad i = 1, \cdots, n \end{aligned} \tag{6.2}$$

where m is the number of lines, and o is the number of DER in the network. P_{ld_i} represents the load connected at the ith bus, P_{ls_i} represents the line losses in the ith line and P_i^{DER} represents the active power injected by DER on ith bus.

The power injected by the DER on the ith bus is given by,

$$P_i^{DER} = \frac{P_i^{DER^*}}{1 + sT_i^{DER}} \tag{6.3}$$

where $P_i^{DER^*}$ power reference for ith DER system and T_i^{DER} is the DER system response time constant for ith DER.

From (6.2) and (6.3), it can be observed that the power output of DER can have an impact on system frequency dynamics even though DER themselves are operating in asynchronous mode.

6.3 Multichannel Identification Applied to Power System

Based on the subspace identification framework proposed in Chapter 1 the projected matrix is calculated from the Hankel matrices

The projected matrix O is expressed as,

$$\underset{\mathbb{R}^{i\times j}}{O} = \begin{cases} L_{21}, \text{if only output measurements are used} \\ L_{32}, \text{if both input and output are used} \end{cases} \tag{6.4}$$

The system matrices A, B, C, D can be extracted with the help of weighted projection matrix O. Singular value decomposition (SVD) is performed on the weighted projected matrix to obtain U_1 and S_1. Both W_1 and W_2 are considered to be identity matrices.

$$W_1 O W_2 = U S V^T \tag{6.5}$$

$$U_1 = U(1:n); S_1 = S(1:n), n \;\; modelorder \tag{6.6}$$

$$\Gamma_i = U_1 \sqrt{S_1}, \Gamma_{i-1} = \bar{\Gamma}_i \tag{6.7}$$

Solve the set of linear equations for calculating A and C,

$$\frac{\Gamma_{i-1}^{\dagger}.Z_{i+1}}{Y_i} = (\frac{A}{C}).\Gamma_i^{\dagger} Z_i + K U_f + P \tag{6.8}$$

$$K = (\begin{bmatrix} B|\Gamma_{i-1}^{\dagger}.H_{i-1}^d - A.\Gamma_i^{\dagger}.H_i^d \\ D|0 - C.\Gamma_i^{\dagger.H_i^d} \end{bmatrix}) \tag{6.9}$$

where $Z_i = Y_f/[W_p U_f]$,$Z_{i+1} = [Y_f^- W_p^+ U_f^-]$ and P is the residual.And then B and D is calculated by solving the least square problem described in (6.10). The details of how to solve the least square problem can be found in (61).

$$\frac{\Gamma_{i-1}^{\dagger}.Z_{i+1}}{Y_i} = (\frac{A}{C}).\Gamma_i^{\dagger}Z_i + KU_f + P \tag{6.10}$$

$$K = (\begin{bmatrix} B|\Gamma_{i-1}^{\dagger}.H_{i-1}^{d} - A.\Gamma_i^{\dagger}.H_i^{d} \\ D|0 - C.\Gamma_i^{\dagger.H_i^{d}} \end{bmatrix}) \tag{6.11}$$

The matrices extracted are used to formulate the identified model of the system.

The transfer function for the multi-input-multi-output(MIMO) system is derived from the state space matrices,

$$G(s) = \mathbf{C}SI - A^{-1}\mathbf{B} + D \tag{6.12}$$

If the inputs and outputs of the system are determined, the system model can be represented as:

$$G(s) = \begin{bmatrix} G_{11}(s) & \cdots & G_{1r}(s) \\ G_{21}(s) & \cdots & G_{2r}(s) \\ \vdots & \cdots & \vdots \\ G_{p1}(s) & \cdots & G_{pr}(s) \end{bmatrix} \begin{bmatrix} u_1(s) \\ u_2(s) \\ \vdots \\ u_r(s) \end{bmatrix} = \begin{bmatrix} y_1(s) \\ y_2(s) \\ \vdots \\ y_p(s) \end{bmatrix} \tag{6.13}$$

where $u_i(s)$ and $y_j(s)$ are the ith and jth elements of the input vector and the output vector, respectively. G_{ij} is the element of the G matrix at position (i, j). p and r are the number of system outputs and number of system inputs, respectively.

6.4 Augmentation of DER Local Controller with Proposed WADC Technique

A general representation of the proposed SI based adaptive controller applied to DER is shown in Fig. 6.1. The controller action of DER with the proposed augmentation with WADC comprises of two parts as,

$$u(t) = u^{d}(t) + u^{loc}(t) \tag{6.14}$$

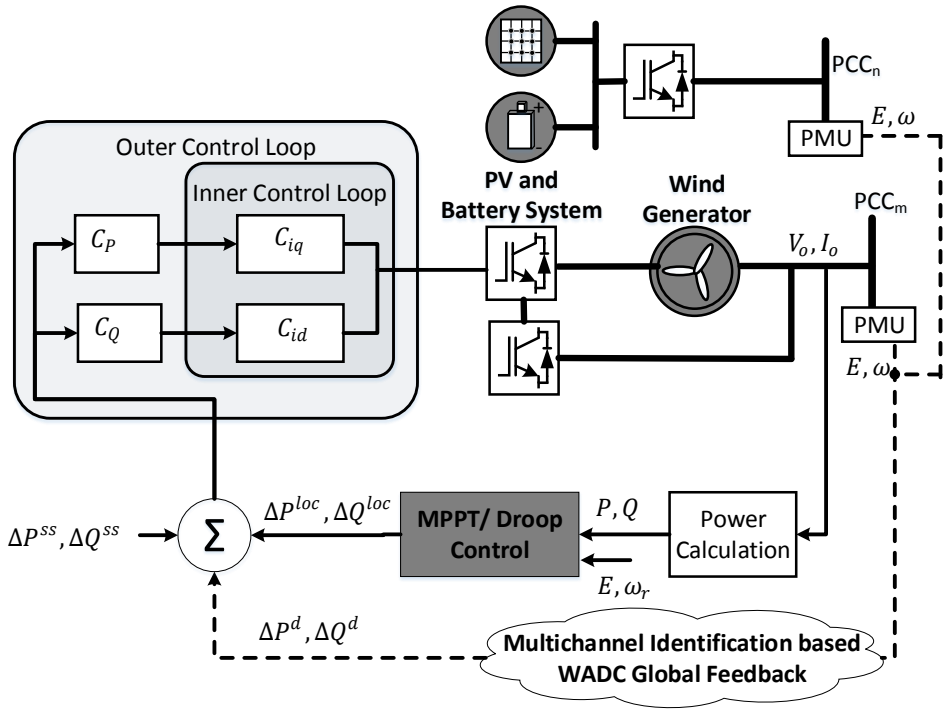

Figure 6.2: Augmentation of DER LC using proposed WADC signal.

where u^d is the damping component of the control input provided by the DC designed using identified system parameters in 6.3 and u^{loc} is the component of control signal required to track the local reference input. For the SI, inter-area speed deviation $\Delta\omega_{ij}$ is considered as the system output and the ΔP_{DER} is considered as the system input. The identified linearized model of the system is then utilized for the design of DC. The goal is to enhance the overall system stability while minimizing the inter-area speed deviation.

It is worth noting that in this work the focus is to utilize this architecture and augment DER LCs such that DER can take part in damping the system oscillations. For DER, the objective of LC is to track the reference set-point provided either by maximum power point tracking (MPPT) controller or by the DER operator. The goal of the WADC is to damp the system oscillations by appropriately modifying the active and reactive power output of DER system. The augmentation of the LC of DER to incorporate the damping functionality is shown in Fig. 6.2. Overall, the active power set-point given to the DER system comprises of three terms: (ΔP^{loc},ΔQ^{loc}) for load sharing or MPPT control as local reference, (ΔP^{ss},ΔQ^{ss}) as a set-point provided by secondary/tertiary level controller from

DER control center and (ΔP^d,ΔQ^d) as a remote set-point signal provided by DC. Once the sum of these three different set-points is available, the tracking of these set-point is achieved through the conventional vector control techniques implemented in DER systems (101). The outer loop controls (C_P,C_Q) the active and reactive power set-points and provides an equivalent current reference to the inner loop control (C_{id},C_{iq}) which track the current flowing out of the DER system.

By controlling the active and reactive power output of the DER system, the speed oscillation brought about by local and wide area disturbances could be mitigated. Thus, the goal of the multichannel identification based WADC is to monitor and identify the local and inter-area oscillations and send proper damping signals to DER systems in order to dampen the system oscillation.

6.4.1 SI Based DC Design

The DC designed for this work is based on MVC architecture used in polynomial methods (102) which solves the optimal control problem of minimizing the output variance of the ARX system identified in Section 6.3 k steps ahead of time. Polynomial method is chosen in this work as opposed to state space form (103) due to easier and simpler implementation and application for practical purposes. The controller designed in this work is based on nth order identification of the system. For $n = 2$, the controller takes in the following form (102):

$$u_1(k) = \frac{a^1 y_1(k) + a^2 y_1(k-1) - b^1_{12} u_1(k-1)}{b^1_{11}} \tag{6.15}$$

for a step ahead prediction error minimization.

6.5 Simulation Results and Discussion

Fig. 6.3 shows the test system that has been utilized to assess the performance of the proposed SI based DC with respect to conventional PSS that has been implemented in the synchronous machine. The test system is a modified version of classic two area four machine system (100). The test system has been implemented in MATLAB-Simulink. The model consists of two areas connected through a tie-line. Area 1 has two synchronous generators each generating 690 MW power and area 2 also has two synchronous generator

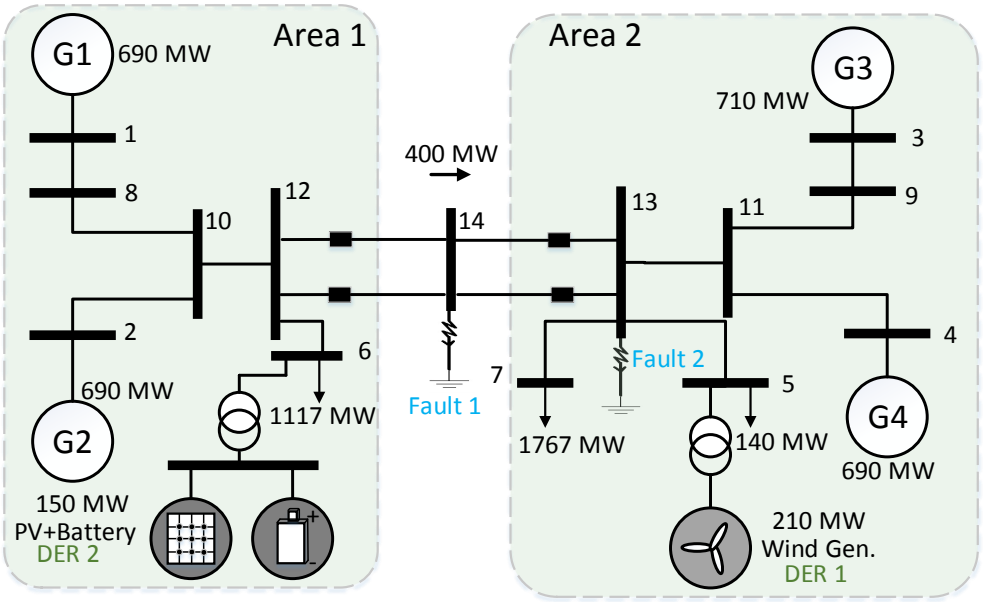

Figure 6.3: Modified classical two-area four-machine system with integrated DER.

each generating 710 MW and 690 MW respectively. In this chapter, the full-order model of the synchronous generators is used with LCs of governor, exciter, and PSS. On top of synchronous machine, each area consists of aggregated DER models. In area 1, a 100 MW PV farm coupled with a 50 MW storage unit is connected to bus 6 along with a 150 MW load and in area 2, a 210 MW wind farm is connected to bus 5 along with a 140 MW load. Two case studies are performed to test the performance of the proposed SI based DC. Fig. 6.4 shows the performance of the proposed multi-channel identification technique for properly capturing the system dynamics. At 10 seconds, when the fault is applied, there is a large error but the parameters are updated recursively and they converge quickly to stable values.

6.5.1 Fault in Middle of Transmission Line

In this case, a bolted three phase fault for 6 cycles is applied to middle of the tie-line connecting Area-1 and Area-2. It is assumed that the fault is auto-cleared after 6 cycles and the circuit breakers on the either end of the line are not opened. This disturbance excites the interarea oscillation in the system.

The purpose of this study is first to show that if not explicilty asked to take part in mitigating the system oscillation, the DER systems basically continue to send the same amount of power to the grid irrespective of the system oscillation. This primarily happens

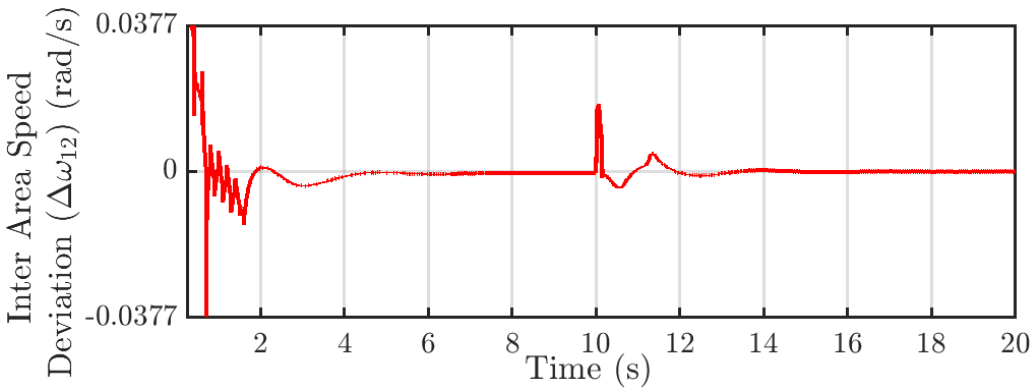

Figure 6.4: Estimation error of the recursive least square multi-channel identification routine.

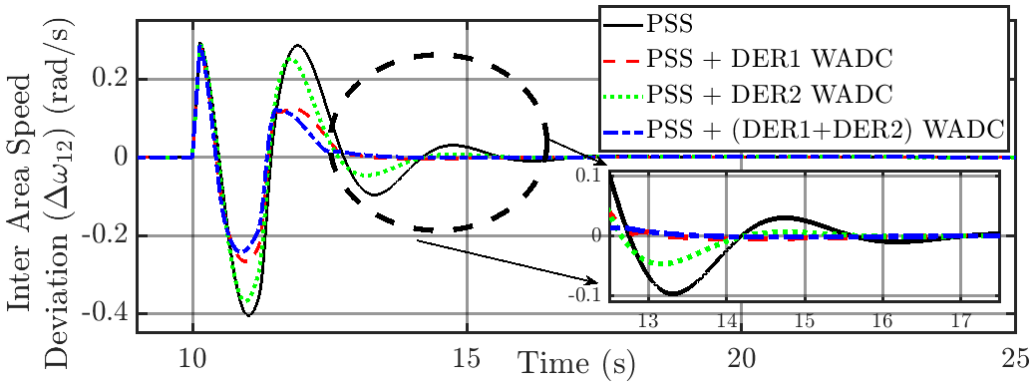

Figure 6.5: Inter-area speed deviation comparison with PSS and proposed technique with multiple combination of DER.

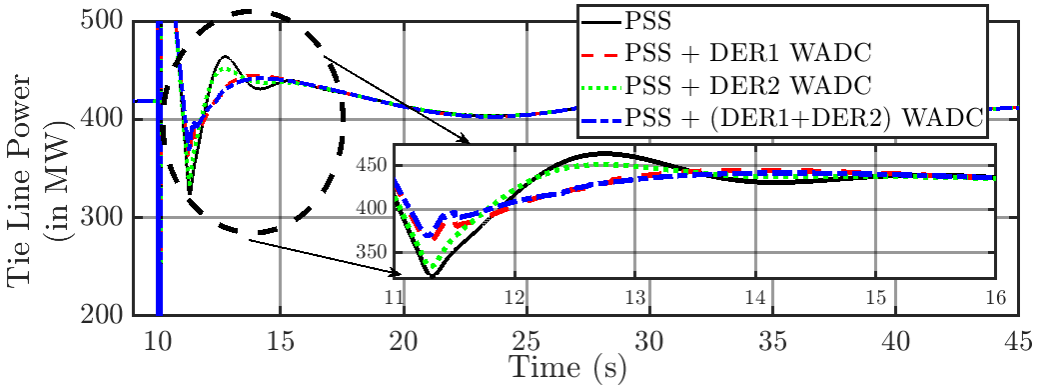

Figure 6.6: Tie-line power flow transfer comparison with PSS and proposed technique with multiple combination of DER.

because of the asynchronous nature of operation of DER systems i.e. their power output naturally does not depend on system speed. Once that is demonstrated, next the capability of WADC augmented DER systems to dampen the system oscillation is shown and the performance is compared with the damping performance of PSS employed in synchronous

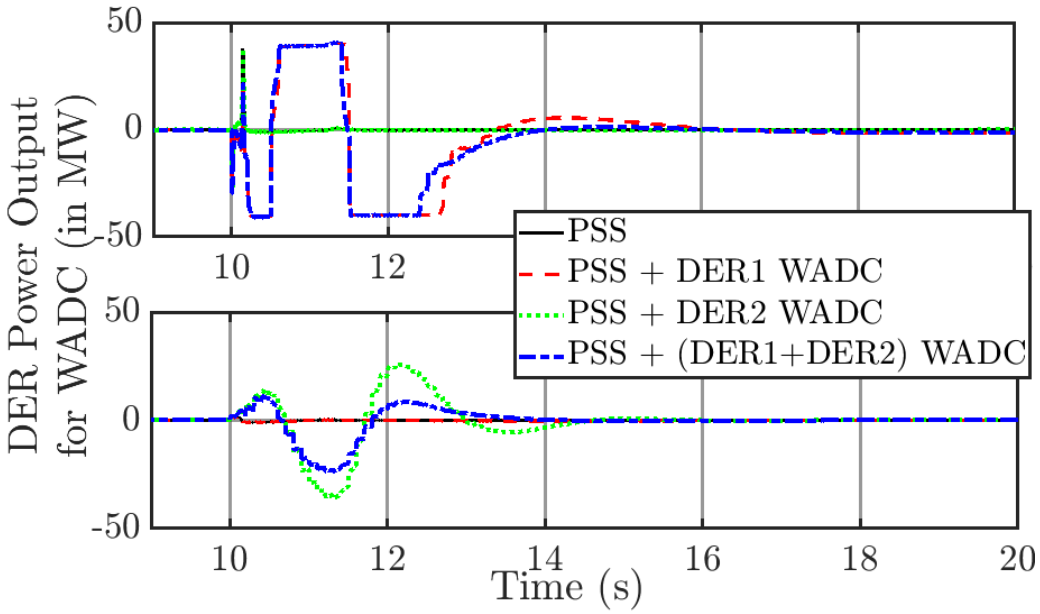

Figure 6.7: DER power output deviation from its local setpoint for WADC contribution a)DER1 b)DER2.

machine.

Fig. 6.5 shows the inter-area speed deviation for four different cases: a) PSS of synchronous machines are enabled and damping control in DERs are disabled b) PSS of synchronous machines are enabled along with DC in DER of area 1 c) PSS of synchronous machines are enabled along with DC in DER of area 2 d) PSS of synchronous machines are enabled along with DC in DER of both area 1 and area 2. It can be observed that with the proposed DC enabled, the dynamic response of system following the fault improves in terms of less overshoot and better damping. It can also be observed that better damping is obtained when DER in both area are utilized and also DER in sending end can provide more damping effect than the DER in area 2.

Fig. 6.6 shows the tie-line power flow for the different cases studied. It can be observed that with the proposed WADC controller implemented on DER the tie-line power oscillations is minimized as well. Fig. 6.7 shows the variation of DER power output in area 1 and area 2 from its local set-point in order to contribute for damping the inter-area mode. It can be observed that the DER only contributes to damping the system oscillation when the WADC signal is enforced. Without the WADC signal it can be observed that the DER strictly forces

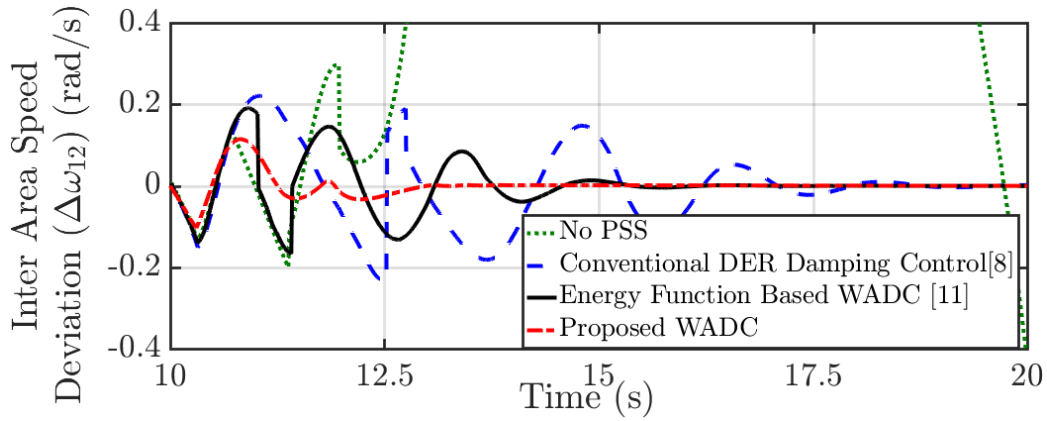

Figure 6.8: Inter-area speed oscillation damping comparison for different WADC schemes.

its power output to the reference level. Also, note that the DER power output variation on both area is limited to ±45 MW to be utilized for WADC application which is low compared to the net system generation of 2800 MW.

6.5.2 Comparison with the Existing WADC architecture for DER

This test case presents the comparison of the proposed WADC with the existing WADC architecture for DER systems proposed in literature. The cases compared are a) No PSS and damping control implemented in DER systems b) With supplementary damping wind PSS designed as conventional WADC as in (48) c)Energy Function based direct intelligent WADC as in (51) and d) Proposed multichannel identification based WADC controller. A fault is applied at the middle of line as in section 6.5.1 at 10 secs for a 300 ms period and various WADC schemes are comapred. The result shown in Fig. 6.8 shows that the proposed WADC technique outperforms the other existing WADC schemes, the major advantage comes in from the fact that the proposed technique is not dependent on knowing the system parameters as the parameters are estimated online on the proposed control technique. Thus it can be seen that the proposed control technique can be a better alternative to the existing WADC scheme employed for DER systems.

6.5.3 Comparison with the Existing SI based Adaptive WADC architecture

This test case presents the comparison of the proposed adaptive WADC with the existing adaptive WADC architecture. The adaptive WADC proposed in (8) was implemented for DER in area 1 and the performance comparison between technique in (8) and proposed

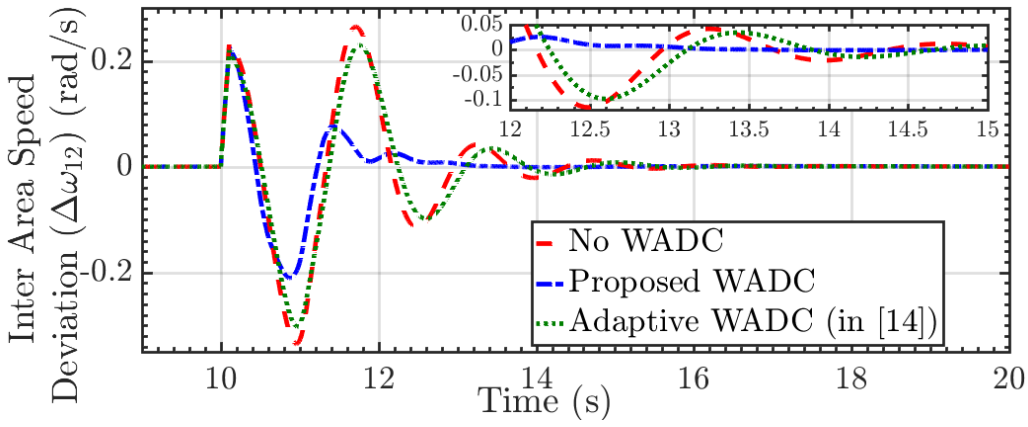

Figure 6.9: Inter-area speed oscillation damping comparison between proposed adaptive WADC and WADC proposed in (8).

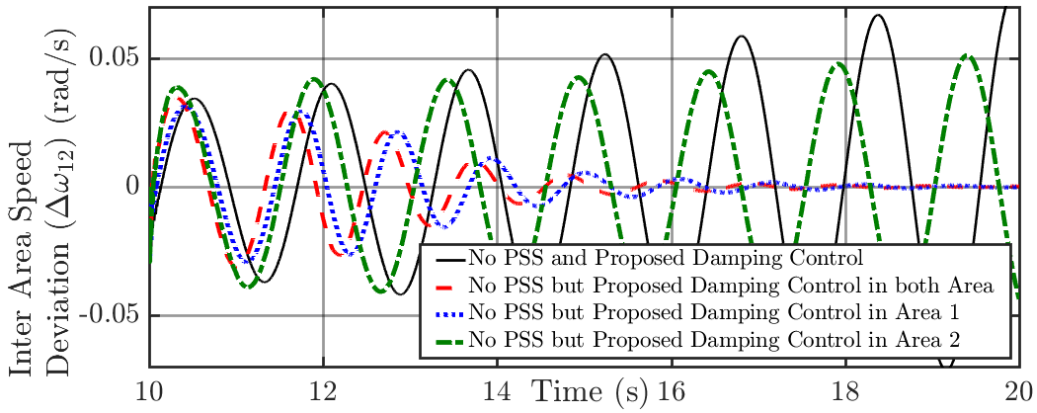

Figure 6.10: Inter-area speed oscillation damping comparison without PSS but only with proposed DC.

technique was performed. Fig. 6.9 shows the performance of the proposed DC and DC in (8) for fault conditions mentioned in Section 6.5.1. It can be observed that the proposed technique has a better response as compared to the technique presented in (8).

6.5.4 Proposed DER DC on System without PSS and Effect of Time Delay

Fig. 6.10 shows the performance of the proposed WADC without the presence of PSS in synchronous machine. As can be seen from Fig. 6.10 without the PSS and no damping control in DER, the interarea speed deviation continues to grow overtime, however with the proposed DER based WADC implementation on both area and area 1 the inter area speed deviation settles down to zero. With the WADC implemented on area 2 DER it can be observed that the oscillation are contained. The delay of the signals in the communication network for WADC implementation can have an detrimental impact on the performance

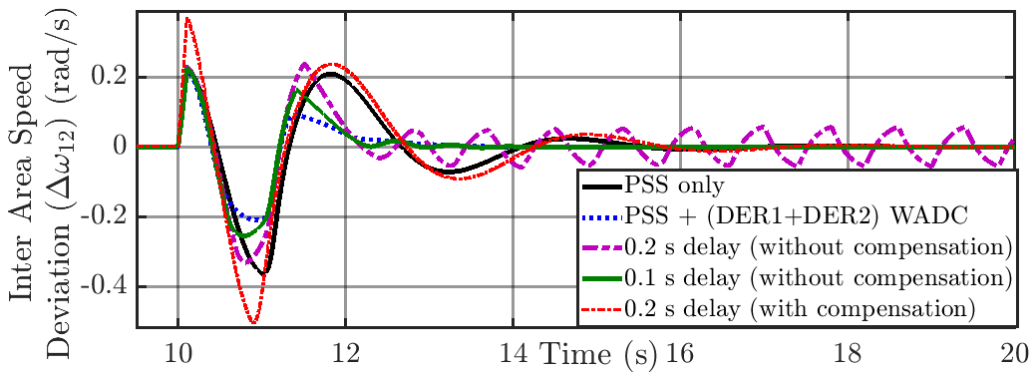

Figure 6.11: Inter-area speed oscillation comparison with and without delay compensation for proposed DER DC.

of the WADC (50). However utilizing the time stamp data from the WADC signal can help determine the delay that have occured between dispatch and arrival of control signal. Once the delay is determined a local time delay compensator can be designed to ensure that the WADC based DER DC still performs well. Fig. 6.11 shows the inter-area speed oscillation damping performance of the proposed controller at different time delays and with and without delay compensation. It can be observed that at larger time delays the proposed DC can damp the first swing however because of larger time delay a sustained oscillation is introduced in the system. It can also be observed that with proper compensation the inter-area oscillations can be damped even with presence of significant time delay.

6.6 Summary

In this chapter, an adaptive WADC for DER integrated power grid is proposed in order to damp the system speed oscillations. Multichannel RLS estimation technique has been utilized to identify the relation between the power system speed deviation as a system output and the power output of DER as a system input. The proposed approach augments the existing LC of DER to achieve the goal of damping the system speed oscillations. The results based on dynamic simulation of two area system in MATLAB Simulink shows better damping functionality of the proposed technique. Some of the issues regarding the practical implementation of the proposed method are model order selection, signal selection, and identifying the system from ambient data which is the data. These issues will be studied in the extension of this work.

CHAPTER 7: CONCLUSIONS

In this dissertation, an integrated framework based on subspace identification is proposed that can detect the presence of forced oscillation in PMU measurements and can estimate the electromechanical modes accurately in the presence of forced oscillations.Comparison of proposed approach is performed with state of the art mode estimation approaches and the proposed framework accurately estimates the oscillatory modes. Further, to decrease the computational time of mode estimation algorithm for large power systems a spectral clustering based method is proposed. The proposed method shows uses subspace affinity to form a similarity graph and then uses spectral clustering to divide the signals into weak and small groups for critical mode of interest. This helps to reduce the number of signals needed for estimating the critical oscillatory mode accurately. The proposed grouping also helps to indicate the location of oscillation source. An oscillation source location method is proposed that can locate the source of oscillation properly for single and multiple oscillation source locations. Locating the source of oscillation is the most crucial step in mitigating oscillation.

Moreover, a model-measurement based hybrid model is proposed which can help studying the effect of unmodeled dynamics. The proposed approach can help the system operators in short time planning giving them an indication about the difference between model and measurement response. This enhances the situational awareness of the operators. The system identification based approach developed is used further to design a minimum variance controller for mitigating the oscillations using renewable energy resources (RER). The proposed controller is a multi-input-multi-output (MIMO) controller and can effectively coordinate between multiple damping resources to mitigate power system oscillations.

The work proposed in this dissertation leads to an number of research plans for developing analytical tools that can provide in depth power system dynamics analysis and for developing

robust control approaches that can adapt with the changing system condition to damp oscillations faster. Some of the future works are

- All the methods developed in this dissertation are being compiled to create a MATLAB based tool that can help increasing research and understanding in this field of work
- In this dissertation, network and communication constraints have not been considered. As part of future work the effect of latency, communication protocol etc on the proposed approaches will be studied
- The proposed system identification techniques can be used to study other data driven power system problems like voltage stability, microgrid inverter coordination, MIMO DFIG control,
- The proposed adaptive control architecture can be enhanced to include the forced oscillation detection in control action, The control action will widely vary depending on the type of oscillation

LIST OF PUBLICATIONS

[1] M. Ahmed, R. Bhattarai, **S. J. Hossain**, S. Abdelrazek, and S. Kamalasadan. Coordinated voltage control strategy for voltage regulators and voltage source converters integrated distribution system. In *2017 IEEE Industry Applications Society Annual Meeting*, pages 1–8, Oct 2017.

[2] M. Ahmed, R. Bhattarai, **S. J. Hossain**, S. Abdelrazek, and S. Kamalasadan. Coordinated voltage control strategy for voltage regulators and voltage source converters integrated distribution system. *IEEE Transactions on Industry Applications*, 55(4):4235–4246, July 2019.

[3] R. Bhattarai, **S. J. Hossain**, J. Qi, J. Wang, and S. Kamalasadan. Sustained system oscillation by malicious cyber attacks on distributed energy resources. In *2018 IEEE Power Energy Society General Meeting (PESGM)*, pages 1–5, Aug 2018.

[4] T. G. Paul, **S. J. Hossain**, S. Ghosh, P. Mandal, and S. Kamalasadan. A quadratic programming based optimal power and battery dispatch for grid-connected microgrid. *IEEE Transactions on Industry Applications*, 54(2):1793–1805, March 2018.

[5] **S. J. Hossain**, R. Bhattarai, M. Ahmed, S. Abdelrazek, and S. Kamalasadan. Operational cost value assessment and value based stacked energy storage management for active power distribution systems. In *2017 IEEE Industry Applications Society Annual Meeting*, pages 1–8, Oct 2017.

[6] **S. J. Hossain**, R. Bhattarai, R. Yousefian, and S. Kamalasadan. Adaptive wide area damping controller for distributed energy resources integrated power grid. In *2018 IEEE Power Energy Society General Meeting (PESGM)*, pages 1–5, Aug 2018.

[7] **S. J. Hossain**, B. D. Biswas, R. Bhattarai, M. Ahmed, S. Abdelrazek, and S. Kamalasadan. Operational value-based energy storage management for photovoltaic (pv) integrated active power distribution systems. *IEEE Transactions on Industry Applications*, 55(5):5320–5330, Sep. 2019.

[8] **S. J. Hossain** and S. Kamalasadan. Investigation on evaluating the unmodeled dynamics of power system and its effects on characterizing power system oscillations. In *2018 North American Power Symposium (NAPS)*, pages 1–6, Sep. 2018.

[9] **S. J. Hossain** and S. Kamalasadan. Combined deterministic-stochastic online subspace identification for power system modeestimation and oscillation classification. In *2019 IEEE Industry Applications Society Annual Meeting*, Oct 2019.

[10] **S. J. Hossain** and S. Kamalasadan. Online measurement based power system reduced order model generation and validation. In *2019 North American Power Symposium (NAPS)*, pages 1–6, Oct. 2019.

[11] **S. J. Hossain**, T. G. Paul, R. Bisht, A. Suresh, and S. Kamalasadan. An integrated battery optimal power dispatch architecture for end-user-driven microgrid in islanded and grid-connected mode of operation. *IEEE Transactions on Industry Applications*, 54(4):3806–3819, July 2018.

[12] A. Thakallapelli, **S. J. Hossain**, and S. Kamalasadan. Coherency based online wide area control of wind integrated power grid. In *2016 IEEE International Conference on Power Electronics, Drives and Energy Systems (PEDES)*, pages 1–6, Dec 2016.

[13] A. Thakallapelli, **S. J. Hossain**, and S. Kamalasadan. Coherency and online signal selection based wide area control of wind integrated power grid. *IEEE Transactions on Industry Applications*, 54(4):3712–3722, July 2018.

REFERENCES

[1] S. Maslennikov, B. Wang, Q. Zhang, a. Ma, a. Luo, a. Sun, and E. Litvinov, "A test cases library for methods locating the sources of sustained oscillations," in *2016 IEEE Power and Energy Society General Meeting (PESGM)*.

[2] J. W. Pierre, D. Trudnowski, M. Donnelly, N. Zhou, F. K. Tuffner, and L. Dosiek, "Overview of system identification for power systems from measured responses1," *IFAC Proceedings Volumes*, vol. 45, no. 16, pp. 989 – 1000, 2012. 16th IFAC Symposium on System Identification.

[3] S. A. N. Sarmadi and V. Venkatasubramanian, "Inter-area resonance in power systems from forced oscillations," *IEEE Transactions on Power Systems*, vol. 31, pp. 378–386, Jan 2016.

[4] V. S. PeriÄ, X. Bombois, and L. Vanfretti, "Optimal signal selection for power system ambient mode estimation using a prediction error criterion," *IEEE Transactions on Power Systems*, vol. 31, pp. 2621–2633, July 2016.

[5] R. Xie and D. Trudnowski, "Distinguishing features of natural and forced oscillations," in *2015 IEEE Power Energy Society General Meeting*, pp. 1–5, July 2015.

[6] P. Anderson, A. Fouad, I. of Electrical, and E. Engineers, *Power System Control and Stability*. IEEE Press, 1977.

[7] A. Pai, *Energy Function Analysis for Power System Stability*. Power Electronics and Power Systems, Springer US, 1989.

[8] F. Bai, L. Zhu, Y. Liu, X. Wang, K. Sun, Y. Ma, M. Patel, E. Farantatos, and N. Bhatt, "Design and implementation of a measurement-based adaptive wide-area damping con-

troller considering time delays," *Electric Power Systems Research*, vol. 130, pp. 1 – 9, 2016.

[9] P. Kundur, *Power System Stability And Control*. EPRI power system engineering series, McGraw-Hill, 1994.

[10] A. K. Singh; and B. C. Pal, "Ieee pes task force on benchmark systems for stability controls report on the 68-bus, 16-machine, 5-area system."

[11] P. Pourbeik, P. S. Kundur, and C. W. Taylor, "The anatomy of a power grid blackout - root causes and dynamics of recent major blackouts," *IEEE Power and Energy Magazine*, vol. 4, pp. 22–29, Sept 2006.

[12] "Identification of electromechanical modes in power systems," 2012.

[13] N. Zhou, D. J. Trudnowski, J. W. Pierre, and W. A. Mittelstadt, "Electromechanical mode online estimation using regularized robust rls methods," *IEEE Transactions on Power Systems*, vol. 23, pp. 1670–1680, Nov 2008.

[14] S. A. N. Sarmadi and V. Venkatasubramanian, "Electromechanical mode estimation using recursive adaptive stochastic subspace identification," *IEEE Transactions on Power Systems*, vol. 29, pp. 349–358, Jan 2014.

[15] T. Jiang, H. Yuan, H. Jia, N. Zhou, and F. Li, "Stochastic subspace identification-based approach for tracking inter-area oscillatory modes in bulk power system utilising synchrophasor measurements," *IET Generation, Transmission Distribution*, vol. 9, no. 15, pp. 2409–2418, 2015.

[16] B. Peeters and G. D. Roeck, "Stochastic system identification for operational modal analysis : A review," 2001.

[17] M. Ghorbaniparvar, "Survey on forced oscillations in power system," *Journal of Modern Power Systems and Clean Energy*, vol. 5, pp. 671–682, Sep 2017.

[18] V. S. PeriÄ and L. Vanfretti, "Power-system ambient-mode estimation considering spectral load properties," *IEEE Transactions on Power Systems*, vol. 29, pp. 1133–1143, May 2014.

[19] NERC, "Interconnection oscillation analysis."

[20] D. N. Kosterev, C. W. Taylor, and W. A. Mittelstadt, "Model validation for the august 10, 1996 wscc system outage," *IEEE Transactions on Power Systems*, vol. 14, pp. 967–979, Aug 1999.

[21] J. J. S.-G. et. al., "Identification of electromechanical modes in power systems," June 2012.

[22] J. W. Pierre, D. Trudnowski, M. Donnelly, N. Zhou, F. K. Tuffner, and L. Dosiek, "Overview of system identification for power systems from measured responses," *IFAC Proceedings Volumes*, vol. 45, no. 16, pp. 989 – 1000, 2012. 16th IFAC Symposium on System Identification.

[23] J. W. Pierre, N. Zhou, F. K. Tuffner, J. F. Hauer, D. J. Trudnowski, and W. A. Mittelstadt, "Probing signal design for power system identification," *IEEE Transactions on Power Systems*, vol. 25, pp. 835–843, May 2010.

[24] J. SeppÃnen, J. Turunen, A. NikkilÃ, and L. Haarla, "Resonance of forcing oscillations and inter-area modes in the nordic power system," in *2018 IEEE PES Innovative Smart Grid Technologies Conference Europe (ISGT-Europe)*, pp. 1–6, Oct 2018.

[25] NERC, "Reliability guideline forced oscillation monitoring and mitigation."

[26] J. Ning, S. A. N. Sarmadi, and V. Venkatasubramanian, "Two-level ambient oscillation modal estimation from synchrophasor measurements," *IEEE Transactions on Power Systems*, vol. 30, pp. 2913–2922, Nov 2015.

[27] J. Zhang, C. Wu, and Y. Han, "A power spectrum density based signal selection approach for electromechanical mode estimation," in *2012 IEEE Power and Energy Society General Meeting*, pp. 1–7, July 2012.

[28] Q. F. Zhang, X. Luo, E. Litvinov, N. Dahal, M. Parashar, K. Hay, and D. Wilson, "Advanced grid event analysis at iso new england using phasorpoint," in *2014 IEEE PES General Meeting | Conference Exposition*, pp. 1–5, July 2014.

[29] F. P. Demello and C. Concordia, "Concepts of synchronous machine stability as affected by excitation control," *IEEE Transactions on Power Apparatus and Systems*, vol. PAS-88, pp. 316–329, April 1969.

[30] N. Rostamkolai, R. J. Piwko, and A. S. Matusik, "Evaluation of the impact of a large cyclic load on the lilco power system using time simulation and frequency domain techniques," *IEEE Transactions on Power Systems*, vol. 9, pp. 1411–1416, Aug 1994.

[31] J. S. Thorp, C. E. Seyler, and A. G. Phadke, "Electromechanical wave propagation in large electric power systems," *IEEE Transactions on Circuits and Systems I: Fundamental Theory and Applications*, vol. 45, pp. 614–622, June 1998.

[32] F. P. Demello and C. Concordia, "Concepts of synchronous machine stability as affected by excitation control," *IEEE Transactions on Power Apparatus and Systems*, vol. PAS-88, pp. 316–329, April 1969.

[33] L. Dosiek, N. Zhou, J. W. Pierre, Z. Huang, and D. J. Trudnowski, "Mode shape estimation algorithms under ambient conditions: A comparative review," *IEEE Transactions on Power Systems*, vol. 28, pp. 779–787, May 2013.

[34] S. Maslennikov, B. Wang, and E. Litvinov, "Dissipating energy flow method for locating the source of sustained oscillations," *International Journal of Electrical Power Energy Systems*, vol. 88, pp. 55 – 62, 2017.

[35] M. Klein, G. J. Rogers, and P. Kundur, "A fundamental study of inter-area oscillations in power systems," *IEEE Transactions on Power Systems*, vol. 6, pp. 914–921, Aug 1991.

[36] P. Pourbeik, P. S. Kundur, and C. W. Taylor, "The anatomy of a power grid blackout - root causes and dynamics of recent major blackouts," *IEEE Power and Energy Magazine*, vol. 4, pp. 22–29, Sept 2006.

[37] "Real-time application of synchrophasors for improving reliability," May 2018.

[38] R. B. Myers and D. J. Trudnowski, "Effects of forced oscillations on spectral-based mode-shape estimation," in *2013 IEEE Power Energy Society General Meeting*, pp. 1–6, July 2013.

[39] M. GHORBANIPARVAR, "Survey on forced oscillations in power system," *Journal of Modern Power Systems and Clean Energy*, vol. 5, pp. 671–682, Sep 2017.

[40] J. Follum, J. W. Pierre, and R. Martin, "Simultaneous estimation of electromechanical modes and forced oscillations," *IEEE Transactions on Power Systems*, vol. 32, pp. 3958–3967, Sept 2017.

[41] S. Maslennikov, B. Wang, Q. Zhang, a. Ma, a. Luo, a. Sun, and E. Litvinov, "A test cases library for methods locating the sources of sustained oscillations," in *2016 IEEE Power and Energy Society General Meeting (PESGM)*, pp. 1–5, July 2016.

[42] H. Ye, Y. Liu, P. Zhang, and Z. Du, "Analysis and detection of forced oscillation in power system," *IEEE Transactions on Power Systems*, vol. 32, pp. 1149–1160, March 2017.

[43] I. R. Cabrera, B. Wang, and K. Sun, "A method to locate the source of forced oscillations based on linearized model and system measurements," in *2017 IEEE Power Energy Society General Meeting*, pp. 1–5, July 2017.

[44] D. J. Trudnowski and J. E. Dagle, "Effects of generator and static-load nonlinearities on electromechanical oscillations," *IEEE Transactions on Power Systems*, vol. 12, pp. 1283–1289, Aug 1997.

[45] D. Gautam, L. Goel, R. Ayyanar, V. Vittal, and T. Harbour, "Control strategy to mitigate the impact of reduced inertia due to doubly fed induction generators on large power systems," *IEEE Transactions on Power Systems*, vol. 26, pp. 214–224, Feb 2011.

[46] F. M. Hughes, O. Anaya-Lara, N. Jenkins, and G. Strbac, "Control of dfig-based wind generation for power network support," *IEEE Transactions on Power Systems*, vol. 20, pp. 1958–1966, Nov 2005.

[47] J. L. DomÃnguez-GarcÃa, O. Gomis-Bellmunt, F. D. Bianchi, and A. Sumper, "Power oscillation damping supported by wind power: A review," *Renewable and Sustainable Energy Reviews*, vol. 16, no. 7, pp. 4994 – 5006, 2012.

[48] Z. Miao, L. Fan, D. Osborn, and S. Yuvarajan, "Control of dfig-based wind generation to improve interarea oscillation damping," *IEEE Transactions on Energy Conversion*, vol. 24, pp. 415–422, June 2009.

[49] M. Singh, A. J. Allen, E. Muljadi, V. Gevorgian, Y. Zhang, and S. Santoso, "Interarea oscillation damping controls for wind power plants," *IEEE Transactions on Sustainable Energy*, vol. 6, pp. 967–975, July 2015.

[50] R. Yousefian, R. Bhattarai, and S. Kamalasadan, "Transient stability enhancement of power grid with integrated wide area control of wind farms and synchronous generators," *IEEE Transactions on Power Systems*, vol. 32, pp. 4818–4831, Nov 2017.

[51] R. Yousefian, S. Kamalasadan, and R. Bhattarai, "Direct intelligent wide-area damping controller for wind integrated power system," in *2016 IEEE Power and Energy Society General Meeting (PESGM)*, pp. 1–5, July 2016.

[52] S. A. N. Sarmadi and V. Venkatasubramanian, "Electromechanical mode estimation using recursive adaptive stochastic subspace identification," *IEEE Transactions on Power Systems*, vol. 29, pp. 349–358, Jan 2014.

[53] H. Liu, L. Zhu, Z. Pan, F. Bai, Y. Liu, Y. Liu, M. Patel, E. Farantatos, and N. Bhatt, "Armax-based transfer function model identification using wide-area measurement for

adaptive and coordinated damping control," *IEEE Transactions on Smart Grid*, vol. 8, pp. 1105–1115, May 2017.

[54] B. Pal and B. Chaudhuri, *Robust Control in Power Systems*. Power Electronics and Power Systems, Springer US, 2006.

[55] R. Bhattarai, S. J. Hossain, J. Qi, J. Wang, and S. Kamalasadan, "Sustained system oscillation by malicious cyber attacks on distributed energy resources," in *2018 IEEE Power Energy Society General Meeting (PESGM)*, pp. 1–5, Aug 2018.

[56] A. Thakallapelli, S. J. Hossain, and S. Kamalasadan, "Coherency and online signal selection based wide area control of wind integrated power grid," *IEEE Transactions on Industry Applications*, vol. 54, pp. 3712–3722, July 2018.

[57] S. J. Hossain, R. Bhattarai, R. Yousefian, and S. Kamalasadan, "Adaptive wide area damping controller for distributed energy resources integrated power grid," in *2018 IEEE Power Energy Society General Meeting (PESGM)*, pp. 1–5, Aug 2018.

[58] U. Agrawal, J. Follum, J. W. Pierre, and D. Duan, "Electromechanical mode estimation in the presence of periodic forced oscillations," *IEEE Transactions on Power Systems*, vol. 34, pp. 1579–1588, March 2019.

[59] Ruichao Xie and D. Trudnowski, "Distinguishing features of natural and forced oscillations," in *2015 IEEE Power Energy Society General Meeting*, pp. 1–5, July 2015.

[60] V. S. PeriÄ and L. Vanfretti, "Power-system ambient-mode estimation considering spectral load properties," *IEEE Transactions on Power Systems*, vol. 29, pp. 1133–1143, May 2014.

[61] P. van Overschee and B. de Moor, *Subspace Identification for Linear Systems: Theory* $\tilde{A}\hat{a}\neg Implementation\neg Applications. SpringerUS$, 2011.

[62] T. Wu, V. M. Venkatasubramanian, and A. Pothen, "Fast parallel stochastic subspace algorithms for large-scale ambient oscillation monitoring," *IEEE Transactions on Smart Grid*, vol. 8, pp. 1494–1503, May 2017.

[63] W. Li, M. Wang, and J. H. Chow, "Real-time event identification through low-dimensional subspace characterization of high-dimensional synchrophasor data," *IEEE Transactions on Power Systems*, vol. 33, pp. 4937–4947, Sep. 2018.

[64] K. D. Cock, G. MercÃšre, and B. D. Moor, "Recursive subspace identification for in-flight modal analysis of airplanes."

[65] J. Munier and G. Y. Delisle, "Spatial analysis using new properties of the cross-spectral matrix," *IEEE Transactions on Signal Processing*, vol. 39, pp. 746–749, March 1991.

[66] C. W. Taylor, D. C. Erickson, K. E. Martin, R. E. Wilson, and V. Venkatasubramanian, "Wacs-wide-area stability and voltage control system: R d and online demonstration," *Proceedings of the IEEE*, vol. 93, pp. 892–906, May 2005.

[67] U. Agrawal, J. Follum, J. W. Pierre, and D. Duan, "Electromechanical mode estimation in the presence of periodic forced oscillations," *IEEE Transactions on Power Systems*, vol. 34, pp. 1579–1588, March 2019.

[68] D. A. Gray, M. J. Gibbard, and D. J. Vowles, "Characterisation of ambient noise in electricity power grids," in *Proceedings of the Eighth International Symposium on Signal Processing and Its Applications, 2005.*, vol. 2, pp. 835–838, Aug 2005.

[69] **S. J. Hossain** and S. Kamalasadan, "Combined deterministic-stochastic online subspace identification for power system modeestimation and oscillation classification," in *2019 IEEE Industry Applications Society Annual Meeting*, Oct 2019.

[70] P. Gao, M. Wang, S. G. Ghiocel, J. H. Chow, B. Fardanesh, and G. Stefopoulos, "Missing data recovery by exploiting low-dimensionality in power system synchrophasor measurements," *IEEE Transactions on Power Systems*, vol. 31, pp. 1006–1013, March 2016.

[71] and J. Malik, "Normalized cuts and image segmentation," *IEEE Transactions on Pattern Analysis and Machine Intelligence*, vol. 22, pp. 888–905, Aug 2000.

[72] R. A. Horn and C. R. Johnson, eds., *Matrix Analysis*. New York, NY, USA: Cambridge University Press, 1986.

[73] L. Vanfretti and J. H. Chow, "Analysis of power system oscillations for developing synchrophasor data applications," in *2010 IREP Symposium Bulk Power System Dynamics and Control - VIII (IREP)*, pp. 1–17, Aug 2010.

[74] D. J. Vowles and M. J. Gibbard, "Illustration of an analytical method for selecting signals and locations for power system modal-estimators," in *IEEE PES General Meeting*, pp. 1–7, July 2010.

[75] J. Zhang, C. Wu, and Y. Han, "A power spectrum density based signal selection approach for electromechanical mode estimation," in *2012 IEEE Power and Energy Society General Meeting*, pp. 1–7, July 2012.

[76] J. SeppÃnen, A. NikkilÃ, J. Turunen, and L. Haarla, "Operational experiences of wams-based damping estimation methods," in *2017 IEEE Manchester PowerTech*, pp. 1–6, June 2017.

[77] S. Maslennikov, B. Wang, and E. Litvinov, "Dissipating energy flow method for locating the source of sustained oscillations," *International Journal of Electrical Power Energy Systems*, vol. 88, pp. 55 – 62, 2017.

[78] M. Ghorbaniparvar and N. Zhou, "A survey on forced oscillations in power system," *CoRR*, vol. abs/1612.04718, 2016.

[79] B. WANG and K. SUN, "Location methods of oscillation sources in power systems: a survey," *Journal of Modern Power Systems and Clean Energy*, vol. 5, pp. 151–159, Mar 2017.

[80] L. Chen, F. Xu, Y. Min, M. Wang, and W. Hu, "Transient energy dissipation of resistances and its effect on power system damping," *International Journal of Electrical Power Energy Systems*, vol. 91, pp. 201 – 208, 2017.

[81] S. Chevalier, P. Vorobev, K. Turitsyn, B. Wang, and S. Maslennikov, "Using passivity theory to interpret the dissipating energy flow method," *CoRR*, vol. abs/1811.03260, 2018.

[82] S. Chevalier, P. Vorobev, and K. Turitsyn, "Using effective generator impedance for forced oscillation source location," *CoRR*, vol. abs/1708.01893, 2017.

[83] L. Chen, Y. Min, and W. Hu, "An energy-based method for location of power system oscillation source," *IEEE Transactions on Power Systems*, vol. 28, pp. 828–836, May 2013.

[84] S. Feng, B. Zheng, P. Jiang, and J. Lei, "A two-level forced oscillations source location method based on phasor and energy analysis," *IEEE Access*, vol. 6, pp. 44318–44327, 2018.

[85] **S. J. Hossain** and S. Kamalasadan, "Online measurement based power system reduced order model generation and validation," in *2019 North American Power Symposium (NAPS)*, pp. 1–6, Oct. 2019.

[86] **S. J. Hossain** and S. Kamalasadan, "Investigation on evaluating the unmodeled dynamics of power system and its effects on characterizing power system oscillations," in *2018 North American Power Symposium (NAPS)*, pp. 1–6, Sep. 2018.

[87] J. Follum, J. W. Pierre, and R. Martin, "Simultaneous estimation of electromechanical modes and forced oscillations," *IEEE Transactions on Power Systems*, vol. 32, pp. 3958–3967, Sept 2017.

[88] J. Follum, J. W. Pierre, and R. Martin, "Simultaneous estimation of electromechanical modes and forced oscillations," *IEEE Transactions on Power Systems*, vol. 32, pp. 3958–3967, Sept 2017.

[89] J.-H. Weng and C.-H. Loh, "Recursive subspace identification for on-line tracking of structural modal parameter," *Mechanical Systems and Signal Processing*, vol. 25, no. 8, pp. 2923 – 2937, 2011.

[90] D. F. Enns, "Model reduction with balanced realizations: An error bound and a frequency weighted generalization," in *The 23rd IEEE Conference on Decision and Control*, pp. 127–132, Dec 1984.

[91] J. H. Chow and K. W. Cheung, "A toolbox for power system dynamics and control engineering education and research," *IEEE Transactions on Power Systems*, vol. 7, pp. 1559–1564, Nov 1992.

[92] E. B. Cano, "Nyiso case studies of system events analysis using pmu data," *NASPI Work Group Meeting*, March 2014.

[93] **S. J. Hossain**, R. Bhattarai, R. Yousefian, and S. Kamalasadan, "Adaptive wide area damping controller for distributed energy resources integrated power grid," in *2018 IEEE Power Energy Society General Meeting (PESGM)*, pp. 1–5, Aug 2018.

[94] R. Bhattarai, **S. J. Hossain**, J. Qi, J. Wang, and S. Kamalasadan, "Sustained system oscillation by malicious cyber attacks on distributed energy resources," in *2018 IEEE Power Energy Society General Meeting (PESGM)*, pp. 1–5, Aug 2018.

[95] A. Ulbig, T. S. Borsche, and G. Andersson, "Impact of low rotational inertia on power system stability and operation," *IFAC Proceedings Volumes*, vol. 47, no. 3, pp. 7290 – 7297, 2014. 19th IFAC World Congress.

[96] S. Eftekharnejad, V. Vittal, G. T. Heydt, B. Keel, and J. Loehr, "Impact of increased penetration of photovoltaic generation on power systems," *IEEE Transactions on Power Systems*, vol. 28, pp. 893–901, May 2013.

[97] D. Gautam, V. Vittal, and T. Harbour, "Impact of increased penetration of dfig-based wind turbine generators on transient and small signal stability of power systems," *IEEE Transactions on Power Systems*, vol. 24, pp. 1426–1434, Aug 2009.

[98] S. Eftekharnejad, V. Vittal, G. T. Heydt, B. Keel, and J. Loehr, "Impact of increased penetration of photovoltaic generation on power systems," *IEEE Transactions on Power Systems*, vol. 28, pp. 893–901, May 2013.

[99] A. Thakallapelli, **S. J. Hossain**, and S. Kamalasadan, "Coherency and online signal selection based wide area control of wind integrated power grid," *IEEE Transactions on Industry Applications*, vol. 54, pp. 3712–3722, July 2018.

[100] P. Kundur, N. J. Balu, and M. G. Lauby, *Power system stability and control*, vol. 7. McGraw-hill New York, 1994.

[101] R. Pena, J. Clare, and G. Asher, "Doubly fed induction generator using back-to-back pwm converters and its application to variable-speed wind-energy generation," *IEE Proceedings-Electric Power Applications*, vol. 143, no. 3, pp. 231–241, 1996.

[102] R. Bhattarai, N. Gurung, and S. Kamalasadan, "Minimum variance controller based adaptive control for doubly fed induction generator," in *2016 North American Power Symposium (NAPS)*, pp. 1–6, Sept 2016.

[103] R. Trentini, R. Kutzner, and L. Hofmann, "State-space generalized minimum variance controller based pss for damping of interarea modes," in *2016 18th Mediterranean Electrotechnical Conference (MELECON)*, pp. 1–6, April 2016.

APPENDIX A: TEST SYSTEMS DESCRIPTION

A.1 Two Area System

Two area test system is a well known model studied for inter area oscillation (9).The model consists of two areas connected through a tie-line. Area 1 has two synchronous generators each generating 700 MW power and area 2 also has two synchronous generator each generating 719 MW and 700 MW respectively. Area 1 has a local load of 967 MW and area 2 has a local load of 1767 MW. Both the areas are connected through a weak transmission line and area 1 exports 400 MW to area 2. The 'IEEE Type EXAC4A' is used for voltage regulation, governor type 'TGOV1' is used for governor model and type 'STAB1' is used for power system stabilizer model. Details are given in Figs. A.2 and A.3.

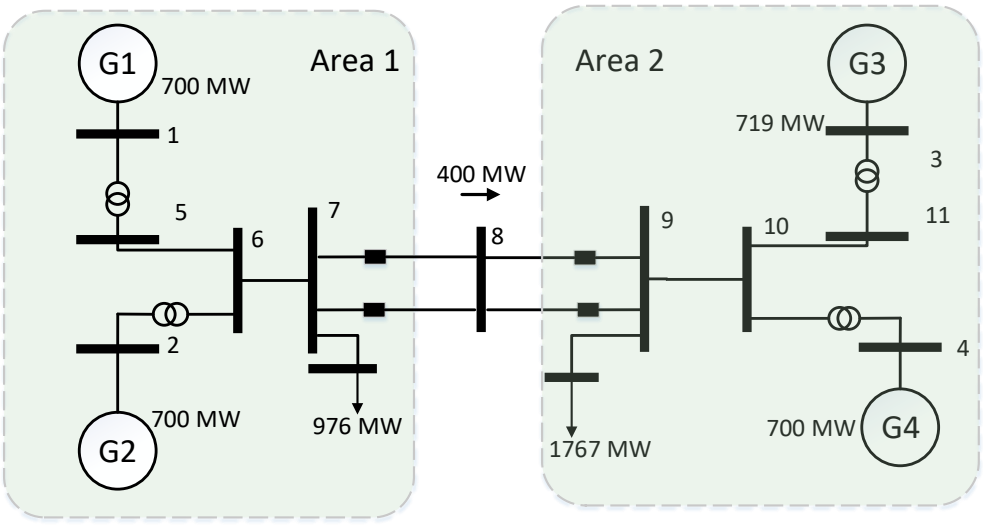

Figure A.1: Two area test System (9).

GEN	R	T1	Vmax	Vmin	T2	T3	Dt
1	0.05	0.05	10.00	-10.00	2.1	7.0	0.0
2	0.05	0.05	10.00	-10.00	2.1	7.0	0.0
3	0.05	0.05	10.00	-10.00	2.1	7.0	0.0
4	0.05	0.05	10.00	-10.00	2.1	7.0	0.0

Figure A.2: Governor data for the two area system.

GEN	K/T	T	T1/T3	T3	T2/T4	T2	HLIM
1	3.0	2.0	2.0	0.04	2.0	0.04	0.1
2	3.0	2.0	2.0	0.04	2.0	0.04	0.1
3	3.0	2.0	2.0	0.04	2.0	0.04	0.1
4	3.0	2.0	2.0	0.04	2.0	0.04	0.1

Figure A.3: Power system stabilizer (PSS) data for the two area system.

A.2 IEEE 39 Bus Test System

IEEE 39-Bus system is a reduced equivalent of the New England test system (NETS). Fig. A.4 shows the one line diagram of the test system (7).This system has 10 generators and 39 buses. Generator 1 located at bus 39 is an aggregated generator and hence has high inertia and output power. Exciter model used for voltage regulation is of 'IEEE type 1' and governor model is of type 'TGOV1'.The governor data is added for EMT simulation studies compared to (7). Details are given in Figs. A.5.

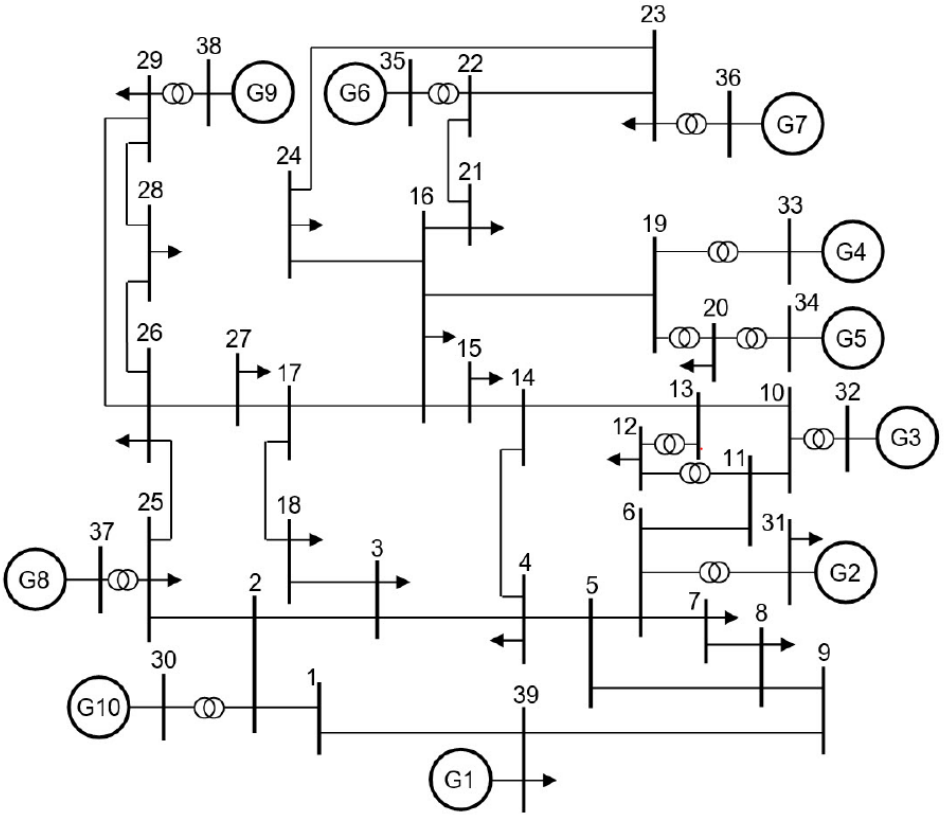

Figure A.4: IEEE 39 bus test system (7).

GEN	R	T1	Vmax	Vmin	T2	T3	Dt
2	0.05	0.05	1.00	-1.00	2.1	7.0	0.0
3	0.05	0.05	1.00	-1.00	2.1	7.0	0.0
4	0.05	0.05	1.00	-1.00	2.1	7.0	0.0
5	0.05	0.05	1.00	-1.00	2.1	7.0	0.0
6	0.05	0.05	1.00	-1.00	2.1	7.0	0.0
7	0.05	0.05	1.00	-1.00	2.1	7.0	0.0
8	0.05	0.05	1.00	-1.00	2.1	7.0	0.0
9	0.05	0.05	1.00	-1.00	2.1	7.0	0.0
10	0.05	0.05	1.00	-1.00	2.1	7.0	0.0

Figure A.5: Governor data for the 39 bus system.

A.3 IEEE 68 Bus Test System

The 68-bus system is a reduced order equivalent of the inter-connected New England test system (NETS) and New York power system (NYPS), with five geographical regions out of which NETS and NYPS are represented by a group of generators whereas, the power import from each of the three other neighboring areas are approximated by equivalent generator models. Fig. A.6 shows the one line diagram of the test system (10).This system has 16 generators and 68 buses. Generator 14,15 and 16 are aggregated generators and hence has high inertia and output power. Exciter model used for voltage regulation is of 'DC4B' and 'ST1A'. Governor model is of type 'TGOV1'.The governor data is added for EMT simulation studies compared to (10). Details are given in Figs. A.7.

A.4 miniWECC System

miniWECC system is consist of a reduced WECC 179-bus, 29-machine system (1). The one-line diagram of the system is shown in Fig. A.8. All generators are represented as the GENCLS model from Siemens PTI PSS/E, i.e. a classical second-order differential model reflecting the motion of the rotor; damping parameter D for all generators are set to 4; all loads are modeled as constant MVA. Generators where the disturbances are applied are represented as GENROU model from Siemens PTI PSS/E.

Note: (i) generator inertia data were recreated reflecting the dynamics of interests in the Western Interconnection system and does not match exactly the actual system parameters; (ii) damping parameter D for each generator was artificially created such that the natural modes not of interests are reasonably damped.

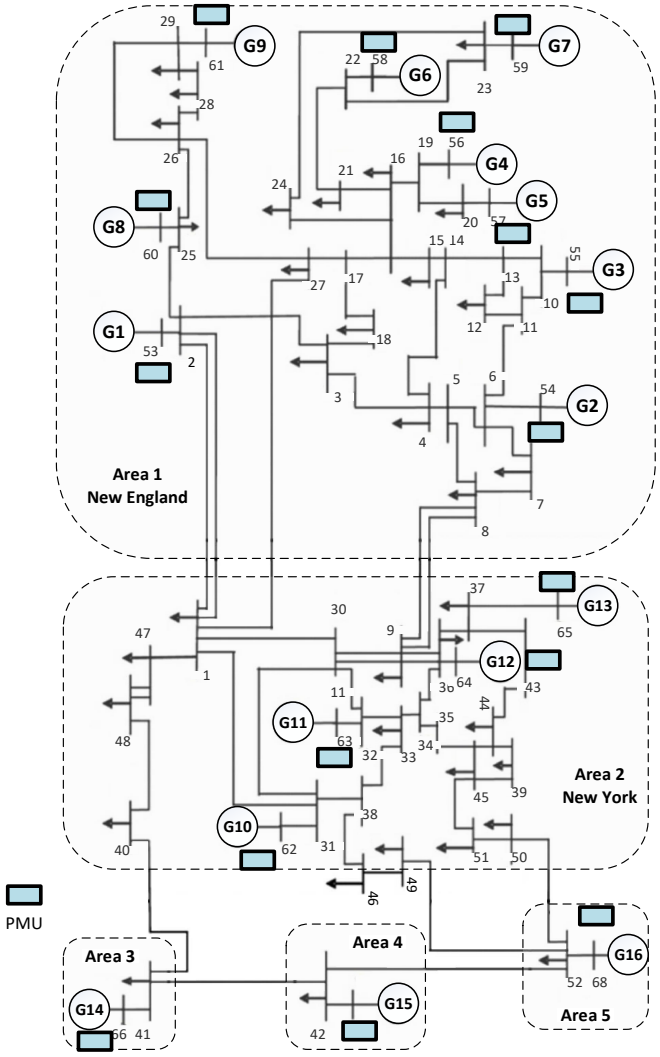

Figure A.6: IEEE 68 bus test system (10).

IBUS	Bus	Area	I	R	T1	VMAX	VMIN	T2	T3	Dt	MVA Base	Pgen (Powerflow)	Pmax (Powerflow)	Pmin (Powerflow)	Status
1	1	1	1	0.002	0	500	0	0	1	0	200	250	9999	0	1
2	2	1	1	0.002	0	500	0	0	1	0	200	545	9999	0	1
3	3	1	1	0.002	0	500	0	0	1	0	200	650	9999	0	1
4	4	1	1	0.002	0	500	0	0	1	0	200	632	9999	0	1
5	5	1	1	0.002	0	500	0	0	1	0	200	505	9999	0	1
6	6	1	1	0.002	0	500	0	0	1	0	200	700	9999	0	1
7	7	1	1	0.002	0	500	0	0	1	0	200	560	9999	0	1
8	8	1	1	0.002	0	500	0	0	1	0	200	540	9999	0	1
9	9	1	1	0.002	0	500	0	0	1	0	200	800	9999	0	1
10	10	2	1	0.002	0	500	0	0	1	0	200	500	9999	0	1
11	11	2	1	0.002	0	500	0	0	1	0	600	1000	9999	0	1
12	12	2	1	0.002	0	500	0	0	1	0	200	1350	9999	0	1
13	13	2	1	0.002	0	500	0	0	1	0	6000	3591	9999	0	1
14	14	3	1	0.002	0	500	0	0	1	0	3000	1785	9999	0	1
15	15	4	1	0.002	0	500	0	0	1	0	3000	1000	9999	0	1
16	16	5	1	1E-04	0	500	0	0	1	0	6000	3379.5681	9999	0	1

Figure A.7: Governor data for the 68 bus system.

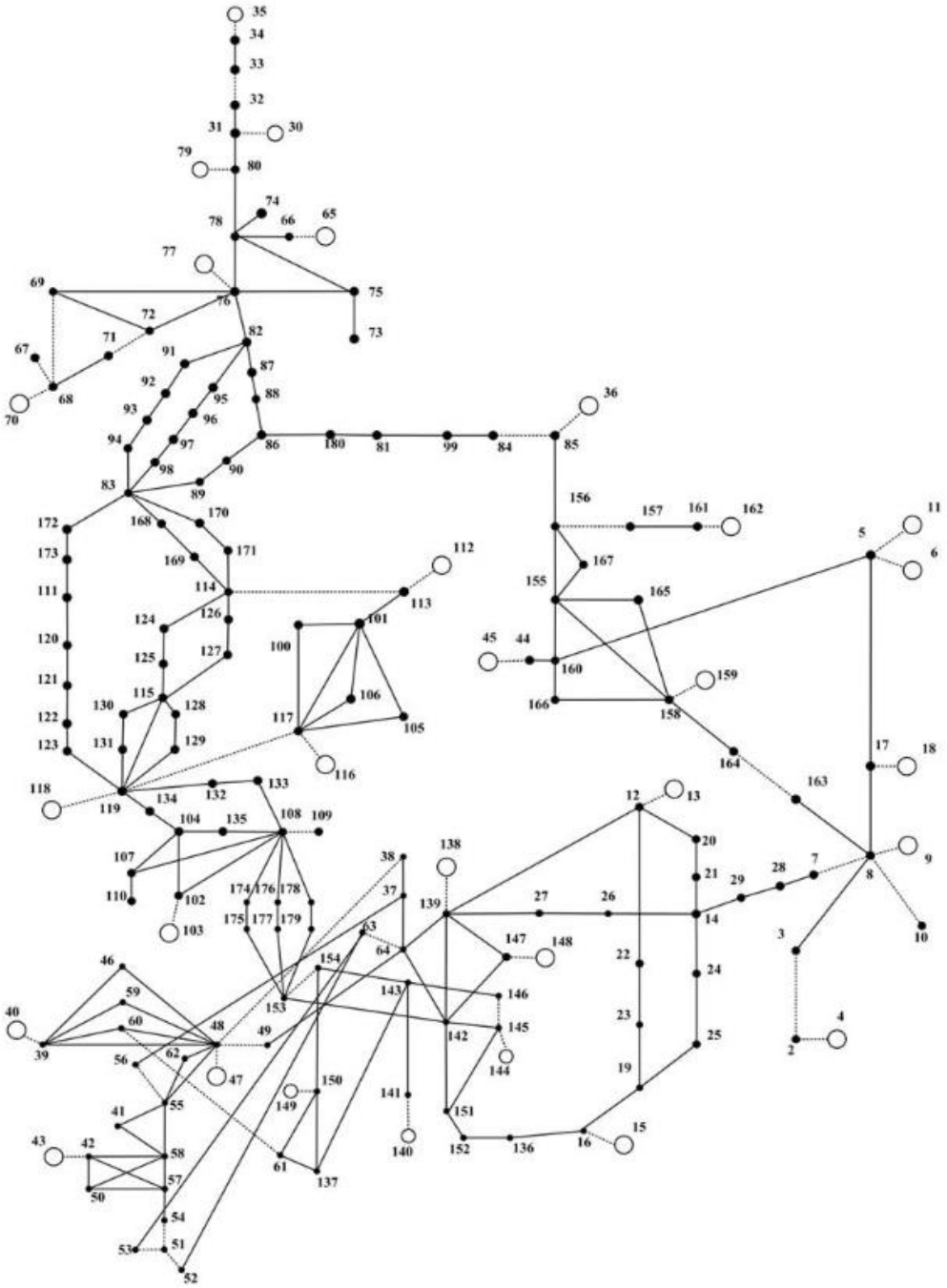

Figure A.8: miniWECC test system (1).

APPENDIX B: SIGNAL PROCESSING METHODOLOGY

In this section, the typical process of dealing with PMU measurements are presented. And some preliminary background for method like prony, periodogram are shown. It also shows how mode shape can be extracted from measurement.

Figure B.1: Flow chart of the study method .

B.1 PMU Data Concentration

First step is to gather the PMU measurements for different output channels. In this study, results are obtained from simulation, so data integrity problems related to PMU data which includes outliers and missing data are not considered. Fig. B.2 shows the active power output of 29 generator buses in the miniWECC system for a studied case.

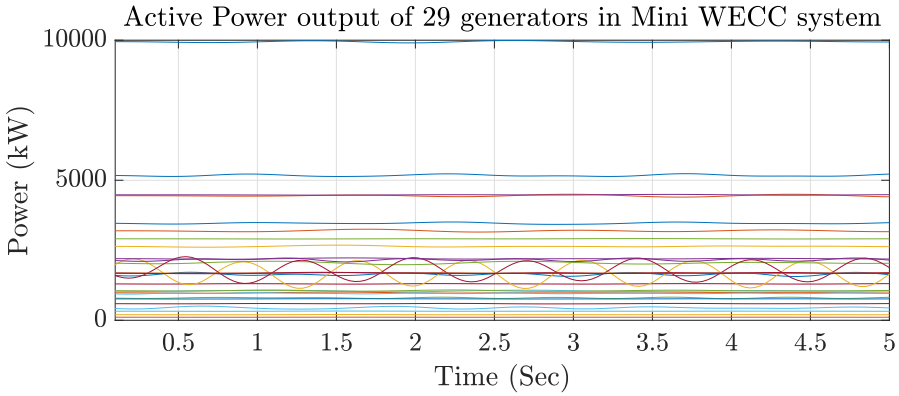

Figure B.2: Data acquisition from different output channels.

B.2 Data Preprocessing

Acquired data is generally preprocessed before detection algorithms are applied to it. Data preprocessing includes passing the data through a low pass filter and down sampled as only the electromechanical modes are of interest. Then the data is detrended to remove any DC offset which might bias the oscillation detection algorithms. Fig. B.3 shows the detreneded and downsampled data for this example.

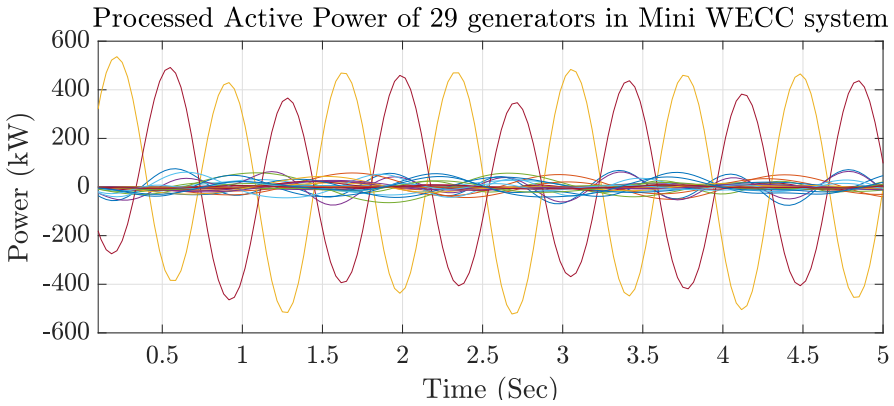

Figure B.3: Processed data from different output channels.

B.3 Signal selection

After processing the data signals are selected based upon oscillation magnitudes for detecting oscillation and it's characteristics. Fig. B.4 shows the signals which has the highest oscillation magnitude. Highest magnitude of oscillation is seen at generator 10 which is located at bus 159 and this signal is used for further analysis.

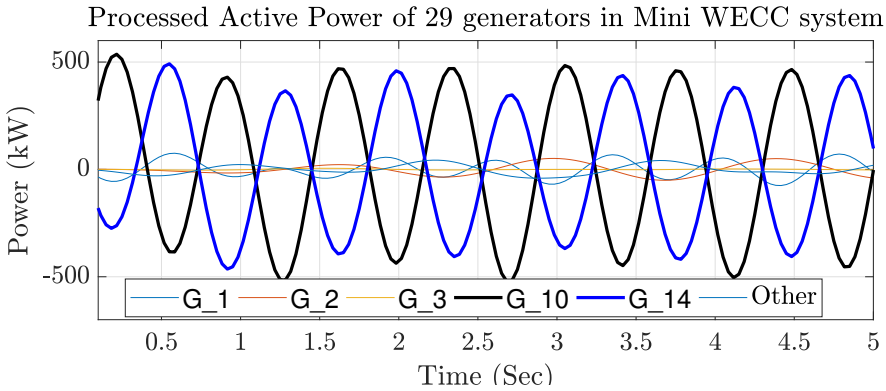

Figure B.4: Selected signals from different output channels.

B.4 Oscillation detection

The selected signal from previous step is analyzed to estimate the frequency of oscillation. Both parametric and non parametric methods have been used for the estimation. The data window length used for estimation is 20 second. Prony analysis have been used for parametric method and welch's periodogram is used for non parametric method. Table B.1 shows that both the parametric and nonparametric methods are able to identify the same

oscillation frequency. Fig. B.5 illustrates the selected signal and the estimation from welch's periodogram. Prony analysis approximates a signal as a summation of damped sinusoids and the general expression is given in (B.1). For the example case order of the system $n = 6$ and table B.2 shows the phase, amplitude and damping estimates of different frequencies for prony analysis.

$$y_r(t) = \sum_{m=1}^{n} A_m e^{\sigma_m t} cos(\omega_m t + \phi_m) \tag{B.1}$$

Table B.1: Estimation of oscillation frequency and damping ratio.

Method (Hz)	Frequency	Damping ratio
Prony analysis	1.41	0
Welch's Periodogram	1.41	NA

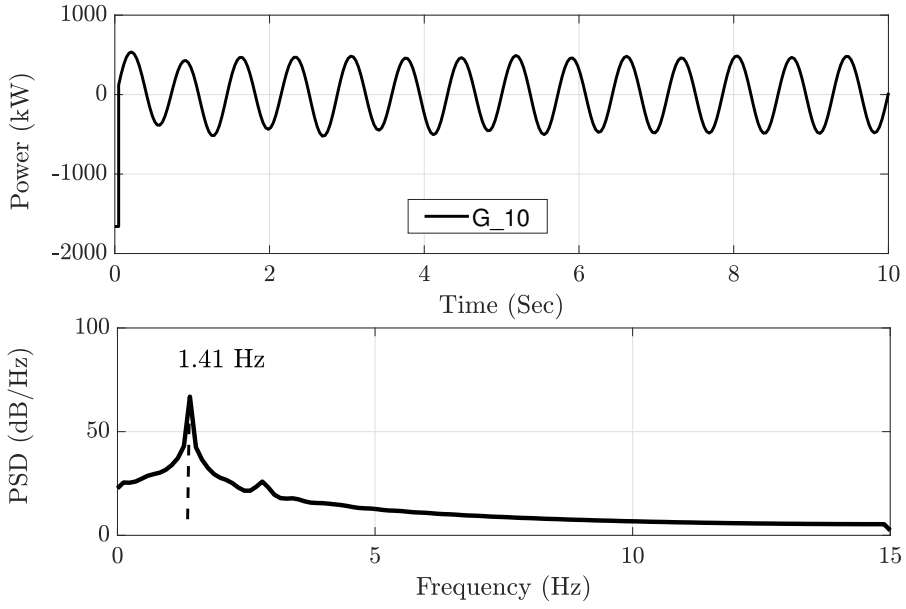

Figure B.5: Selected signal and oscillation frequency identification.

B.5 Oscillation shape estimation

Once thee oscillation frequency is identified then it is important to know which generator are contributing to that particular oscillation and at which generator output power that

Table B.2: Prony analysis signal components.

Frequency(f_m) (Hz)	Amplitude(A_m)	Phase (ϕ_m) (rad)	damping (σ_m)
1.4026	245.2940	-2.3410	0
1.4026	245.2940	2.3410	0
2.5357	9.4039	0.2040	0
2.5357	9.4039	-0.2040	0
3.4037	5.3608	3.0988	0
3.4037	5.3608	-3.0988	0

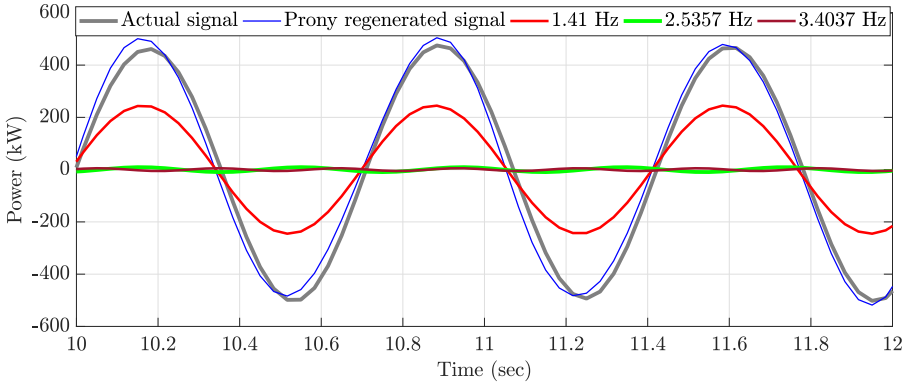

Figure B.6: Portion of the regenerated signals using Prony

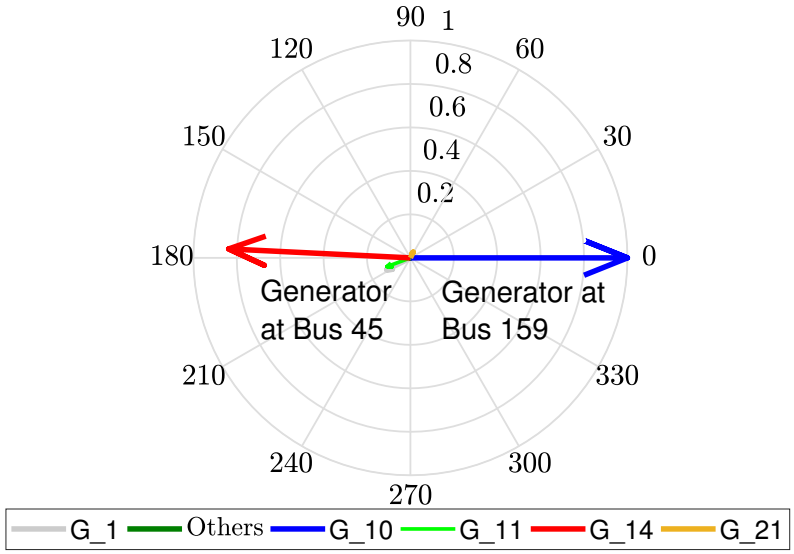

Figure B.7: Oscillation shape estimation.

oscillation is more prominent. A combination of these two factors is seen in the oscillation shape. Oscillation shape involves extracting the magnitude and phase of the oscillation frequency of interest from all the available output channels. Fig. B.7 shows the normalized oscillations shape for the 1.41 Hz oscillation mode. It shows that the highest magnitude is seen in generator at bus 159 although the source of the oscillation is at generator at bus 45 for this case. So, the bus near the oscillation source will have highest magnitude is not necessarily true always.